The University of Nottingham

Institute of Engineering Surveying and Space Geodesy

Investigations Into Un-mitigated Troposphere and Multipath Effects on Kinematic GPS for 3-Dimensional Monitoring of High Rise Building Movements.

By

Azman Bin Mohd Suldi
B.Surv., M.Sc.

Thesis submitted to the University of Nottingham for the degree of Doctor of Philosophy

June 2006

Abstract

Monitoring is a process of observing any changes on a monitored subject. Deformation monitoring is a process which consists of four stages: specification, design, implementation and analysis [*Kennie et al.*, 1990], with the structure being monitored on a daily, hourly or continuous basis for any changes in position, size and shape. With the Global Positioning System (GPS), a 24-hour all weather monitoring system can be established. However, for kinematic GPS, un-mitigated troposphere and multipath remain as the main source of errors in the position residuals. These were investigated in detail using data from field trials conducted by the author which suite their particular purposes. The investigations were made using static and moving stations, and included stations at the same altitude, and stations with a high difference in altitude, and baseline lengths of less than ten kilometres. Using Adaptive Filtering (AF) technique, common signals in two time series can be extracted. By performing AF and interchanging position residuals time series as reference and desired (Forward and Backward) using consecutive days of data will show the multipath and this can be confirmed with a third day of data. While same day AF can be used to separate un-mitigated troposphere and movements from receiver noise. The position residuals considered in this thesis were processed with Leica Ski-Pro Version 3.0 software. These were validated and through comparisons made using a kinematic GPS processing software named KINPOS, developed by previous researchers at the IESSG, University of Nottingham and the use of Virtual Reference Station (VRS) data were also investigated by comparing with actual data. Through the field trials carried out on Snowdon, University campus, Humber Bridge and Forth Road Bridge, the novelty of this thesis is that it demonstrates that by better understanding the trends in un-mitigated troposphere and multipath, the use of kinematic GPS for monitoring tall structures can be improved, making the results more suitable for engineers and building owners or managers to better assess building performance during extreme motions caused by traffic, earthquakes, strong winds, and other climatic conditions.

Acknowledgements

The three years of research that has gone into this thesis were carried out at the Institute of Engineering Surveying and Space Geodesy (IESSG).

I would like to express my gratitude to all those who gave me the opportunity and possibility to complete this thesis. Firstly, I would like to thank everyone at the IESSG for their help, particularly my supervisors Dr. Gethin W. Roberts and Dr. Richard M. Bingley, for their help and supporting advice throughout the three years. I would also like to thank Sean Ince and Dr. Samantha Waugh, for their assistance with my field trials which would not have been possible without their help, Dr. Xiaolin Meng, for his guidance on Adaptive Filter, Dr. Chris Hide, for his valuable knowledge on KINPOS, Dr. Norman Teferle, for his PERL scripts related to TEQC, and Collin Fane at the Ordnance Survey for the Virtual Reference Station (VRS) data. Also, to the Snowdonia National Park Authority and council, the Humber Bridge Board and the Forth Estuary Transport Authority (FETA) which is responsible for managing the Forth Road Bridge for their permissions and cooperation with my trials. Finally, I would like to thank my fellow colleagues doing their PhD's and MSc's at the IESSG who gave continuous support and their precious time in making my field trials possible.

Last but not least, my special thanks to my lovely wife, Rosidah and my two kids, Amirul Hakeem and Azliya Ashiqeen for their full understanding of my commitment to my research work till completion.

Contents

List of Figures

List of Tables

Glossary

AF	-	Adaptive Filtering
BSW4.2	-	Bernese SoftWare version 4.2
DOD	-	United States Department of Defense
DOY	-	Day Of Year
ETRS89	-	European Terrestrial Reference System 1989
FIG	-	International Federation of Surveyors
GALILEO	-	Equivalent to GPS but built by the European union
GDOP	-	Geometric Dilution of Precision
GLONASS	-	Global Navigation Satellite System
GNSS	-	Global Navigation Satellite System
GPRS	-	General Packet Radio Service
GPS	-	Global Positioning System
GSM	-	Global System for Mobile communications
IAG	-	International Association of Geodesy
ICAO	-	International Civil Aviation Organization
IESSG	-	Institute of Engineering Surveying and Space Geodesy
IGS	-	International GPS Service
LAN	-	Local Area Network
NGS	-	National Geodetic Survey
NOAA	-	National Oceanic and Atmospheric Administration
OSNET	-	Ordnance Survey NETwork, United Kingdom
OTF	-	On The Fly
PPP	-	Precise Point Positioning
PRN	-	Pseudo Random Noise
RFI	-	Radio Frequency Interference
RINEX	-	Receiver Independent Exchange Format Version 2
RMS	-	Root Mean Square
RTK	-	Real Time Kinematic
RZTD	-	Relative Zenithal Tropospheric Delay
SVN	-	Satellite Vehicle Number

TEC	-	Total Electron Content
TEQC	-	Translate/Edit/Quality Check
USNO	-	United States Naval Observatory
UT	-	Universal Time
VRS	-	Virtual Reference Station
ZHD	-	Zenith Hydrostatic Delay
ZWD	-	Zenith Wet Delay

Chapter 1

Introduction

Developments in the construction industry have resulted in the rapid growth of large structures such as long suspension bridges, towers and tall buildings, which may vibrate and displace due to temperature change, wind load change, traffic, subsidence, settlement and ground movements. These changes, pose concern to the safety of the occupants and the structure itself. An experience such as the fall of Highland Towers in Malaysia in 1993 [*HighTower*, 2006] shows that no or insufficient monitoring was done professionally, to assess any movements on the building before it was too late, which resulted in heavy losses of life and a setback to engineers.

Monitoring is a process of observing any changes on a monitored subject. Deformation monitoring is a process which consists of four stages: specification, design, implementation and analysis [*Kennie et al*, 1990], with the structure being monitored on a daily, hourly or continuous basis for any changes in position, size and shape. The International Federation of Surveyors (FIG) for example, under COMMISSION 6, has a working group 6.1 dedicated in deformation measurement and analysis. Construction engineers in particular, are very interested to know how their buildings perform under real weather and site conditions. Even though all precautions can be accounted for during the design stage, it should be of high interest to engineers to be able to receive and analyse three-dimensional (3D) positional information, which are accurate and reliable, for them to further improve their designs. It is the task of surveyors to provide this information.

The Global Positioning System (GPS) is funded and controlled by the United States Department of Defense (DOD). Using the coded signals, with a minimum of four satellites, a user with a receiver on the surface of the earth can compute position, velocity and time. Relative positioning using the phase signals can be achieved to high accuracies of millimetre level [*Hofmann-Wellenhof et al.*, 2001; *Leick*, 2004].

Many studies have been conducted on deformation monitoring to provide the above information accurately, using GPS alone or as part of an intergrated system, e.g. GPS alone [*Lovse et al.*, 1995; *Duff and Hyzak*, 1997; *Behr et al.*, 1998; *Rutledge et al.*, 2001; *Cheng et al.*, 2002; *Kijewski-Correa and Kareem* 2003], GPS with accelerometers [*Ogaja et al.*, 2001; *Meng*, 2002; *Li et al.*, 2006], GPS with optical fibre sensors [*Ge et al.*, 2002a].

Using GPS alone, *Lovse et al.* [1995] measured the dynamic vibrations of the 160 m high Calgary Tower using a single GPS antenna with a base station 1 km away from the tower. Movements with amplitudes of $\pm$30 mm were reported in both the North-South and East-West directions, caused by temperature changes rather than wind loading.

A structural monitoring project using RTK-GPS (Real Time Kinematic – GPS) was developed for the 280 m high Republic Plaza Building in Singapore [*Ogaja et al.*, 2001]. The use of GPS was to complement and corroborate the results from accelerometers and anemometers which, have been in operation since 1995. The GPS system included a communication link, which allows real time solutions at the rover station with data sampled at 10Hz.

Ge et al. [2002a] incorporated the optical fibre Bragg grating (FBG) sensors with a GPS based monitoring system. While GPS provides 3D positional results for determination of building strain, tilt and rotation, the optical fibre sensors are placed vertically along the edge of the building to measure both strain and temperature.

In Chicago, a GPS based program for monitoring three of the city's tall buildings was carried out by *Kijewski-Correa and Kareem* [2003]. The reference station

was set-up on top of a 20 storey high building due to the denseness of its surrounding which allows only 70% coverage to the sky. The displacements in north-south and east-west components were reported as within a few centimetres.

Li et al. [2006] used GPS-RTK (GPS–Real Time Kinematic) for monitoring a 108 m steel tower in Japan using a GPS and accelerometer system with data sampled at 10Hz and 20Hz respectively. Comparing between the two systems showed that GPS-RTK can follow movement better when they are larger than two centimetres.

On monitoring the height deflections of the Humber Bridge, *Roberts et al.*, [2000; 2001] showed that with the Kinematic GPS technique, using data sampled at 5Hz, the precision that can be achieved is in the order of a few millimetres. This and other research has proven that GPS is capable of producing results with precisions at the millimetre level, which would be sufficient for the purpose of deformation monitoring of structures. Whence, this could lead to the development of a real time structural failure alarm system as well as the computation of long term cumulative deterioration factors, which are essential to the maintenance and integrity of the structure [*Roberts et al.*, 2000].

In general, all the above works accounted for combinations of multipath, radio frequency interference, satellite geometry, baseline lengths, receiver and antenna calibrations with structural movements; however, no un-mitigated troposphere effects were being addressed except by *Meng* [2002]. It may be based on the assumption that atmospheric effects have been totally mitigated using appropriate models such as the *Saastamoinen* [1973] or *Hopfield* [1969] but this may only be true if both base and rover stations were very near to each other and at the same altitude, as shown below.

To monitor relative positions between two points with GPS, one can simply place a receiver on a fixed station (reference) and another receiver on a station that needs to be monitored (rover). By processing the data in kinematic mode, the differences in the position of the rover with respect to the reference can be seen, and interpreted as movements. However, sample results from the Snowdon Trial carried out by the author, show that even if both the reference and rover stations

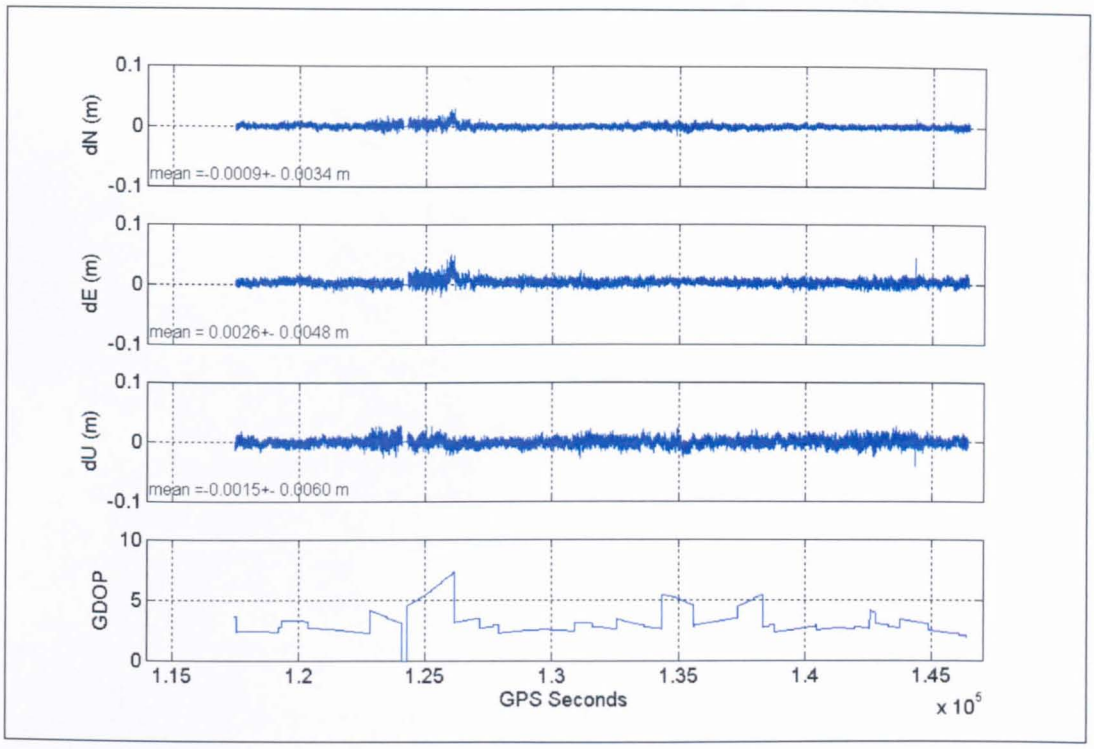

Figure 1.1 Ski-Pro outputs of baseline 100a – 100b position residuals with their GDOPs, Snowdon Trial, 16th June 2003.

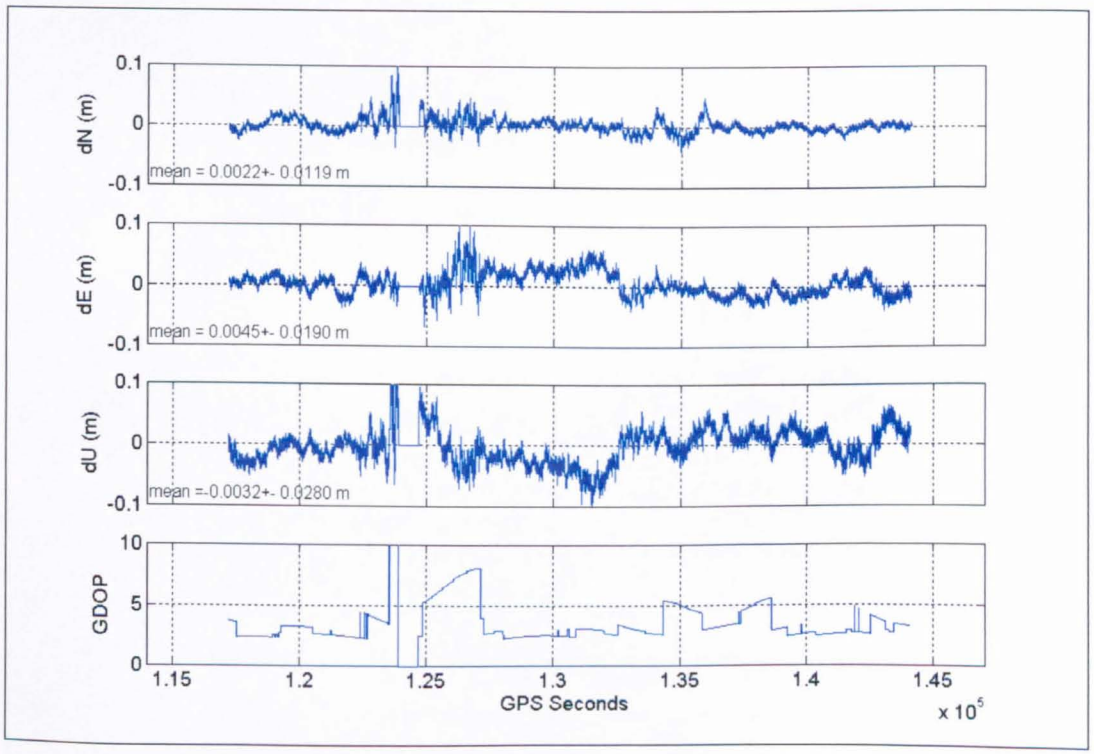

Figure 1.2 Ski-Pro outputs of baseline 100a – 400a position residuals with their GDOPs, Snowdon Trial, 16th June 2003.

are static, the position residuals do not produce a smooth horizontal line representing zero movement. Figure 1.1 shows the position residuals, arithmetic mean and standard deviations in all three coordinate components and GDOPs (Geometric Dilution of Precision, described in chapter 3) for two static stations that are very close to each other (less than 15 metres) and at effectively the same altitude. Figure 1.2 shows the corresponding plots for two static stations that are about 9 km apart and have a 48 m difference in altitude.

As can be seen from Figure 1.1, in this case there is no significant variation or changes in the time series apart from the ones that are due to changes of the satellite geometry, as shown by the GDOPs. These results are well expected based on the fact that as they were located near to each other (14 m apart), both stations should be experiencing the same systematic biases and errors which are then cancelled out during the computing process whence, producing an almost smooth horizontal line, with some noise. In contrast, Figure 1.2 shows apparent movement of the rover with respect to the reference station. Since all three stations were static, we would expect to see the same results as in Figure 1.1, but this is not the case in Figure 1.2. Hence, if GPS is to be used for monitoring purposes, it is vital to investigate the cause for these variations in the position residuals so that any un-mitigated systematic biases and errors are not misinterpreted as movements.

Generally, in relative positioning with short baselines and appropriate processing techniques (double-difference), most of the systematic biases and errors such as the clock errors and ionosphere, can be mitigated [*Hofmann-Wellenhof et al.* 2001; *Leick*, 2004]. However, this is not the case for the tropospheric delay and multipath. In kinematic GPS, although some of the tropospheric delay can be mitigated using a standard model, these are based on assumptions (from historical long-term observations) and do not represent the actual climate of the location at the time of observation. Also, there are no models for multipath that can be applied. Hence, both of these will have un-mitigated effects which could show up as variations in the position residuals.

Furthermore, deformation monitoring for tall structures involves having baselines with substantial difference in altitude. Both the reference and rover will be

experiencing different atmospheric effects as it is well known that the atmospheric pressure decreases with height. If the atmospheric conditions during the observations are the same as the profile used for creation of the tropospheric model, this should not be a problem. In reality, the atmosphere is not consistent and varies in time. Hence, although the troposphere has been modelled with standard atmospheric parameters, it is suspected that un-mitigated troposphere still exists in the position residuals.

To date, not many studies have been dedicated to investigate the problems of relative tropospheric delay and multipath effects on kinematic GPS for monitoring tall structures. *Tor* [2002] applied Kalman Filter time series analysis in deformation analysis to filter and smooth GPS time series by extracting the true signal of the state of deformation. *Ge et al.* [2000] used Adaptive Filtering (AF) to separate multipath with tectonic and fault movements from baseline solutions while *Dodson et al.* [2001a] on mitigating multipath and its applications on structural deflection monitoring.

Meng [2002] conducted a comprehensive study on real-time bridge deformation monitoring. He proved that the Adaptive Filtering is capable of filtering out common errors due to multipath, GPS receiver noise and relative tropospheric delay, leaving reasonably clean results which show displacements due to actual bridge movements. He also highlighted relative tropospheric delay as one of the major error sources in such a GPS based monitoring system, with the microclimate factor playing a major role in contributing to such errors. *Collins et al.* [1997] pointed out that under unusual conditions, the vertical profiles of total pressure or water vapour be significantly different from average profiles. Surface pressure differences on the order of 80 millibars from the global average could cause an unmodelled range error on the order of 2 metres at an elevation angle of five degrees.

Meng [2002] suggested further studies be undertaken on the tropospheric effects on GPS based monitoring if it were to be used with longer baselines and substantial differences in altitude between the reference and rover stations. Although much of research has been conducted on the troposphere, most of it has been based on static processing [*Tregoning et al.*, 1998; *Jensen et al.*, 2002b], and

oceanic regional coverage [*Chadwell and Bock*, 2001]. This is sufficient for long term monitoring but insufficient for real-time monitoring, as vibrations or movements can occur in a matter of seconds.

Attempts have been made to solve for the tropospheric delay as an extra unknown during GPS processing as shown in *Dodson et al.* [1996] where, this improved the solution of GPS height estimates for a baseline of 134 km in length, and in *Collins et al.* [1997]. *Dodson et al.* [2001b] extended the technique of solving for the tropospheric delay on a moving antenna which was later adopted by *Pattinson* [2002], who developed a modified version of the IESSG's KINPOS software to include the solving for the tropospheric delay from GPS observations made by a moving receiver. However, the solved delays achieved at that time were considered suitable for meteorological applications and its use in monitoring had not been validated before this study.

The highest man-made high-rise building as listed on the internet [*Emporis*, 2005], is the Taipei 101 (509m), followed by the Kuala Lumpur City Center Twin Towers (KLCC, 452m), the Sears Tower, Chicago (442m). These buildings are in the lower band of microclimate weather, where, if monitoring of movements with high accuracy from stations on the ground to stations on top of the building were to be made, relative tropospheric delay must be properly taken into account.

The main objective of the author's research was to further employ the techniques proposed by *Meng* [2002], i.e. the adaptive filtering method in order to investigate the effects of un-mitigated troposphere and multipath on deformation monitoring. The main kinematic GPS processing software used in this study was Leica Ski-Pro Version 3.0, and this was compared with the IESSG's KINPOS software. Bernese software version 4.2 has also been used for static processing, as required, and TEQC has also been used to produce Multipath values from the RINEX observation data files at the respective station.

Separately, new developments Network RTK have included VRS (Virtual Reference Station, described in chapter 3). Usually, the existing active stations which form a network were located a significant distance apart, such as for the Ordnance Survey of Great Britain where the stations were separated at 27 to 98

km apart [*Fane*, 2004]). For RTK GPS positioning, studies have shown that if high precision is required, and to be able to rapidly and reliably resolve the carrier phase ambiguities, the baseline lengths between the reference and rover receiver must not exceed 10 to 20 km [*Rizos et al.*, 2002; *Wanninger*, 2004]. With actual reference stations and long distances, the observation precision will be degraded. This is not so with VRS as they are supposed to be capable of creating or bringing a virtual reference station nearer to the rover receiver, thus reducing the baseline length and increasing position accuracy. The generated virtual reference station data should have taken into account the ionosphere and troposphere. However, *Wanninger* [2002] stated that the quality of the VRS data mainly depends on two aspects; firstly, on the reference station multipath biases and secondly, on ionosphere and troposphere disturbances. Many researches have been undertaken to quantify the quality of the results from VRS. For example, *Häkli* [2004], demonstrates that, for VRS networks in Finland, centimetre-level of measurement precision can be achieved considering measurement factors such as the satellite geometry and initialisation times. In GPS-based aircraft positioning for subsequent airborne mapping projects, studied in the Western Australian Centre for Geodesy at Curtin University of Technology, Perth [*Castleden*, 2004], initial comparisons of the Precise Point Positioning (PPP) and VRS techniques with an independently well-controlled aircraft trajectory and ground-based stations in Norway show that each deliver precisions of around 3 cm.

It is in the interest of the author to include VRS in this study to investigate if the generated VRS station can be an ideal replacement for an actual reference station. This is important for monitoring purposes which, apart from saving on costs (on equipment and labour), shorter baseline length means higher precision as the troposphere and multipath effects can be effectively mitigated.

By better understanding the trends in un-mitigated troposphere and multipath, the aim of the author's research was to demonstrate that the use of kinematic GPS for monitoring structures could be improved, making the results more suitable for engineers and building owners or managers to better assess building performance during extreme motions caused by earthquakes, strong winds, and other climatic conditions.

As a summary, the main research objectives for this study are as follows:

- Post-process GPS data in kinematic mode using Leica Ski-Pro Version 3.0 and compare the results with KINPOS.
- Identify the impact of un-mitigated troposphere for baselines with high differences in altitude.
- Identify the presence of multipath with the AF approach.
- Assess the quality of 3D position time series that could be provided to engineers for studies on the movement of structures.
- Investigate the use of VRS data for improved mitigation of tropospheric delay.

The thesis has been written in nine chapters.

The contents of this thesis begin with the introduction in the first chapter where the author includes a literature review and identifies the problem.

Chapter two describes the characteristics of the Earth's atmosphere through which the GPS signals travel from satellites to the receiver. Particular attention was given to the troposphere, to show the differences of weather conditions relating to location, topography and land activities such as plantations, buildings or factories.

Chapter three provides information on kinematic GPS, which includes the formation of the equations and basic definitions of the terms used throughout this thesis, brief description on the VRS concept were also given in line to chapter 8.

Chapter four contains information on the field trials conducted by the author for the purpose of this thesis. Basic information was provided to give some idea on the scenario of the trials.

To validate the results processed with Leica Ski-Pro Version 3.0, comparisons were made using a kinematic GPS processing software named KINPOS, developed by previous researchers at the IESSG, University of Nottingham. The results are detailed in chapter five, which also contains brief descriptions of the

software used for the purpose of this study with particular attention given to AF as it will be used extensively in further chapters.

Chapter six consists of analyses on static receiver positions, which allowed investigations on un-mitigated troposphere and multipath using data from field trials conducted on Snowdon and on the University campus (Trial #1). While, chapter seven includes investigations on data collected with receivers placed on top of a suspected moving structure, namely the bridge towers of the Humber Bridge and the Forth Road Bridge.

Chapter eight shows how the created VRS data were compared with actual data from the University Trial #2, to investigate its capabilities in solving for the troposphere, whence, on its potential use for high precision monitoring purposes.

Conclusions, recommendations and suggestions for further work are then given in chapter nine.

Chapter 2

The Atmosphere

This chapter describes the characteristics of the Earth's atmosphere, to allow better understanding of the atmospheric factors and how they affect radio wave signals. Emphasis is given on the troposphere as it is found to be more variant due to effects from wind, urban area activities and microclimates. Modelling of the troposphere is also mentioned, where without actual meteorological data, assumptions based on the ideal gas laws using standard atmospheric parameters were adopted, which resulted in the actual troposphere effect not being mitigated properly.

2.1 The Earth's Atmosphere

GPS works by transmitting radio signals from satellites, where these signals travel through the Earth's atmosphere to a receiver located on the surface of the Earth.

An atmosphere is defined as the gaseous envelope that surrounds a celestial body. Therefore, the Earth, like other planets in the solar system, has an atmosphere, which is retained by gravitational attraction and largely rotates with it [*Metoff*, 2005].

Half of the atmosphere's mass lies between the Earth's surface and an altitude of about 5.5 km with about 99% of the atmosphere's mass below 32 km. In terms of air pressure, at an altitude of only 32 km, air pressure is less than 1% of its average sea level value. At altitudes up to 85 km, the atmosphere consists of approximately 78% nitrogen and 21% oxygen. The remainder is made up of argon, carbon dioxide, several other gases, and water vapour. Water vapour acts

as an independent gas and is found only in the lower levels of the atmosphere. From the standpoint of weather, however, it is the most important component of the air; because it can change into water droplets or ice crystals under changes in atmospheric conditions of temperature and pressure and is responsible for the formation of clouds and fog. However, it is difficult to predict when and under what conditions water vapour will change to a visible form. It is made more difficult by the fact that the amount of water vapour in the air is never constant, but varies from day to day and even from hour to hour.

Based on the average vertical temperature profile, the atmosphere can be subdivided into four concentric layers: troposphere, stratosphere, mesosphere, and thermosphere. Each layer is characterised by a uniform change in temperature with increasing altitude. In some layers there is an increase in temperature with altitude, whilst in others it decreases with increasing altitude. The top or boundary of each layer is denoted by a 'pause' where the temperature profile abruptly changes, as shown in Figure 2.1.

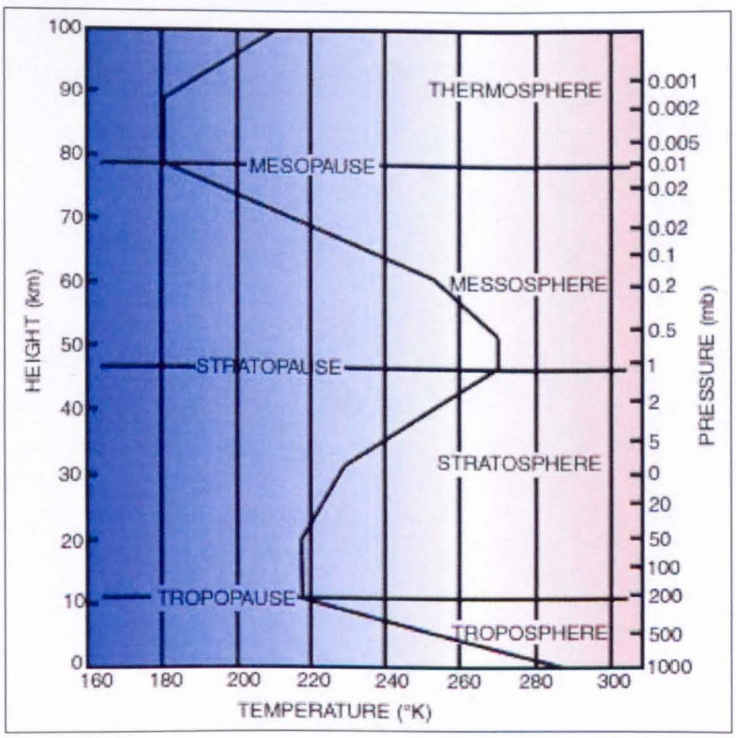

Figure 2.1 Vertical temperature profile of the ICAO (International Civil Aviation Organization) Standard Atmosphere [*Metoff*, 2005].

In GPS terminology, the Earth's atmosphere can be divided into two major parts, i.e. the ionosphere and the troposphere.

2.1.1 The Ionosphere

The ionosphere is the region within the mesosphere and thermosphere; that contains a relatively high concentration of ions; electrically charged particles. Within the ionosphere, the charged subatomic particles delay the code and advance the phase signals of electromagnetic waves by equal amounts, which for GPS can be up to tens of metres [*Leick*, 2004].

Based on electron density, the ionosphere can be subdivided into three layers: D-layer (60 to 90 km), E-layer (90 to 140 km), and F-layer (above 140 km). Since electron density increases nearly continuously with altitude to a maximum at an average level close to 300 km, the D-, E- and F-layers are not discrete, rather they differ from each other on the reflection of electromagnetic waves.

There are also local disturbances of electron density in the ionosphere. Such irregularities can cause amplitude fading and phase scintillation of GPS signals while larger disturbances impact the Total Electron Content (TEC). These will result in receivers losing lock, or receivers not being able to maintain lock for a prolonged period of time [*Leick*, 2004].

The ionospheric refractivity is given by *Leick* [2004] as

$$N_I = \frac{40.30}{f^2} N_e << 1 \qquad [2.1]$$

where,

N_e = local electron density

f = satellite carrier frequency

The total electron content (TEC) along the path from receiver to the end of the effective ionosphere is

$$\text{TEC} = \int N_e \, ds \quad (\text{where } ds \text{ is the partial difference of distance} = c \, dt) \qquad [2.2]$$

The TEC represents the number of free electrons in a 1-square-metre column along the path and is given in units of (el/m^2).

The ionospheric delay can be computed in units of distance (metres) by

$$I_{f,P} = \frac{40.30}{f^2} \int N_e \, ds \qquad [2.3]$$

The value is the same for the code delay and the phase advance, but with a different sign.

The primary purpose of multiple frequencies in GNSS (Global Navigation Satellite System) is to neutralize the effect of the ionosphere on position determination.

2.1.2 Troposphere

The word troposphere stems from the Greek "tropos" for "turning" or "mixing". This region, constantly in motion, is the densest layer. Nitrogen and oxygen are the primary gases within this region. [*Centipedia*, 2005]

The troposphere ranges from between 0 to 8 km (at the poles) and 16 km (over the equator), extending up to 50 km is the stratosphere. The troposphere is the most active region of variable atmospheric water vapour or moisture where the pressure, density and temperature all decrease rapidly with height. Most of the weather occurs in the troposphere, because of the presence of water vapour and strong vertical currents. The change of temperature with height is larger than in other layers, the temperature decreasing from approximately +17°C at sea level to

approximately –52 °C at the beginning of the tropopause. This is known as adiabatic cooling, i.e. a change in temperature caused by a decrease in pressure.

The troposphere's thermal profile is largely the result of the heating of the Earth's surface by incoming solar radiation. Heat is then transferred up through the troposphere by a combination of convective and turbulent transfer. This is in direct contrast with the stratosphere, where warming is the result of the direct absorption of solar radiation.

The troposphere is denser than the layers of the atmosphere above it (because of the weight compressing it), and it contains up to 75% of the mass of the atmosphere. It is primarily composed of nitrogen (78%) and oxygen (21%) with only small concentrations of other trace gases. It causes the GPS signals to refract from their original path, as a function of pressure, temperature, and humidity along the signal path, and this causes the speed of propagation to be reduced, so the arrival of the signal is delayed compared to if the signal travelled through a vacuum. This is commonly known as the tropospheric delay [*Bisnath et al.*, 1997].

In contrast to the troposphere, temperatures in the stratosphere rise with increasing altitude. Another distinctive feature of the stratosphere is the absorption of ultraviolet radiation by ozone (O_3), which is greatest around 50 km (stratopause). Temperatures reach a maximum here, and according to latitude and season, they range from –30 °C over the winter pole to +20 °C over the summer pole. As well as a noticeable change in temperature, the move from the troposphere into the stratosphere is also marked by an abrupt change in the concentrations of the variable trace constituents. Water vapour decreases sharply, whilst ozone concentrations increase. These strong contrasts in concentrations are a reflection of little mixing between the moist, ozone-poor troposphere and the dry, ozone-rich stratosphere.

Unlike ionospheric delay/advance, tropospheric delay cannot be eliminated with dual frequency signals because it is not frequency dependent. It is also known to be one of the major errors in GPS. Without modelling for the tropospheric delay, a zenithal path delay of the order of 2.3 metres for a station at sea level with standard atmospheric conditions can be expected [*Hugentobler et al.*, 2001]. The

delay also varies with elevation angle because lower elevation angles produce a longer path length through the troposphere [*Parkinson et al.*, 1996].

In GPS positioning, the tropospheric delay is normally handled by utilizing a global tropospheric delay model, for determining the signal delay in the zenith direction. The zenith tropospheric delay is then combined with a mapping function, where the delay is mapped down to the elevation angle of the received signal [*Niell*, 1996].

Many models have been developed to overcome the effects of tropospheric delay such as the Magnet [*Hatch and Larsen*, 1985], *Saastamoinen* [1973], and *Hopfield* [1969]. An assessment of 15 models is summarized by *Bisnath et al.* [1997]. Comments on the importance of proper estimation of tropospheric delay have also been described by *Collins et al.* [1998]; *Chang et al.*, [1999]; *Boehm et al.*, [2001] and *Jensen*, [2002a, 2002b].

In the context of these models, the tropospheric delay, can be divided into two main parts, ie. hydrostatic and wet parts. The hydrostatic part constitutes about 90% of the error and it is relatively easy to predict the Zenith Hydrostatic Delay (ZHD) to a few millimetres accuracy. However, the wet part is much more difficult to predict, due to rapid changes in the microclimate which results in high variations of water vapour content; prediction of the Zenith Wet Delay (ZWD) using conventional surface meteorological measurements yields an accuracy of no better than 1 – 2 cm. This effect of the delay is maximum near the surface of the earth and decreases as the altitude increases [*Hofmann-Wellenhof et al.*, 2001; *Bisnath et al.*, 1997 and *Ge et al.*, 2002b].

A standard atmosphere model, using height dependent values can be estimated as [*Berg*, 1948]

$$p = p_r \cdot \left(1 - 0.0000226 \cdot \left(h - h_r\right)\right)^{5.225} \qquad [2.4a]$$

$$T = T_r - 0.0065 \cdot \left(h - h_r\right) \qquad [2.4b]$$

$$H = H_r \cdot e^{-0.0006396 \cdot (h - h_r)} \qquad [2.4c]$$

where, p, T, H are pressure, temperature (Kelvin), and humidity at height h (metres) of the site; p_r, T_r, H_r are the corresponding values at reference height h_r, e.g. the reference values given in the Bernese software manual [*Hugentobler et al.*, 2001] are $h_r = 0$ metre, $p_r = 1013.25$ mbar, $T_r = 18^\circ$ Celcius, $H_r = 50$ %.

In the context of using GPS for monitoring structural movements it is important that tropospheric delay is handled with care as any un-mitigated tropospheric delay can be misunderstood as movement by the engineers and could raise a false alarm in a monitoring system.

2.2 Tropospheric Models

As mentioned in the previous section, there are many troposphere models available. In this section two of these models are described in more detail. These are the MAGNET model [*Hatch and Larsen*, 1985], which is available in KINPOS, and the *Saastamoinen* [1973] model, which is available in Ski-Pro.

2.2.1 The MAGNET model [*Hatch and Larsen*, 1985]

The MAGNET model was used by *Pattinson* [2002] in KINPOS.

The zenith hydrostatic delay (ZHD) for a point can be computed as

$$\text{ZHD} = 0.002276\, P \qquad [2.5]$$

Where, the pressure

$$P = (1015.0 - 1.75 \cos \phi)\, e^{-hx} \text{ mbar} \qquad [2.6]$$

$$x = 0.113 + 0.001h + 0.017 \sin \phi\, (1 + 0.382 \cos (0.0174\, (J - 30))) \qquad [2.7]$$

with ϕ - latitude, h – height of point in km and J – Julian day.

It should be noted that the reference pressure value used by KINPOS is 1015.0 mbar which is different from the standard value of 1013.25 mbar.

KINPOS works by computing the ZHD for each satellite, which is then mapped down with the *Niell* [1996] mapping function.

2.2.2 Saastamoinen Model [*Saastamoinen*, 1973; *Hugentobler et al.*, 2001]

The *Saastamoinen* [1973] hydrostatic model is written as follows [*Pattinson*, 2002; *Zheng et al.*, 2004];

$$\text{ZHD} = 0.0022768\, P\, (1 - 0.00266 \cos 2\phi - 0.00028\, h)^{-1} \qquad [2.8]$$

The total tropospheric delay as written in the Bernese software manual, gives the following equation,

$$\Delta_{\text{delay}} = \frac{0.002277}{\cos z}\left[p + \left(\frac{1255}{T} + 0.05 \right) e - \tan^2 z \right] \qquad [2.9a]$$

where the atmospheric pressure p and the partial water vapour pressure e are given in millibars, the temperature T in degrees Kelvin; the result is given in metres.

A more refined model [*Hofmann-Wellenhof et al.*, 2001; *Baueršíma, 1983*] gives special correction terms B and δR.

$$\Delta_{\text{delay}} = \frac{0.002277}{\cos z}\left[p + \left(\frac{1255}{T} + 0.05 \right) e - B \tan^2 z \right] + \delta R \qquad [2.9b]$$

Note : Leica Geosystems AG confirmed that they use equation [2.9b] without the ray bending term (δR) in the Ski-Pro software, with the standard atmosphere parameters based on equations [2.4a, 2.4b and 2.4c]. The correction term B can be interpolated from Table 6.3 in *Hofmann-Wellenhof et al.* [2001], while the T and e terms represent the wet delay and z, the zenith angle, for the mapping function.

2.3 Microclimates

Within the troposphere, as described above, there is a distinctive microclimate for every type of environment on the Earth's surface.

A microclimate is the distinctive climate of a small-scale area, such as a valley or part of a city. The weather variables in a microclimate, such as temperature, rainfall, wind or humidity, may be subtly different to the conditions prevailing over the area as a whole and from those that might be reasonably expected under certain types of pressure or cloud cover. Indeed, it is the amalgam of many, slightly different microclimates that actually makes up the climate for a town or city [*Metoff*, 2005].

Urban microclimates are perhaps the most complex of all microclimates. There are various elements that constitute an urban microclimate and their values, as compared to rural areas in the United Kingdom, can be seen in Table 2.1.

Sunshine duration	5 to 15% less
Annual mean temperature	1 to 2 degrees warmer
Temperatures on sunny days	2 to 6 degrees higher
Occurrence of frosts	2 to 3 weeks fewer
Relative humidity in winter	2% less
Relative humidity in summer	8 to 10% less
Total precipitation	5 to 30% more
Number of rain days	10% more
Number of days with snow	14% fewer
Cloud cover	5 to 10% more
Occurrence of fog in winter	100% more
Amount of condensation nuclei	10 times more

Table 2.1 Differences in various weather elements in urban areas compared with rural locations [*Metoff*, 2005].

Marked differences in air temperature are some of the most important contrasts between urban and rural areas, as shown in the table above. Two major results of such microclimates are urban heat islands and urban winds.

2.3.1 Urban heat islands

Urban heat islands are separations between relatively warm urban areas and relatively less warm surroundings. As can be seen in Figure 2.2, the city of London is the hottest area as compared to its surroundings.

The formation of a heat island is the result of the interaction of the following general factors:

- the absorption and reflection of solar radiation by building materials.
- the emission of pollutants from cars and heavy industry act as condensation nuclei, leading to the formation of cloud and smog, which can trap radiation. In some cases, a pollution dome can also build up.
- the absence of strong winds to both disperse the heat and bring in cooler air from rural and suburban areas.

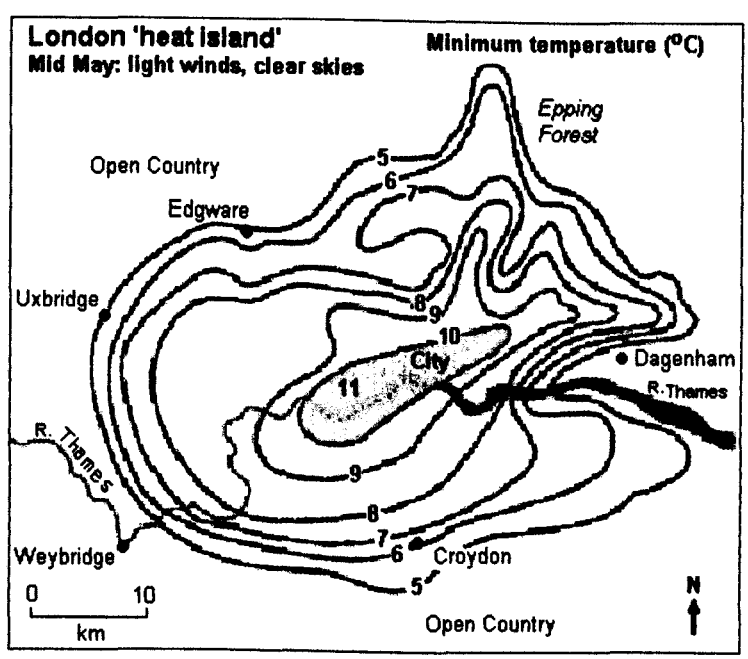

Figure 2.2 Heat island for London [*Metoff*, 2005].

The precise nature of the heat island varies from urban area to urban area, and it depends on the presence of large areas of open space, rivers, the distribution of industries and the density and height of buildings. In general, the temperatures are highest in the central areas and gradually decline towards the suburbs. In some cities, a temperature cliff occurs on the edge of town. This can be seen on the heat profile for Chester in Figure 2.3 [*Metoff*, 2005].

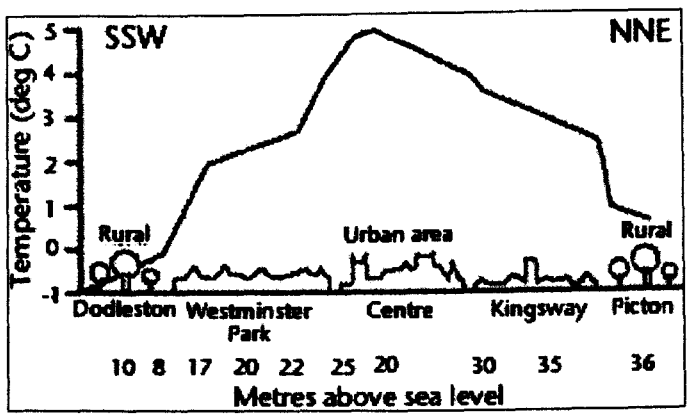

Figure 2.3 Urban heat island in Chester [*Metoff*, 2005].

2.3.2 Urban winds

Wind is an air motion relative to the Earth's surface. It is a vector quantity, that has both direction and magnitude. Hence, acceleration in wind may consist of a change in speed or direction or both. The forces that affect horizontal and vertical air motions in the atmosphere are i) pressure gradient force, ii) centripetal force, iii) coriolis force, iv) friction, and v) gravity [*Tokay*, 2005].

Developments in the construction and design of tall buildings in urban areas can obviously disturb the airflow. These structures create a surface friction, which can deflect or slow down the airflow over urban areas. These result in urban areas, in general, experiencing less wind than, surrounding rural areas. However, a cluster of buildings can result in a windier environment, with quite marked gusts. This is the result of the increased surface roughness that the urban skyline creates, leading to strong vortices and eddies. In some cases, these faster, turbulent winds are funnelled in between buildings, producing higher velocity, swirling up litter and making walking along the pavements quite difficult.

The typical effects of wind as it strikes buildings are shown in Figures 2.4 and 2.5 where it results in turbulence of eddies and vortices. Wind is not constant either with height or with time; it is not uniform over the side of a building, and does not always cause positive pressure. In fact, wind is a very complicated phenomenon; it is air in turbulent flow, which means that the motion of individual air particles is so erratic that in studying wind one ought to be concerned with statistical distributions of speeds and directions rather than with simple averages or fixed physical quantities.

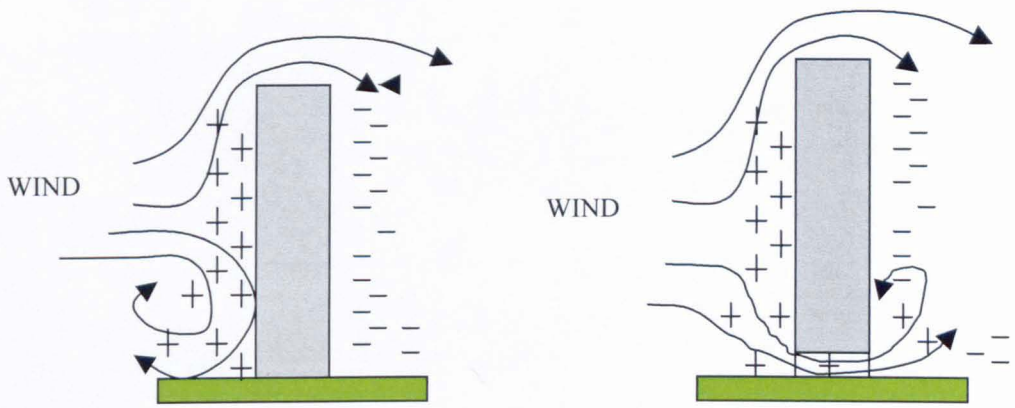

Figure 2.4 Flows of wind to a solid building (left) and a ventilated building (right) [*Schueller*, 1977].

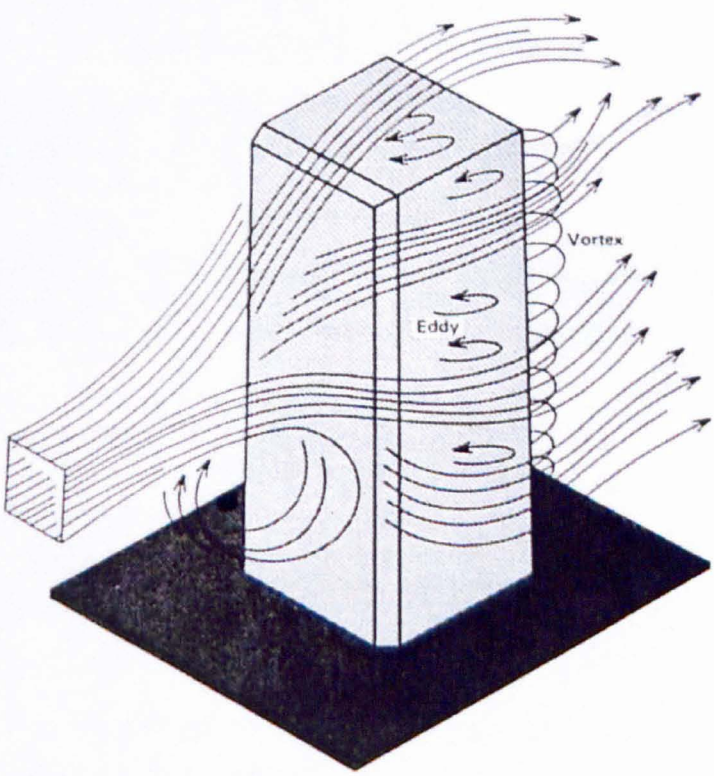

Figure 2.5 Formations of eddies and vortices [*Schueller*, 1977].

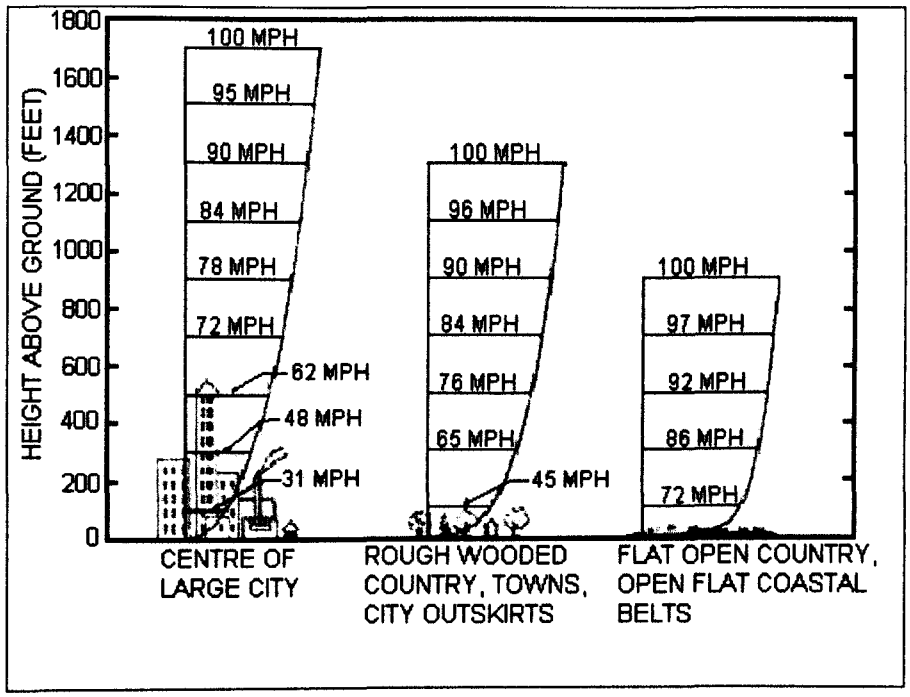

Figure 2.6 Mean velocity profiles over terrain with three different roughness characteristics for a gradient wind of 100 mph [*Glenridge*, 2005].

In general, wind velocity increases with height and its rate of increase is dependent on ground roughness. The more the intervention, (i.e. by trees, cars, buildings, etc.), the higher the altitude, at which maximum velocity will occur. Wind is usually much stronger over the brow of a hill or ridge because the flow lines converge over the obstructing feature and to pass the same quantity of air a higher speed is required. Large valleys often have a strong funnelling effect that increases the wind speed along the axis of the valley.

2.4 Summary

It has been shown that at any location on the surface of the Earth, a different microclimate will be experienced. The change in atmospheric parameters such as the temperature, water vapour and wind will not be uniform with the change in topography, but will also be influenced by urban areas. It is also shown that the atmosphere varies considerably within the urban area itself. If one is to consider using GPS for monitoring purposes, these phenomena must be taken into account

where stations forming the baselines should, in an ideal case, be located in the same environment i.e. the length of the baseline to be as short as possible and the altitude of the stations the same so that the atmospheric effect can be relatively mitigated. From the wind profiles, it is obvious that as the altitude increases from the surface of the ground, with tall buildings in the urban areas, different characteristics of the wind can be seen. GPS processing tools use standard atmospheric parameters to apply corrections for the tropospheric delay. Based on the variations of the atmosphere in urban areas, it must be assumed that un-mitigated troposphere will, therefore, exist in the computed positions. This assumption will be investigated further in chapter 6 and 7.

Chapter 3

Kinematic GPS

The full deployment of the Global Positioning System (GPS) since the 1980's has brought a new era in surveying. Unlike conventional methods, GPS provides a continuous 24 hour daily referencing system to any user on the surface of the Earth, in any weather conditions. As of 10th February 2006, the current GPS constellation consists of 29 satellites (Block II/IIA/IIR/IIR-M) with the most recent Block IIR-M satellite launched on September 26, 2005 [*USNO*, 2006]. The constellation was designed with approximately 11 hour 58 minutes orbits inclined at 55° to the equatorial plane so that, at any instance, it provides the sufficient minimum of four of satellites in good geometric position almost anywhere on the surface of the Earth. Depending on the selected elevation angle, there are often, more than the minimum number of satellites available for use and it is during these periods that surveyors often perform kinematic surveys. In fact, at a ten degrees elevation angle, there can be brief periods where up to 11 to 12 GPS satellites are visible on the earth.

Primarily with GPS, a user with suitable receiving ground equipment can determine their position, expressed for example as geodetic coordinates, i.e. latitude, longitude and elevation. This can be achieved by the simple resection of "true" measured ranges from the user to the satellites.

Hofmann-Wellenhof et al. [2001] illustrate the principle of satellite positioning which, at any given instant, assuming the satellites to be static, and the ground receiver clock set precisely to GPS system time, the time taken for the satellite signal to reach the receiver can be converted to true distance or range (ρ) using the following equation

$$\rho = \left\| \underline{\rho}^S - \underline{\rho}_R \right\| \qquad [3.1]$$

where $\underline{\rho}^S$ is the geocentric vector to satellite and $\underline{\rho}_R$ is the geocentric vector to the user as can be seen in Figure 3.1. Hence, by having ranges to three satellites, it is sufficient to uniquely solve the user position with three equations.

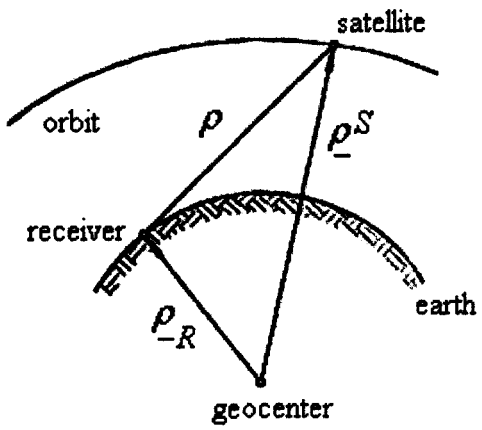

Figure 3.1 Principle of satellite positioning *Hofmann-Wellenhof et al.* [2001].

However, in reality, a more inexpensive clock is usually employed in GPS receivers, which results in an offset from true GPS time. This offset causes the distance measured to the satellite to be slightly longer or shorter than the "true" range. The offset, treated as an unknown, makes the total number of unknowns to four, where with a current three satellite configuration, it is not possible to be solved. Whence, a measured distance to an extra satellite is needed to overcome this problem. Now, the distances are called pseudoranges (R) since they are the true range plus a small (positive or negative) range correction $\Delta\rho$ resulting from the receiver clock offset δ. A simple model for the pseudorange is

$$R = \rho + \Delta\rho = \rho + c\delta \qquad [3.2]$$

with c being the velocity of light in a vacuum.

Equation [3.2] above is the basic equation in GPS positioning. To solve for the four unknowns, i.e. the three components of position and the time unknown, four pseudoranges are needed for a unique solution which means that a minimum of four satellites need to be observed simultaneously. Additional satellite(s) or pseudorange(s) introduces redundancy by having extra equations whence, a least squares solution can be applied.

3.1 Satellite signal

Based on the fundamental L-band frequency of 10.23 MHz, GPS space vehicles (SVs) or satellites transmit signals on two frequencies, namely L1 (1575.42 MHz) and L2 (1227.60 MHz). The actual carrier frequencies broadcast by the satellites are modulated by spread spectrum signals with a unique pseudo random noise (PRN) associated with each satellite, to make it less subject to intentional (or unintentional) jamming, commonly used today by such diverse equipment as hydrographic positioning ranging systems and wireless Local Area Network (LAN) systems [*Hofmann-Wellenhof et al.*, 2001]. The modulated codes are the C/A-code for civilian use, and the P(Y)-code for military use, while the navigation message consists of status information, satellite clock offsets and satellite (broadcast) ephemerides. Modernised GPS will introduce additional civilian codes on L2 and a new carrier L5 (1176.45 MHz) [*Landau et al.*, 2004; *Leick*, 2004]. Block IIR-M1 (PRN17/SVN53) is the first modernised GPS satellite that will broadcast two new military signals and a second civil signal L2C [*USNO*, 2006]. For more information see: *http://www.spaceflightnow.com/delta/d313a/*. In the future, GALILEO will also provide additional signals to the existing GPS system and developments in receiver hardware are expected to allow augmentation between GPS and GALILEO signals. The first GALILEO satellite was launched on 28th December 2005 [*ESA*, 2006].

3.2 GPS Observables

There are two types of GPS observable for each frequency signal. The first is the code pseudorange, which is the distance deduced from the measured difference in time taken for the signal to travel from the satellite to the receiver. The second observable, the carrier phase, is the difference between the received phase and the phase of the receiver oscillator at the epoch of measurement. The code pseudorange is widely used for navigation purposes while the carrier phase is used for surveying, as it enables millimetre-level measurement accuracy [*Kaplan*, 1996].

3.3 Errors affecting GPS signals

In reality, the code pseudoranges and phase pseudoranges, do not represent the true distance from receiver to satellite. As the signal travels from the satellite to the receiver, they are affected both by, systematic errors and offsets and random noise. *Hofmann-Wellenhof et al.* [2001] classified the error sources into three groups, namely satellite related errors, propagation medium related errors, and receiver related errors with some of the range biases as listed in Table 3.1.

Source	Effect
Satellite related	Clock offset
	Orbital errors
Signal propagation	Ionospheric refraction
	Tropospheric refraction
Receiver	Antenna phase center variation
	Clock offset
	Multipath

Table 3.1 Range biases [*Hofmann-Wellenhof et al.*, 2001].

In general, the true range from satellite to receiver with all the possible errors can be shown as follows,

$$\rho_{true} = R - (\delta\rho_{clock} + \delta\rho_{orbit} + \delta\rho_{iono} + \delta\rho_{trop} + \delta\rho_{noise\&res} + \delta\rho_{mp} + \delta\rho_{hw}) \qquad [3.3]$$

where

$\delta\rho_{clock}$ - satellite and receiver clock offsets

$\delta\rho_{orbit}$ - orbit error

$\delta\rho_{iono}$ - error due to the ionosphere

$\delta\rho_{trop}$ - error due to the troposphere

$\delta\rho_{noise\&res}$ - noise and resolution error

$\delta\rho_{mp}$ - multipath offset

$\delta\rho_{hw}$ - receiver hardware offsets

Atomic clocks (Caesium or Rubidium [*USNO*, 2006]) are used on GPS satellites to control all onboard timing operations including broadcast signal generation. Although they are known to be highly stable, they may deviate by up to 1 msec from GPS time, which translates to a 300 km pseudorange error [*Kaplan*, 1996]. Both the clocks and the orbital error are affected by the relativistic effect due to the earth rotation and the motion of satellite. *Hofmann-Wellenhof et al.*, [2001], states that the effects of gravitational field of the Earth are considered whilst the effects from the sun, moon and other masses in the solar system are negligible. These types of biases can be safely removed by the double-difference method.

The ionosphere and the troposphere error are the atmospheric effects on the satellite signal as they propagate from satellite to the receiver. Using a dual frequency receiver the ionosphere effects can be eliminated by the *ionosphere-free* combination [*Hofmann-Wellenhof et al.*, 2001; *Leick*, 2004]. The tropospheric delay cannot be eliminated with a dual-frequency receiver as the neutral atmosphere is a non-dispersive medium and not frequency dependent. This type of delay can be modelled as described in chapter two and applied to the

observed ranges prior to solving for the coordinates. However, since the models are based on several assumptions, the effects of tropospheric delay will not be fully mitigated.

Multipath is a major effect that introduces errors in positions. It is caused by multiple reflections of the signal at the receiver and also at the satellite during signal emission. The reflections can be from permanent features surrounding the receiver such as buildings, ground, water surfaces and trees, while temporary multipath can be from large passing vehicles near the antenna, which can appear as noise. Multipath is frequency dependent, *Hofmann-Wellenhof et al.* [2001] states that carrier phase are less affected than code pseudoranges. An assessment on multipath by *Apostolidis* [2003] also shows that with code processing, there is significant correlation between times of bad positional accuracy and times of high multipath.

Permanent multipath can be identified, by comparing the trends of the results for consecutive days [*Meng*, 2002], however, it is difficult to quantify the amount of the effects. Whence, to reduce the effect, the location of the receiver should be chosen where minimal interference occurs and the use of choke-ring antennas such as the Leica AT503 and AT504, can greatly reduce multipath effects from below and along it's horizon [*Meng*, 2002]. Several other multipath mitigation techniques are given in *Lau* [2004].

The receiver hardware offset can include errors from the antenna phase centre variations, particularly from combinations of receiver hardware and antennas. The antenna phase centre is the point where the GPS signal is referred to for measurement and generally, it is not the same as the geometric antenna centre. Different types of antenna will have a different set of offsets and variations and even the same type of antenna for a different unit might have different values [*Hofmann-Wellenhof et al.*, 2001]. Corrections based on antenna calibrations are readily available in the Leica Ski-Pro version 3.0 software but these are only given for Leica antennas and whenever a different type of antenna is used, values for these can be imported from the National Geodetic Survey (NGS) website [*Mader*, 2006]. With relative positioning, it does not matter if relative or absolute antenna calibrations were used as they will be

mitigated. However, care must be taken to ensure that the same type of either relative or absolute values is being used throughout the whole period of GPS processing. Relative antenna calibrations are computed with respect to the AOAD/M_T antenna while absolute antenna calibrations consists of all the relative variations that the NGS has computed and added with the absolute values for AOAD/M_T antenna (*Mader*, 2006].

The noise and resolution error can include the actual observation noise plus random constituents of temporary multipath and the un-mitigated tropospheric delay. *Staton* [2003] investigated the error caused by radio frequency interference (RFI) and found that it affects L2 more than L1, with increased noise and data loss rather than loss of lock.

3.4 Relative Positioning Techniques

There are a variety of positioning techniques with GPS [*Walsh*, 1994; *Wylde and Featherstone,* 1995; *Hofmann-Wellenhof et al.*, 2001; *Leick*, 2004]. Relative positioning is the major technique used for surveying purposes, where high accuracy can be required. This technique involves making precise measurements of the vector between two GPS instruments; the differences in position of a rover station with respect to a reference station. The advantage is that most of the relativistic effects due to the Earth rotating and gravitational force cancel or become negligible [*Leick*, 2004].

Considering figure 3.2, we have two ground stations with receivers namely *A* (reference) and *B* (rover), with two visible satellites, *j* and *k*.

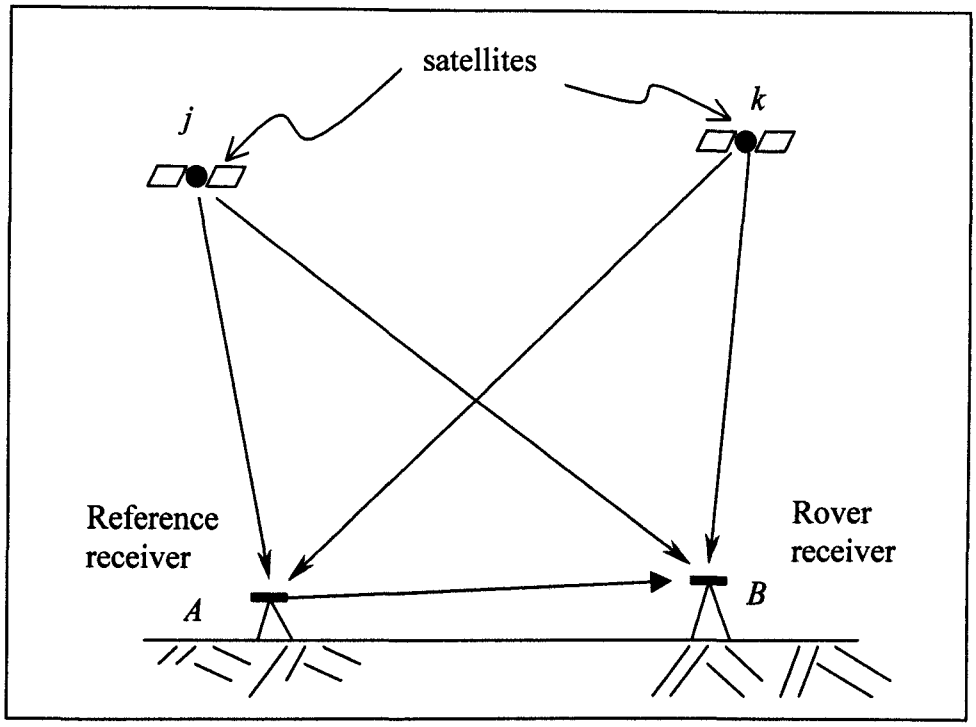

Figure 3.2 Relative Positioning.

The mathematical model for the double-difference equation is

$$\Phi_{AB}^{jk}(t) = \frac{1}{\lambda}\rho_{AB}^{jk}(t) + N_{AB}^{jk} \qquad [3.4]$$

where

$$\Phi_{AB}^{jk}(t) = \Phi_B^k(t) - \Phi_B^j(t) - \Phi_A^k(t) + \Phi_A^j(t)$$

$$\rho_{AB}^{jk}(t) = \rho_B^k(t) - \rho_B^j(t) - \rho_A^k(t) + \rho_A^j(t)$$

$$N_{AB}^{jk} = N_B^k - N_B^j - N_A^k + N_A^j$$

with

Φ - phase pseudorange

ρ - the distance between the satellite at emission epoch t and the receiver at reception epoch $t + \Delta t$

N - integer ambiguity

λ - wavelength

It should be noted that, through single-difference (using A and B to *j*), the satellite clock offset is eliminated. The unknown receiver clock offsets are then removed by double-differencing or combining two single-difference equations (using A and B to *j* and *k*).

A detailed derivation of equation [3.4] can be found in *Hofmann-Wellenhof et al.* [2001]. Triple-differences can be obtained by differencing the double-difference equation between two epochs. The advantage is the cancelling effect for the time independent ambiguities, thus, enabling detection of cycle slips. The equations for the triple-differences can also be seen in *Hofmann-Wellenhof et al.* [2001], while for a detailed description of cycle slips the reader is referred to *Leick* [2004].

3.4.1 Static Positioning

The observation technique where both receivers involved remain fixed in position is called static positioning. The static method formally requires hours of observations and was the technique that was primarily used for early GPS surveys and is generally used for establishing control stations to the highest accuracy. Improvements made on the algorithms for faster solving of the integer ambiguity introduces "fast static" or "rapid static" positioning. A typical period of 5-15 minutes static observations are required for short baselines (less than 15km) but more time is needed for longer baselines [*Rizos et al.*, 1999].

3.4.2 Kinematic Positioning

The technique of kinematic positioning is where one receiver remains fixed, while the second receiver moves. Kinematic surveys require initialization, to allow for the integer ambiguities to be resolved, then the roving antenna/receiver can be on the move while continuously locked to the satellites. Real Time Kinematic (RTK) is the term widely used today for systems that work with an active reference station and ambiguity resolution being carried out using a "on-the-fly" (OTF) algorithm in real time. This allows the rover receiver to keep on moving on site such as on GPS-guided bulldozers and excavators [*Roberts et al.*,

2002] and mapping [*Erener and GÖKALP*, 2004] applications. For real time positioning, the reference station must have the capabilities to transmit the "correction parameters" which, when received by the roving receiver, enable real time positions of up to centimetre level accuracy to be obtained [*Rizos et al.*, 1999]. Without the communication facility, or if real time results are not necessary, post-processing can be performed at a later stage. The RTK system with a single reference station has limitation where it is confined to baseline lengths of about 10 - 20 km to maintain its accuracy level. However, this can be overcome with the use of multiple-reference stations [*Rizos et al.*, 1999; *Kashani et al.*, 2004] i.e. Network RTK or more recently, the Virtual Reference Station (VRS) Network RTK system.

For the purpose of this thesis, data were collected on static and dynamic positions but post-processed as OTF in kinematic mode in order to achieve epoch to epoch results.

3.4.3 The Virtual Reference Station Concept

RTK requires the user to set up a local reference station near the area to be surveyed, which then transmits its raw measurements or observation corrections to a rover receiver via some sort of data communication link (e.g. VHF or UHF radio, cellular telephone). The need for a local reference station is that existing reference stations are usually spread over quite a distance (e.g for the United Kingdom, at 27 to 98 km apart [*Fane*, 2004]), whereas, for RTK, the maximum distance between reference and rover receiver must not exceed 10 to 20 km in order to be able to rapidly and reliably resolve the carrier phase ambiguities [*Wanninger*, 2004]. Multiple reference stations can improve systematic bias and error mitigation and reduce RTK initialization time *Vollath et al.*, [2003], but increase operating costs by having several sets of equipment in different locations [*Rizos et al.*, 2002]. The VRS concept is based on the idea of creating virtual data for a reference station nearer to the rover, thus, eliminating the above problems [*Vollath et al.*, 2002].

3.4.4 How do VRS systems work?

In general, a VRS system consists of a control centre, a network of reference stations and a roving receiver. Communications between the reference stations and the control centre (Hub) are usually via dedicated landline connections while between the rover and the Hub via a GSM (Global System for Mobile communications) / GPRS (General Packet Radio Service) mobile phone connection.

Generation of the VRS data consists of three major steps (Figure 3.3);

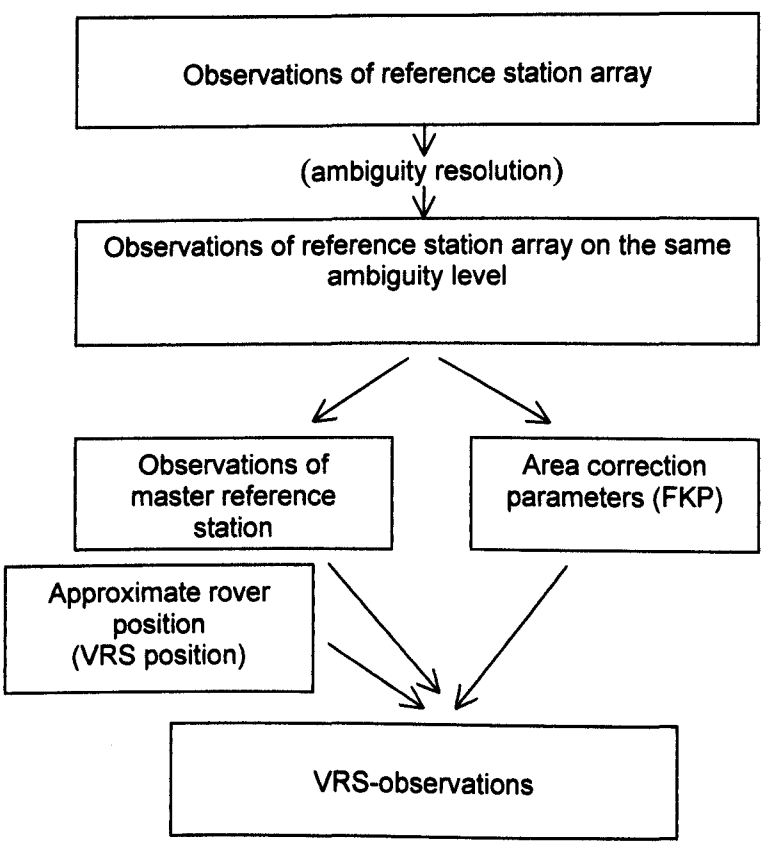

Figure 3.3 Computations of VRS-observations [*Wanninger*, 2002].

i. Observed data at each individual reference station in the network are checked and corrected for cycle slips and data quality. Good data is then used to fix the ambiguities. With the ambiguities fixed, the system then proceeds with the identification of the orbital errors, the dispersive ionospheric delay/advance and the non-dispersive tropospheric delay.

ii. The orbit biases are modelled individually for each satellite while the ionospheric and tropospheric corrections are estimated per station, to produce model coefficients that enable interpolation or extrapolation to the VRS location.

iii. The observations at the nearest (or master) reference station are then shifted, based on the coordinate differences to the approximate rover position and model coefficients (area correction parameters). This results in VRS data which, can be used by the rover receiver to determine its position using a short baseline to the VRS rather than a longer baseline to an actual reference station.

Further information on VRS was described in Chapter 8.

3.5 Ambiguity Resolution

Using the phase pseudorange observable, the integer ambiguity (N) must be correctly resolved in order to obtain accurate results. It is important for RTK that the ambiguity can be resolved in a very short period of time and while the receiver is on the move (for detection movements in deformation monitoring purposes) especially when lost of lock to the satellite signals occurs. Developments in ambiguity resolution algorithms, advance in computing technology, and the use of dual frequency receivers, mean that the ambiguity can potentially be resolved with data from a single epoch [*Rizos et al.*, 1999].

In KINPOS, the method used is the Least Squares AMBiguity Decorrelation Adjustment (LAMBDA) search [*De Jong and Tiberius*, 1996; *Pattinson*, 2002], while Leica Ski-Pro Version 3.0 uses the Repeated Search Process [*Euler et al.*, 2000; *Kotthoff et al.*, 2005].

For more information on the ambiguity resolution search technique, the reader can refer to *Walsh* [1994], *Hansen* [1996], *Yang et al.* [2002] and *Kim et al.* [2004].

3.6 Dilution of Precision

The geometry of the visible satellites used for determining the position of the receiver plays an important role in predicting the quality of the results. A measure of geometry in GPS is known as Dilution of Precision (DOP) factor [*Hofmann-Wellenhof et al.*, 2001].

A good DOP depends on the distribution of the satellites with respect to the receiver position. The DOP can be geometrically interpreted as a volume of a spherical body formed by the satellites centred at the observing site. The larger the volume of this body, the better the satellite geometry, which can be shown as a low DOP value. The critical scenario is when the body degenerates to a plane and a cone shape is formed with the observing site as apex. There are six types of DOP whose values can be deduced from the cofactor matrix diagonal elements of the pseudorange double-difference solution. They are Geometric (GDOP), Position (PDOP), Horizontal (HDOP), Vertical (VDOP) and Time (TDOP) dilution of precision [*Hofmann-Wellenhof et al.*, 2001].

For surveying work, where high precision is needed, DOPs are useful in providing information such as optimum times for the observations to be carried out. Knowing the approximate coordinates of the station concerned together with the satellite ephemeris, DOPs can be computed from the coefficients of the design matrix for the pseudorange double-difference equations.

An example of GDOP with respect to the position residuals for a kinematic survey, are shown in Figure 3.4. Here, it can be seen that GDOP alone cannot be used to quantify the quality of the results, e.g. there are instances where when the GDOP value is high (e.g. greater than 5), the position residuals are smaller than when the GDOP value is lower than 5 which could mean other factors such as the multipath and un-mitigated troposphere exists.

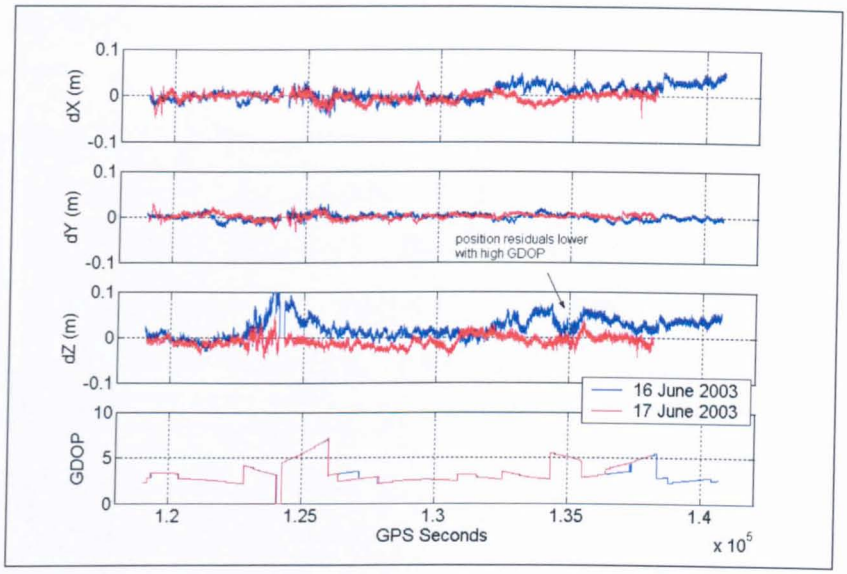

Figure 3.4 Plots of GDOP with position residuals for baseline 100a – 300a on two days from the Snowdon Trial, 2003 processed with Ski-Pro.

3.7 Converting Cartesian to Topocentric coordinates

All computed position residuals i.e. differences in coordinates between computed and "true values" of baselines, can be converted from dX, dY and dZ (cartesian) into dN, dE and dU (topocentric) using the following transformation matrix [*Misra*, 2001].

$$\begin{bmatrix} dN \\ dE \\ dU \end{bmatrix} = \begin{bmatrix} -\sin\phi\cos\lambda & -\sin\phi\sin\lambda & \cos\phi \\ -\sin\lambda & \cos\lambda & 0 \\ \cos\phi\cos\lambda & \cos\phi\sin\lambda & \sin\phi \end{bmatrix} \begin{bmatrix} dX \\ dY \\ dZ \end{bmatrix} \qquad [3.5]$$

where ϕ and λ are the geodetic latitude and longitude for the station.

A Matlab script was written by the author for the above conversion and a sample can be seen in Appendix G.

3.8 Summary

A brief description on GPS was given to provide the reader with an idea on how the system works. Emphasis was given on the carrier phase observable used for kinematic positioning, ambiguity resolution, sources of errors and dilution of precision. The kinematic GPS technique will be employed throughout this project with the computed coordinates on each epoch be compared with the "true coordinates" of the respective station to produce the position residuals. To show the results in a more meaningful manner, a conversion script was written using Matlab to convert the position residuals into local Northing, Easting and Up rather than showing them in X, Y, Z.

Chapter 4

Field Trials

For the purpose of this project, five field trials have been carried out by the author. They were

i. Snowdon Trial, 16th and 17th June 2003
ii. Humber Bridge Trial, 1st,2nd and 4th March 2004
iii. University Trial #1, 19th – 21st May 2004
iv. Forth Road Bridge Trial, 8th – 10th February 2005
v. University Trial #2, 25th – 27th April 2005

The Snowdon and University Trials #1 were used to investigate the un-mitigated troposphere based on static stations. The Humber and Forth Road Bridge Trials were for moving stations, while the University Trial #2 includes the incorporation of VRS data.

A brief description for each of the above trials will be given in this chapter. The receivers and antennas used in the trials are Leica products. For simplification, the Leica SR530 dual-frequency receiver will be denoted as SR530 DF, while the Leica SR510 single-frequency will be named SR510 SF and the Leica GPS 1200 Pro Series dual-frequency as GRX1200. The antennas used were the choke-ring type Leica AT504 and AT503, or a compact AT502 lightweight antenna with built-in ground plane.

4.1 The Snowdon Trial 16th and 17th June 2003

The purpose of this field trial was to collect GPS data at different locations with substantial height differences, to look at the effects of tropospheric delay on GPS signals. Snowdonia was selected, as the mountainous terrain has a large difference in height, which hopefully can show the high variations on the troposphere. The field trial was carried out on the 16th and 17th June 2003, in Snowdonia, which is located about 280 kilometres to the west of Nottingham (Figure 4.1). The Snowdon Mountain railway enabled easy access to the summit and to the 'Half-Way' station. The surrounding area at the base of Snowdon, both to the North and to the South of the summit, was also easily accessed by road.

Figure 4.1 Location map for Snowdon. (*www.multimap.com*)

The layout of the Snowdon network is illustrated in Figure 4.2. Four survey locations at different altitudes were established: Llanberis at an altitude of about 162 m above sea level, Half-Way station at about 569 m, Summit at about 1135 m, and Nantgwynant at about 114 m. A pair of receivers were located at both Llanberis and Nantgwynant; one receiver was located, each at Half-Way railway station and Summit on DOY 167. DOY is the Day-Of-Year which begins at 1st January of each year.

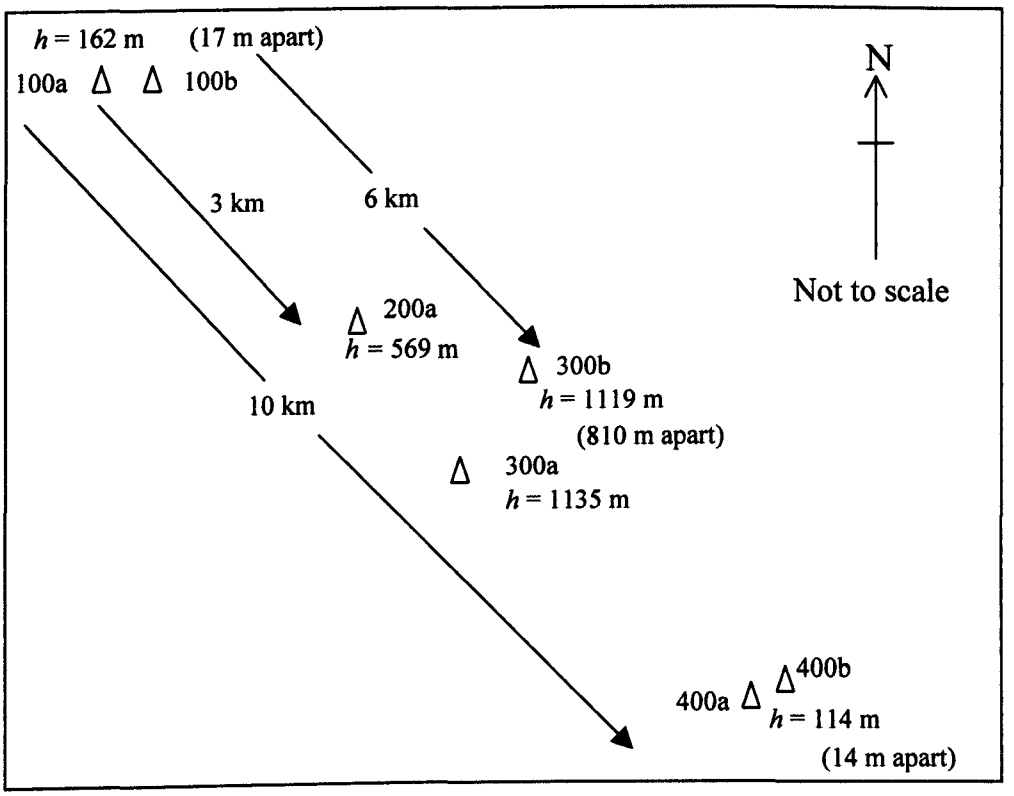

Figure 4.2 Layout of stations with their altitude (h) above mean sea level for the Snowdon Trial. Station 200a (DOY 167 only) and 300b (DOY 168 only).

The network extended from Llanberis (stations 100a and 100b) for approximately ten kilometres to Nantgwynant (stations 400a and 400b). The summit of Snowdon (station 300a) was just over six kilometres slope distance from Llanberis. The Half-Way railway station (station 200a) was just under three kilometres slope distance from Llanberis. Crib Y Ddysgl (station 300b) was less than one kilometre from the summit towards Llanberis. The two survey stations at Llanberis, were about seventeen metres apart, and at Nantgwynant were about fourteen metres apart. The purpose of having two receivers close to each other at these two low level locations was to provide a degree of control when computing baselines to other points; the effect of the troposphere would be expected to be the same at the two receivers only a few metres apart.

The receivers used were the SR530 DF with AT503 antennas on tripod for all stations. All survey stations were reoccupied on the second day of data acquisition, except for station 200a (Half-Way railway station). On the second day, the receiver from station 200a was located at a new point, 300b on Crib Y

Ddysgl, at an altitude of about 1,119 metres, and a slope distance of about 810 metres from Summit. Table 4.1 shows the antenna height for each station on each day. The difference in antenna height between two stations at the same location were set to no more than 10 cm to ensure that multipath effect of the neighbouring antenna was minimized. Between the two days, the antennas at 100a and 100b were lower by 15 cm and the most at 400b by about 31 cm.

Snowdon Trial				Antenna Height (metres)	
Station	Receiver	Antenna	Station height (m)	16th June 2003	17th June 2003
100a	SR530 DF	AT503	162.0	1.520	1.398
100b	SR530 DF	AT503	161.8	1.606	1.445
200a	SR530 DF	AT503	568.7	1.496	-
300a	SR530 DF	AT503	1135.1	1.499	1.517
300b	SR530 DF	AT503	1119.6	-	1.743
400a	SR530 DF	AT503	114.1	1.374	1.530
400b	SR530 DF	AT503	114.0	1.295	1.612

Table 4.1 Receivers, antennas and antenna heights for the Snowdon Trial stations.

The observations were carried out for two days; it was successful on the first day but encountered problems with a power supply on the second day, which caused the observation period to be shortened. Other than the above, the trial was successful with the data rate at 1Hz, and cut-off satellite elevation of 15 degrees due to the topography of the surrounding area. The period of observation for each station can be seen in Figure 4.3.

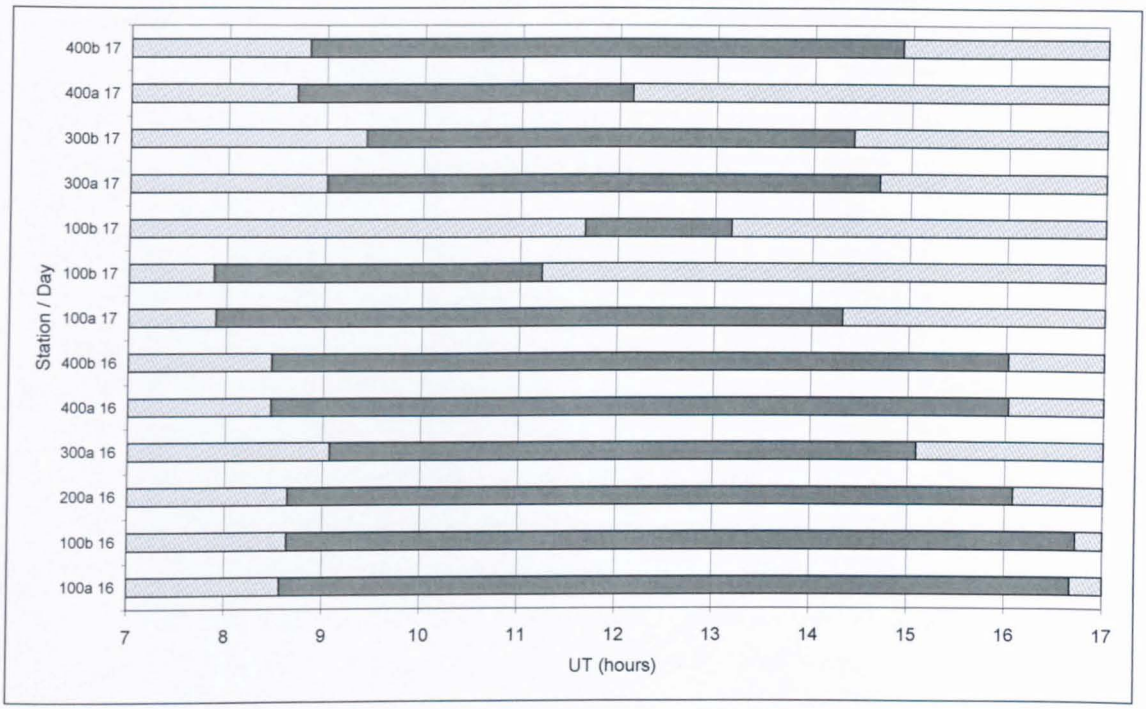

Figure 4.3 Period of actual data collected for the Snowdon Trial.

Figure 4.4 Stations 100a and 100b – Llanberis were established in the area with the most open aspect. There were a number of buildings and trees nearby giving the possibility of multipath.

The stations on the south side of Snowdon (400a/b) were positioned next to a road and the landscape surrounding the points had dense tree coverage on hillsides gradually rising to mountains (Figures 4.5 and 4.6). Thus, there was the possibility

of temporary multipath from passing vehicles at this location, which is unavoidable. Also, there are transmission lines running above 400b, which could introduce interference to the signals.

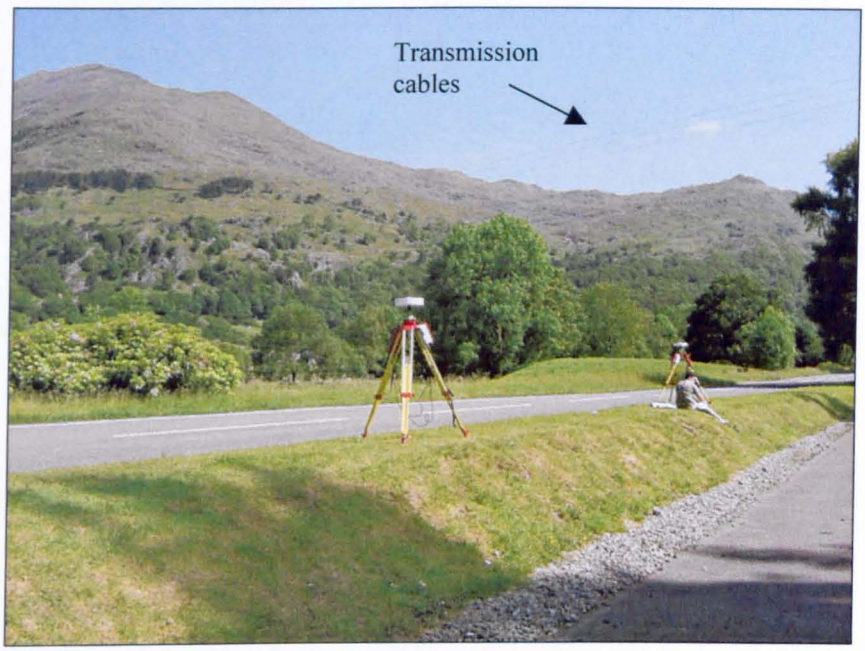

Figure 4.5 Stations 400a (near) and 400b – Nantgwynant, Snowdon.

Figure 4.6 Stations 400b (near) and 400a – Nantgwynant, Snowdon.

Figure 4.7 Station 300a – Summit on DOY 167, Snowdon Trial.

Figure 4.8 Station 300a – Summit on DOY 168, Snowdon Trial.

Station 300a (Figures 4.7 and 4.8), on the Summit was established on an open area a few metres from the Ordnance Survey Triangulation Pillar. The Pillar was not used under consideration that tourists might introduce multipath interference by being around the Pillar. Station 200a, which was only occupied on DOY 167, was on an open sloping hillside, which faced west, with the slope rising above the point to the east. Station 300b, which was occupied only on DOY 168, was on the

top of a ridge with an open aspect about one kilometre from 300a. As can be seen from the two figures of the Summit, the weather conditions did vary on successive days where it is clear on DOY 167 and foggy/cloudy on DOY 168, where we can not see any background view.

4.2 Humber Bridge Trial 1st, 2nd and 4th March 2004

A trial was conducted at the Humber Bridge, which is about 120 kilometres to the North of Nottingham. With a middle span of 1,410 metres, the Humber Bridge held the world record as the longest single span suspension bridge for 17 years after it was first opened to public in June 1981. The bridge is constantly moving and it bends more than three metres in the middle in winds of 80 mph and the towers bend inwardly at the top [*Humberbridge*, 2005]. The purpose of this trial was to use the substantial height difference between the bridge deck and the tower to look at any effects of the troposphere. With the tower holding the middle span, it is expected to move with the loads due to traffic flow and wind.

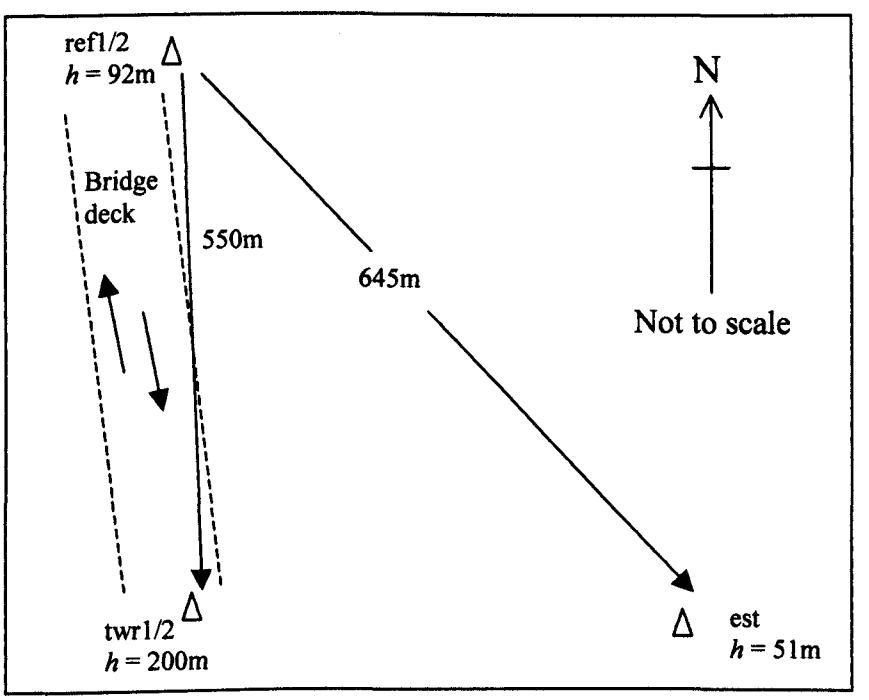

Figure 4.9 Layout of stations for the Humber Bridge Trial.

The layout of the network (Figure 4.9) includes the roof of the Bridge Control Building (ref), top of the North Tower (twr) and the estuary (est, Figure 4.10). The receivers and antennas used together with the antenna heights were as shown in Table 4.2. The difference in altitude of station est is about –40 m from ref1 and the tower stations (twr) 110 m higher. The twr1 and twr2 stations are at the base joining the two towers (Figure 4.11) sharing the same antenna using a splitter. The antenna at twr was fixed to the handrail using a tribrach on a G–clamp as can be seen in Figure 4.12. Due to site constraints, i.e. surrounded by the tower walls and bridge deck cables, twr1/2 were expected to experience poor satellite visibility and high multipath interference.

Humber Bridge Trial				Antenna Height (metres)		
				March 2004		
Station	Receiver	Antenna	Station height (m)	1st	2nd	4th
ref1	SR530 DF	AT504	91.8	0.947	0.946	1.101
ref2	SR510 SF	AT503	91.8	1.043	1.040	1.131
est	SR530 DF	AT502	51.6	1.417	1.494	1.596
twr1	SR530 DF	AT504	200.3	0.234	0.234	0.234
twr2	SR510 SF	AT504	200.3	0.234	0.234	0.234

Table 4.2 Receivers, antennas and antenna heights for the Humber Bridge Trial stations.

The antenna heights for twr1/2 remain the same as it was fixed on a G-clamp throughout the period of this trial, thus, the same view to the satellites can be expected. However, for the ref1/2 stations, they were the same for the first two days (stays overnight) but slightly different (+10 mm) on 4th March 2004 (re-set-up). While for the est station, using tripod, need to be set-up on each day which result with differences of +20 cm between 1st and 4th March 2004.

Figure 4.10 Location of the est station for the Humber Bridge Trial.

Figure 4.11 Location of the ref1/2 stations and view of the tower (twr1/2) used for the Humber Bridge Trial.

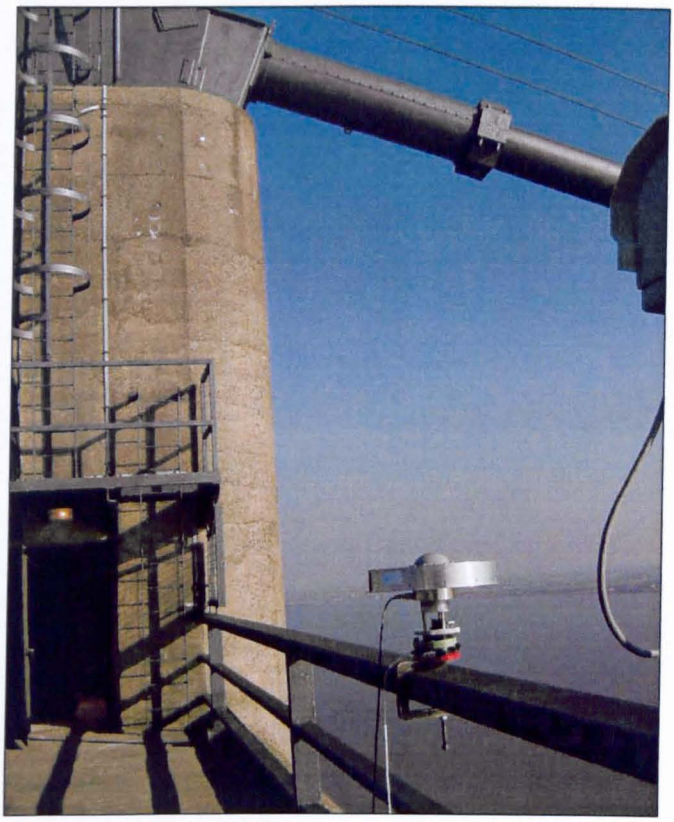

Figure 4.12 The AT504 on tribrach with G-clamp for twr1/2 stations for the Humber Bridge Trial.

The trial was a success for the three days with no major problems encountered. About 4 hours of common data were collected on each day at 1 second interval, with the cut-off satellite elevation angle set to zero degrees.

4.3 University Trial #1 19th – 21st May 2004

A trial was conducted at the University of Nottingham grounds on the 19th – 21st May 2004. Three locations (Figure 4.13) were selected, i.e. on top of the Electronic Tower Building (twr1/2), in front of the Trent Building (tre1/2) and near the Sports Centre (sc1/2). Two receivers with antennas on tripods were placed at each location, while the reference station for coordinate determination was the Ordnance Survey active station NOTT. The receivers used were the SR530 DF and SR510 SF with choke-ring antennas AT504 and AT503 on tripod. A pair of dual-frequency receiver were located on top of the tower, and a combination of both dual and single frequency receivers were used at each ground location. Between the top of the tower and the ground stations, there is about fifty

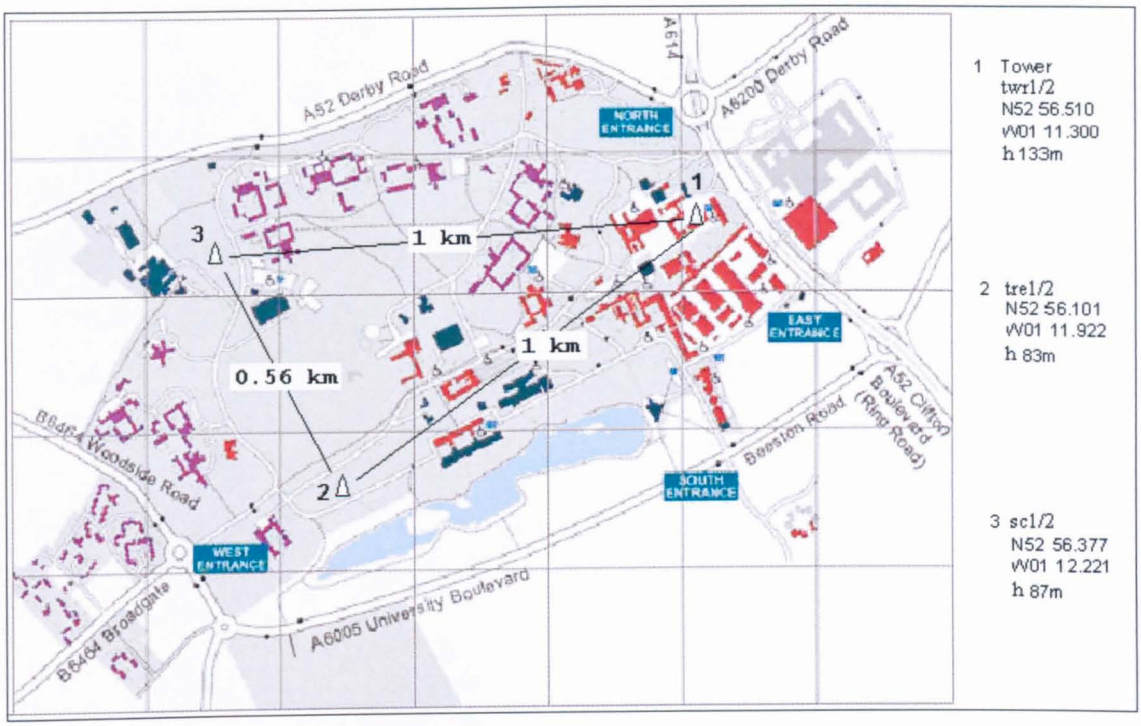

Figure 4.13 Location of stations for the University Trial #1.

metres difference in altitude and they are separated by a hill which makes sighting from the ground stations to the tower impossible. The antenna heights for each station on the three days can be seen in Table 4.3. The differences in height between adjacent antenna were kept within 10 cm in order to minimize any multipath effect due to adjacent stations being 2 - 4 metres apart. The large height difference at the tower stations is due to the marker for twr1 were raised by about 30 cm from the floor of the roof. Both the antennas at the tower stations were left in place throughout the trial period and the difference of about 10 mm at twr1 on the third day is due to the antenna being re-levelled.

University Trial #1				Antenna Height (metres)		
				May 2004		
Station	Receiver	Antenna	Station height (m)	19th	20th	21st
twr1	SR530 DF	AT504	133.7	1.277	1.277	1.267
twr2	SR530 DF	AT503	133.4	1.570	1.570	1.570
tre1	SR530 DF	AT504	82.2	1.445	1.443	1.507
tre2	SR510 SF	AT503	82.3	1.452	1.444	1.405
sc1	SR530 DF	AT504	87.5	1.421	1.391	1.363
sc2	SR510 SF	AT503	87.6	1.439	1.358	1.340

Table 4.3 Receivers, antennas and antenna heights for the University Trial #1 stations.

The layout for the station locations, were selected in such a way that both ground stations have equal distances to the tower stations. The purpose was to look at the relative effects of un-mitigated troposphere from the ground to top of the tower. Also, will the separation of tre and sc stations possibly experiencing different troposphere effects, while providing additional station as a check for multipath. Of the three locations, the sc location was expected to have disturbance from temporary multipath as the receivers were sited near a road with the possibility of interference by buses and lorries passing by.

Photo 4.14 Location of the twr1/2 stations for the University Trial #1.

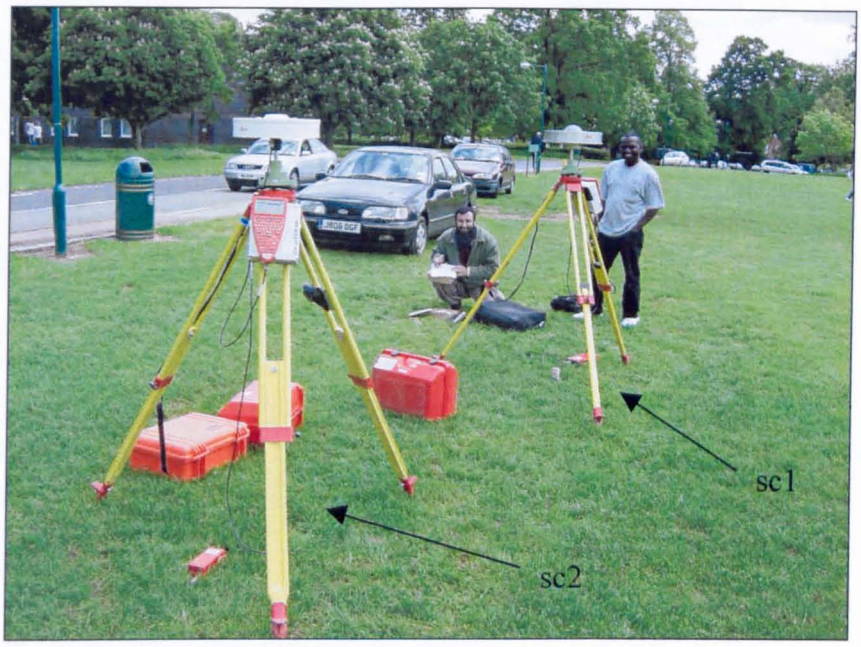

Photo 4.15 Location of the sc1/2 stations for the University Trial #1.

The weather for the first two days was sunny and windy, while it rained on the third day throughout the observation period. About four hours of common data were successfully collected on each day at the rate of 1 second epoch with zero degree cut-off elevation angle.

4.4 The Forth Road Bridge Trial 8th -10th February 2005

The Forth Road Bridge, located west of Edinburgh was opened on 4th September 1964. At that time, it was the largest suspension bridge in Europe, fourth largest in the world, with a main span of 1,005 metres and overall length of 2.5 km [*Feta*, 2005], its towers are over 150 metres high which is the reason for this trial. The interest was on the effects of the troposphere due to high difference in height and the heavy traffic over the bridge (frequently exceeding 60,000 cars per day) making it suitable for monitoring purposes.

The plan for the trial was to make GPS observations continuously for a period of 48 hours with scheduled breaks for data downloading. The Forth Estuary Transport Authority (FETA), responsible for maintaining and operating the

bridge, gave full corporation in providing the G-clamps and the power outlet for the receivers.

For the purpose of this project, four stations were established. They were ref1 and ref2 on the roof of the Bridge Building and on top of the South Tower twre (east side) and twrw (west side). The layout is as shown in Figure 4.16.

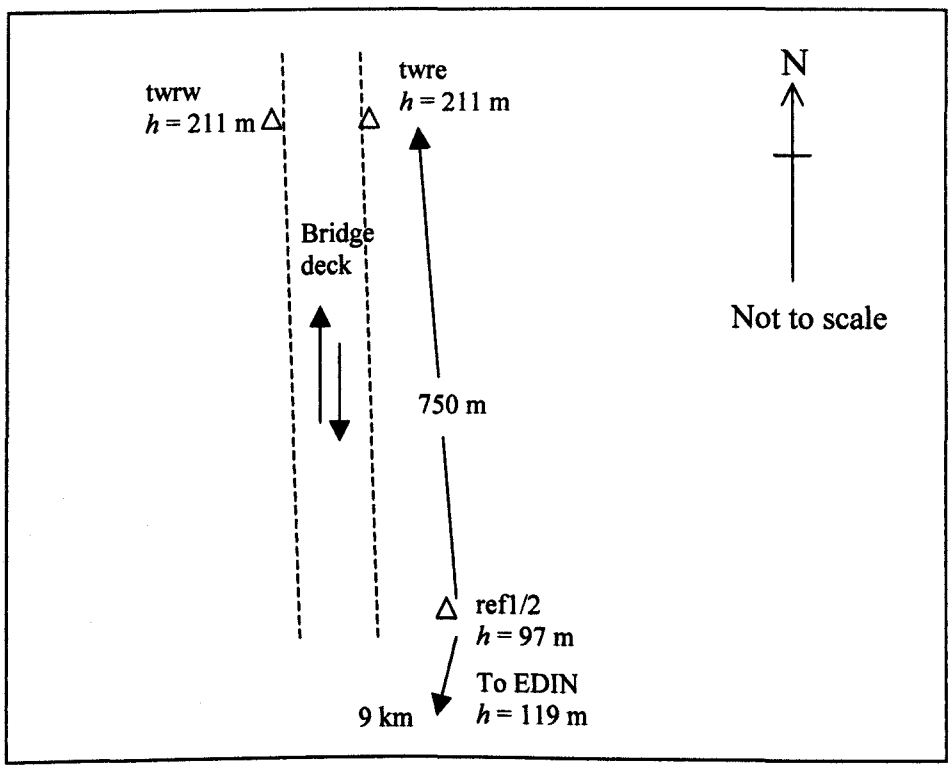

Figure 4.16 Location of stations for the Forth Road Bridge Trial.

The SR530 DF were placed at ref1 and twre coupled with the AT503 and AT504 antennas respectively, GRX1200 for ref2 with the AT503 on tripod and SR510 SF for twrw with AT502 on G-clamp. The GRX1200 is the newest receiver from Leica Geosystems AG and runs with a laptop and a Spider dongle. Intermittent problems were experienced with the GRX1200 where, at times it did not record any satellite as visible.

The antenna heights can be seen in Table 4.4. They are the same throughout the period of this trial as the data were gathered continuously.

Forth Road Bridge Trial				Antenna Height (metres)
Station	Receiver	Antenna	Station height (m)	8^{th} – 10^{th} Feb. 2005
ref1	SR530 DF	AT503	96.7	1.721
ref2	GRX1200	AT503	96.7	1.669
twre	SR530 DF	AT504	211.0	1.496
twrw	SR510 SF	AT502	211.0	1.499

Table 4.4 Receivers, antennas and antenna heights for the Forth Road Bridge Trial stations.

Figure 4.17 The Forth Road Bridge viewed from South side (Tol Plaza). The nearer tower is where the stations are i.e. twrw (left) and twre (right).

The trial was a success for the two days but with the problem encountered for station ref2 (GRX1200) the amount of common data were anticipated to be around two hours only. The data were collected on each day at 1 second interval, with the cut-off satellite elevation angle set to zero degrees.

4.5 University Trial #2 25th – 27th April 2005

The second University Trial (University Trial #2) was conducted at the University of Nottingham grounds on 25th to 27th April 2005. Three locations, which are about the same as in University Trial #1 (Figure 4.13) were selected and shown in Figure 4.18. The stations at the top of the tower building (twr1 and twr2) and in front of the Trent Building (tre1 and tre2) were equipped with the SR530 DF receivers and AT503 antennas, whereas the stations at the Sports Field (sf01 and sf02) had GRX1200 receivers and AT504 antennas.

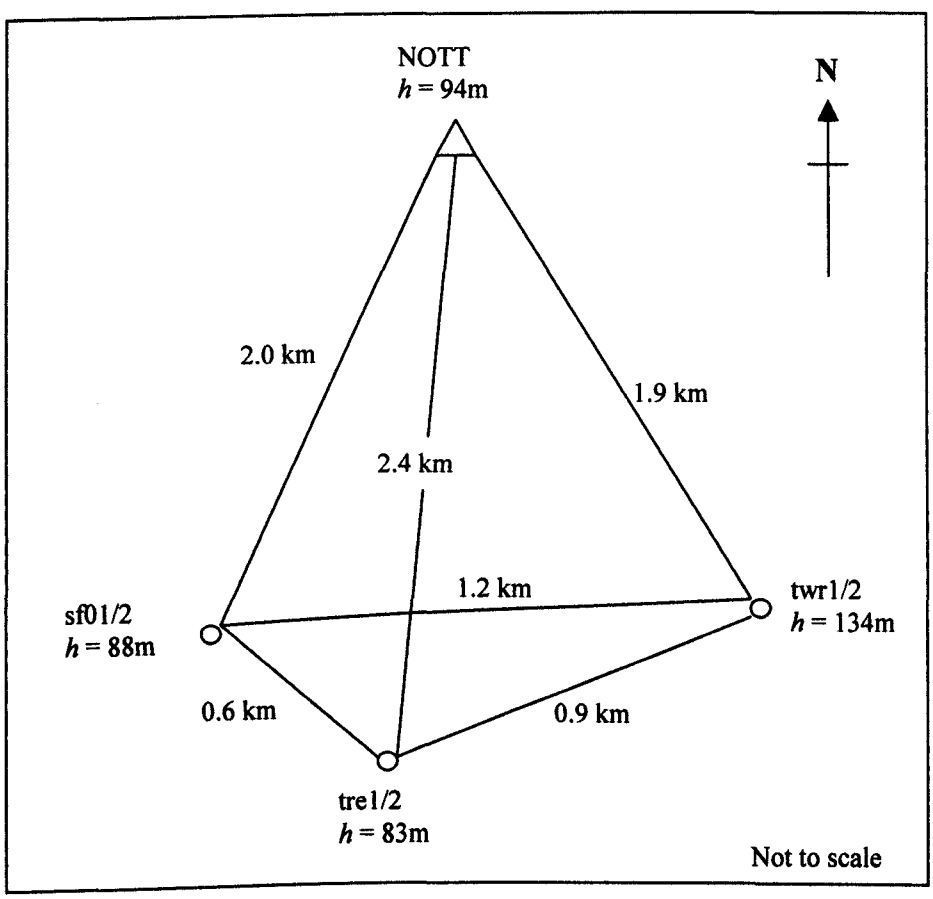

Figure 4.18 Location of stations for the University Trial #2 on 25th to 27th April 2005.

The antenna heights were shown in Table 4.5, where it can be seen that the differences in height at each location were kept to within 20 cm in order to minimize any multipath effect from adjacent antenna. Both the tower stations

remained fixed throughout the period of this trial with slight adjustment on levelling of the antenna which resulted with slight difference in height.

University Trial #2				Antenna Height (metres)		
				April 2005		
Station	Receiver	Antenna	Station height (m)	25th	26th	27th
twr1	SR530 DF	AT503	133.7	1.328	1.321	1.321
twr2	SR530 DF	AT503	133.4	1.696	1.690	1.691
tre1	SR530 DF	AT503	83.1	1.362	1.414	1.370
tre2	SR530 DF	AT503	83.1	1.334	1.376	1.350
sf01	GRX 1200	AT504	87.7	1.404	1.382	1.563
sf02	GRX 1200	AT504	87.8	1.237	1.309	1.333

Table 4.5 Receivers, antennas and antenna heights for the University Trial #2 stations.

The period of observation at each station for the three days can be seen in Figure 4.19. Data from sf stations were available for less than two hours while for the tre stations, slightly more than four hours.

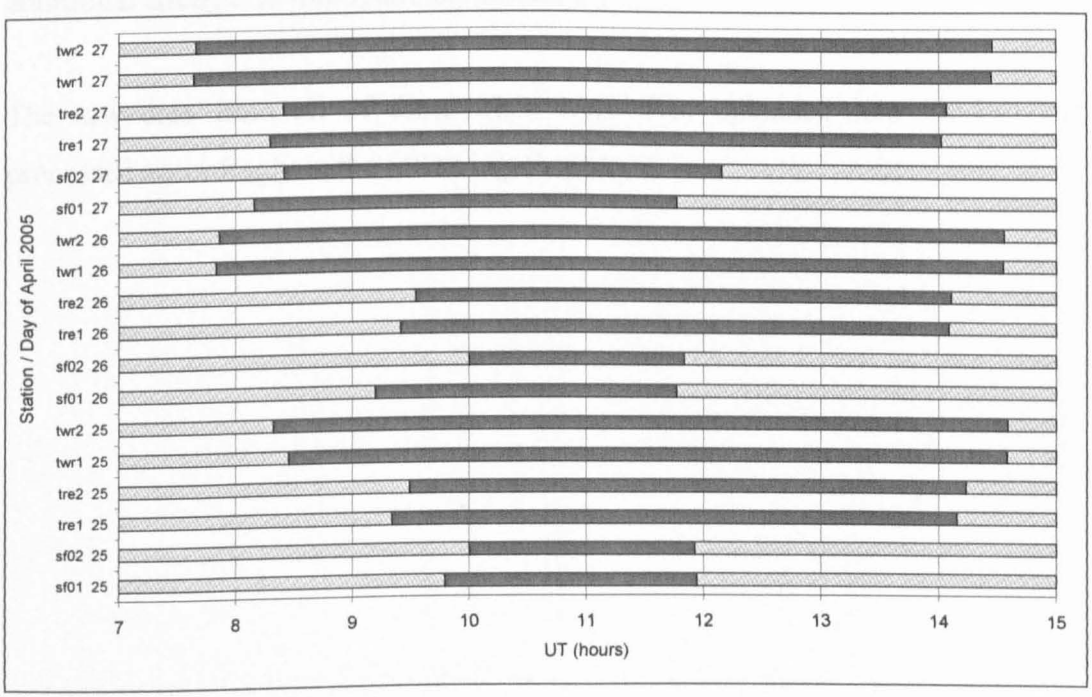

Figure 4.19 Plot of observation period for the three days for the University Trial #2 stations on 25th to 27th April 2005.

In all cases, two receivers with separate antennas were placed on two tripods about 3 metres apart and data were recorded at a 1 second epoch interval with zero degrees cut-off elevation angle over the three day period. Concurrent data for the OS active station NOTT was also obtained from the Ordnance Survey.

The weather for the first day was bright with sunshine. It was cloudy on the second day with rain after 13:00 hours UT. On the third day it was rainy with intermittent sunshine, clouds and windy.

4.6 Summary

All the trials were successfully conducted, although there were problems with the power supply for the Snowdon Trial and logistic factors, which restricted the amount of common data, that could be obtained. The problem with the GRX1200 also result with only two hours of common data available for the Forth Road Bridge Trial. Nevertheless, the amount of data gathered in two days for the Snowdon and Forth Road Bridge trials were sufficient for the purpose of this thesis while three days data for both University and Humber Bridge trials provides additional strength to multipath identification.

The raw data from all of these trials were then uploaded into Ski-Pro and processed accordingly in the following chapters.

Chapter 5

Software and Comparing Ski-Pro Version 3.0 Results with KINPOS

The processing of GPS data from raw to final coordinates requires careful planning and management. Any slight mistake during the process will lead to an incorrect result and reprocessing can be time consuming, and can raise unnecessary confusions.

In this chapter, the author will describe the steps taken in processing the GPS data available from the field trials; however, minute details such as editing and common computing processes will not be mentioned. Several software packages have been used for this study. Only a brief description of each software will be given and readers are advised to read on the particular reference if further information is required on a software. Extra attention has been given to KINPOS as it forms the main part of this chapter in comparing the Ski-Pro results.

5.1 Software

5.1.1 Matlab Version 6.5

Matlab Version 6.5, a product of The MathWorks, Inc. [*http://www.mathworks.com/*], was used as the main tool in this study for analysis and plotting of the results. Several scripts were written by the author which help in reducing the amount of computations and plotting of figures that would have been required if using Microsoft Excel, for example. To name a few, the computing scripts were: to convert time from hours, minutes and seconds to GPS

seconds; to convert from dx, dy, dz to dN, dE, dU using equation [3.5]; to compute RMS values; and to produce all figures in this chapter and most figures in other chapters. It was also the main tool for performing the Adaptive Filter runs on the time series of position residuals with the *lms.m* script [*Meng*, 2002].

5.1.2 Bernese Software Version 4.2

Released in 2001, Bernese Software Version 4.2 (BSW4.2) is a static GPS processing software which is claimed to meet the highest quality standards for geodetic applications using GPS as well as GLONASS data. It was developed at the Astronomical Institute, University of Berne (AIUB) in Swtizerland. This software was made available to the author in UNIX format (on the navix server) and has been used extensively by researchers and fellow students for post-processing GPS data in static mode.

Due to its robustness and the capability to estimate tropospheric delay, this software was used to compute the coordinates of reference stations in each of the local field trial GPS networks in static mode. These were then regarded as "*true values*" in further processing using Ski-Pro and KINPOS.

Before BSW4.2 can be used to process the data, several preparations need to be made. They are described as follows:

i. All relevant files such as for the *Earth Rotation Parameter Information (POLE)*, *Satellite Problem Information (SATCRUX)*, *Phase centre corrections (PHASE_IGS.01)* and *Translation table*, must be updated accordingly for the current period from information given at *ftp://ftp.unibe.ch/aiub/BSWUSER/GEN/*.

ii. If the *PHASE_IGS.01* file does not contain the information for the type of receiver and antenna used, this file must be updated with information on the antenna phase centre corrections available from the National Geodetic Survey website [*Mader*, 2006].

iii. The RINEX observation files exported from Ski-Pro were then transferred to UNIX using wsftp.exe in ASCII mode. These files are then translated into BSW4.2 format for every 15 second epoch.

5.1.3 Leica Ski-Pro Version 3.0

Leica Ski-Pro Version 3.0 software is produced by Leica Geosystems AG. It is a commercial GPS software and is known to be able to post-process data both in Static and Kinematic mode (both OTF and Stop-and-Go). It is also capable of performing network adjustment and providing analysis of the results in graphical form. Ski-Pro interacts with a graphical menu system, which makes it easier to use. Since it is a commercial GPS software, not much is known on how and what are the equations actually used in Ski-Pro. However, from correspondence with Leica Geosystems AG, it is now known that Ski-Pro uses the *Saastamoinen* [1973] model as in equation [2.9b], without the δR term, and with standard atmosphere parameters based on equations [2.4a, 2.4b and 2.4c], as mentioned in Chapter 2. Secondly, *Kotthoff et al.* [2005] described the method of repeated search processing to fix the ambiguities in Ski-Pro, which explains why solutions from Ski-Pro is more consistent than KINPOS as found in section 5.4.

5.1.4 KINPOS

KINPOS is the IESSG's in-house developed kinematic GPS processing software. It was originally developed by *Dr. Wu Chen* and later improved by *Pattinson* [2002]. The KINPOS program consists of source code written in FORTRAN77 which allows upgrading. The software is able to process dual frequency GPS data with the double-difference method, and uses a Kalman Filter to combine the measured and predicted double-differences ranges to form estimates of the position, velocity and acceleration of a roving receiver. It is also able to solve for the relative tropospheric delay at the rover with respect to the reference receiver. Some analysis on the performance and capabilities of KINPOS were carried out by *Pattinson* [2002].

For the purpose of this project, KINPOS was used to obtain coordinates in Kinematic mode, for comparison with results from Ski-Pro. The kinematic solution when solving for the relative troposphere was used by the author to compare the results from Ski-Pro and only minor revisions were introduced to the program beyond that given in *Pattinson* [2002] i.e. the output of the *Azimuth, Elevation* and *Residual* for identification of each satellite used in the computations, and the *Tropospheric Delay* at each station for every epoch, as detailed in Appendix A. Recent antenna calibration informations were also added to KINPOS.

5.1.5 Adaptive Filter

The Adaptive Filtering (AF) technique used in this project was the one described by *Meng* [2002]. The studies showed that the AF approach is a reliable signal isolation tool; it can be employed flexibly to any kind of time series pairs with potential cross-correlation and is applicable especially to series with unknown low and high frequencies, contaminated by similar frequency band noises. For further reading on the fundamentals and applications basics of AF, readers are referred to *Haykin* [1996], *Gustafsson* [2001], and *Treichler et al.* [2001].

To perform AF, two sets of data series of same size are required, each recognised as Reference and Desired. The results from AF will be the COM and OUT part, where the COM part should represent the common values to both time series while the OUT part contains the differences between the Desired time series and the COM part. A correlation factor provides an indication on the relation between the Reference and Desired time series with a value of –1 to +1. For example, a +0.5 correlation value means that fifty percent of the data points in both time series have common trends and a correlation with the negative sign means that there is no correlation at all between the two time series.

Sample plots of results from AF on consecutive days with high correlation of 0.8114 were as shown in Figure 5.1.

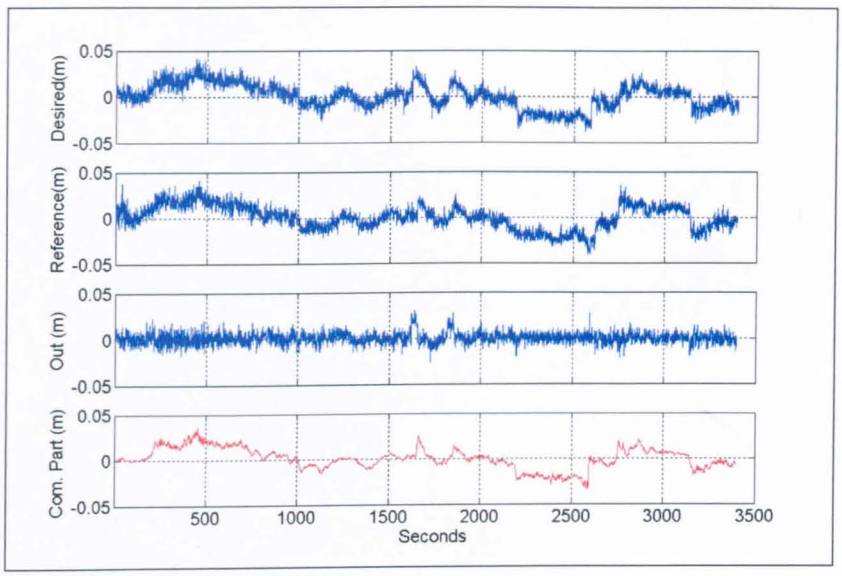

Figure 5.1 Plots of AF on two days for baseline ref1 – twr1 in dU component for 1st (Reference) to 2nd (Desired) March 2004, Humber Bridge Trial.

To verify the result from AF, the two time series must be interchanged as Reference and Desired known as Forward and Backward runs respectively.

For example, as shown in Figure 5.2a, we have position residuals time series in the dU component of baseline 100a – 400a computed from data observed on 16th June 2003 and 17th June 2003 from the Snowdon Trial. For this example, from AF, there are four plots where

A - Desired (position residuals time series on 17th June 2003

B - Reference (position residuals time series on 16th June 2003

C - OUT part (differences between the Desired time series and the COM part)

D - COM or COMMON part extracted by AF

A and B are the inputs while C and D are the outputs. The above setting is known as Forward run. The correlation factor given by AF for this case is 0.2574, which means, of the total data being filtered, only 25.74 percent were found to have common trends.

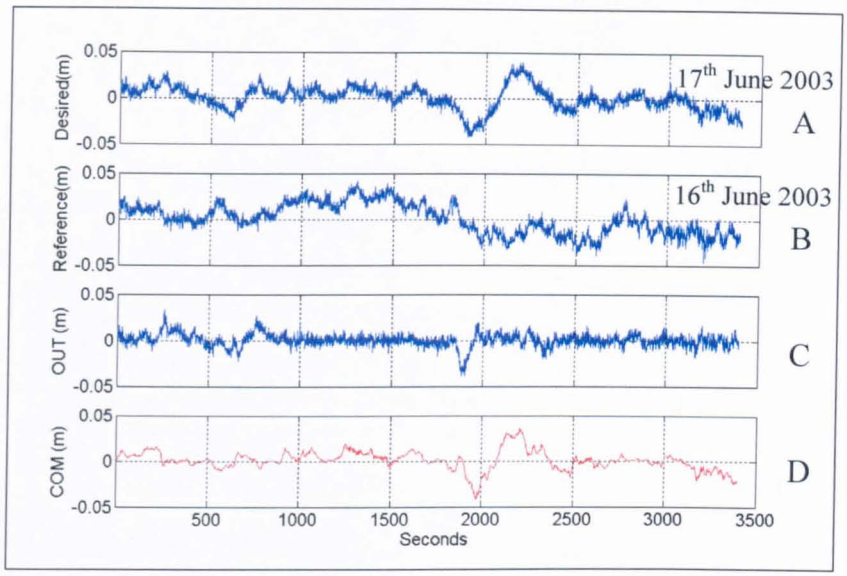

Figure 5.2a Plots of AF on two days for baseline 100a – 400a in dU component for 16th (Reference) to 17th (Desired) June 2003 (Forward), Snowdon Trial.

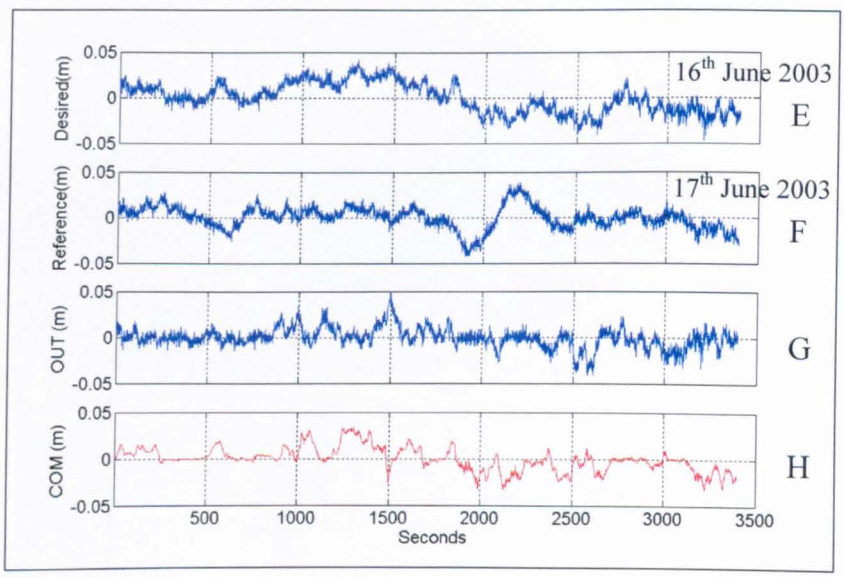

Figure 5.2b Plots of AF on two days for baseline 100a – 400a in dU component for 17th (Reference) to 16th (Desired) June 2003 (Backward), Snowdon Trial.

To verify if the COM part from the Forward run above contain common trends, a Backward run need to be perform with AF. This was carried out by interchanging the position residuals time series input for Desired with 16th June 2003 and Reference with 17th June 2003 as shown in Figure 5.2b where

E - Desired (position residuals time series on 16th June 2003

F - Reference (position residuals time series on 17th June 2003

G - OUT part (differences between the Desired time series and the COM part)

H - COM or COMMON part

Note : The Backward run will produce the same correlation factor value as the Forward run.

By plotting the two OUT parts (C and G) and COM parts (D and H) together as shown in Figure 5.2c, we should be able to see if there is any common or similar trends resulting from AF on the two time series. As implied by the correlation factor, not much of the COM parts show the same trends in the two time series A and B above.

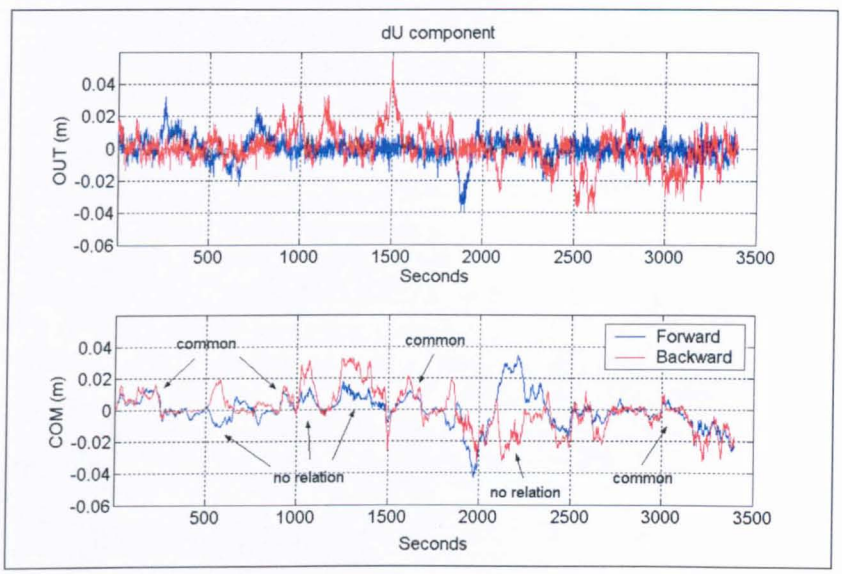

Figure 5.2c Plots of OUT and COM parts for baseline 100a – 400a from AF between two days [(Forward (16^{th}–17^{th}), and Backward (17^{th}–16^{th})] from the Snowdon Trial on 16^{th} and 17^{th} June 2003.

AF is the main tool that will be used in chapter 6, 7 and 8. For this project, AF was performed in one of the three ways below;

i. **SAME DAY AF** using position residual time series of two baselines for the same day; this is for baselines from two nearby stations to a distant station or, from a single station to two distant stations near to each other, observed on the same day. The COM part of the result here should contain the relative un-mitigated troposphere, multipath and station movement while the OUT part is noise.

ii. **CONSECUTIVE DAYS AF** using the COM parts above (i) for a single baseline; this run uses the COM part results from the same day AF (i) where the noise have been removed earlier, and runs were made using both results on consecutive days for the same baseline taking into account the four minutes delay. The purpose is to separate multipath (COM part) from un-mitigated troposphere and station movements (OUT part), based on the fact that multipath should be the same on consecutive days.

iii. **CONSECUTIVE DAYS AF** for a single baseline where **SAME DAY AF** has not been performed; this is for a single baseline observed on consecutive days taking into account the four minutes delay. The resulting COM part should give the multipath, while the OUT part gives the relative un-mitigated troposphere, station movement plus noises, based on the fact that multipath should be the same on consecutive days.

Based on runs in the forthcoming chapters, by performing AF between two days, using the time series from either (ii) or (iii) above, produce the same or a slightly different result for the COM part, while the result for the OUT part, will have differences depending on the amount of noise which have been removed in (i).

5.2 Data Processing Strategy

The Raw GPS data recorded from the field trials were first imported into Ski-Pro. A check and corrections were made (where necessary), particularly to the station name, antenna height and antenna type to ensure that the correct information had been used in the data file. The data were then exported and saved in RINEX format. Two sets of RINEX data file were created i.e. the Static and Kinematic RINEX data files. To create the kinematic data, a "2" was inserted on a new line at column 40 after the End of Header in the RINEX file. This is necessary so as to allow Ski-Pro to recognise and process them as kinematic data.

Final precise orbits, which, are only available after approximately thirteen days from the day of observation, were used and downloaded from the International

GNSS Service website [*IGS*, 2006]. Comparing between broadcast and precise ephemerides, no significant differences were seen for all the field trials, due to the limited baseline lengths used.

To relate the local field trial GPS network to the Ordnance Survey's ETRS89 coordinate system, the nearest Ordnance Survey active station was selected and their RINEX data files were downloaded from the Ordnance Survey GPS website http://www.gps.gov.uk. These were then imported in Ski-Pro or BSW4.2 and held fixed when processing the baseline from them to the reference station of the local network for each trial. For the Snowdon and Humber Bridge trials, Ski-Pro was unable to resolve the ambiguities, which might be due to their distances; whence, BSW4.2 was used for both trials and successfully resolved the ambiguities. For the University #1 and #2 and Forth Road Bridge trials, the ambiguities were resolved successfully in static mode processing with Ski-Pro. This is because the distances from the active stations to the local field trial network were much less. One field trial station was selected as reference and by performing static GPS processing, using a baseline from the nearest active station, the ETRS89 coordinates for the field trial networks were established. The station name for each field trial and the corresponding active station used as reference, were as shown in Table 5.1.

Trials	Local Reference Station	OS Active Station	Distance (km)	Processed by
Snowdon	100a	LYN2	29	BSW4.2
Humber Bridge	ref1	LEED	80	BSW4.2
University #1 and #2	tre1	NOTT	3	Ski-Pro 3.0
Forth Road Bridge	ref1	EDIN	9	Ski-Pro 3.0

Table 5.1 The local reference and active stations used for each field trial.

The local reference station was then held fixed for the determination of the coordinates of other local stations with Ski-Pro 3.0. These coordinates were then adopted as "*true values*" for the analysis of the kinematic processing carried out using Ski-Pro 3.0 and KINPOS.

5.3 Processing with KINPOS

To run KINPOS, it is not as straight forward as with Ski-Pro. One needs to have a good understanding on how the GPS data are to be processed, and what options or settings need to be used in the KINPOS control file. A full example of the control file together with a description of the settings can be seen in Appendix A.

Several test runs were carried out with KINPOS to select the best or correct settings to be used and these are discussed in the following sections. Only results from four major settings will be described here where the author felt it is important for obtaining the best results from KINPOS. The tests were made using the Snowdon Trial data on day 16th June 2003. Runs with KINPOS were made from 100a to three stations namely, 100b, 300a and 400a, to form three baselines namely 100a – 100b, 100a – 300a and 100a – 400a, which are about 15 m, 6 km and 9 km in distance, respectively.

5.3.1 Effects of Kalman Filter Constant Acceleration or Random Walk

The POSITIONMODEL option allows the user to select which model is to be used for predicting the position of the rover in the Kalman Filter. Two options are available, 'CONSTACC' for Constant Acceleration and 'RW' for Random Walk model. Comparisons carried out by the author shows that there is only a very slight difference of less than 2 mm on the position residuals between 'CONSTACC' and 'RW' as can be seen in Table 5.2 (for epochs with resolved ambiguity). The highest is for baseline 100a – 400a which is the longest baseline (9 km). Based on the small difference for this trial data, it does not matter which setting to be used.

Baseline	dN (mm)	dE (mm)	dU (mm)
100a–100b	<1.0	<1.0	<1.5
100a–300a	<1.0	<1.0	<1.5
100a–400a	<1.0	<1.0	<2.0

Table 5.2 Difference of position residuals between Constant Acceleration and Random Walk model processed with KINPOS for sample baselines from the Snowdon Trial.

5.3.2 Effects of Different Frequency

The FREQUENCY options in the KINPOS control file allow the user to select which frequency to be used for processing. The available options are 0 for ionospherically free (quoted as L0), 1 for L1 and 2 for L2. The purpose of these tests was to assess which frequency to use, as with dual frequency data, all three options are available.

All three baselines were successfully run with KINPOS using the three frequency options, which showed that they are equally able to resolve ambiguities. A minimum of 5 and maximum of 8 satellites were available for baseline 100a – 300a. KINPOS marks the resolved ambiguity code with a "1", which means that the ambiguities were resolved with redundancy, and a "2" without redundancy.

The plots of the time series for baseline 100a – 300a using the three frequencies can be seen in Figure 5.3 in the dN, dE and dU components respectively. By looking at the plots, with the ambiguities successfully resolved, we can see that the position residuals computed with the L1 frequency (red) give the best time series when compared to L2 (green) and L0 (blue) as they have lower variations both in minimum and maximum values.

Looking at the bar charts of the values of standard deviations and ranges between the minimum and maximum values for the three baselines (Figure 5.4, 5.5 and 5.6), it is clear that L1 gives the best result as it has the lowest standard deviations and ranges. The standard deviation seems to agree between the three frequencies with no significant differences although they increase in magnitude, as the baseline is longer. Also, as the length of the baselines increases, the variation in maximum and minimum values seems to expand higher, with L0 produces higher variation when compared to L1 and L2, with L1 the lowest. Not surprising that L0 (ionosphere free) gives higher values as this is a linear combination and therefore noise increases.

Based on the above results, with the maximum baseline length of nine kilometres, which can be considered as a short baseline, it was considered best to use the L1 frequency for further processing with KINPOS.

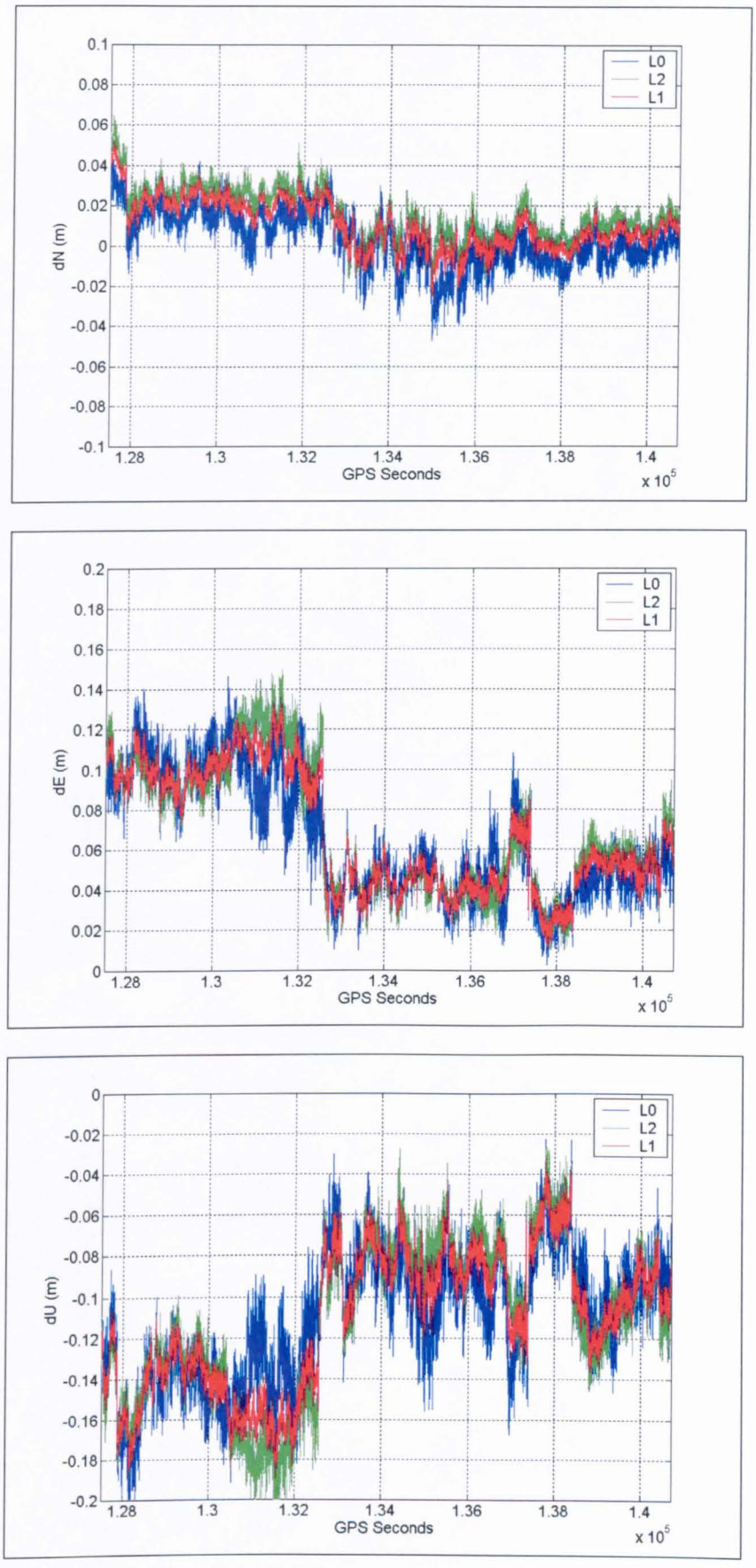

Figure 5.3 Plots of position residuals using different processing frequencies with KINPOS for baseline 100a – 300a (dN, dE and dU components), Snowdon Trial 16th June 2003.

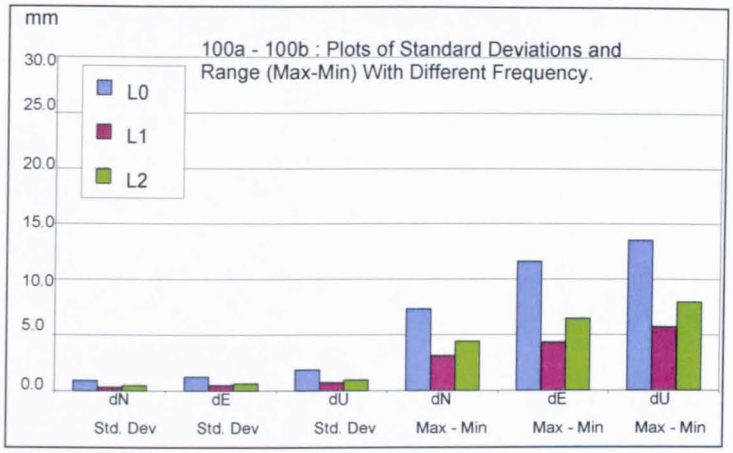

Figure 5.4 Standard Deviations and Range (Max – Min) values for the position residuals from KINPOS for baseline 100a – 100b Snowdon Trial, 16th June 2003.

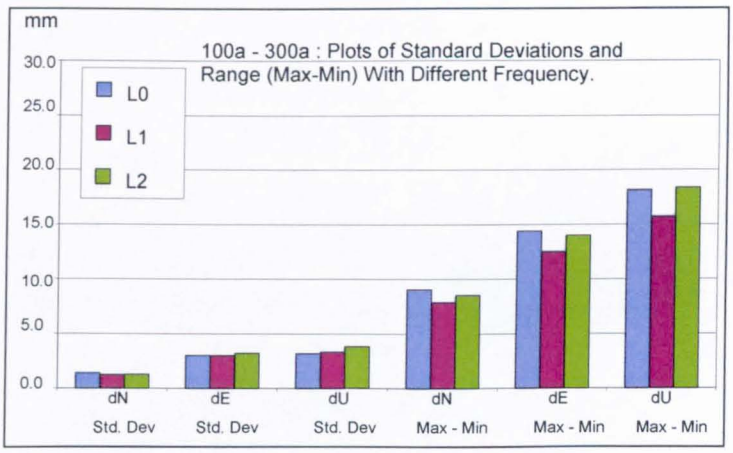

Figure 5.5 Standard Deviations and Range (Max – Min) values for the position residuals from KINPOS for baseline 100a – 300a Snowdon Trial, 16th June 2003.

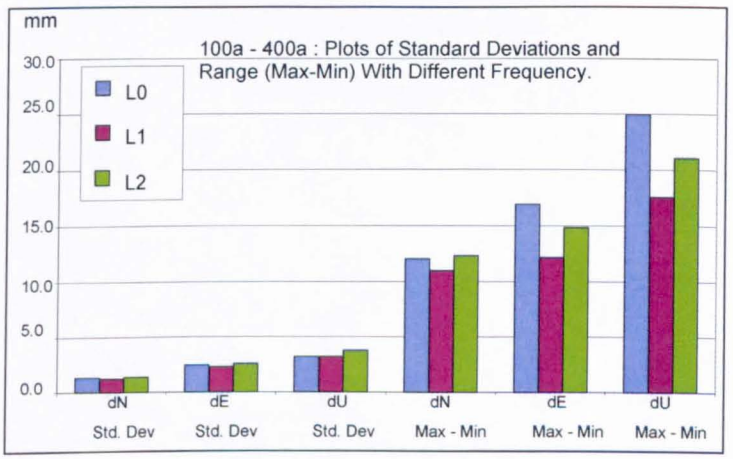

Figure 5.6 Standard Deviations and Range (Max – Min) values for the position residuals from KINPOS for baseline 100a – 400a Snowdon Trial, 16th June 2003.

5.3.3 Solving for the troposphere with KINPOS

Processing with KINPOS to solve for the relative zenith tropospheric delay needs a full understandings on how the computations are carried out. Any mistakes in the settings can produce results which may look correct but in reality are wrong. After lots of test runs, the main settings for the KINPOS control file were chosen as follows;

i. POSITIONMODEL – Random Walk (RW) was selected to allow freedom in prediction of state by the Kalman filter. Furthermore, the difference between RW and CONSTACC were a mere ± 2 mm, due to the distance between stations being considered as short.

ii. FREQUENCY – L1 only was used as the distance between points was considered short, ie. less than 10 km. Runs with different frequency settings showed that L1 gives a more consistent result, with smaller variations in the positions.

iii. Starting Time – When using an initial starting time of 09:08:00 hours, ambiguity resolution for all baselines were mostly found to be unresolved with KINPOS which at times caused the program to halt. This was because the ambiguity resolution process in KINPOS is a continuous process with the normal equations for each epoch being accumulated between epochs, hence, with cycle slips, insufficient number of satellites available (less than 5) and some period of data loss, the ambiguity could not be resolved by KINPOS. Whence, a starting time of 11:25:00 was chosen, with the ending time of 15:05:06.

iv. Troposphere Model – Only MAGNET was found to be able to be used in KINPOS and set as modelled for the hydrostatic part for the base station, while KINPOS solved relatively for the rover station. No wet model were applied to the base station.

v. Process Noise – This is a major point in KINPOS as it defines the weight used by the Kalman filter. Smaller values result in a tight constraint, while

larger values could be too loose. To look at the effects of the process noise (PROCNOISE), values ranging from 0.001 to 0.500 cm/√hr were tested.

In these tests, each plot in the dN, dE and dU component consists of five line plots which represents the position residuals produced from modelled troposphere (MAGNET) and solving the zenith tropospheric delay with PROCNOISE values of 0.001, 0.100, 0.250 and 0.500 cm/√hr (with the initial zenith tropospheric value of zero). The RZTD plot shows the RZTD for each settings of PROCNOISE together with the modelled values.

5.3.3.1 Testing Baselines 100a – 400a and 400a – 100a

Referring to Figure 5.7, for baseline 100a as reference to 400a as rover (difference in altitude of -48 m), the dN component seems to have no significant difference as the PROCNOISE value is increased. There are some variations in the dE component but the dU shows greater variations, where the solved position residuals changes around the modelled values with the results from using the 0.500 cm/√hr *process noise* being closest to the modelled results. However, the RZTD values (Figure 5.8) do not show a consistent result as it also expands as the PROCNOISE value increases. These show the influences of the Kalman filter estimates in KINPOS.

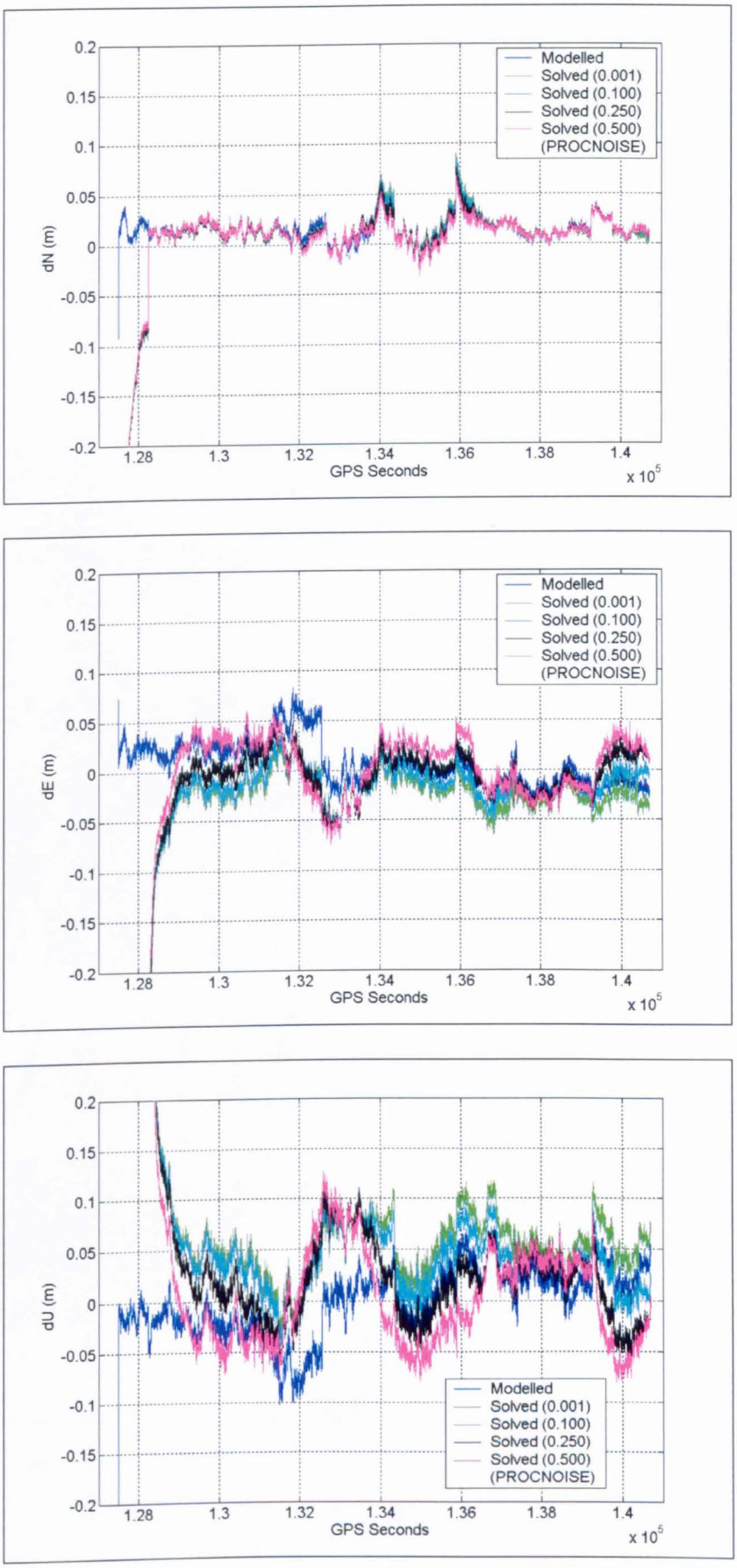

Figure 5.7 Plots of position residuals and with solve all option for the troposphere in KINPOS for baseline 100a – 400a, Snowdon Trial on 16th June 2003.

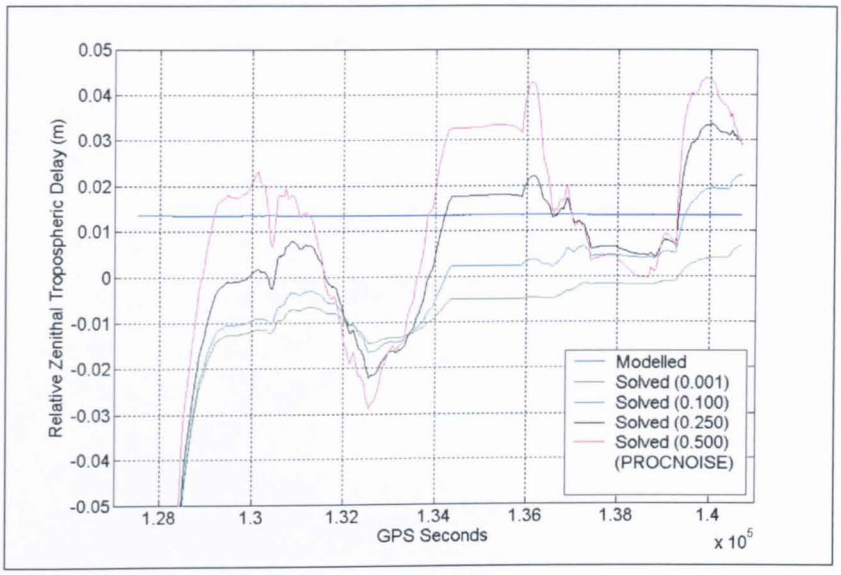

Figure 5.8 Plots of RZTD with solve all option for the troposphere in KINPOS for baseline 100a – 400a, Snowdon Trial on 16th June 2003.

Two common characteristics can be derived from the plots, i.e. firstly, KINPOS needs some period of time to converge (about 1,500 seconds for this baseline), and secondly, as the PROCNOISE value increase, higher variations can be seen in both the RZTD and the position residuals. Hence, a question as to what value of the PROCNOISE should be used can be raised? However, since the purpose of this test is to compare results between KINPOS and Ski-Pro, in some ways it does not matter which PROCNOISE value is used as what we are interested is in the trends of the time series of the position residuals.

The solved position residuals differ from the modelled values by up to 40 mm in the dU component. For a difference in altitude of 48 m, it is estimated that the relative hydrostatic delay is around 14 mm, whence, the above differences were suspected to be unrealistic because it is well known that the wet delay is only about 10% of the total delay.

To investigate these findings, further runs were made on the same baseline but this time with 400a as reference and 100a as the rover. This created a scenario in which the altitude difference had a positive sign. The plots of the results can be seen in Figures 5.9 and 5.10 where a more reasonable pattern can be seen. This is shown by the RZTD plots (Figure 5.10) where they are centered around the modelled values which is more appropriate, except when the *process noise* values were higher.

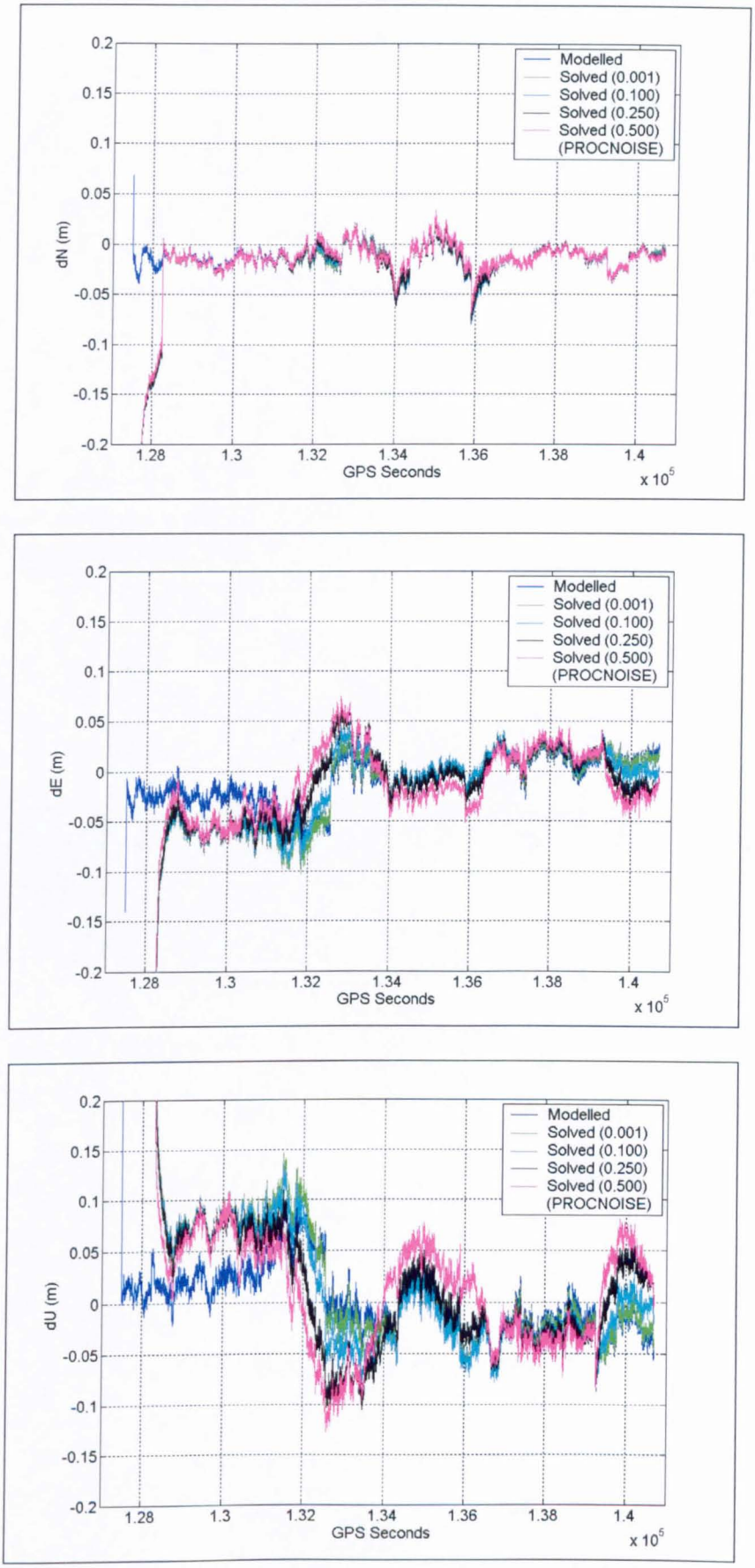

Figure 5.9 Plots of position residuals with solve all option for the troposphere in KINPOS for baseline 400a – 100a, Snowdon Trial on 16th June 2003.

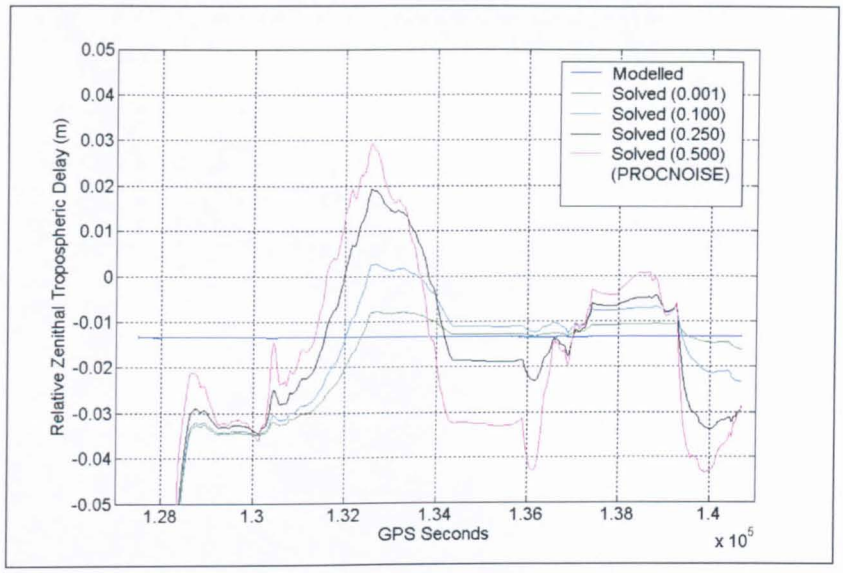

Figure 5.10 Plots of RZTD with the solve all option for the troposphere in KINPOS for baseline 400a – 100a, Snowdon Trial on 16th June 2003.

5.3.3.2 Testing Baseline 100a – 300a

For baseline 100a – 300a (difference in altitude of 980 m), as shown in Figure 5.11, a small bias can be seen in the dN component, which is higher in dE and dU components between the modelled and solved results with KINPOS. This is expected as the modelled KINPOS only takes into account the hydrostatic part of the troposphere. Upon solving for the troposphere, it can be seen that the position residuals moved nearer or centered about the zero mark. What is evident from these results is that the effects of the tropospheric delay is not only in the dU component but also affects the dN and dE component, although the magnitude is lower.

Another effect is that at epochs where the number of satellites change, there seems to be a drastic change on the position residuals when the troposphere is modelled. For example, at the 132,557 GPS seconds mark, the number of satellites changes from 7 to 6, with SV05 lost from sight, and at 134,358 GPS seconds when SV07 is lost from sight leaving a total of 5 from 6. These kind of jumps affect all other baselines too, which is why the differences are not consistent. However, many of these were corrected by KINPOS when solving for the troposphere. The effects on the RZTD values (Figure 5.12) were the same as in section 5.3.3.1, i.e., when the PROCNOISE value were higher, the variations increase.

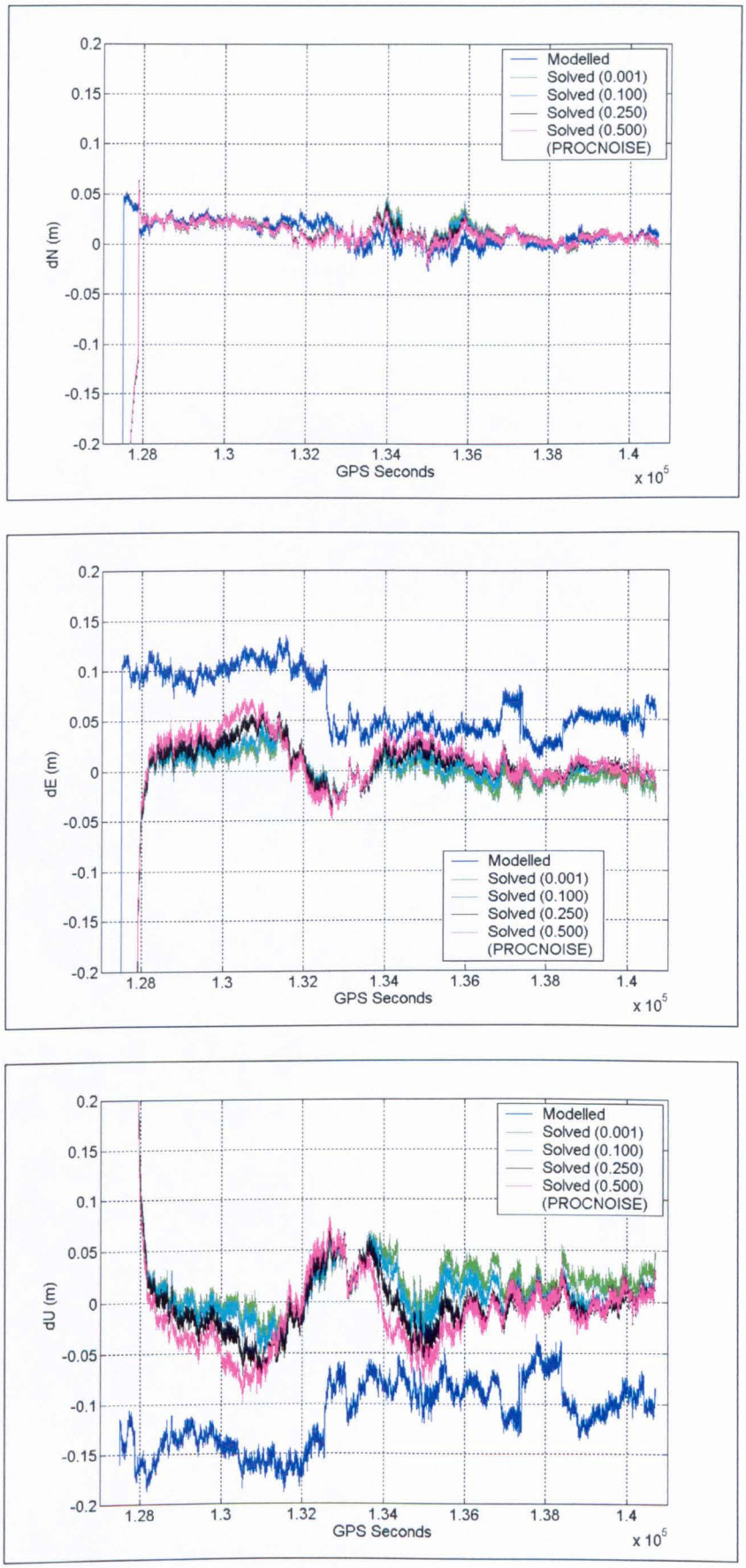

Figure 5.11 Plots of position residuals with solve all option for the troposphere in KINPOS for baseline 100a – 300a, Snowdon Trial on 16th June 2003.

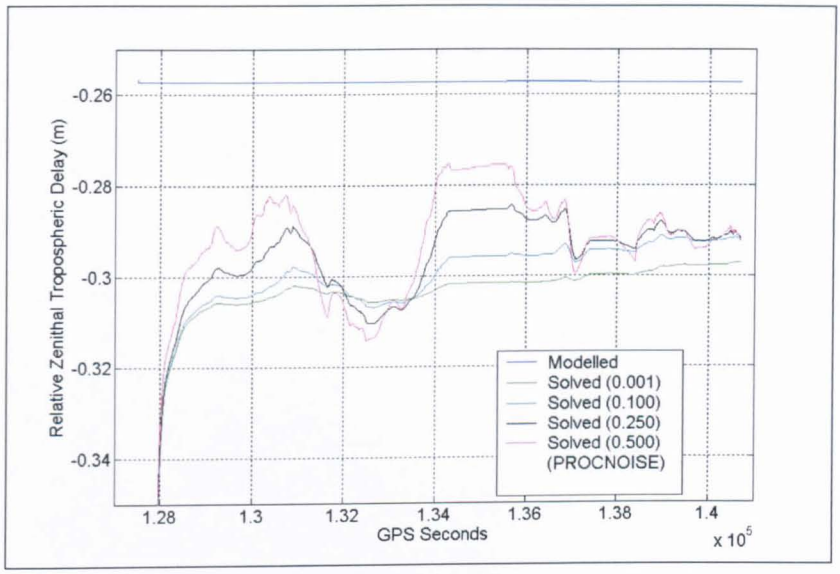

Figure 5.12 Plots of RZTD with solve all option for the troposphere in KINPOS for baseline 100a – 300a, Snowdon Trial on 16th June 2003.

As the Snowdon points were static, it is clear that the option of solving for the RZTD in KINPOS should be used in preference to the option of modelling the RZTD.

5.3.4 The Effects of Initial Troposphere Value

This section investigates the effects of using an initial troposphere value to see if it influences the convergence time for solving the RZTD in KINPOS. With a PROCNOISE value of 0.01 cm/√hr, the initial values used were 0.0, 3.00 m and the troposphere value for the respective station, e.g. for station 100a, 2.2618 m, while for 300a is 2.0045 m. The position residuals and the RZTD were plotted together with the results for when the troposphere is modelled and can be seen in Figures 5.13 and 5.15 for baseline 400a – 100a, and Figures 5.14 and 5.16 for 100a – 300a respectively.

For baseline 400a – 100a (Figure 5.13), no differences can be seen in the dN component, whereas a bias can be seen in the dE and dU components. This is reflected in the RZTD plots (Figure 5.15) where, as the initial value increases, a bias is created but it looks like converging towards the end of the time series. This means that the initial value does have an effect on the position residuals; however,

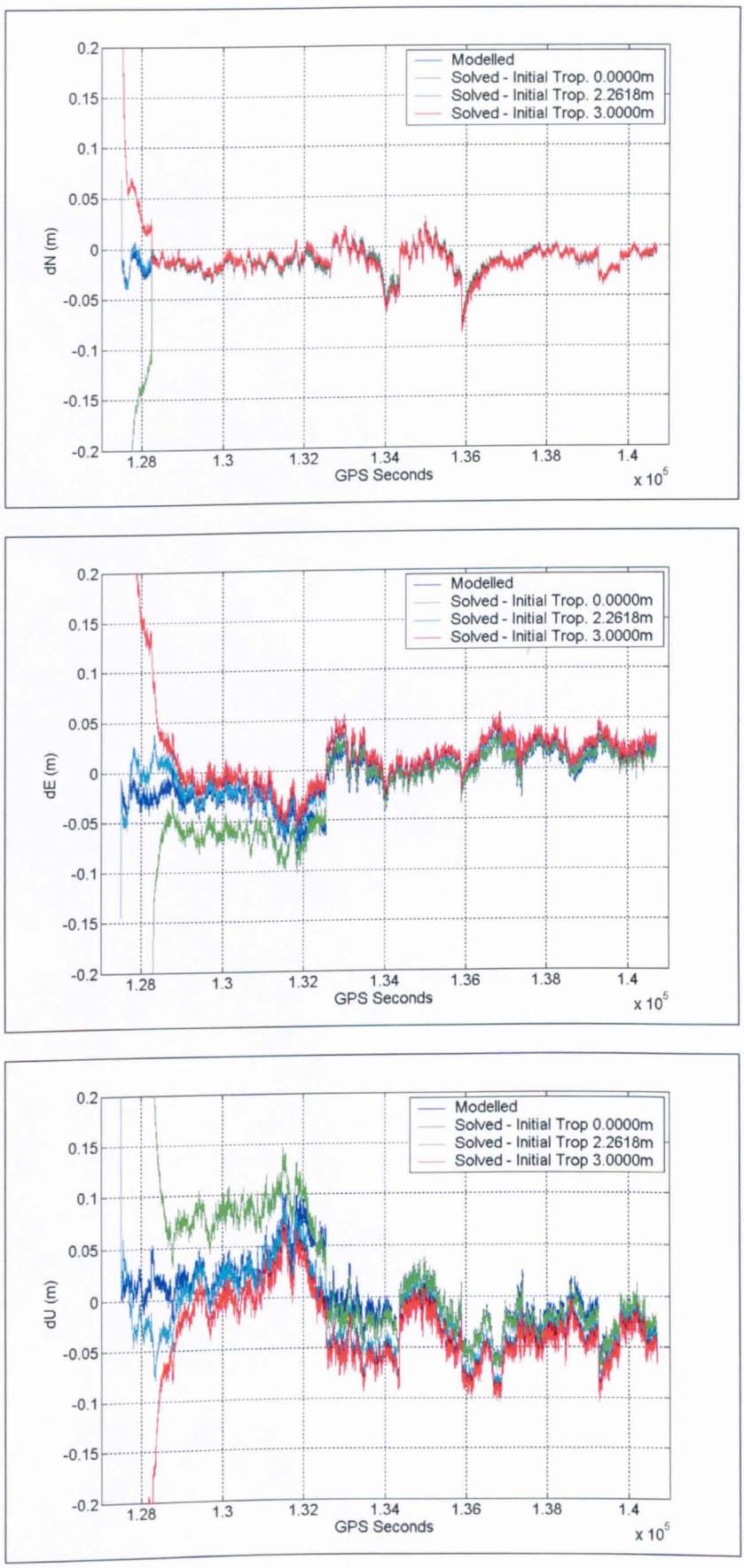

Figure 5.13 Plots of position residuals with solve all option for the troposphere using different initial troposphere values in KINPOS for baseline 400a – 100a, Snowdon Trial on 16th June 2003.

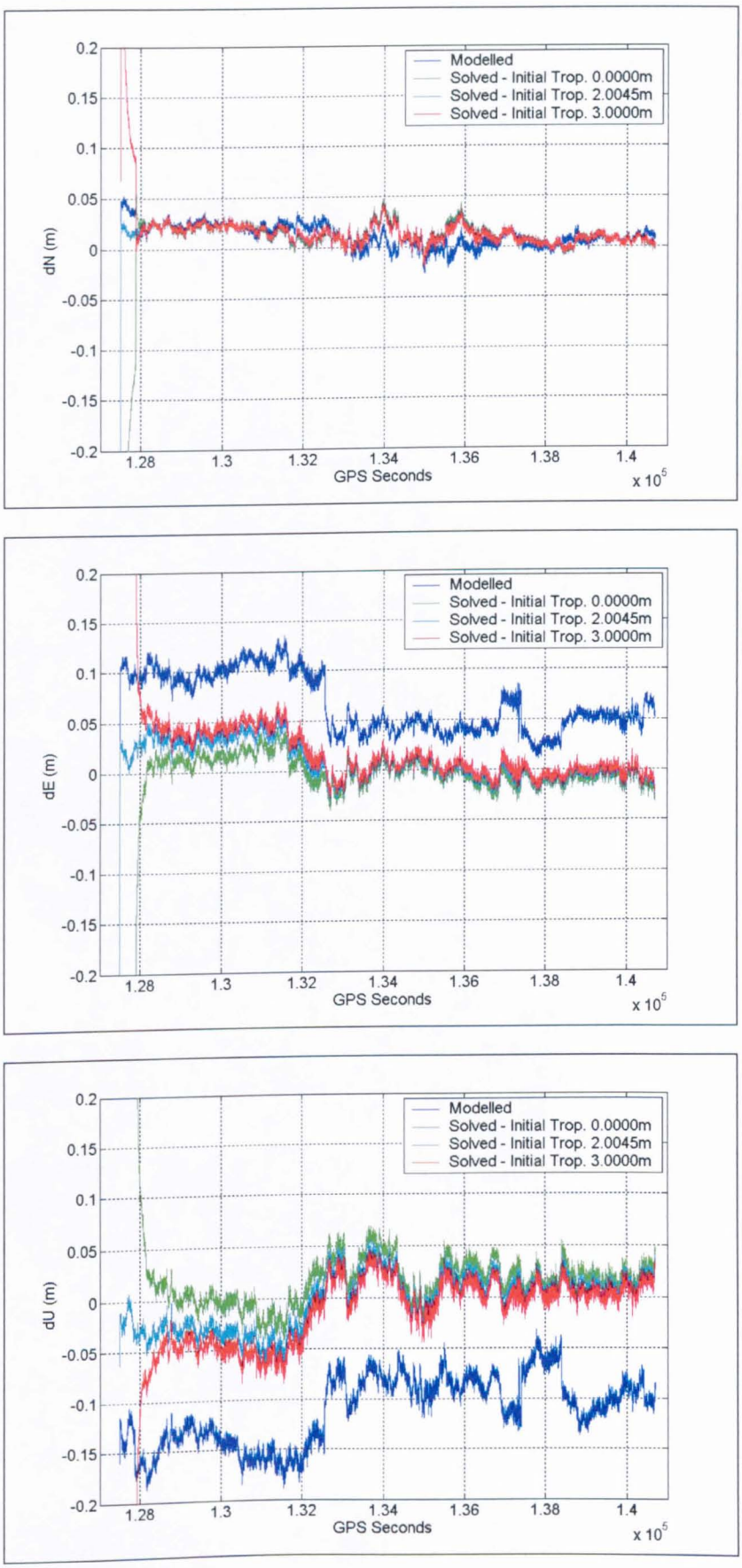

Figure 5.14 Plots of position residuals with solve all option for the troposphere using different initial troposphere values in KINPOS for baseline 100a – 300a, Snowdon Trial on 16th June 2003.

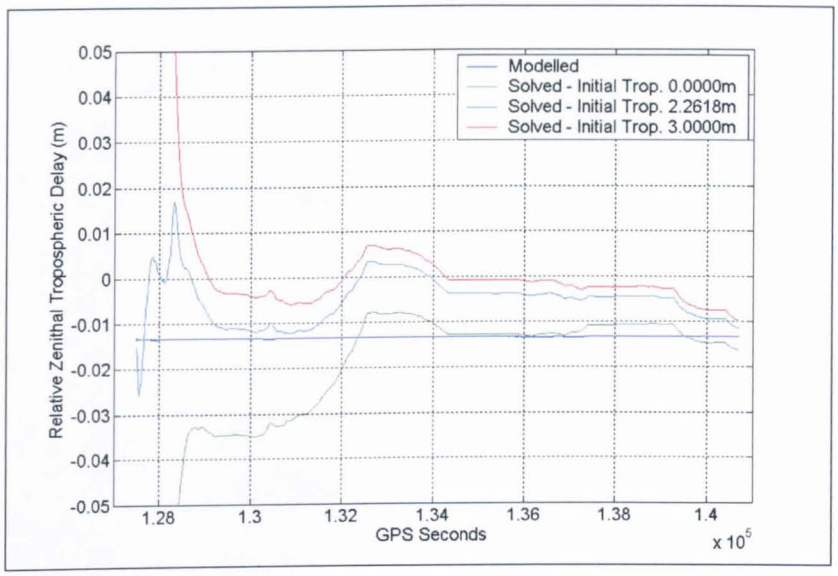

Figure 5.15 Plots of RZTD with solve all option for the troposphere using different initial troposphere values in KINPOS for baseline 400a – 100a, Snowdon Trial on 16th June 2003.

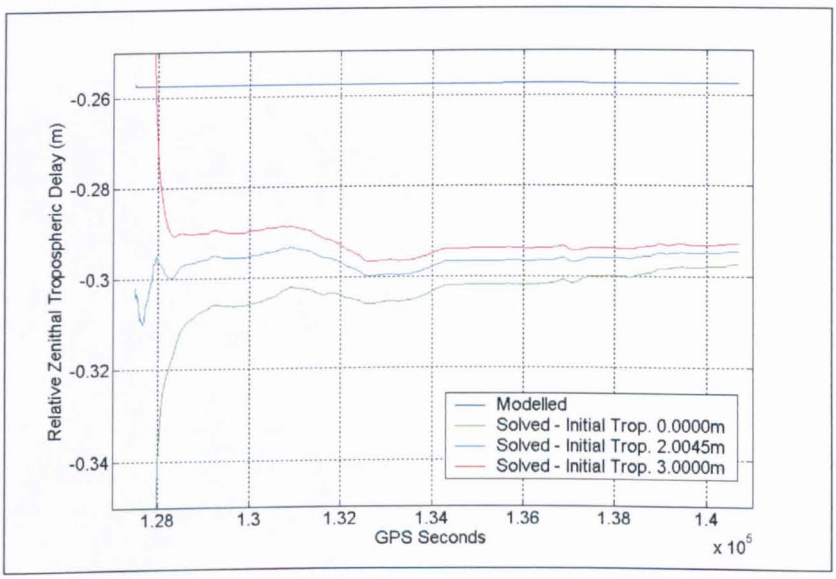

Figure 5.16 Plots of RZTD with solve all option for the troposphere using different initial troposphere values in KINPOS for baseline 100a – 300a, Snowdon Trial on 16th June 2003.

it is not clear which value provides the correct setting but, based on the plots, it is clear that a zero initial value is sufficient.

The same trends of results can be seen for baseline 100a – 300a when using different initial troposphere values results in different biases. Their numerical RMS difference can be seen in Table 5.3, while their values for the mean with their standard deviation from modelled values can be seen in Table 5.4.

16 June 2003	Initial Troposphere Value	RMS difference		
Baseline		dN (mm)	dE (mm)	dU (mm)
400a–100a	0.0000	0.4	1.4	3.0
	2.2618	3.0	10.6	22.3
	3.0000	3.9	13.7	28.8
100a–300a	0.0000	15.4	50.7	106.4
	2.0045	13.6	45.1	94.4
	3.0000	12.7	42.2	88.2

Table 5.3 RMS difference in position residuals from different initial troposphere values with the solve all option compared to using modelled values in KINPOS for baselines 400a – 100a and 100a – 300a for epochs of 134,000 to 138,175 GPS seconds, Snowdon Trial on 16th June 2003.

16 June 2003	Initial Troposphere Value	dN (mm)		dE (mm)		dU (mm)	
Baseline		Mean	Std. Dev	Mean	Std. Dev	Mean	Std. Dev
400a–100a	modelled	-16.4	17.0	3.5	14.1	-18.9	22.5
	0.0000	-0.2	0.3	1.2	0.9	-2.5	1.8
	2.2618	-2.2	2.1	10.3	2.4	-21.8	4.6
	3.0000	-2.9	2.7	13.3	3.1	-28.2	6.1
100a–300a	Modelled	0.2	7.1	42.7	13.3	-83.6	17.4
	0.0000	11.3	10.4	-48.8	13.6	104.4	20.1
	2.0045	10.0	9.2	-43.4	12.3	92.8	17.7
	3.0000	9.3	8.6	-40.6	11.6	86.6	16.4

Table 5.4 Mean and standard deviation of the difference in position residuals from different initial troposphere values with the solve all option compared to using modelled values in KINPOS for baselines 400a – 100a and 100a – 300a for epochs of 134,000 to 138,175 GPS seconds, Snowdon Trial on 16th June 2003.

These tables provide further confirmation that the initial value does have an effect on the position residuals, but it can be seen that a zero initial value is sufficient.

5.4 Comparing Ski-Pro Version 3.0 Results with KINPOS

As mentioned in the previous section, the main purpose of using KINPOS was to compare results from Ski-Pro Version 3.0. It is not the intention of the author to highlight any weaknesses of either software but solely as a comparison to validate that results from Ski-Pro are sufficiently acceptable for this project, as claimed by Leica Geosystems AG.

Three categories of different station altitudes were investigated: less than 100 m, 400 m and about 1,000 m. Three baselines from the Snowdon Trial on day 16th June 2003 were used, i.e., 100a – 400a (less than 100 m difference in altitude), 100a – 200a and 100a – 300a with a difference in altitude of 400 m and 1,000 m respectively. Data from University Trial #1, 19th May 2004 were also used i.e. baseline trel – twrl, which has about 50 m difference in altitude. For the Snowdon Trial data, the start time was 11:25:00 and the stop time was 15:05:06 with a 15 degree cut-off elevation angle. Although the observations were collected earlier, a different start time was selected as KINPOS could not resolve the ambiguities prior to 11:25:00. For the University Trial #1 data, the start time was 10:00:55 with a stop time of 14:01:25. For Ski-Pro, the frequency was set to "auto" and Saastamoinen was selected for the troposphere model. Although the frequency is set to "auto", due to the short baseline lengths, L1 was used by Ski-Pro to compute the coordinates. This can be seen from Figures 5.17 to 5.22, where plots of the position residuals in all components shows that there are similarity in the magnitude of the results.

For KINPOS, the selected frequency was L1 and the troposphere model was MAGNET. Firstly, only the hydrostatic part of both reference and rover were modelled in KINPOS, with *Niell* [1996] used as the mapping function, which means that the tropospheric delay is not solved, whence the PROCNOISE option is redundant. Then, the troposphere at the reference station was modelled, and the troposphere at the rover was solved using a PROCNOISE value of 0.01 cm/$\sqrt{\text{hr}}$ and initial troposphere value of zero.

5.4.1 Baselines of less than 100 metres difference in altitude

5.4.1.1 Baseline 100a – 400a and vice-versa, Snowdon Trial

The plots of the position residuals for the baseline 100a – 400a in all three components can be seen in Figure 5.17 and for baseline 400a – 100a in Figure 5.18. Looking at both Figures 5.17 and 5.18 for the dN component, the results from both KINPOS settings are almost similar in trend with a slight bias. Taking into account that the results from using the solve all troposphere option in KINPOS takes about 1,500 seconds to stabilise, when compared to results from Ski-Pro, in general, they have an almost similar pattern but with a bias. In the dE and dU component, it is obvious that the result from 'solved KINPOS' departs away from both Ski-Pro and 'modelled KINPOS'. Their RMS difference can be seen in Table 5.5. It is clear that the bias from both KINPOS results with respect to Ski-Pro is almost the same. The larger bias of about 19 mm in the RMS difference in the dN component is still unexplainable.

16 June 2003	KINPOS	RMS difference		
Baseline		dN (mm)	dE (mm)	dU (mm)
100a–400a	Modelled	18.0	7.3	10.0
	Solved	22.9	17.3	48.3
400a–100a	Modelled	18.5	6.2	11.3
	Solved	18.7	6.0	13.2
100a–200a	Modelled	6.8	31.2	64.0
	Solved	6.4	8.3	9.7
100a–300a	Modelled	12.5	58.9	120.8
	Solved	5.1	9.4	15.8

Table 5.5 RMS difference in position residuals from modelled and solved KINPOS compared to Ski-Pro for baselines 100a – 400a, 400a – 100a, 100a – 200a and 100a – 300a for epochs of 134,000 to 138,175 GPS seconds, Snowdon Trial on 16th June 2003.

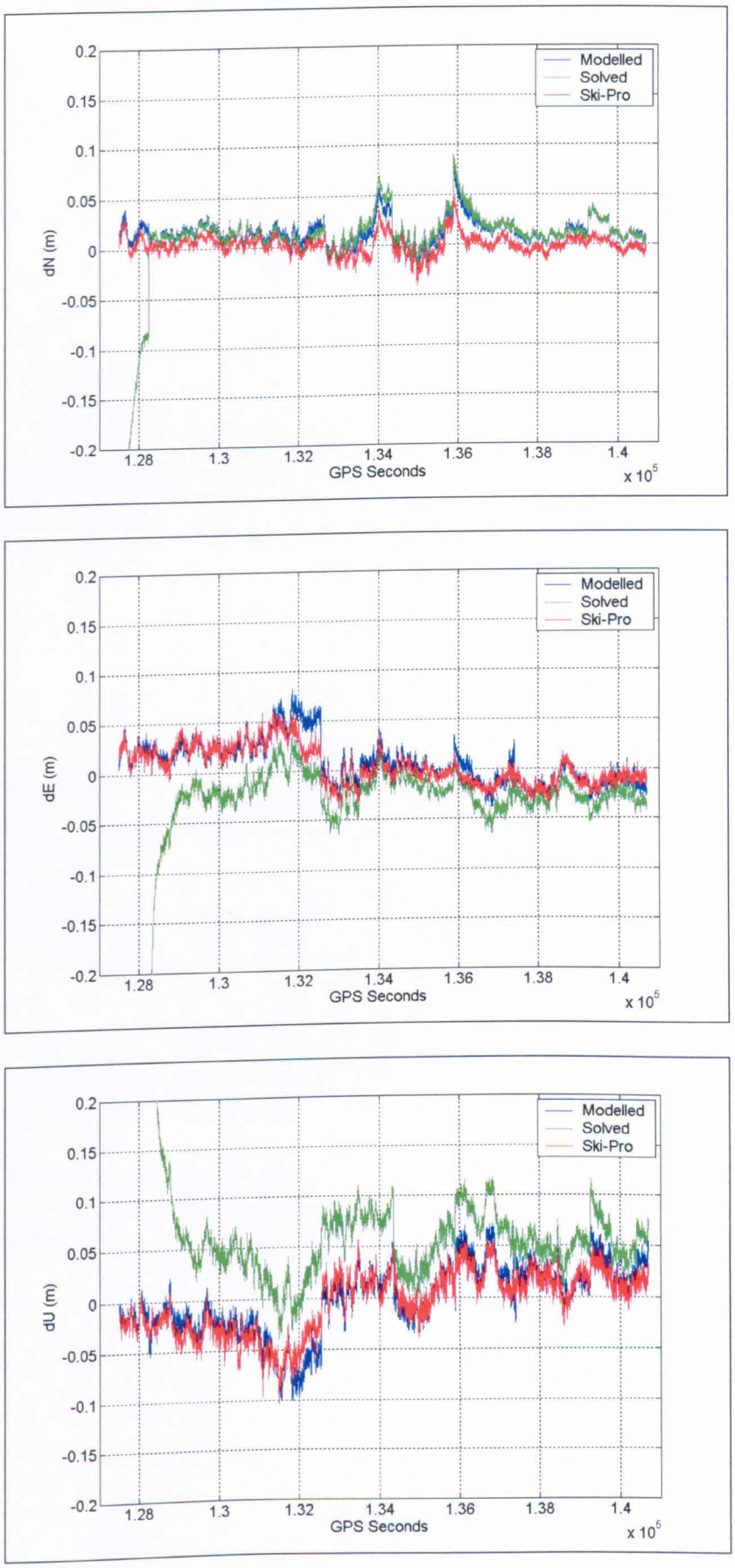

Figure 5.17 Plots of position residuals for baseline 100a – 400a from modelled and solved KINPOS with Ski-Pro for the Snowdon Trial on 16th June 2003.

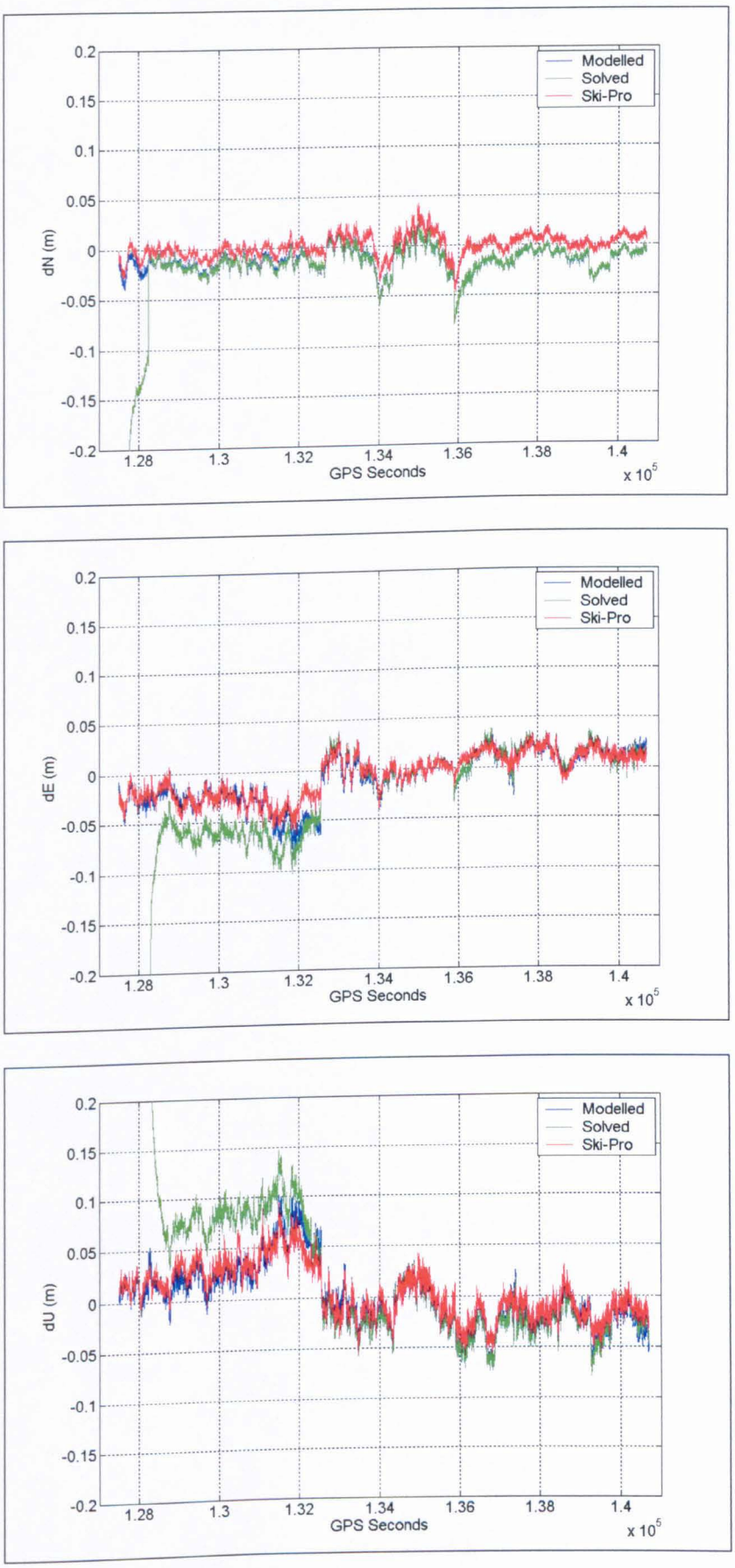

Figure 5.18 Plots of position residuals for baseline 400a – 100a from modelled and solved KINPOS with Ski-Pro for the Snowdon Trial on 16th June 2003.

5.4.1.2 Baseline trel – twrl, University Trial #1 19th May 2004

A baseline from the University Trial #1 was also investigated to compare Ski-Pro with KINPOS. refl was selected as base and twrl as rover. Station twrl is about 51 m above trel with a plan distance of about 1 km. Initially, the start time of 10:00:55 (295,255 GPS seconds) with the stop time of 14:01:25 (309,685 GPS seconds) were selected. The plots of the results for the three runs namely; Ski-Pro, 'modelled KINPOS' and 'solved KINPOS', are as shown in Figure 5.19 for the three components. It can be seen that KINPOS took sometime to converge while solving for the troposphere. There is also a jump recorded by KINPOS around the 302,000 seconds mark, which is probably due to the ambiguities being incorrectly resolved. A check on the satellites shows that only 4 satellites were available during that period. The RMS difference for both KINPOS results with respect to Ski-Pro can be seen in Table 5.6. To maintain consistency of the RMS values between the results, only epochs between 303,000 to 309,685 GPS seconds were considered. Whence, the effects from epochs during the convergence period and around the 302,000 seconds from the solved KINPOS do not influence the RMS difference.

19 May 2004	KINPOS	RMS difference		
Baseline		dN (mm)	dE (mm)	dU (mm)
Computed from epochs 303,000–309,685 seconds				
trel–twrl	Modelled	3.1	5.9	10.9
	Solved	3.4	15.6	28.4
Computed from epochs 305,000–309,685 seconds				
trel–twrl	Modelled	3.1	6.1	11.4
	Solved	3.0	5.1	7.0

Table 5.6 RMS difference in position residuals from modelled and solved KINPOS compared to Ski-Pro for baselines trel – twrl for epochs of 303,000 to 309,685 GPS seconds, and 305,000 to 309,685 GPS seconds, University Trial #1 on 19th May 2004.

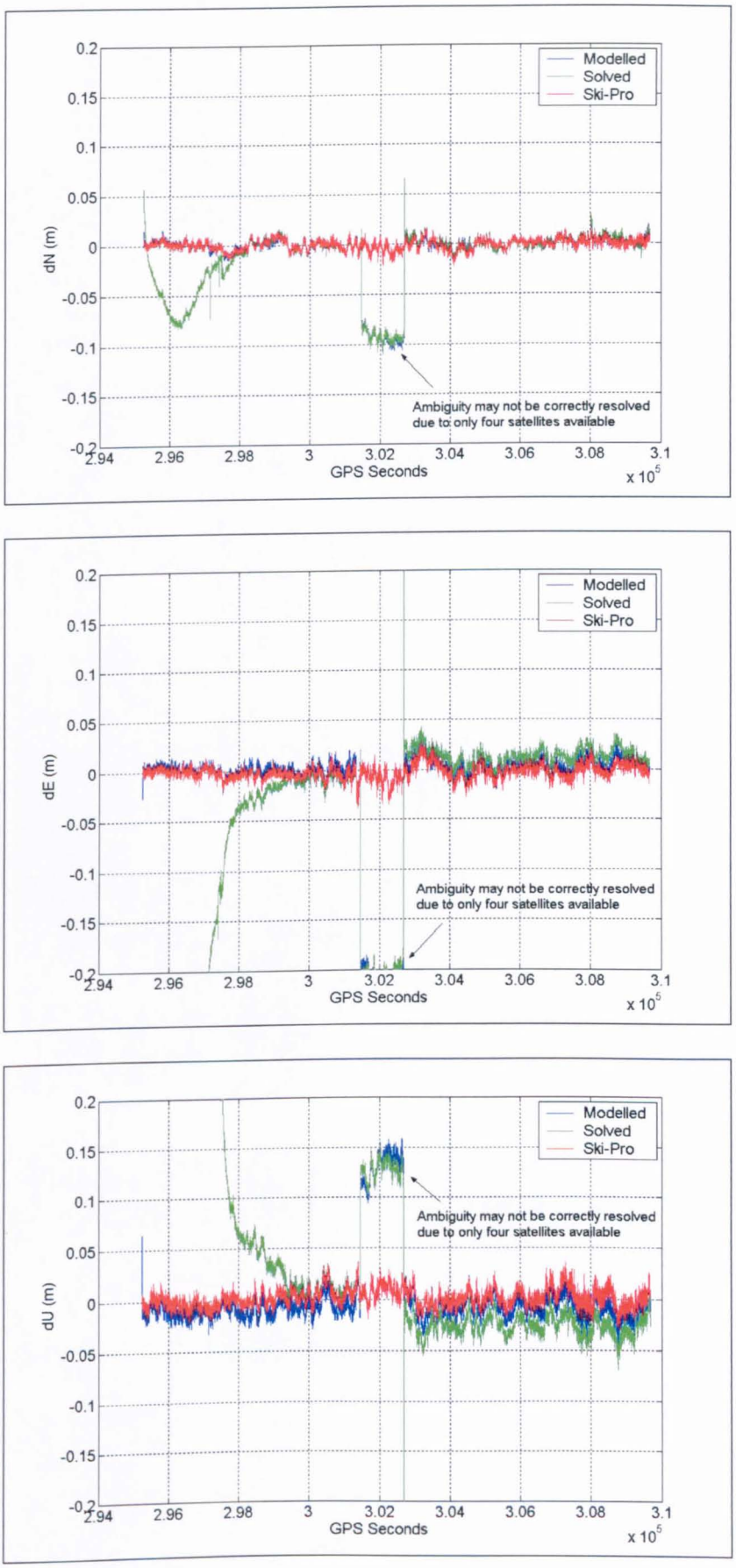

Figure 5.19 Plots of position residuals for baseline tre1 – twr1 with start time 295,255 GPS seconds from modelled and solved KINPOS with Ski-Pro for the University Trial#1 on 19th May 2004.

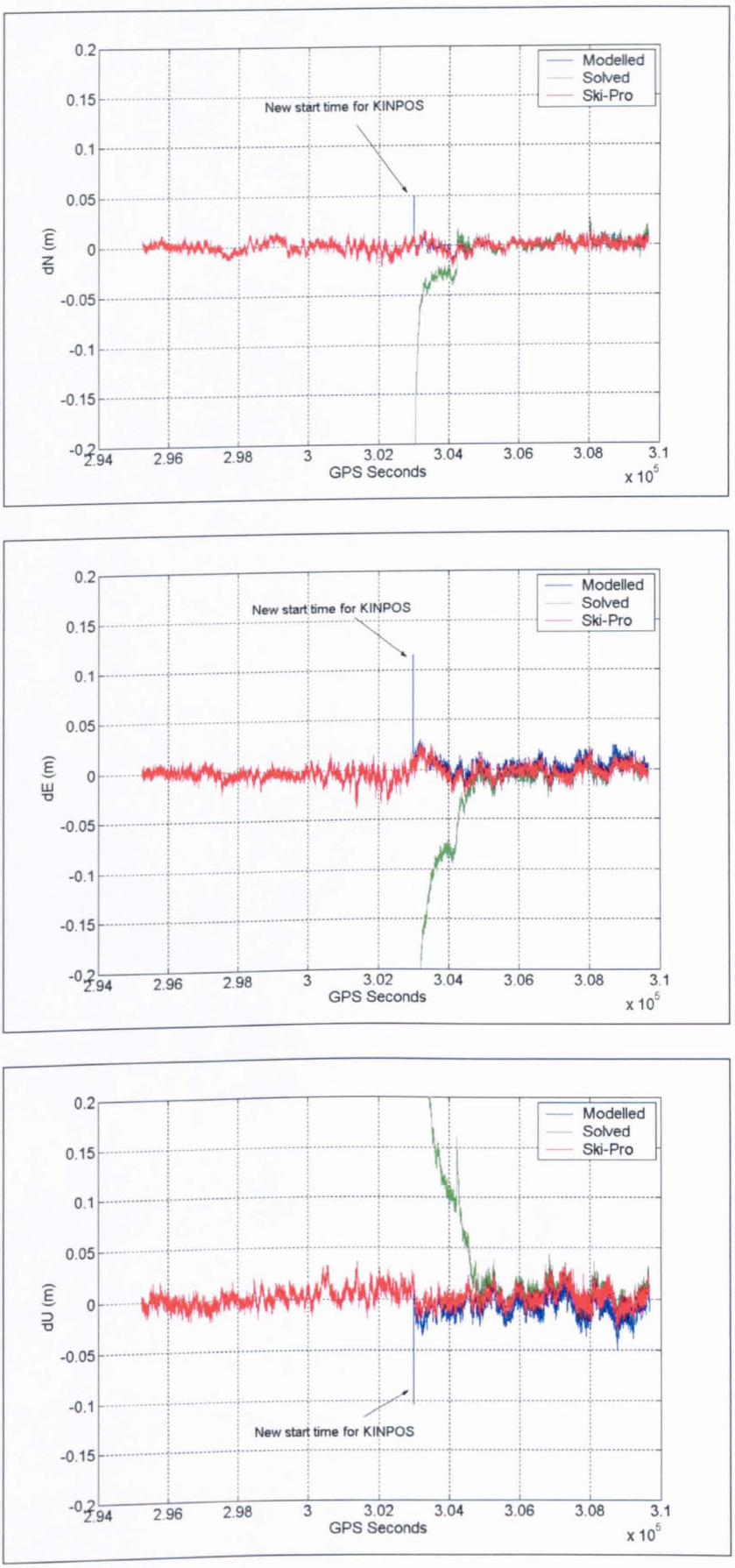

Figure 5.20 Plots of position residuals for baseline tre1 – twr1 with start time 303,000 GPS seconds from modelled and solved KINPOS with Ski-Pro for the University Trial#1 on 19th May 2004.

A different approach was used by changing to a new start time of 295,255 GPS seconds (after the problematic period). Much more realistic results can be seen as shown in Figure 5.20 and in Table 5.6 when only epochs from 305,000 – 309,685 GPS seconds were considered, as a period of 2,000 seconds were needed for KINPOS to converge or stabilized.

From the RMS difference values, it can be seen that the result from solved KINPOS using the new start time have lower differences when compared to the initial start time. Between modelled and solved KINPOS, almost no differences were recorded in the dN and dE components, while 4 mm can be seen in the dU component. The trends of all three time series were almost similar to each other.

5.4.2 Baseline of 400 metres difference in altitude

5.4.2.1 Baseline 100a – 200a

As mentioned earlier in 5.3.3.1, 'modelled KINPOS' estimates the troposphere using the MAGNET model which explains why the position residuals are away from both 'solved KINPOS' and Ski-Pro. The plots in Figure 5.21 show that the pattern between Ski-Pro and 'solved KINPOS' was almost the same with RMS difference of 6.4 mm in dN, 8.3 mm in dE and 9.7 mm in dU components (Table 5.5). The converging time is also smaller as compared to the baseline considered in section 5.4.1.1.

5.4.3 Baseline of 1000 metres difference in altitude

5.4.3.1 Baseline 100a – 300a

For this baseline, where station 300a is about 980 metres above 100a, the RMS difference is 5.1 mm in dN, 9.4 mm in dE and 15.8 mm in dU components (Table 5.5). Plots for this baseline are as shown in Figure 5.22. Comparing to plots for baseline 100a – 200a, the patterns of the time series are almost similar between solved KINPOS and Ski-Pro except for the slight differences towards the end of the time series. The graphical difference in the position residuals between solved KINPOS and Ski-Pro are shown in Figure 5.23.

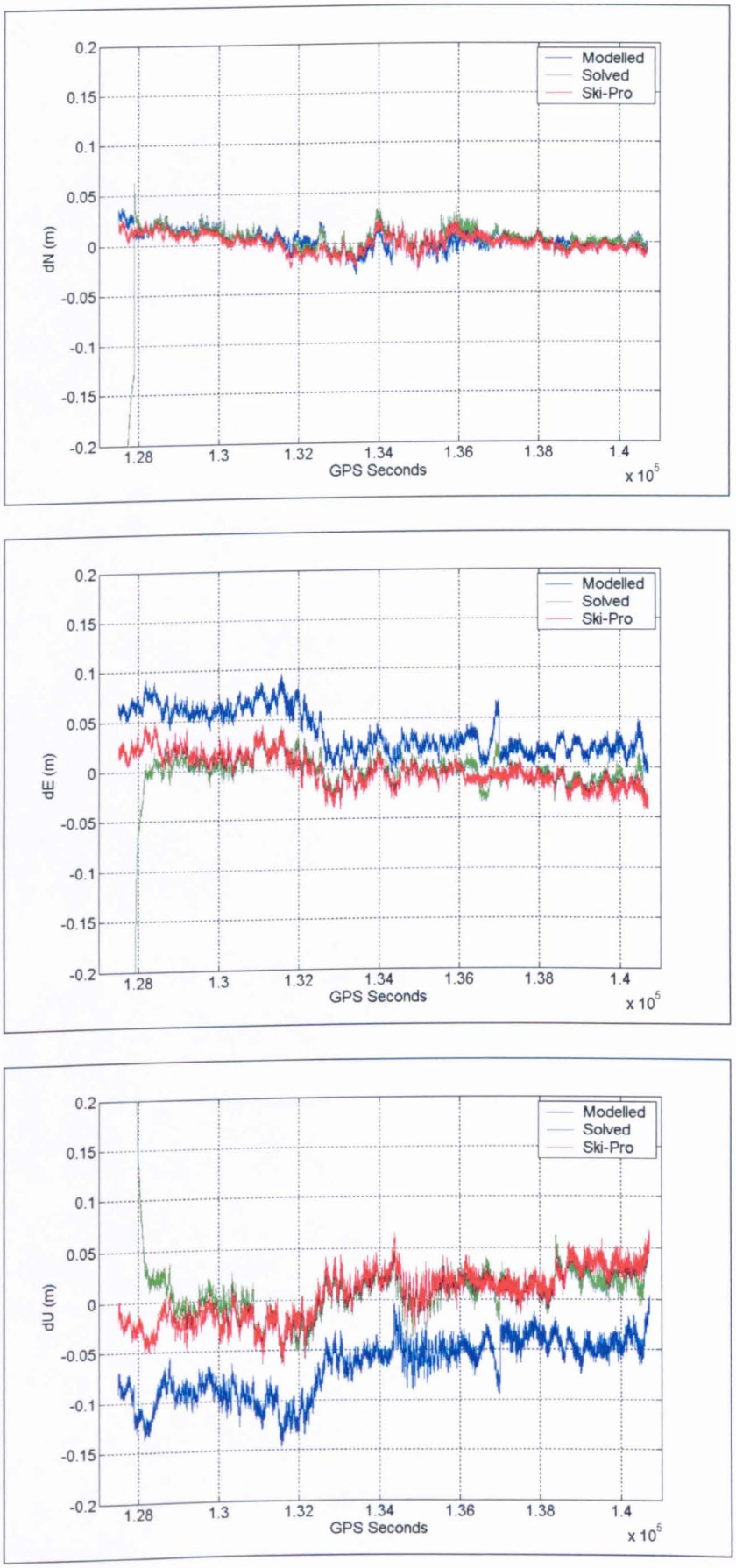

Figure 5.21 Plots of position residuals for baseline 100a – 200a from modelled and solved KINPOS with Ski-Pro for the Snowdon Trial on 16th June 2003.

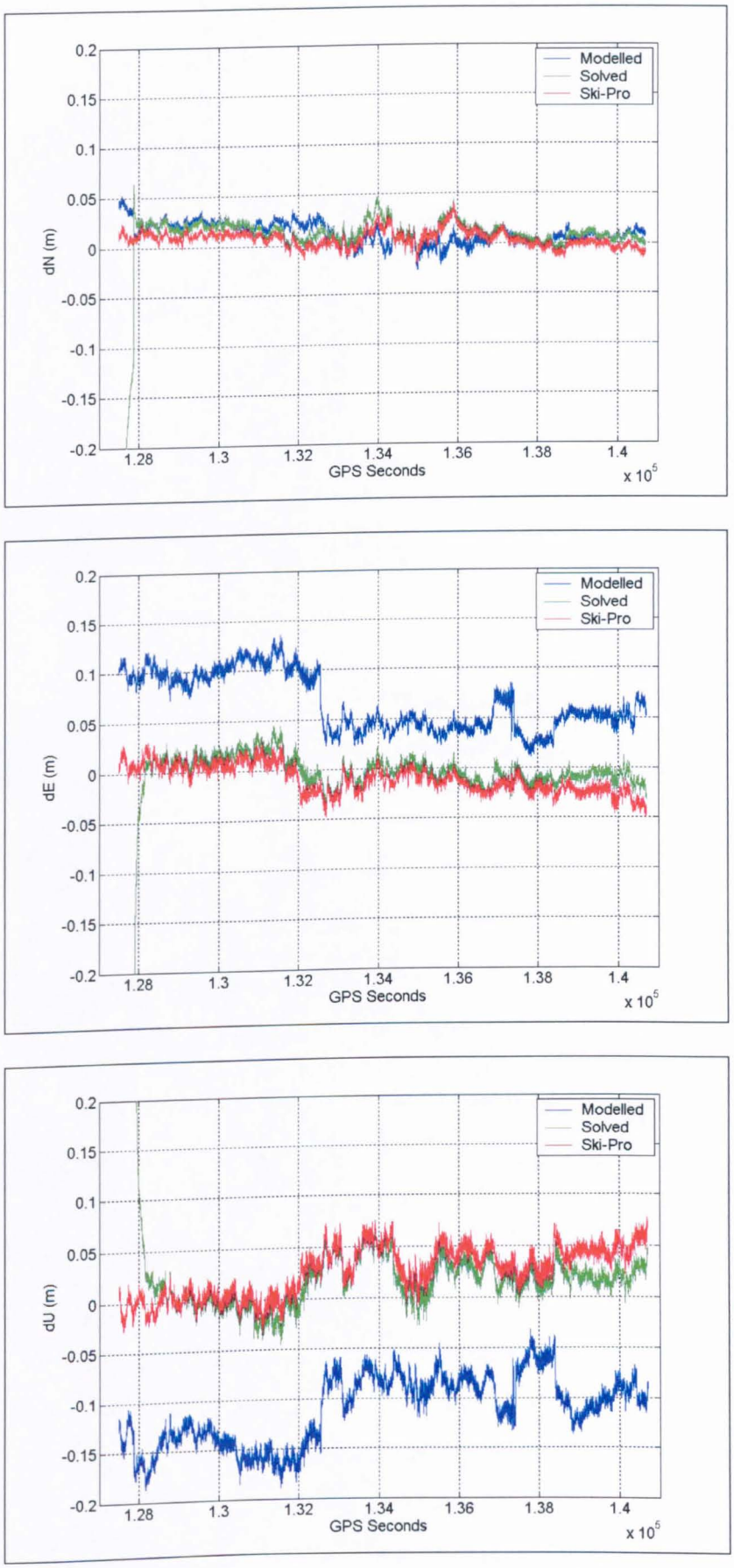

Figure 5.22 Plots of position residuals for baseline 100a – 300a from modelled and solved KINPOS with Ski-Pro for the Snowdon Trial on 16th June 2003.

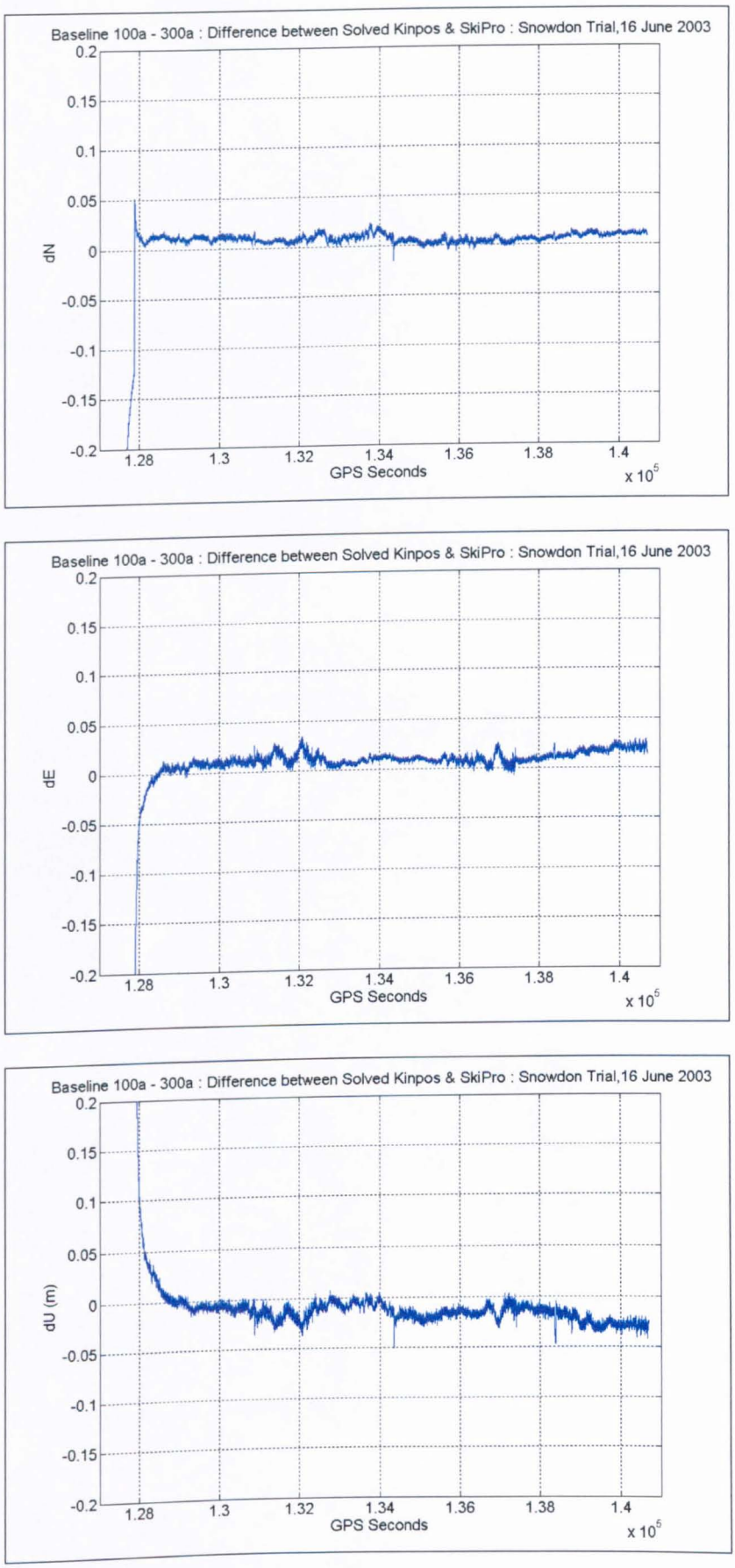

Figure 5.23 Plots of position residuals difference for baseline 100a – 300a between solved KINPOS and Ski-Pro for the Snowdon Trial on 16th June 2003.

5.5 Summary

It can be summarized that;

i. For baselines with a low difference in altitude (less than 100 metres), 'modelled KINPOS' produces similar results to Ski-Pro Version 3.0. This is due to the fact that relatively, the troposphere effects should be very small.

ii. For baselines with higher differences in altitude (400 and 1,000 metres), Ski-Pro Version 3.0 or 'solved KINPOS' should be used, as the 'modelled KINPOS' only takes into account the hydrostatic part of the troposphere.

iii. Data processed with Ski-Pro Version 3.0 can begin with resolved ambiguity as early as the start time for the data itself, which is the same as for 'modelled KINPOS'. However, for 'solved KINPOS', a convergence period is needed which results in a waste of data, which can be up to two hours. Whence, the total number of acceptable epochs is much greater with Ski-Pro Version 3.0 and 'modelled KINPOS', except for epochs where the ambiguities are not resolved.

iv. Comparing Ski-Pro Version 3.0 and 'solved KINPOS' as shown in Figure 5.23, the differences could be due to the fact that KINPOS do not take into account the wet delay for the base station. Although KINPOS attempt to take into account the total tropospheric delay with the solved option, there are still trends or patterns that are probably signs of un-mitigated troposphere and multipath in the position residuals, and also from changes in satellite geometry. This can be seen from all the plots of the position residuals where they show an undulating time series.

Based on the above findings, Ski-Pro Version 3.0 results were found to be more stable and consistent and hence, it was decided that for the purpose of this project in investigating the un-mitigated troposphere and multipath, only the results from Ski-Pro Version 3.0 would be used in the analysis for the remaining chapters.

Chapter 6

Analysis of Results from Static Stations

In this chapter, the author will investigate results from static stations only, using stations from the Snowdon and University Trial #1. Computed coordinates for the local GPS network for both trials can be seen in Appendix B. They were processed in static mode using Ski-Pro version 3.0 and averaged for the days of observation for the respective trial. These have then been used as the "true" values to obtain the position residuals for each epoch from the OTF kinematic processing. Overall, the coordinates were determined to a high precision as shown by their standard deviations in Table B1 (Snowdon Trial) with a maximum of 12 mm, and B3 (University Trial #1) of Appendix B with a maximum of 2 mm. Station 400b from the Snowdon Trial recorded poorer standard deviations than station 400a which could mean that it was experiencing disturbances, such as multipath. TEQC runs on the RINEX file for each station and plots of multipath, show that station 400b is the most affected by multipath, particularly on signals from SV07 and SV18 as can be seen in Figure 6.1.

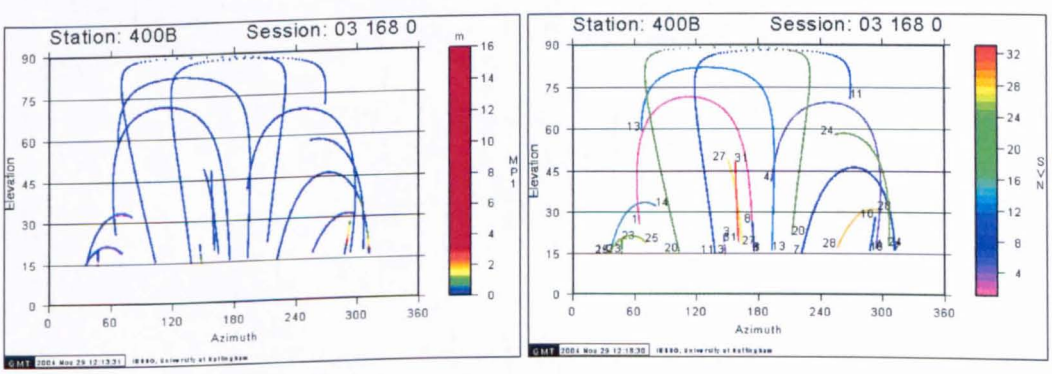

Figure 6.1 Multipath (MP) from TEQC runs on the RINEX file for station 400b on DOY 168 (17th June 2003) of the Snowdon Trial.

Sky plots of the satellite constellation also show that between the two days, all stations were observing the same satellites. An example of the plots from station 100a can be seen in Figure 6.2.

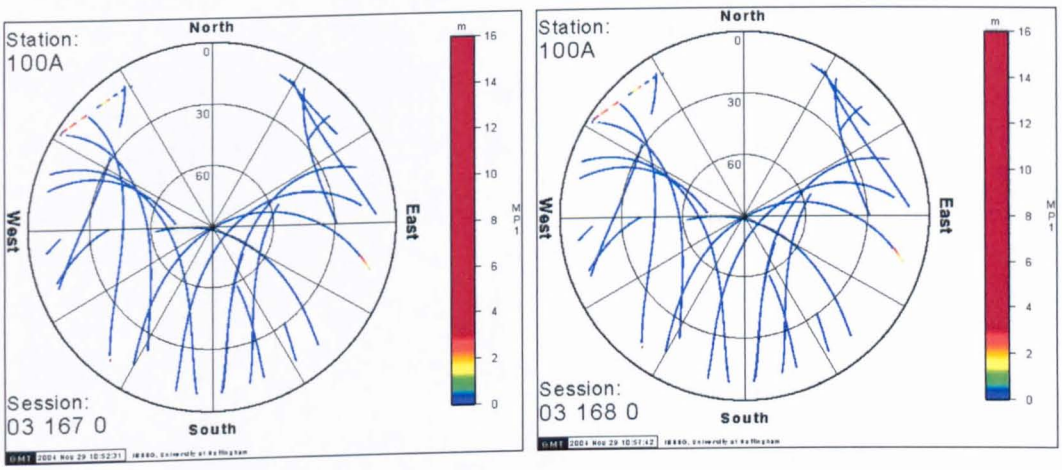

Figure 6.2 Sky plots of satellites as viewed from station 100a on DOY 167 (16th June 2003, left) and DOY 168 (17th June 2003, right) of the Snowdon Trial.

The data were processed in OTF kinematic mode using the whole duration of available epochs for all possible baselines, using station 100a as reference for the Snowdon Trial and tre1 for the University Trial #1. The plots of position residuals for the Snowdon Trial on the two days (16th and 17th June 2003) can be seen in Appendix C, and for the University Trial #1 on three days (19th to 21st May 2004) in Appendix D. For the Snowdon Trial time series, the main reason for the variation of the results for the two days around the 125,000 seconds mark, is that there were only four satellites available and a corresponding increase in GDOP. However, the plots show that GDOP alone cannot be used as a measure to quantify the quality of the results as e.g. baseline 100a – 300a, where, at the 135,000 seconds mark, there is the same GDOP value on both days but the position residuals are not the same. This means that other factors, such as un-mitigated troposphere and multipath exist and may be different during the respective period of observations.

To perform AF, we need to cross-correlate between baselines, hence, it is a must to have common epochs for each baseline. For the Snowdon Trial, due to the partial unavailability of data for station 100b on DOY 168 (17th June 2003), unresolved ambiguities mostly on station 400a, and a delayed start and early stop

time for the duration of observations, only a small period of common epochs were available if all stations were to be considered. A total of 3399 epochs were common to all baselines effectively from two periods: from 120,511 to 122,188 and 128,614 to 130,336 GPS seconds on DOY 167 (16th June 2003) and from 206,671 to 208,348 and 214,774 to 216,496 GPS seconds on DOY 168 (17th June 2003). The first part is before the period where the number of satellites was minimal and the other is after the period. The percentage of common data can be seen from Table 6.1; it varies because the start and end times of observation differ for each baseline. Looking at the baseline with the least period of observation, it can be seen that a maximum of 15.8% of data are available for analysis on DOY 167 (16th June 2003) and 35.1% on DOY 168 (17th June 2003).

	16th June 2003		17th June 2003	
Baseline	Total Seconds	% Usable	Total Seconds	% Usable
100a–100b	28,729	11.8	17,204	19.8
100a–200a / 300b	26,606	12.8	17,461	19.5
100a–300a	21,471	15.8	18,890	18.0
100a–400a	26,062	13.0	9,686	35.1
100a–400b	26,403	12.9	19,251	17.7

Table 6.1 Percentage of common data (3399 seconds) with respect to observed period for the Snowdon Trial on 16th and 17th June 2003.

Examples of plots of common data for the two days are shown in Figure 6.3 for baseline 100a – 400a, and Figure 6.4 for baseline 100a – 300a. The point where the selected epochs joins are also shown (at the 1,700 seconds mark).

Table 6.2 presents the mean and standard deviation of position residuals for the filtered baselines from station 100a. Here it can be seen that the difference between the mean on the two days is always less than 10 mm in dN, but can reach values of 40 mm in dE and 35 mm in dU. Since we know that this trial consists of static stations, with periods of poor GDOP removed, it is clear that values which could be wrongly interpreted as movements are still present. The maximum and minimum values of the position residuals for each baseline are shown in Table

6.3. These reinforce the potential for misinterpreted station movements, with ranges of up to 65 mm in dN, 100 mm in dE and 115 mm in dU.

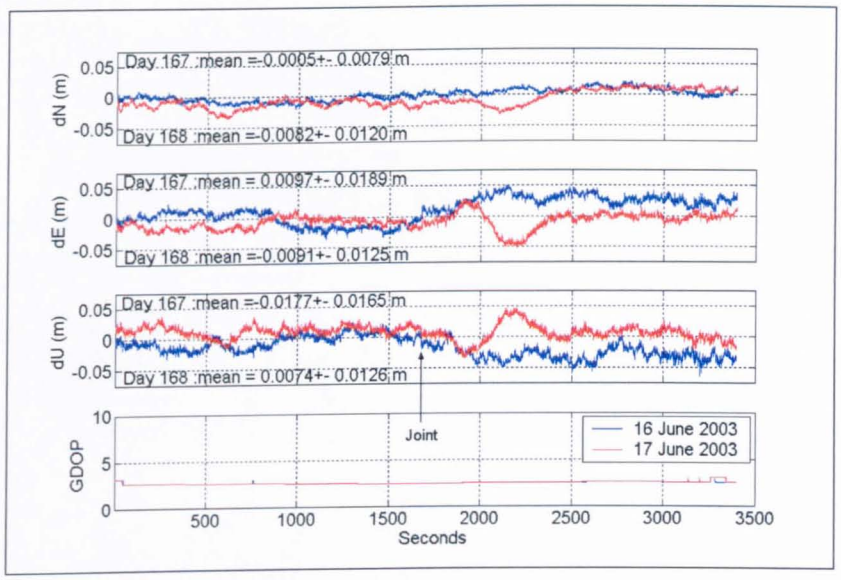

Figure 6.3 Selected position residuals and GDOPs for baseline 100a – 400a, on two days (DOY 167 and 168) of the Snowdon Trial on 16th and 17th June 2003.

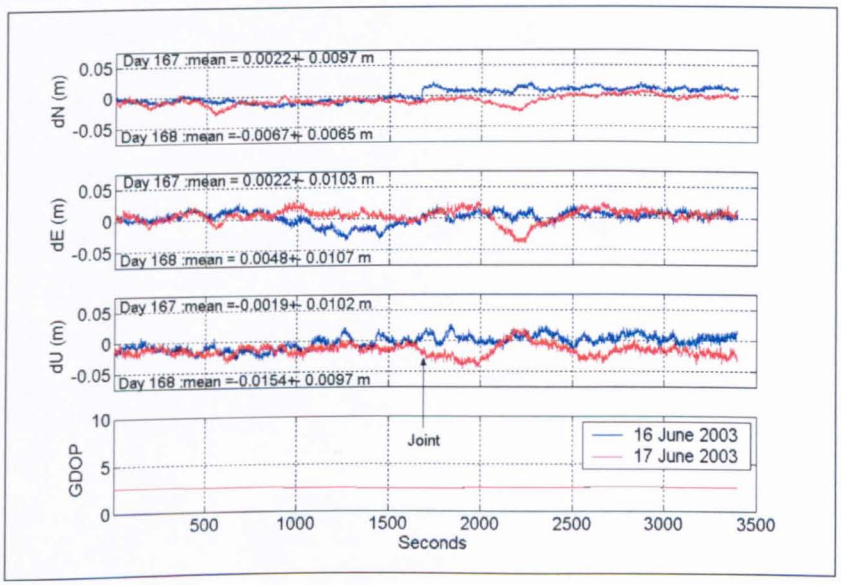

Figure 6.4 Selected position residuals and GDOPs for baseline 100a – 300a on two days (DOY 167 and 168) of the Snowdon Trial on 16th and 17th June 2003.

16 June 2003	dN (mm)		dE (mm)		dU (mm)	
Baseline	Mean	Std. Dev	Mean	Std. Dev	Mean	Std. Dev
100a–100b	-1.8	2.5	1.9	4.0	-2.0	4.8
100a–200a	-0.4	10.8	8.7	12.9	-17.8	9.3
100a–300a	2.2	9.7	2.2	10.3	-1.9	10.2
100a–400a	-0.5	7.9	9.7	18.9	-17.7	16.5
100a–400b	5.0	8.2	20.9	23.6	-23.5	24.8
17 June 2003	dN (mm)		dE (mm)		dU (mm)	
Baseline	Mean	Std. Dev	Mean	Std. Dev	Mean	Std. Dev
100a–100b	2.6	2.6	-3.2	4.0	2.3	4.6
100a–300b	-2.7	6.4	1.1	9.7	-3.3	8.9
100a–300a	-6.7	6.5	4.8	10.7	-15.4	9.7
100a–400a	-8.2	12.0	-9.1	12.5	7.4	12.6
100a–400b	-5.3	12.2	-19.8	13.5	11.4	15.7

Table 6.2 Mean and Standard Deviations of the position residuals for filtered baselines, from station 100a on DOY 167 and 168 of the Snowdon Trial on 16th and 17th June 2003.

16 June 2003	dN (mm)		dE (mm)		dU (mm)	
Baseline	Min	Max	Min	Max	Min	Max
100a–100b	-12.0	6.2	-15.5	16.5	-19.8	15.5
100a–200a	-24.1	22.4	-29.8	42.7	-50.0	23.6
100a–300a	-20.7	21.2	-34.9	26.6	-30.2	26.5
100a–400a	-21.4	20.2	-38.0	48.5	-64.6	24.2
100a–400b	-19.2	27.0	-37.7	64.2	-76.3	39.5
17 June 2003	dN (mm)		dE (mm)		dU (mm)	
Baseline	Min	Max	Min	Max	Min	Max
100a–100b	-6.1	10.8	-17.9	11.9	-13.4	19.1
100a–300b	-2.4	12.6	-41.7	24.3	-30.1	32.4
100a–300a	-29.5	10.2	-40.0	32.6	-46.5	20.6
100a–400a	-37.5	17.9	-54.8	27.6	-34.9	45.8
100a–400b	-36.5	26.5	-69.7	17.1	-32.1	55.2

Table 6.3 Minimum and Maximum values of the position residuals for filtered baselines from station 100a on DOY 167 and 168 of the Snowdon Trial on 16th and 17th June 2003.

For the University Trial #1, about six hours of common data were available (i.e. from 10:00 to 14:00 hours) with only a small period with GDOP values above 5, which occured at the 301,000 GPS seconds mark. Full length plots of the position residuals from this trial can also be seen in Appendix C.

Re-considering Figures 6.3 and 6.4 again, from the values of GDOP, we can see that despite having the same satellite geometry, the position residuals differ with time. In a general case, the position residual (δ) for each epoch can be said to consist of the following:

$$\delta = \delta\rho_{un-mitigatedtrop} + \delta\rho_{mp} + \delta\rho_{receivernoise} \qquad [6.1]$$

where

$\delta\rho_{un-mitigatedtrop}$ - relative un-mitigated troposphere for the baseline

$\delta\rho_{mp}$ - combined multipath for the baseline

$\delta\rho_{receivernoise}$ - combined receiver noise for the baseline

To attempt to identify each of the above components, AF was run with several combinations of baselines as follows,

a. Stations at the same altitude.
These tests involved both baselines which are very short (distances of less than 15 metres, i.e. 100a to 100b, 400a to 400b from the Snowdon Trial and twr1 to twr2 from the University Trial #1) and a baseline of about 800 metres, (i.e. tre1 to sc1 from the University Trial #1).

b. Stations with a small difference in altitude, i.e. less than 100 metres.
These tests involved baselines from 100a/100b to 400a/400b from the Snowdon Trial, and tre1/sc1 to twr1/twr2 from the University Trial #1, with lengths of about 9 km and 1 km respectively.

c. Stations with a large difference in altitude, i.e. about 1,000 metres. These tests involved baselines from 100a/100b to 300a, 300b and 200a (difference in altitude of about 400 m) from the Snowdon Trial.

The results of these tests are presented in sections 6.1, 6.2 and 6.3 respectively.

6.1 Tests on Stations at the same altitude

For this test, the aim was to identify if both stations were experiencing the same multipath effects or not. Relative un-mitigated troposphere was considered to be zero, since these baselines are very short, less than 15 metres, and the stations are at the same altitude. Thus, leaving the effects of combine multipath (if any) and receiver noise.

AF runs were made on baselines 100a – 100b and 400a – 400b between the two days from the Snowdon Trial [16th – 17th (Forward) and 17th – 16th June 2003 (Backward)]. The results were as shown in Figure 6.5 for baseline 100a – 100b and Figure 6.6 for 400a – 400b. For baseline 100a – 100b, there is no clear indication of multipath in all three components. This means that both stations are either experiencing the same multipath effects or have no significant multipath at all. This is supported by their weak correlations of -0.0577 (dN), -0.0352 (dE) and -0.0619 (dU). For baseline 400a – 400b, it is evident that both stations are experiencing different multipath effects as can be seen in the common part (COM) around the 1,500 seconds and 3,000 seconds marks. The effect of multipath varies at around 20 mm in dN, 40 mm in dE and 60 mm in dU. Furthermore, the un-common part (OUT) for this baseline was noisier, due to their location by the road-side, introducing not only permanent multipath, but also temporary multipath, from passing vehicles. Such events can be seen by the sharp spikes in the OUT part of the dU component.

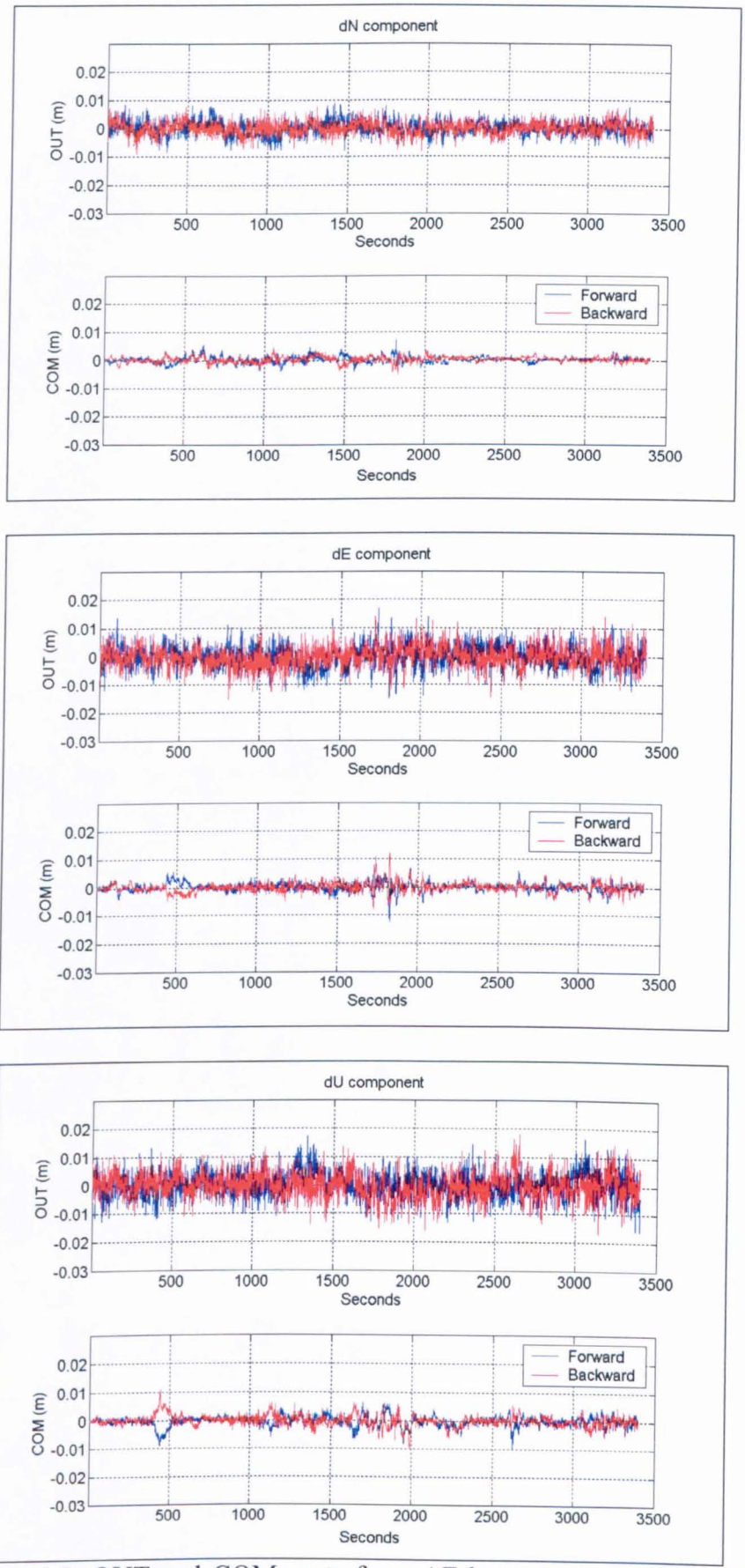

Figure 6.5 OUT and COM parts from AF between two days (DOY 167 and 168), Forward (DOY 167 as Reference and DOY 168 as Desired) and Backward (DOY 168 as Reference and DOY 167 as Desired) for baseline 100a – 100b from the Snowdon Trial, 16th and 17th June 2003.

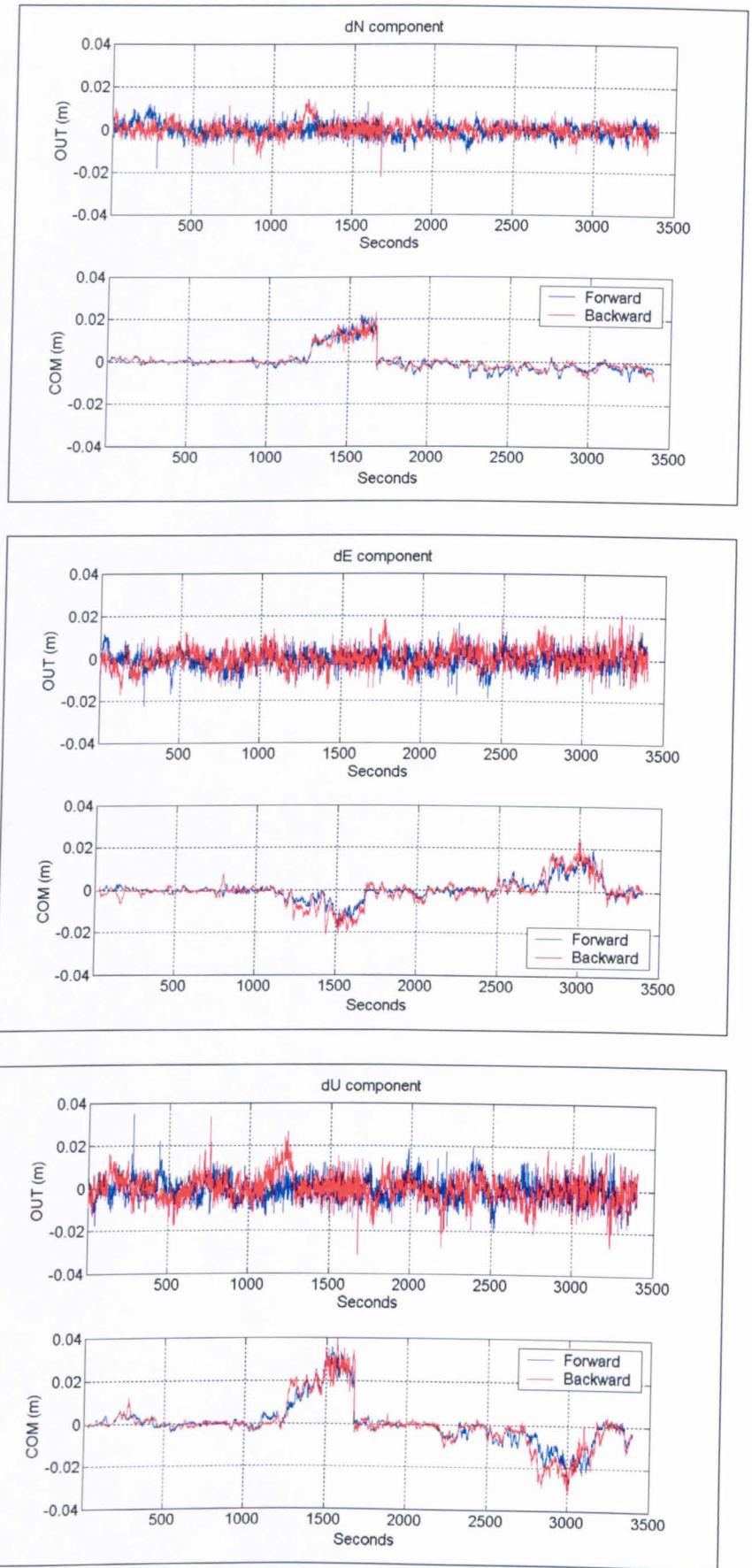

Figure 6.6 OUT and COM parts from AF between two days (DOY 167 and 168), Forward (DOY 167 as Reference and DOY 168 as Desired) and Backward (DOY 168 as Reference and DOY 167 as Desired) for baseline 400a – 400b from the Snowdon Trial, 16th and 17th June 2003.

The RMS of OUT (noise) and COM (multipath) parts can be seen in Table 6.4. High RMS values were recorded for baseline 400a – 400b and the strong correlations in all three components [0.7208 (dN), 0.5549 (dE), 0.7416 (dU)] suggest that multipath has been successfully isolated from the time series for this baseline.

RMS	16th–17th June 2003			17th–16th June 2003		
OUT part	Units in millimetres (mm)					
Baselines	dN	dE	dU	dN	dE	dU
100a–100b	2.5	3.9	4.4	2.4	3.8	4.6
400a–400b	3.2	4.2	5.3	3.3	5.0	6.4
COM part						
100a–100b	1.1	1.5	1.9	1.0	1.7	2.0
400a–400b	5.4	4.9	9.4	4.8	6.3	10.5

Table 6.4 RMS of OUT(noise) and COM (multipath) parts after AF between two days (DOY 167 and 168) for very short baselines with the same altitude from the Snowdon Trial on 16th and 17th June 2003.

Further checks were made on stations 400a and 400b to verify which station causes the difference. The COM part plots (possible multipath) for the dU component from AF runs using DOY 167 (16th June 2003) as Reference and DOY 168 (17th June 2003) as Desired, can be seen in Figure 6.7 (left), and vice-versa (right). These show that the multipath was at station 400b not station 400a.

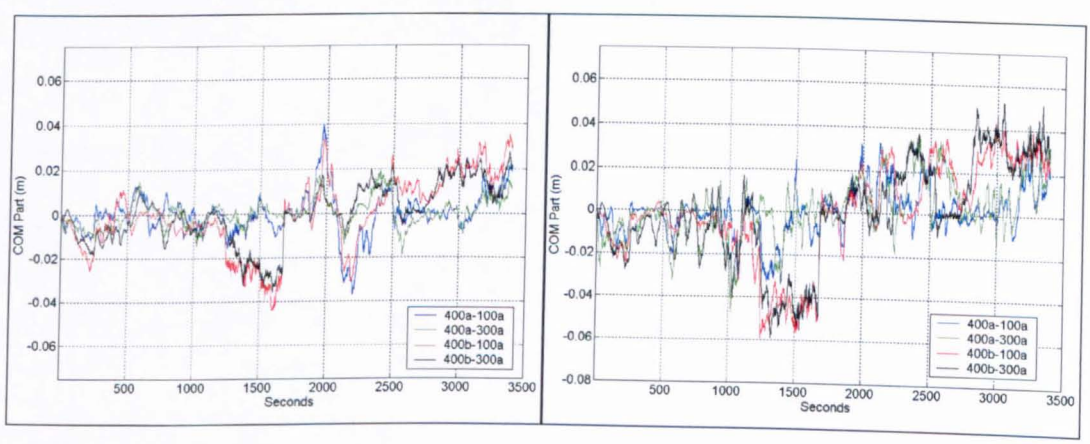

Figure 6.7 Multipath in the dU component from stations 400a and 400b to 100a and 300a respectively from AF for combinations 16th – 17th (left) and 17th – 16th (right) for the Snowdon Trial on 16th and 17th June 2003.

For the University Trial #1, results from runs of AF for baseline twrl to twr2 between days (19^{th} with 20^{th} May, and 20^{th} with 21^{st} May) are shown in Figure 6.8. Although both stations, twrl and twr2 are on top of a tower building, and were expected to be free of multipath, the results from AF suggest that multipath is present most likely due to the existence of other steel structures on top of the tower. However, their magnitude (as the COM part) can be considered as small with the maximum of ±10 mm in the dU component, which is smaller than the noise (OUT part).

Two days	19^{th}–20^{th} May 2004			20^{th}–21^{st} May 2004		
Baselines	dN	dE	dU	dN	dE	dU
twrl–twr2	0.2114	0.2399	0.1890	0.2131	0.2116	0.1715
trel–scl	0.4175	0.4601	0.2484	0.3563	0.4332	0.3131

Table 6.5 Correlations from AF runs between two consecutive days from the University Trial #1 on 19^{th} to 21^{st} May 2004.

Refering to Figure 6.9, for baseline trel to scl which is about 800 metres but with the stations at the same altitude, the trends for the noise and multipath were different. Although there seems to be a pattern of multipath, it is continously being disturbed by sharp spikes which might be due to passing vehicles at station scl. The plots shows that multipath does exist on the baseline between trel and scl, and confirm the assumption of zero un-mitigated troposphere as the noise is more stable, apart from the sharp spikes due to passing vehicles.

Based on these results, for this University Trial #1, further AF runs will be made using baselines from trel to twrl and twr2 as it has been shown that between twrl and twr2, a maximum effect of multipath of magnitude about ±10 mm can be expected in the dU component.

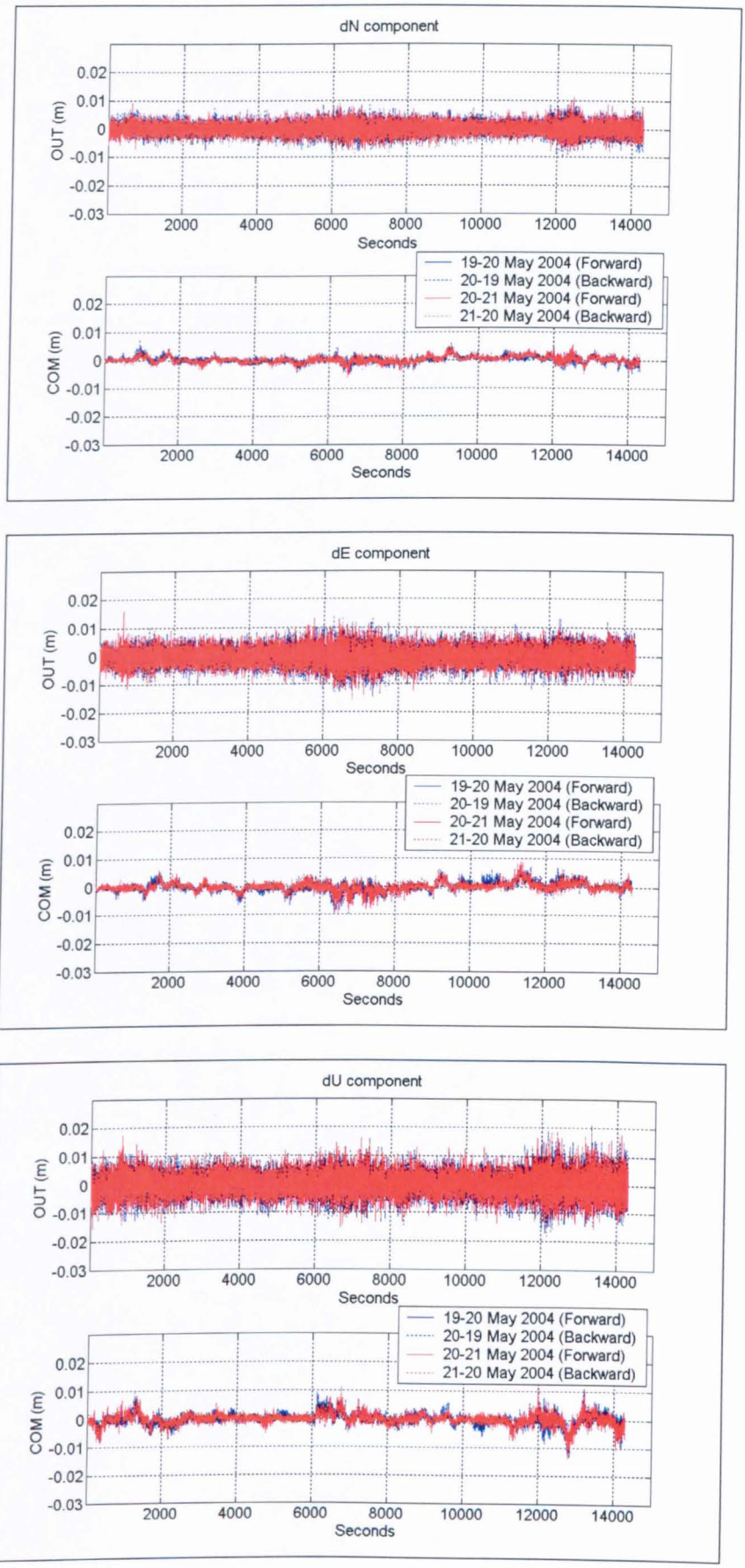

Figure 6.8 OUT and COM parts from AF between days for baselines twr1 to twr2 from the University Trial #1 on 19th to 21st May 2004.

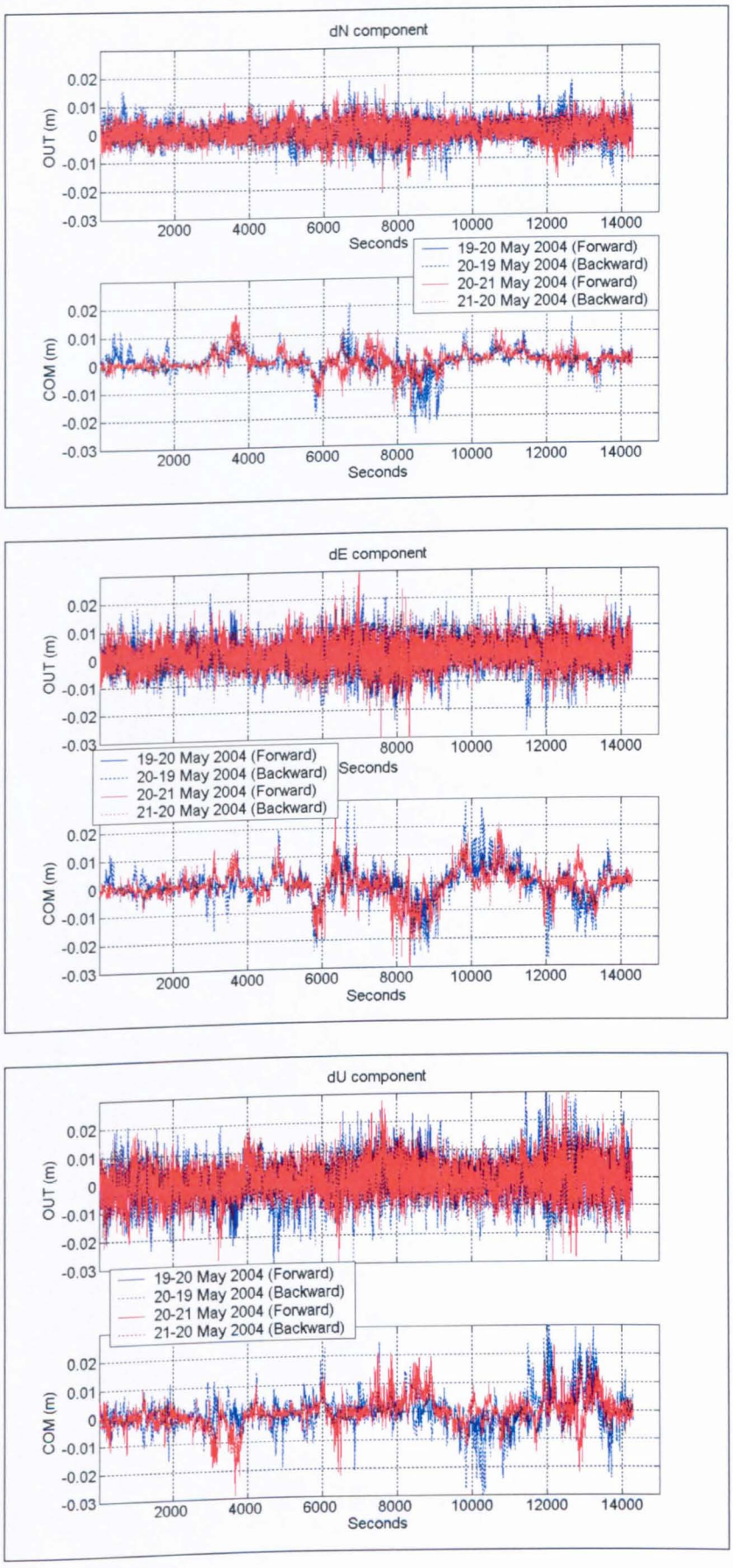

Figure 6.9 OUT and COM parts from AF between days for baselines tre1 to sc1 from the University Trial #1 on 19th to 21st May 2004.

6.2 Tests on Stations with a small difference in altitude

These tests involve stations 100a and 100b to 400a from the Snowdon Trial. These are about 48 metres different in altitude and about 9 km apart. AF runs were carried out between baselines 100a – 400a and 100b – 400a on the same day to isolate noise from un-mitigated troposphere and multipath. The AF was run twice for each pair of baselines, firstly, with 100a – 400a as reference and 100b – 400a as desired (forward), secondly, with 100b – 400a as reference and 100a – 400a as desired (backward). The reason for running the AF in such a way is that, if there are any trends or patterns in the time series, they should be shown in both runs. The plots of the OUT and COM parts of the above runs are shown in Figures 6.10 and 6.11 respectively and the correlations are given in Table 6.6. It can be seen that the COM part has been successfully separated in all three components due to the high correlations between the two time series, as can be seen in Table 6.6. Since it has been shown in Section 6.1 that 100a and 100b were both could be experiencing the same effects of multipath, the time series for the forward and backward runs of AF were almost identical.

In this case, the OUT part should be the receiver noise while the COM part consists of the un-mitigated troposphere and multipath. The RMS for each component for the two days are as shown in Table 6.7 while the ranges i.e. the difference between maximum and minimum values for both the OUT and COM part are shown in Table 6.8.

From Figure 6.11, we can see that the variations are quite small in the dN component with ranges of about $\pm$20 mm on 16th June 2003, but slightly higher on 17th June 2003. The variations in the dE and dU components were almost the same with ranges of about $\pm$40 mm for both days. However, the trends between the two days were totally different even though each station was looking at the same satellites for both days. Between the two days, the RMS differs by about +5 mm, -7 mm and +5 mm in dN, dE and dU components respectively.

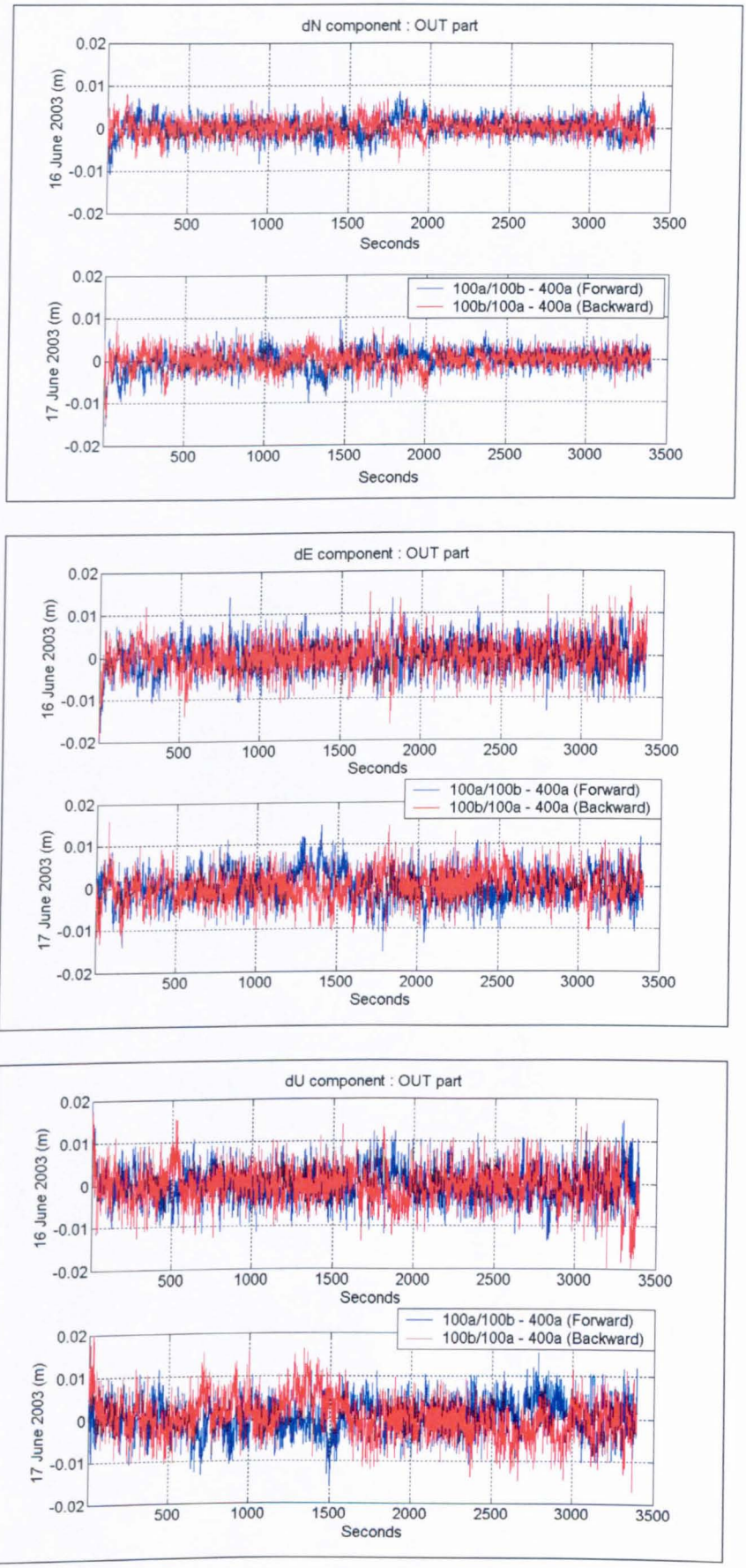

Figure 6.10 OUT part from the AF for baselines from 100a/100b to 400a on the same day from the Snowdon Trial on 16th and 17th June 2003.

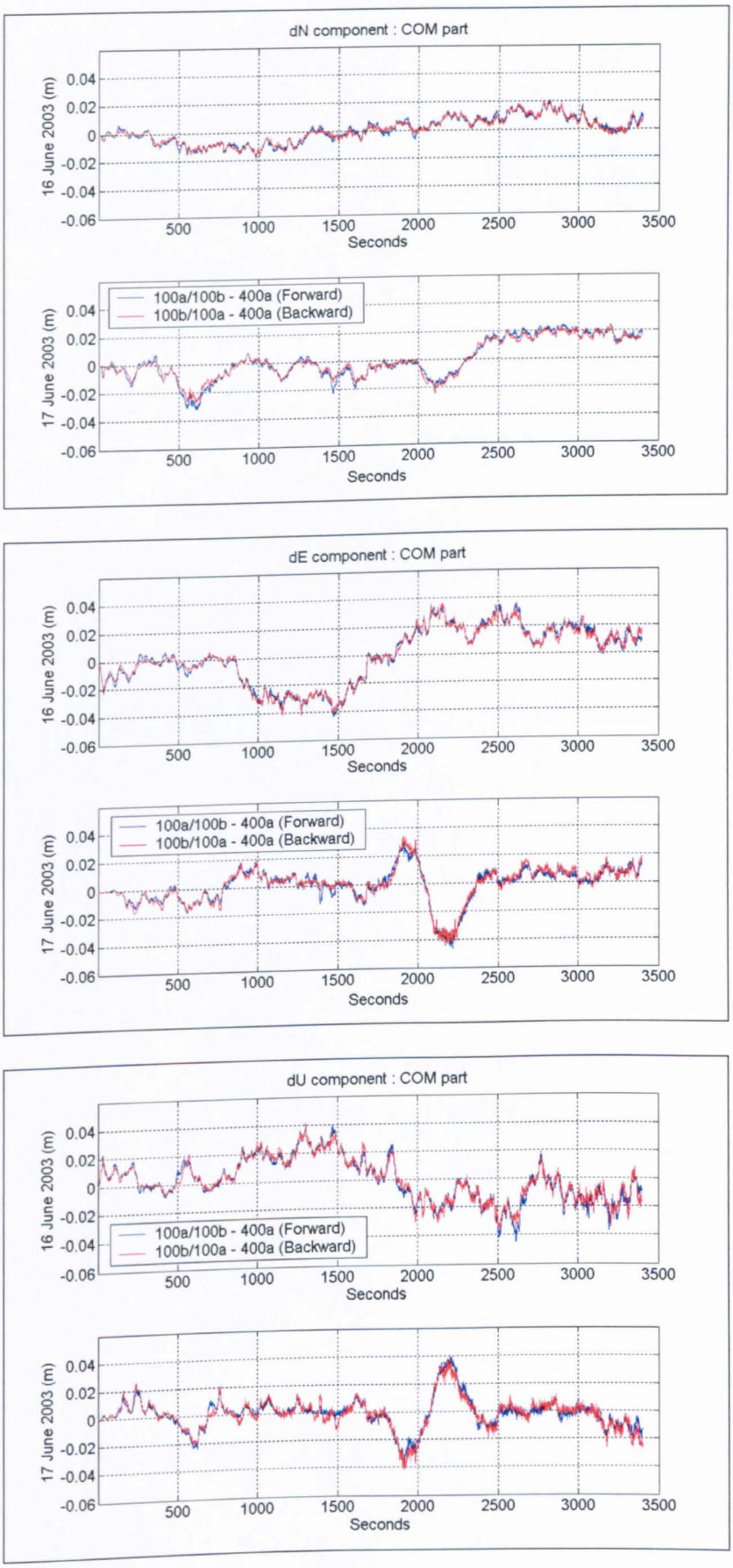

Figure 6.11 COM part from the AF for baselines from 100a/100b to 400a on the same day from the Snowdon Trial on 16th and 17th June 2003.

Same day	16th June 2003			17th June 2003		
Baselines	dN	dE	dU	dN	dE	dU
100a/100b–400a	0.9481	0.9762	0.9548	0.9748	0.9394	0.9016
100a/100b–400b	0.9514	0.9866	0.9832	0.8311	0.9364	0.9308

Table 6.6 Correlations for AF runs on same day for baselines with a low difference in altitude from the Snowdon Trial on 16th and 17th June 2003.

RMS	16th June 2003			17th June 2003		
OUT Part	Units in millimetres (mm)					
Baselines	dN	dE	dU	dN	dE	dU
100a/100b–400a	2.4	3.7	4.2	2.5	3.7	4.1
100b/100a–400a	2.2	3.9	4.5	2.4	3.7	4.8
COM part						
100a/100b–400a	7.9	18.8	16.4	12.9	11.8	11.1
100b/100a–400a	7.6	18.4	15.7	11.7	11.9	11.6

Table 6.7 RMS of OUT and COM parts from AF on the same day for stations with low difference in altitude from the Snowdon Trial on 16th and 17th June 2003.

Ranges (max – min)	16th June 2003			17th June 2003		
	Units in millimetres (mm)					
Baselines	dN	dE	dU	dN	dE	dU
OUT part						
100a/100b–400a	19.3	34.7	36.6	25.0	29.9	31.1
100b/100a–400a	16.5	35.8	42.1	24.1	28.8	37.9
COM part						
100a/100b–400a	39.1	79.9	86.1	56.4	77.5	76.5
100b/100a–400a	38.7	78.7	75.8	50.9	78.0	80.9

Table 6.8 Ranges from minimum and maximum values of OUT and COM parts from AF on the same day for stations with low difference in altitude from the Snowdon Trial on 16th and 17th June 2003.

Further AF runs between these two days were made to isolate the un-mitigated troposphere and multipath using the COM part from Figure 6.11 above. These are as shown in Figure 6.12 and Figure 6.13 show the results for baseline 100a – 400a only. Since, station 100b has the same multipath as station 100a (if any exist as shown in section 6.1), the result from 100b to station 400a was the same, hence, it is not shown here. Comparing between Figures 6.12 and 6.13, we can see that the COM parts (multipath) are almost identical, while the OUT parts (un-mitigated troposphere) differs in magnitude. Their correlations (in Table 6.6) were also the same, which means that it does not matter which combination is run with AF first. It can either be first, for the same day and followed by between days, or vice-versa.

Theoretically, the results shown in the plots of Figure 6.12 should be the separated values for un-mitigated troposphere (OUT part) and multipath (COM part). However, this is not the case, as results from AF runs are dependent on the patterns of the desired time series. If there were to be multipath, the trend should be almost identical as it is well known that multipath will repeat itself daily. For example, looking at the dU plots (COM part) in either Figure 6.12 or 6.13, it is clear that the reversed pattern between the 2,000 to 2,500 seconds (brown) marks is not multipath; and so for any epochs which have significant differences in results from forward and backward runs, it is difficult to separate between un-mitigated troposphere and multipath.

For the dN component, the trends or patterns of the COM part show that multipath probably exists. This is supported by the strong correlation value of 0.5764 registered for the two baselines for the two days (given in Table 6.9). However, since it has been shown before, that for baseline 100a to 100b (Figure 6.5), there is no sign of significant differences, hence, the almost same pattern about the 600 and 2,500 to 3,000 seconds marks (pink), which could be interpreted as multipath but could also be un-mitigated troposphere with the same frequency between the two days. Considering the difference in antenna heights between the two days as mentioned in chapter 4, the above patterns could also be multipath. For this case, periods around the 1,200 seconds mark (green) could be multipath with a magnitude of about 15 mm. For the dE and dU components, it is evident that no

significant multipath exists as can be seen from Figure 6.12, and backed up by their low correlations of –0.1619 and 0.0929 respectively in Table 6.9.

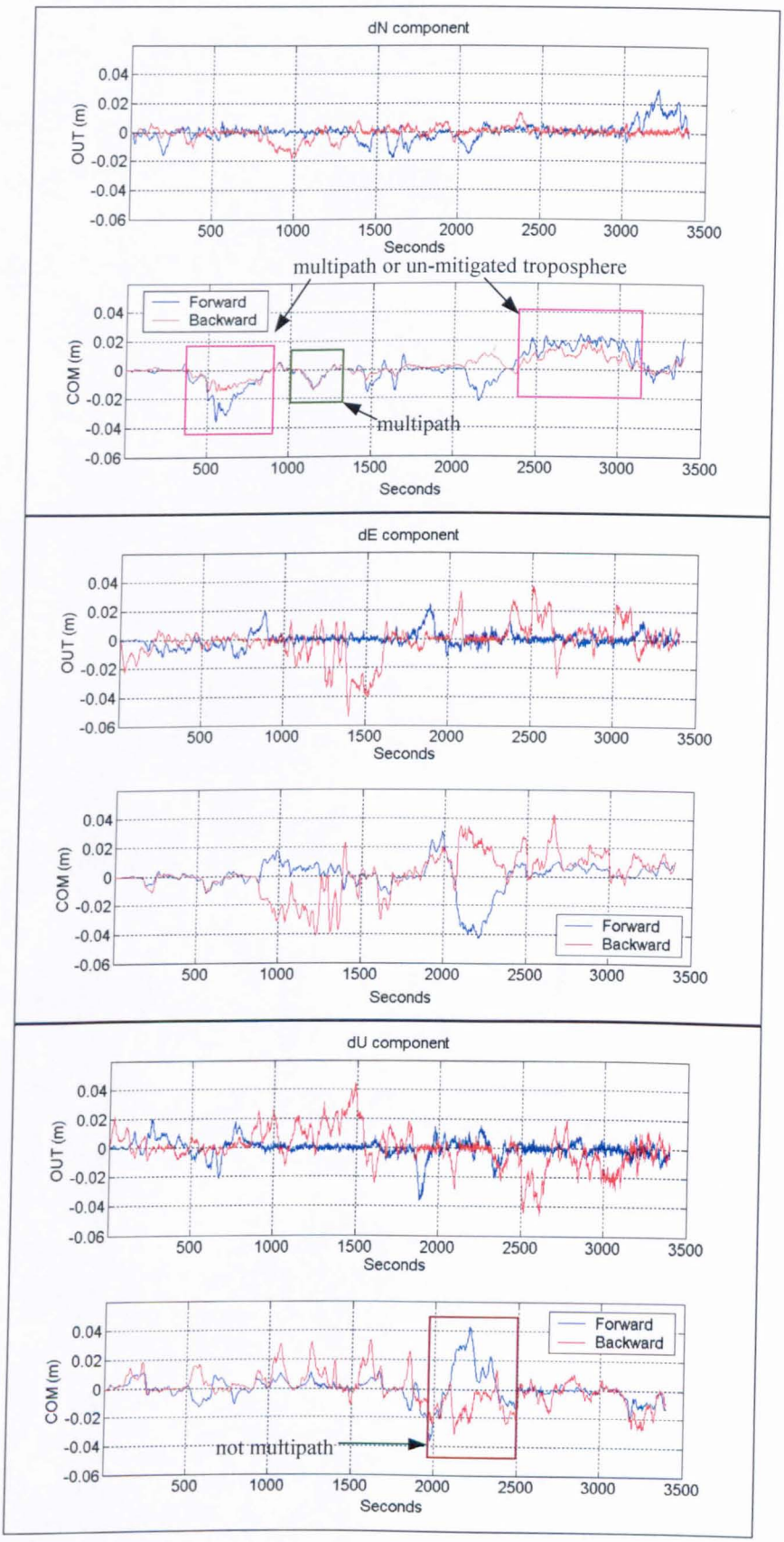

Figure 6.12 OUT and COM parts for baseline 100a/100b to 400a using the COM part (from same day) from AF between two days [(Forward (16^{th}–17^{th}), and Backward (17^{th}–16^{th})] from the Snowdon Trial on 16^{th} and 17^{th} June 2003.

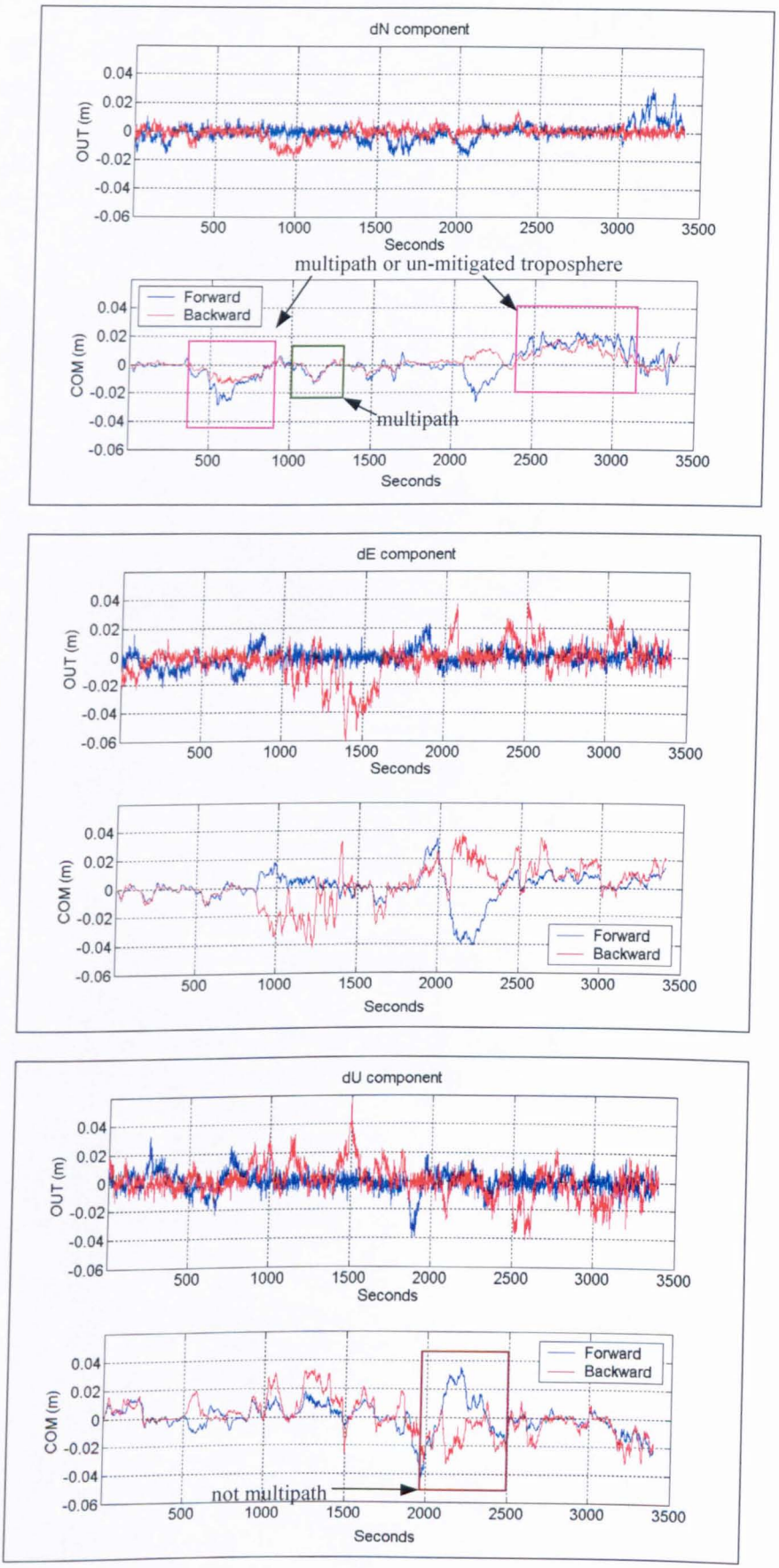

Figure 6.13 OUT and COM parts for baseline 100a–400a from AF between two days [(Forward (16^{th}–17^{th}), and Backward (17^{th}–16^{th})] from the Snowdon Trial on 16^{th} and 17^{th} June 2003.

Two days	16^{th}–17^{th} June 2003		
Baselines	dN	dE	dU
100a/100b–300a	0.4881	0.0277	-0.0159
100a/100b–400a	0.5764	-0.1619	0.0929
100a/100b–400b	0.4511	0.2263	0.6070

Table 6.9 Correlations for AF runs using COM parts from same day for two days from the Snowdon Trial on 16^{th} and 17^{th} June 2003.

For these combinations, we can summarize that un-mitigated troposphere is the dominant factor that influences the position residuals with no significant multipath present except for the dN component. Hence, results of the OUT part from Figure 6.10 of AF runs for the same day gives the noise in the time series, while the COM part (Figure 6.11) is the un-mitigated troposphere. We can then conclude that the un-mitigated troposphere varies in magnitude by ±20 mm in the dN component and ±40 mm in the dE and dU components, with the noise is maximum in the dU component at about ±10 mm.

Results from the University Trial #1 provided better checking for multipath as they have three days of observations (19^{th} to 21^{st} May 2004), so for multipath detection, two sets of consecutive day combinations could be made i.e. (19^{th} and 20^{th}, and 20^{th} and 21^{st} May 2004).

AF runs on a pair of baselines from station trel to twrl and twr2 on the same day for each of the three days were carried out. The AF runs were carried out with first: baseline trel – twrl as reference and trel – twr2 as desired (Forward), and then, baseline trel – twr2 as reference and trel – twrl as desired (Backward). The RMS for the OUT part on each day were similar, in all three components as can be seen in Table 6.10, with the lowest in the dN component and highest in the dU component. A sample plot of the OUT part, assumed to be receiver noise, time series is shown in Figure 6.14 for 19^{th} May 2004.

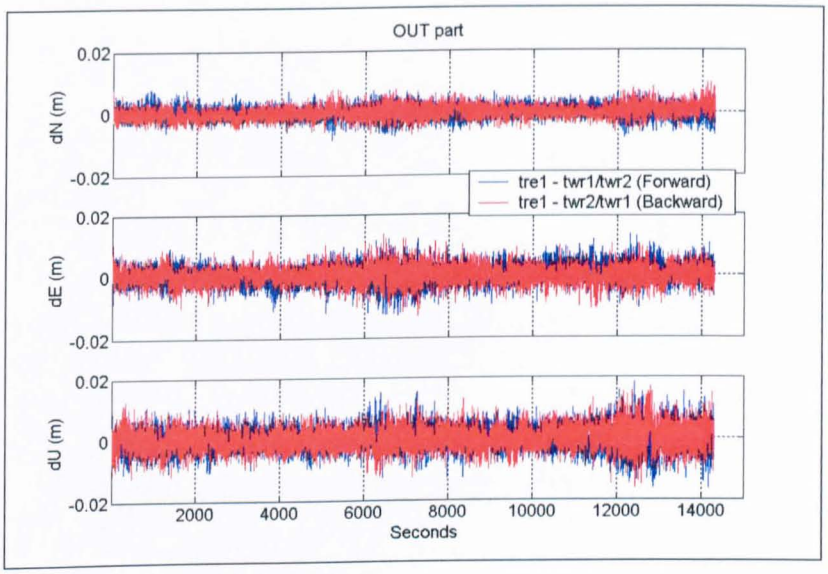

Figure 6.14 OUT part from AF for baseline tre1 to twr1/twr2 from the University Trial #1 on 19th May 2004.

RMS	OUT Part			COM Part		
tre1–twr1/2	Units in millimetres (mm)					
Day	dN	dE	dU	dN	dE	dU
19th May 2004	2.0	3.0	3.6	5.0	6.8	8.4
20th May 2004	1.9	2.9	3.6	3.1	3.9	5.0
21st May 2004	2.0	2.8	3.6	4.8	6.0	7.0

Table 6.10 RMS of OUT and COM part from AF on same day for stations with a small difference in altitude from the University Trial on 19th to 21st May 2004.

A plot of the time series for the COM part for each component for the three days is shown in Figure 6.15. The common (COM) part which comprises of the un-mitigated troposphere and multipath shows different trends between days for each component which suggests that the sites were experiencing different troposphere effects since they have the same constellation of satellites visible. Here, we can see that there is a possibility of multipath about the 4,000 seconds mark (pink) in the dN component, but there is no clear repetition of a trend on any other epochs in all three components. Here, it should also be noted that the RMS of the COM part on 20th May 2004 is lower than other days by about 2 to 3 mm. Table 6.11 also shows that smaller ranges were recorded for 20th May 2004 as compared to the 19th and 21st May 2004.

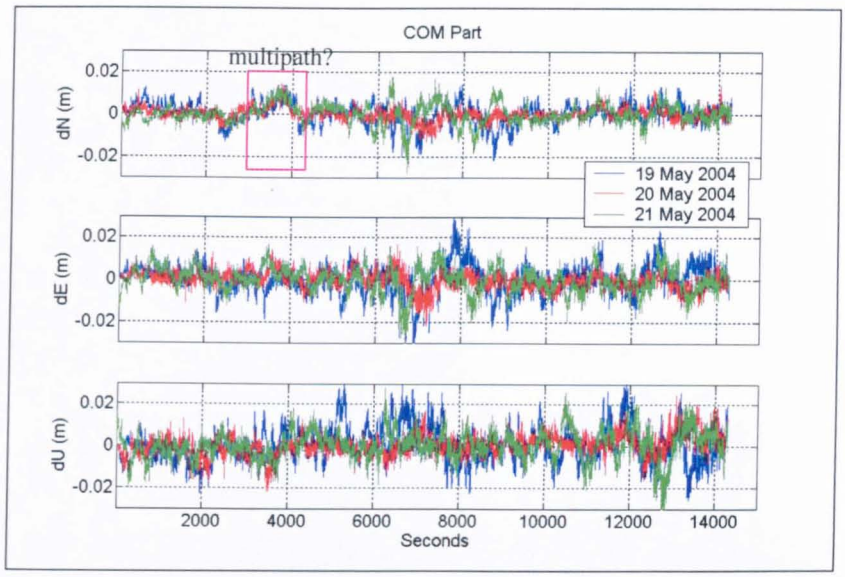

Figure 6.15 COM part from the AF for baseline tre1 to twr1/twr2 on the same day from the University Trial #1 on 19th to 21st May 2004.

Ranges (max – min)	OUT part			COM part		
tre1–twr1/2	Units in millimetres (mm)					
Day	dN	dE	dU	dN	dE	dU
19th May 2004	17.0	25.7	34.6	39.2	66.1	61.5
20th May 2004	16.4	27.8	39.2	27.5	38.7	46.3
21st May 2004	19.1	24.4	34.0	46.0	50.8	67.5

Table 6.11 Ranges from minimum and maximum values of OUT and COM part from AF on the same day for stations with a small difference in altitude from the University Trial #1 on 19th to 21st May 2004.

Baselines tre1–twr1/twr2			
Same day	dN	dE	dU
19th May 2004	0.9084	0.8950	0.8934
20th May 2004	0.8096	0.7617	0.7648
21st May 2004	0.9078	0.8731	0.8516

Table 6.12 Correlations for AF runs on the same day from the University Trial #1 on 19th to 21st May 2004.

To investigate multipath, runs of AF between two consecutive days using the COM part from the same day AF were carried out with the combinations of day 19th and 20th, and 20th and 21st May 2004. The combinations being 19th May as reference and 20th May 2004 as desired (Forward), 20th May as reference and 19th May 2004 as desired (Backward), and the same settings applied for the 20th and 21st May 2004 combination. The results of this are shown in Figures 6.16 (19th and 20th May 2004) and 6.17 (20th and 21st May 2004). Here, we can see that for the COM part of the dN component, there is a repetitive trend around the 3,000 to 4,000 seconds mark (pink). This was registered for both combinations (Figures 6.16 and 6.17) and is surely an indication of multipath, as it is shown that the same trend occurs on all three days. The trend at the 7,000 seconds mark (brown), could also be interpreted as multipath but with the reversed trend as can be seen in the 20th and 21st combination (Figure 6.17, brown), it is not multipath. Instead, it could be un-mitigated troposphere with the same frequency on the 19th and 20th May 2004. The same phenomenon can also be seen in the dE component, around the 7,000 seconds mark (brown), and in the dU component about the 2,000 and 12,000 seconds marks (brown). Their correlations are shown in Table 6.13 and are low. Hence, it can be concluded that un-mitigated troposphere dominates the time series with the period around the 7,000 seconds mark in the dN component an indication of un-mitigated troposphere.

Two days	tre1-twr1/twr2		
Baselines	dN	dE	dU
19 & 20 May 2004	0.3847	0.2188	0.1815
20 & 21 May 2004	0.2054	0.1146	0.2026

Table 6.13 Correlations for AF runs using COM parts for two days from the University Trial #1 on 19th to 21st May 2004.

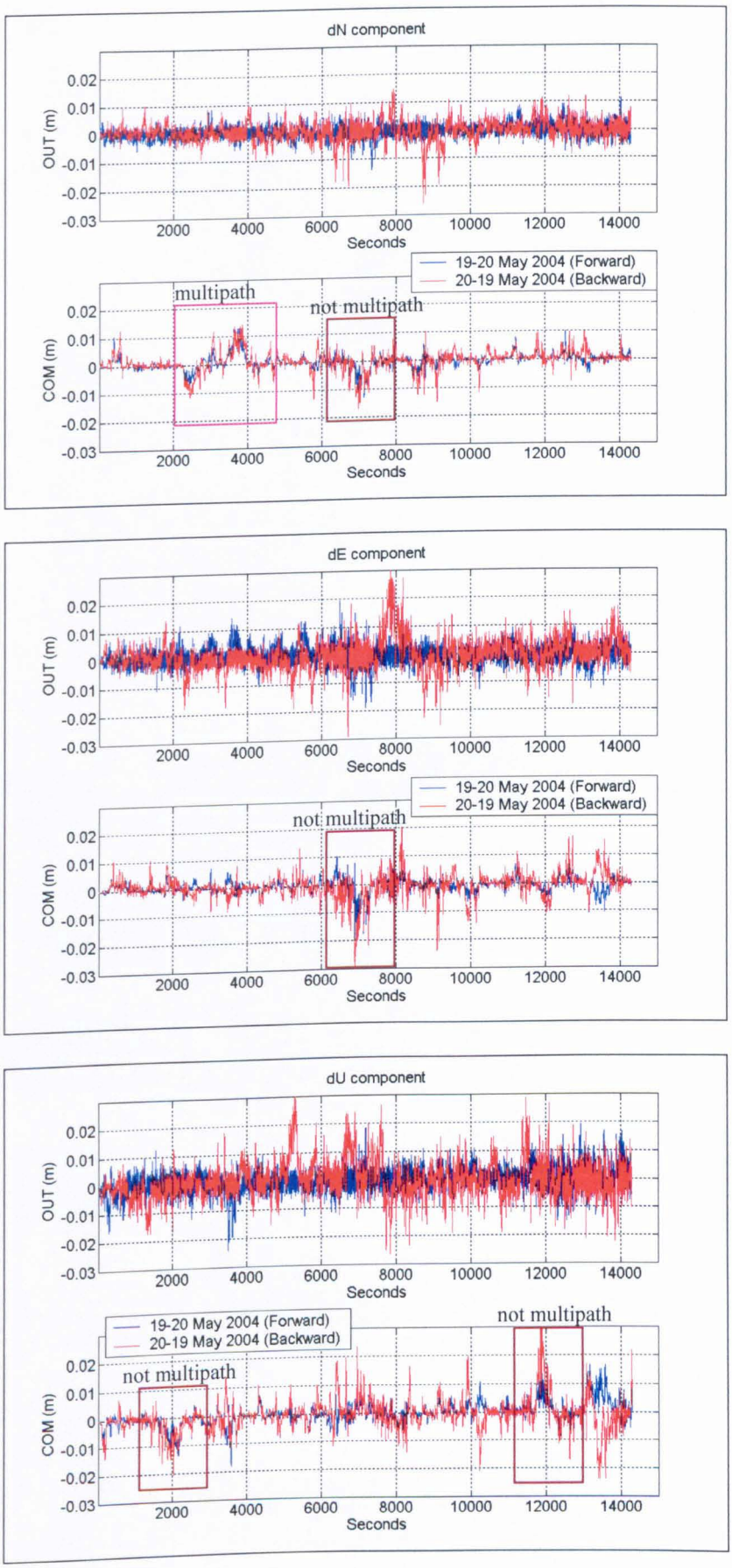

Figure 6.16 OUT and COM part on two consecutive days using the COM part from the same day (tre1 – twr1/twr2), AF runs with combinations 19th and 20th May 2004 from the University Trial #1.

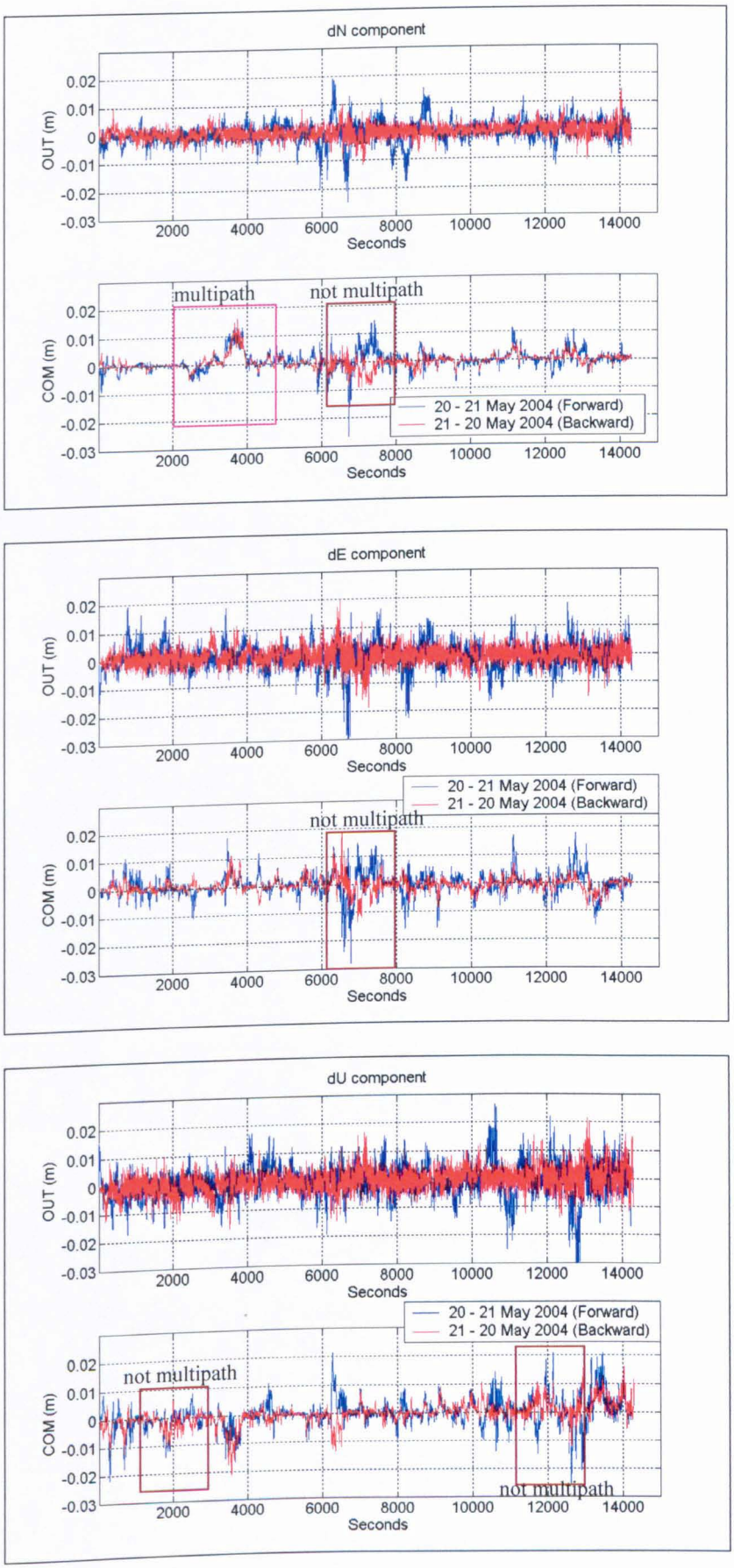

Figure 6.17 OUT and COM part on two consecutive days using the COM part from the same day (tre1 – twr1/twr2), AF runs with combination 20th and 21st May 2004 from the University Trial #1.

6.3 Tests on Stations with a high difference in altitude

In these tests, the baselines involved were from 100a and 100b to 300a, 200a and 300b from the Snowdon Trial. Station 300a is about 5.7 km from 100a with 970 m difference in altitude, station 200a is about 2.7 km with about 400 m difference in altitude and 300b is 5.2 km with 960 m difference in altitude. It should be noted that due to available data at station 200a on 16th June 2003 and 300b on 17th June 2003, only same day AF were performed for baselines involving these stations.

For station 300a, same day AF runs were made using first: baseline 100a – 300a as reference and 100b – 300a as desired (Forward), and 100b – 300a as reference with 100a – 300a as desired (Backward). The plots for both days are as shown in Figure 6.18 (OUT part) and Figure 6.19 (COM part). From both plots, we can see that the OUT and COM part have been successfully extracted. This is supported by their high correlations as in Table 6.14.

The RMS for the OUT and COM parts are as shown in Table 6.15 while the ranges (difference between maximum and minimum) are shown in Table 6.16. Looking at the plots in Figure 6.18, the OUT part (noise) was more consistent between the two days with dU registering the highest RMS value of $\pm$4 mm. The RMS of the COM part (Table 6.15), were around $\pm$10 mm on 16th June 2003 in all three components but slightly lower on 17th June 2003. The trends of the COM part (un-mitigated troposphere and multipath) were different between the two days suggesting that the stations were experiencing different weather conditions for the two days as mentioned in chapter 4. From Figure 6.19, we can see that the variations are quite small in the dN component with ranges of about $\pm$20 mm on 16th June 2003, but slightly higher on 17th June 2003. The variations in the dE component were almost the same with ranges of about –40 mm to +20 mm for both days but for the dU component, varies by about $\pm$20 mm on 16th June 2003 and from –20 mm to +40 mm on 17th June 2003.

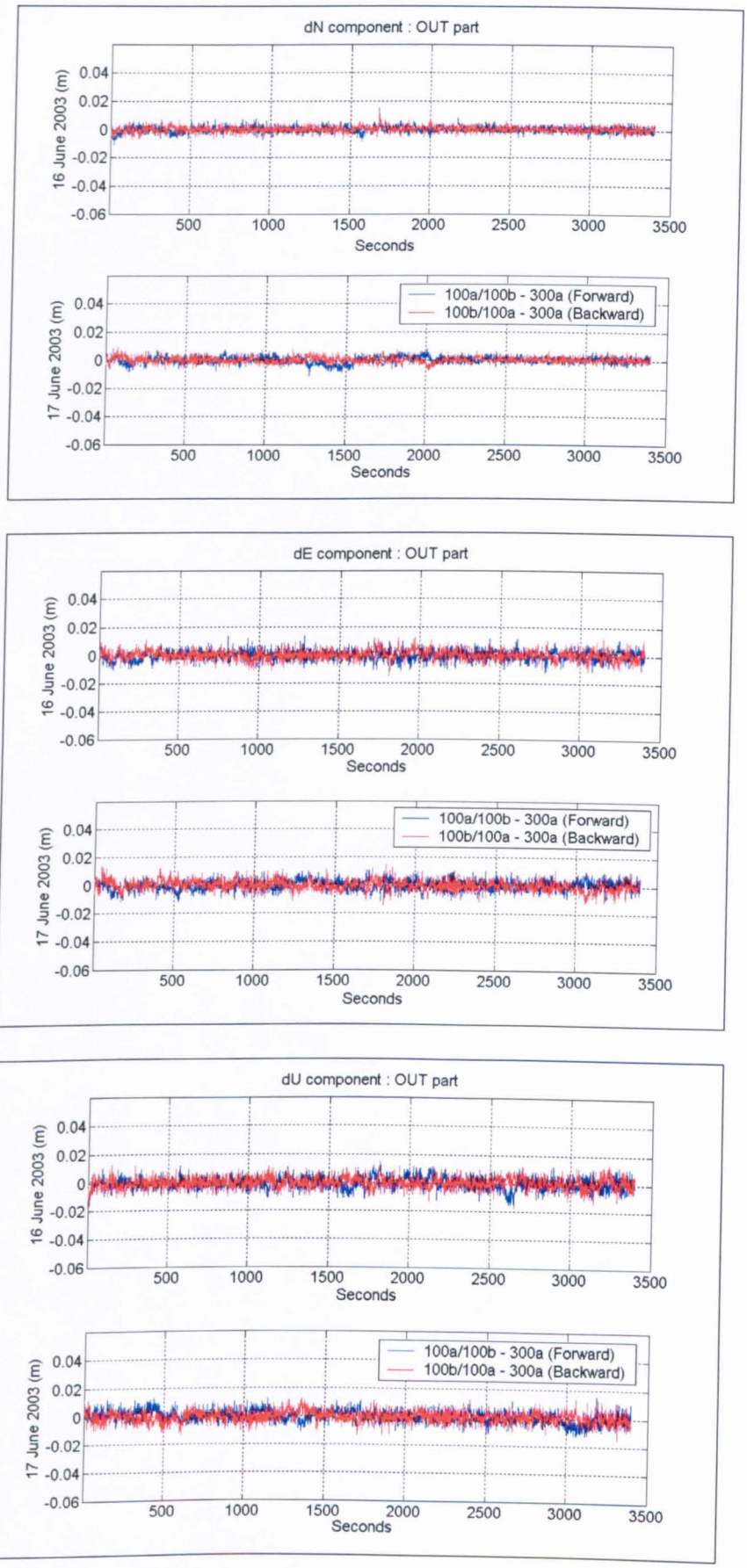

Figure 6.18 OUT part from AF for baselines from 100a/100b to 300a on the same day from the Snowdon Trial on 16th and 17th June 2003.

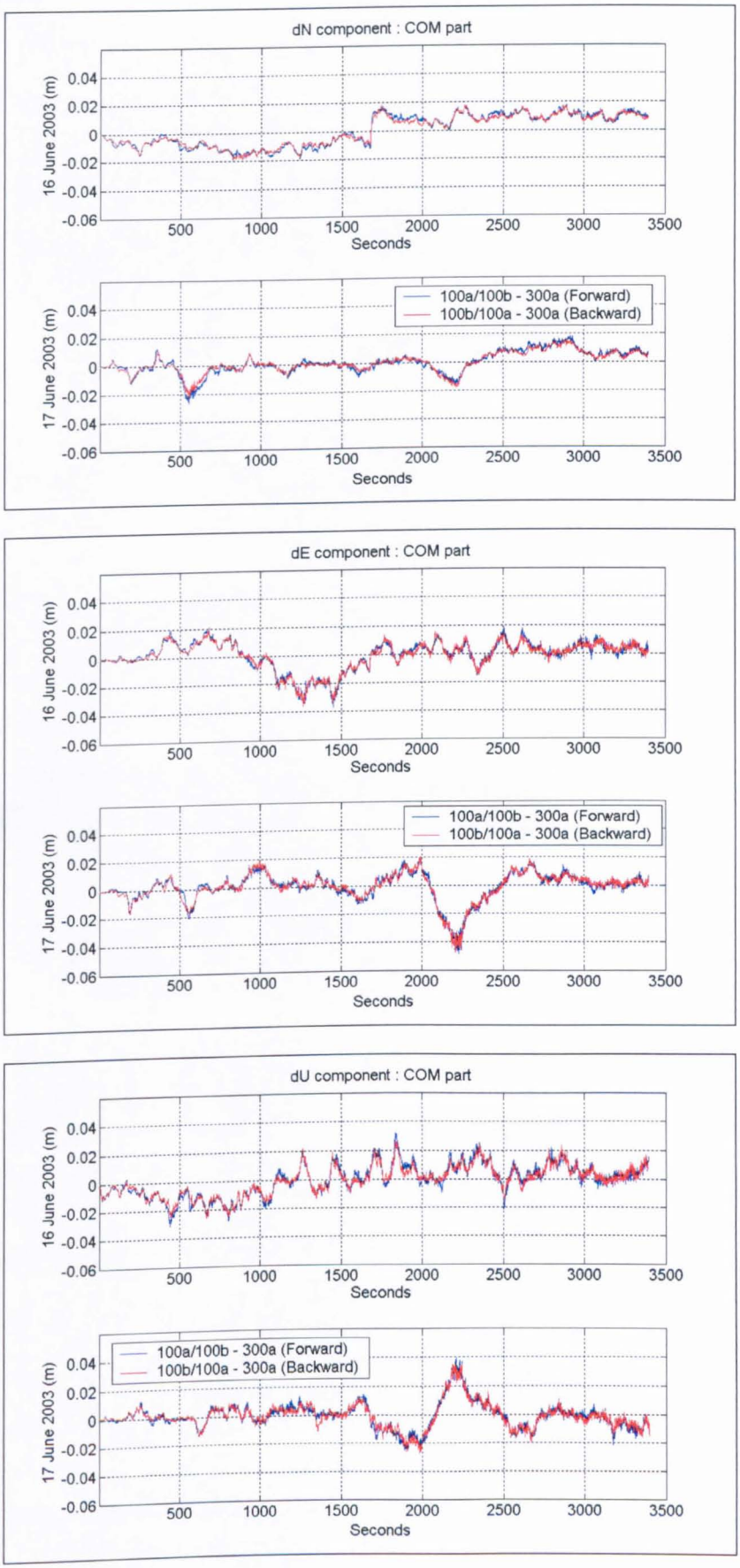

Figure 6.19 COM part from AF for baselines from 100a/100b to 300a on the same day from the Snowdon Trial on 16th and 17th June 2003.

Baselines	Day	dN	dE	dU
100a/100b–300a	16th June 2003	0.9689	0.9296	0.9057
100a/100b–300a	17th June 2003	0.9198	0.9275	0.8872
100a/100b–200a	16th June 2003	0.9747	0.9534	0.8760
100a/100b–300b	17th June 2003	0.9179	0.9173	0.8675

Table 6.14 Correlations for AF runs on the same day for baselines with a high difference in altitude from the Snowdon Trial on 16th and 17th June 2003.

RMS		OUT part			COM part		
		Units in millimetres (mm)					
Baselines	Day	dN	dE	dU	dN	dE	dU
100a/100b–300a	16th June 2003	2.2	3.5	4.0	10.1	10.0	10.4
100a/100b–300a	17th June 2003	2.4	3.6	4.0	7.0	10.1	9.2
100a/100b–200a	16th June 2003	2.2	3.5	4.1	11.0	12.2	8.7
100a/100b–300b	17th June 2003	2.2	3.5	3.7	6.5	9.2	8.1

Table 6.15 RMS of OUT and COM part from AF on the same day for stations with a high difference in altitude from the Snowdon Trial on 16th and 17th June 2003.

Ranges (maximum – mininimum)		OUT part			COM part		
		Units in millimetres (mm)					
Baselines	Day	dN	dE	dU	dN	dE	dU
100a/100b–300a	16th June 2003	25.1	25.7	31.8	36.1	58.2	62.9
100a/100b–300a	17th June 2003	18.9	22.6	28.2	44.9	68.6	64.7
100a/100b–200a	16th June 2003	21.4	36.5	33.3	43.2	71.6	68.1
100a/100b–300b	17th June 2003	16.5	26.7	28.5	35.6	66.3	61.3

Table 6.16 Ranges from minimum and maximum values of OUT and COM part from AF on the same day for stations with a high difference in altitude from the Snowdon Trial on 16th and 17th June 2003.

Further AF runs between these two days were made to isolate the un-mitigated troposphere and multipath using the COM part from Figure 6.19 above (combination 100a/100b – 300a). AF were performed in both Forward (16th June as reference and 17th June 2003 as desired), and Backward (17th June as reference and 16th June 2003 as desired). The results are as shown in Figure 6.20, which theoretically, should be the separated values for un-mitigated troposphere (OUT part) and multipath (COM part).

For the dN component, the trends or patterns of the COM part show that multipath does exist [about the 1,200 and 1,700 seconds mark (pink)], and probably mainly after the 2,500 seconds mark (pink) but their magnitude is lower that un-mitigated troposphere [(e.g. 2,300 seconds mark (brown)]. This is supported by the correlation value of 0.4881 registered by the two baselines for the two days. For the dE and dU components, it is evident that no significant multipath exists, backed up by their low correlations of 0.0277 and –0.0159 respectively.

It can be concluded that for station 300a, multipath is not the dominant factor in the position residuals, whence, the COM parts from Figure 6.19 can be assumed as representing the un-mitigated troposphere.

AF runs on same day were also performed to stations 200a (16th June 2003) and 300b (17th June 2003). The RMS for the OUT part is similar to the RMS for station 300a in both cases but there were slight differences for the COM part as can be seen in Table 6.15, at most 2.2 mm in dE. The ranges as shown in Table 6.16, show that station 200a were experiencing higher variations in the COM part as compared to station 300a by about 13 mm in the dE component. Plots of the COM part in all three components at stations 200a and 300a for day 16th June 2003 were as shown in Figure 6.21. There are slight variations between the two baselines but the trends are still intact as can be seen in the dN component with some differences in the dE and dU components. This is due to 200a being nearer the reference station (100a) with a lower difference in altitude. Assuming no significant multipath is present at station 200a, the COM part represent the un-mitigated troposphere.

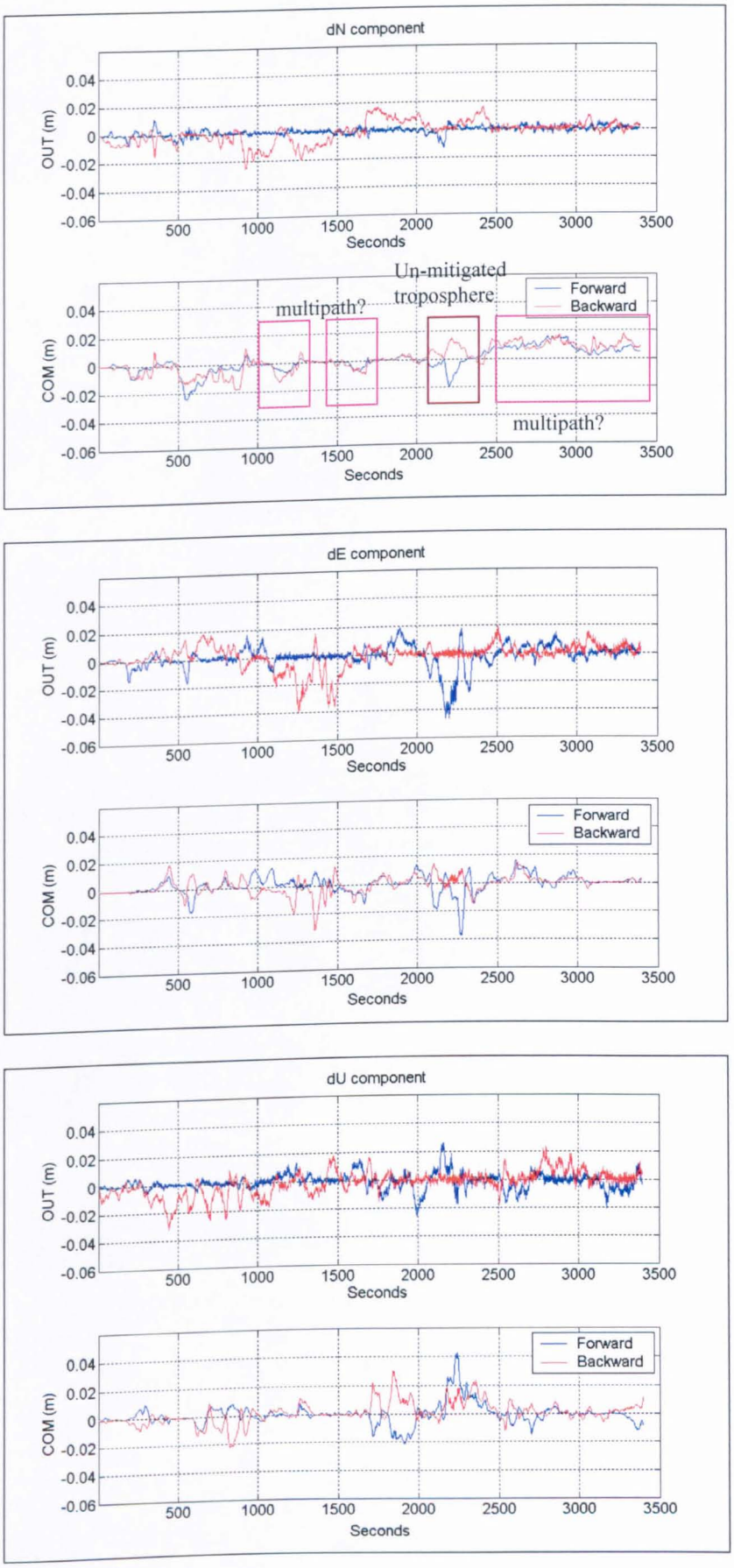

Figure 6.20 OUT and COM parts from the AF for 100a/100b to 300a using the COM part (from same day) from AF between two days [(Forward (16^{th}–17^{th}), and Backward (17^{th}–16^{th})] from the Snowdon Trial on 16^{th} and 17^{th} June 2003.

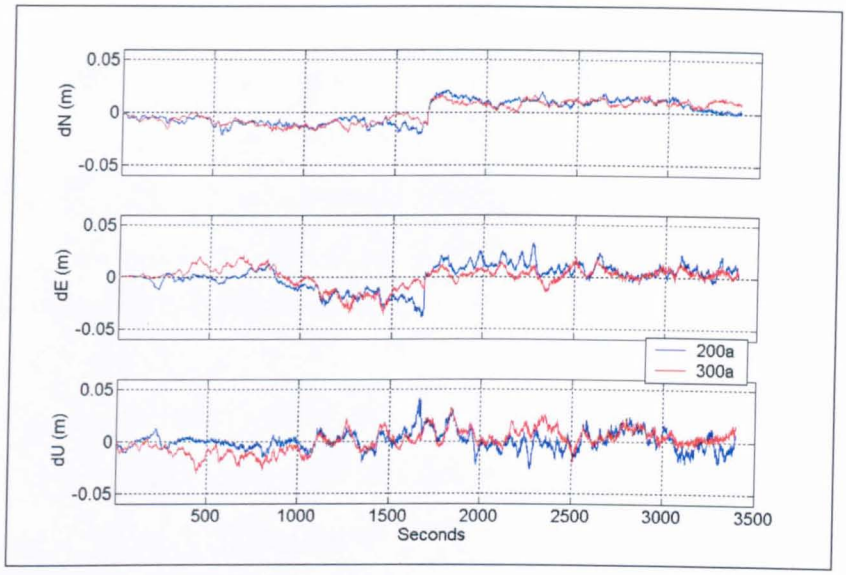

Figure 6.21 Plots of the COM part (un-mitigated troposphere) in all three components for 100a/100b to 200a and 300a on 16th June 2003, Snowdon Trial.

For station 300b on 17th June 2003, plots of the COM part together with 300a are as shown in Figure 6.22. It can be seen that being 810 m from station 300a and 15 m lower in altitude, an almost similar trend resulted. The slight differences on the position residual series mean that both stations were experiencing a slight difference in troposphere. No large differences can be seen on the RMS and ranges as shown in Table 6.15 and 6.16 respectively.

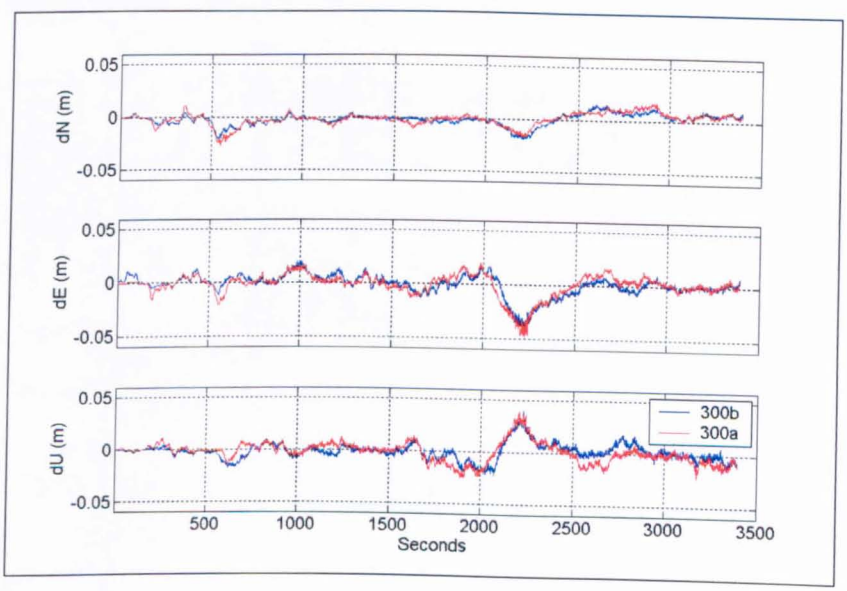

Figure 6.22 Plots of the COM part (un-mitigated troposphere) in all three components for 100a/100b to 300b and 300a on 17th June 2003, Snowdon Trial.

6.4 Discussion and Summary

It has been shown in section 6.1 that by having a pair of stations very near to each other, so that there are no effects from un-mitigated troposphere, multipath can be identified, as can be seen for baseline 400a – 400b and twr1 – twr2.

For both trials, when there is an altitude difference between the stations, it has been shown in sections 6.2 and 6.3 that multipath is not the dominant factor in the position residuals; it is un-mitigated troposphere effects. Considering baseline 100a/100b to 400a as shown in Figure 6.23, the un-mitigated troposphere time series for 16th June 2003 are plotted in blue while for 17th June 2003 in red. Figure 6.24 show the plots for baseline tre1 to twr1/twr2 from the University Trial #1 with the time series for 19th May in blue, 20th May in red and 21st May 2004 in green. Here, we can see that un-mitigated troposphere affects the position residuals in all three components and also changes with time. For the Snowdon Trial results, the magnitude for 16th June 2003 is about $\pm$20 mm in dN, $\pm$40 mm in dE and dU component, with the ranges a bit higher on 17th June 2003. While for the University Trial #1 results, they vary by $\pm$20 mm in dN and up to $\pm$30 mm in dE and dU. However, in this case, for most of the period, the variations were more consistent, with less than $\pm$10 mm in both dN and dE components and $\pm$20 mm in the dU component.

Although both baselines have about the same difference in altitude i.e. 50 metres, it is evident that results from the Snowdon Trial were experiencing higher effects due to un-mitigated troposphere from longer baselines, which is about 9 km for the Snowdon Trial as compared to about 1 km for the University Trial which makes the results for the Snowdon Trial more noisier.. This is supported by their RMS values which were presented in Tables 6.7 and 6.10.

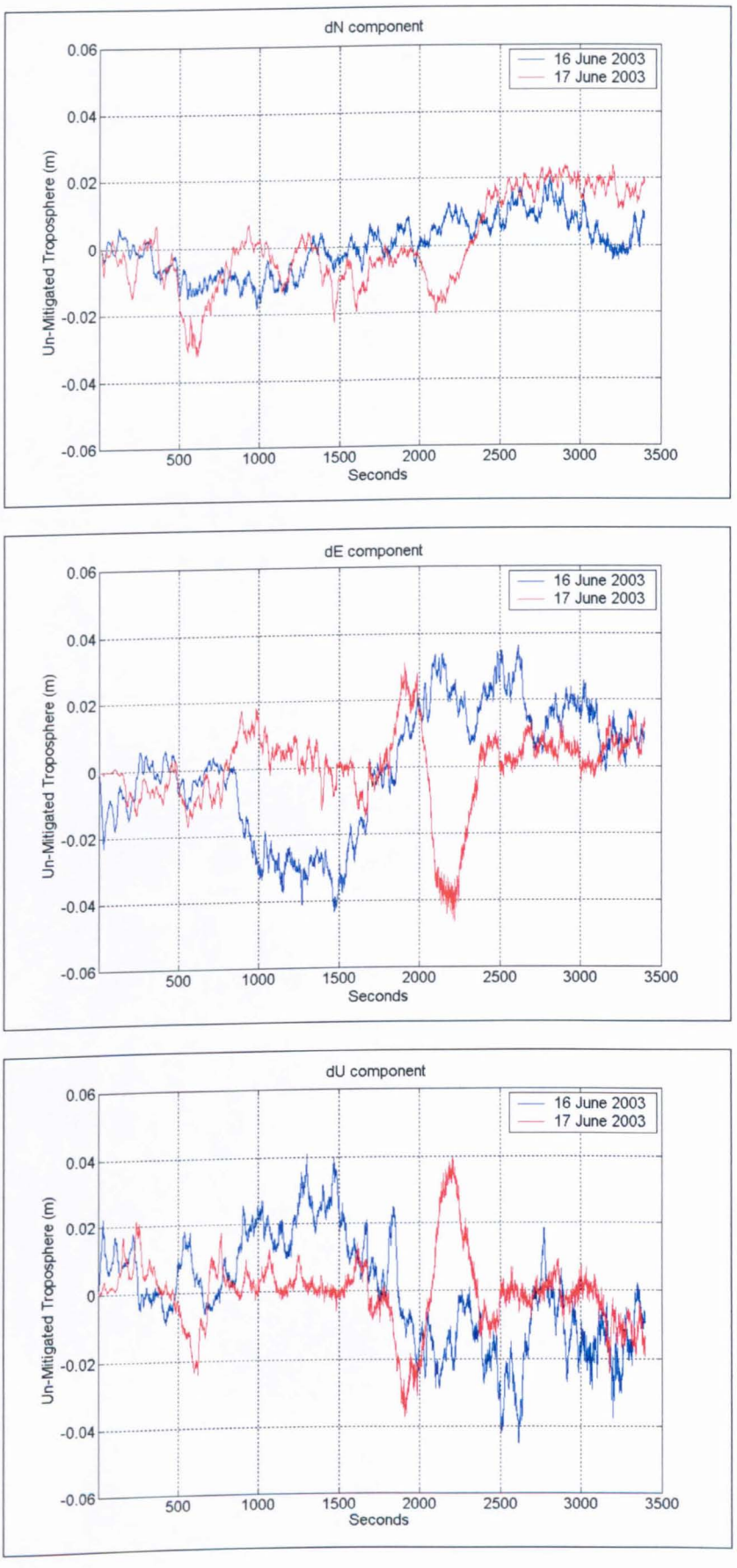

Figure 6.23 Un-Mitigated Troposphere Effects in dN, dE and dU components for baseline 100a/100b to 400a from the Snowdon Trial, 16th and 17th June 2003.

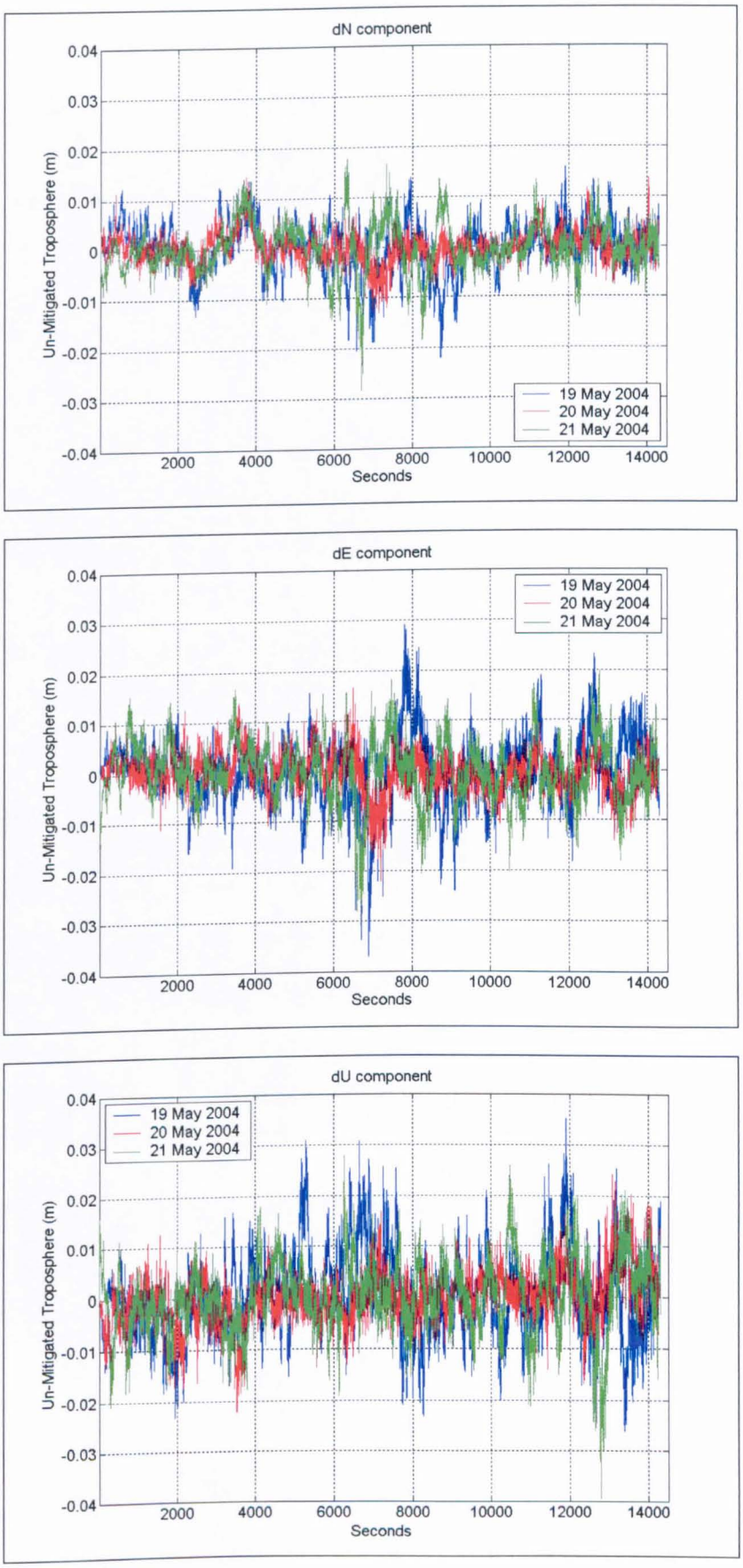

Figure 6.24 Un-Mitigated Troposphere Effects in dN, dE and dU components for baseline tre1 to twr1/twr2 from the University Trial #1, 19th to 21st May 2004.

Baselines with higher differences in altitude were also investigated to see if there were any differences in the un-mitigated troposphere effects. From the results for baseline 100a/100b to 300a, as shown in Figure 6.25, with about 1 km difference in height, a variation of about ±20 mm can be seen in the dN component, -40 mm to +20 mm in dE and –20 mm to nearly +40 mm in dU. These are similar to the results found for baselines with smaller differences in altitude, suggesting that the distance between stations influences the results.

Frequency plots (histogram) for the Noise and Un-Mitigated Troposphere for the respective baselines can be seen in Figures 6.26, 6.27 and 6.28. The plots are for each day for the three components; dN, dE and dU. It is evident that for Noise, most of the epochs are within the ±10 mm limit and there is a good Normal distribution. This is also the case for the un-mitigated troposphere in the University Trial where the values vary within ±15 mm for dN, ±10 mm in dE and about ±20 mm in dU component. However, for the Snowdon Trial this is not the case, as the un-mitigated troposphere effect is different between days as shown by the frequency distributions. For baseline 100a – 300a with high difference in altitude, a better Normal distribution plots of around ±20 mm can be seen in all three components on day 17th June 2003 as compared to day 16th June 2003. For baseline 100a – 400a, although well distributed trends can be seen for the noisier dE and dU, there are clear anomalies in the dN component. This could be due to the fact that station 400a is much further than 300a from station 100a.

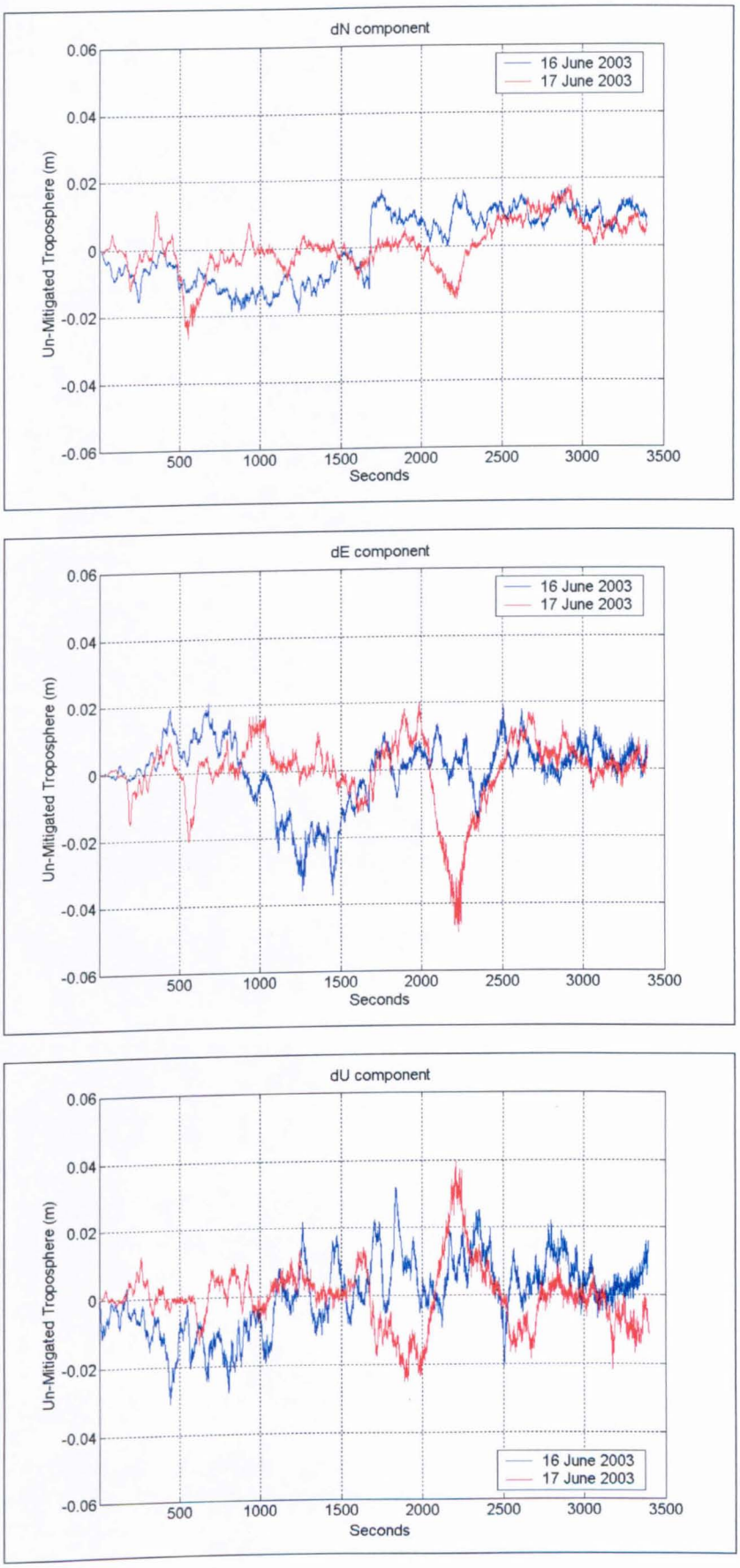

Figure 6.25 Un-Mitigated Troposphere Effects in dN, dE and dU components for baseline 100a/100b to 300a from the Snowdon Trial on 16th and 17th June 2003.

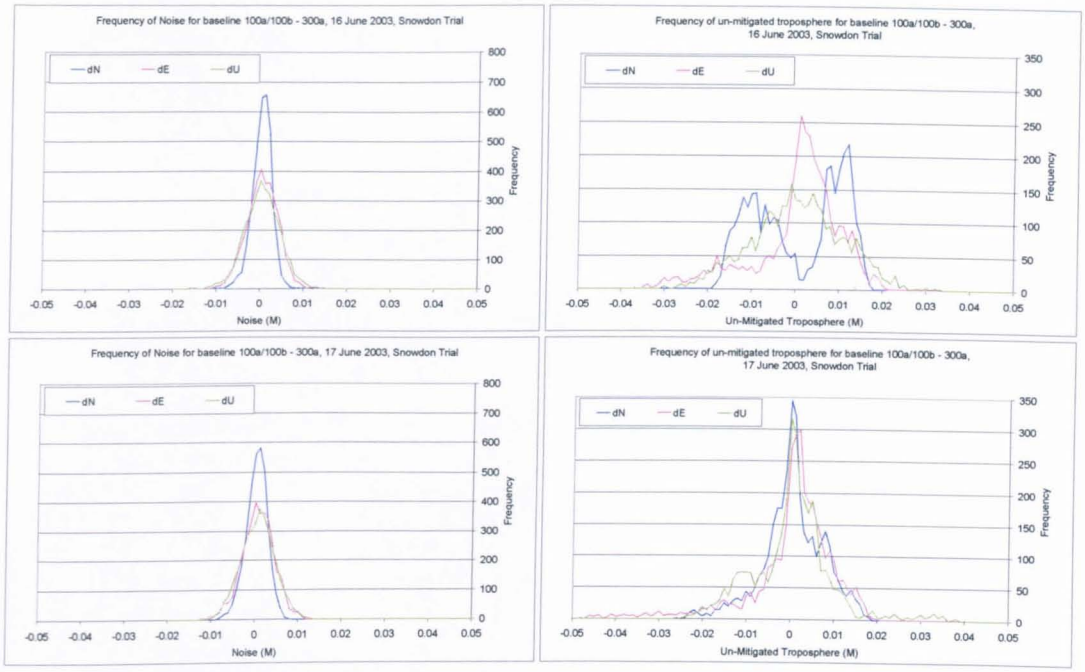

Figure 6.26 Frequency of Noise (left) and Un-Mitigated Troposphere (right) for baseline 100a/100b to 300a from the Snowdon Trial on 16th and 17th June 2003.

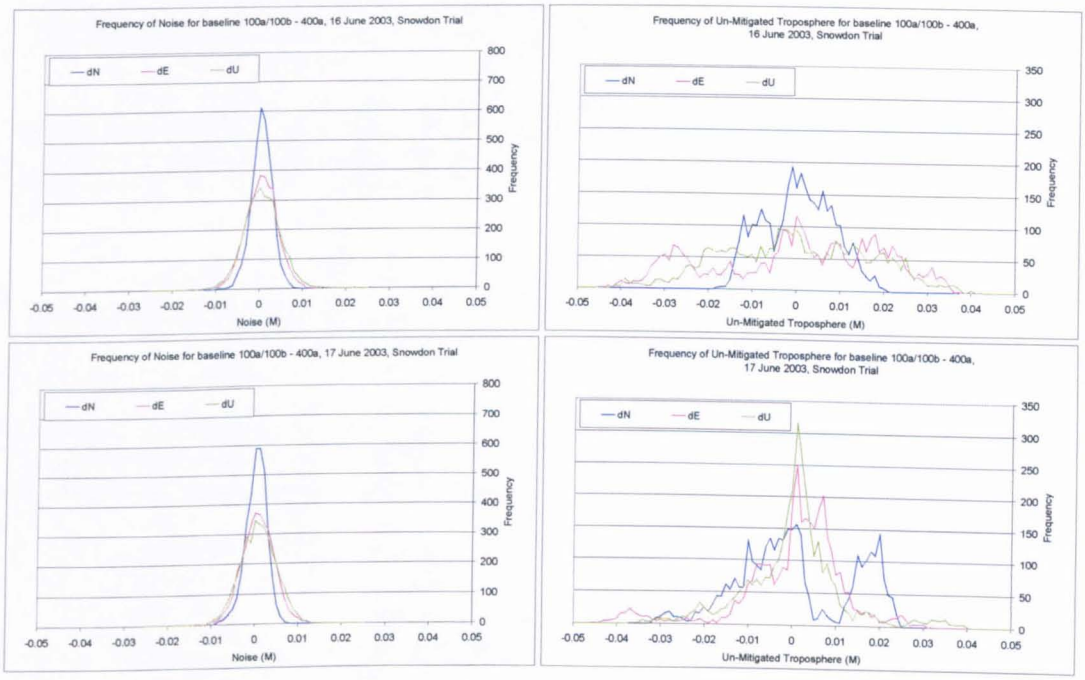

Figure 6.27 Frequency of Noise (left) and Un-Mitigated Troposphere (right) for baseline 100a/100b to 400a from the Snowdon Trial on 16th and 17th June 2003.

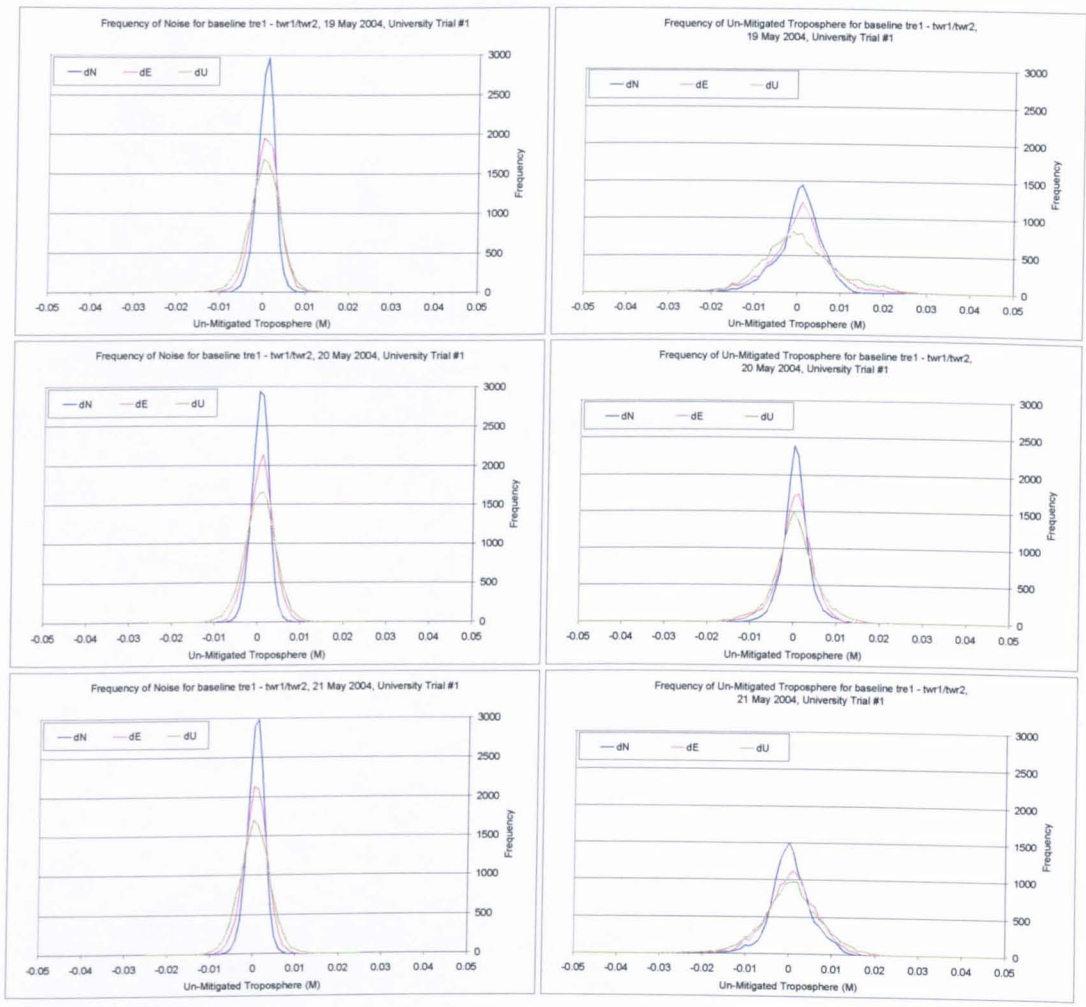

Figure 6.28 Frequency of Noise (left) and Un-Mitigated Troposphere (right) for baseline tre1 to twr1/twr2 from the University Trial #1 on 19th to 21st May 2004.

Based on the above findings, it can be summarized that, tropospheric delay has not been fully mitigated with the Leica Ski-Pro Version 3.0 processing software, although a tropospheric model has been applied. Results from the AF suggest that in all cases, variations in position residuals can be seen which appear to be due to un-mitigated troposphere, based on the fact that

i. The position residuals were computed with reference to the same satellites on consecutive days.

ii. No obvious biases can be seen on the position residuals between days as the variations differs in time which remove the possibilities of wrongly positioned antennas.

iii. It has been proven with AF that the existence of multipath in the tests carried out was minimal, due to the selection of good locations for the stations.

These conclusions are important in the context that it has been demonstrated that the use of kinematic GPS for monitoring tall structures will be limited by the ability to mitigate troposphere delay, and centimetric "apparent movements" in both plan and height can be observed, which must be treated with caution.

Chapter 7

Analysis of Results from Moving Stations

All structures are prone to loads, which will cause them to either change in size, move or be displaced. Generally, there are two basic types of building loads; i.e. dead and live [*Schueller*, 1977].

Dead load is related to the gravitational force that acts on the weight of the structure by pulling it downward. This kind of load will introduce long term settlement and can only be recognised if a long period of monitoring is applied. Since it reacts to gravity, the major effect would be in the vertical direction, however, dependent on the design of the foundations, displacement could also be seen in a horizontal direction.

Live loads are more variable and unpredictable as they occur not only over time but also as a function of location [*Schueller*, 1977]. Examples of live loads that can affect the structure are; occupancy loads created by the weight of people, furnitures, etc; traffic flows on bridge structures; meteorological loads such as rain/snow, temperature, air pressure and wind; and seismic loads.

During the design stage of any structure, all the load effects should have been taken into account to allow the structures to withstand such loads and dampers can be placed in the structure to allow for small movements created by the loads.

For tall buildings, wind loads play an important role. *Schueller* [1977] states that, "with the introduction of the lightweight steel frame, weight was no longer a factor limiting the height of construction." However, this has created new problems, as structures have become less rigid, thereby making lateral stiffness and sway a more important consideration. Some tall buildings that extend into

regions of high wind velocity have been known to sway excessively in strong winds, e.g. the Empire State building (built in 1931), has a total deflection of 10.1 inches (or 257 mm) with an 80 mile per hour (130 km/h) wind [*Schueller*, 1977].

For suspension bridges, traffic loading and wind loading are important. Suspension bridges in the United Kingdom such as the Humber Bridge near Hull, in England and the Forth Road Bridge near Edinburgh, in Scotland were both included in this study. Both bridges were built with a long span platform held by supporting cables, which run along the bridge and are solidly anchored at both sides of the river. To provide sufficient height clearance over the river, concrete towers were built at both ends of the structure, which hold the cables high and allow then to gradually lower to the mid-span of the platform. Traffic and wind loads on the centre platform can cause it to sway and vibrate, which at the same time causes the towers to move. As the purpose of this project is the study of un-mitigated troposphere, multipath and movements on tall structures, only measurement of the tower were of interest, whereas for the bridge platform, readers are advised to read the thesis by *Meng* [2002].

In this chapter, results from trials on the Humber and Forth Road Bridge will be investigated. The substantial difference in altitude between the land and the tower allowing the investigation of the effects of un-mitigated troposphere when monitoring moving stations.

7.1 Analysis of the Humber Bridge Trial, 1st, 2nd and 4th March 2004

Three stations were involved in this trial as shown in Figure 4.9 in chapter 4. They are ref1, located on the roof of the Bridge Control Building, twr1 on the bridge connecting the two North Towers and est at the estuary. Station est is about 40 metres lower in altitude than ref1 while twr1 is 110 metres higher and they both are approximately 600 metres from ref1 in distance and almost perpendicular in directions. Due to site constraints, twr1 was expected to experience poor satellite visibility and high multipath interference.

Full plots of the position residuals with their GDOPs for baselines ref1 – est and ref1 – twr1 from the Humber Bridge Trial are as shown in Figure 7.1 and 7.2 respectively (plots on each day can be seen in Appendix D). These are position residuals, computed using OTF kinematic GPS with respect to "true" positions computed in static mode, which can be seen in Table B2 (Appendix B). For the purpose of the plots, the epochs of the position residuals for 2nd and 4th March have had applied a four minute difference per day with respect to 1st March 2004.

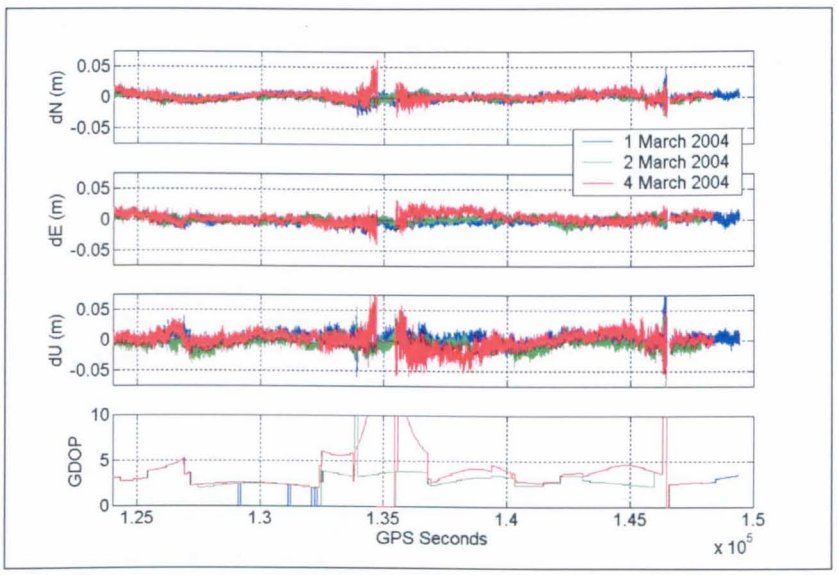

Figure 7.1 Position residuals and GDOPs for baseline ref1 to est from three days of the Humber Bridge Trial, on 1st (blue), 2nd (green) and 4th (red) March 2004.

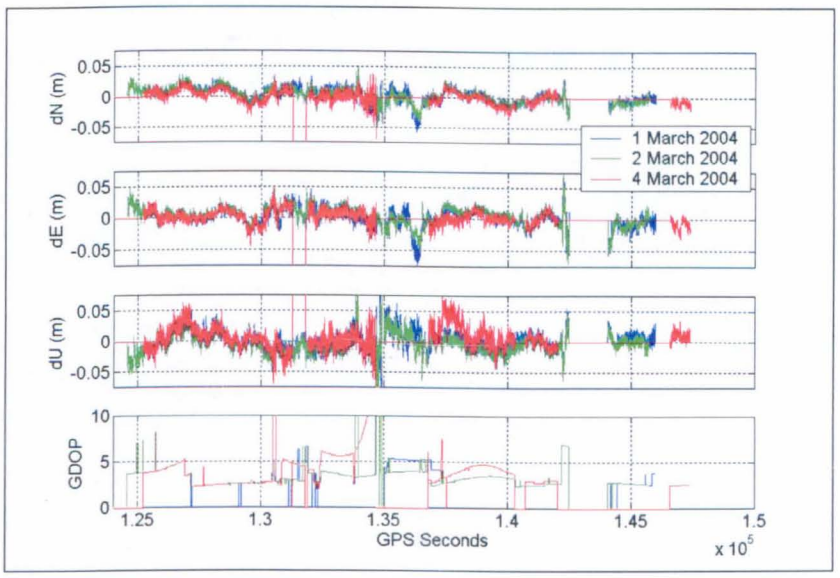

Figure 7.2 Position residuals and GDOPs for baseline ref1 to twr1 from three days of the Humber Bridge Trial, on 1st (blue), 2nd (green) and 4th (red) March 2004.

From Figure 7.1, we can see that there are epochs with intermittent un-resolved ambiguities on 1st March at about the 130,000 GPS seconds mark, on 2nd March at about the 135,000 GPS seconds mark and quite a significant loss on 4th March 2004 at about the 135,000 and 147,000 GPS seconds marks. In general, the same GDOPs were computed on 1st and 2nd March but higher GDOP value were obtained on 4th March between the 132,000 to 147,000 GPS seconds marks. Investigation into the RINEX file using TEQC for the data observed during this period showed that both stations were observing to the same satellites on 1st and 2nd March, however, on 4th March, data from SV31 were corrupted and not being used in the processing, as shown in Figure 7.3.

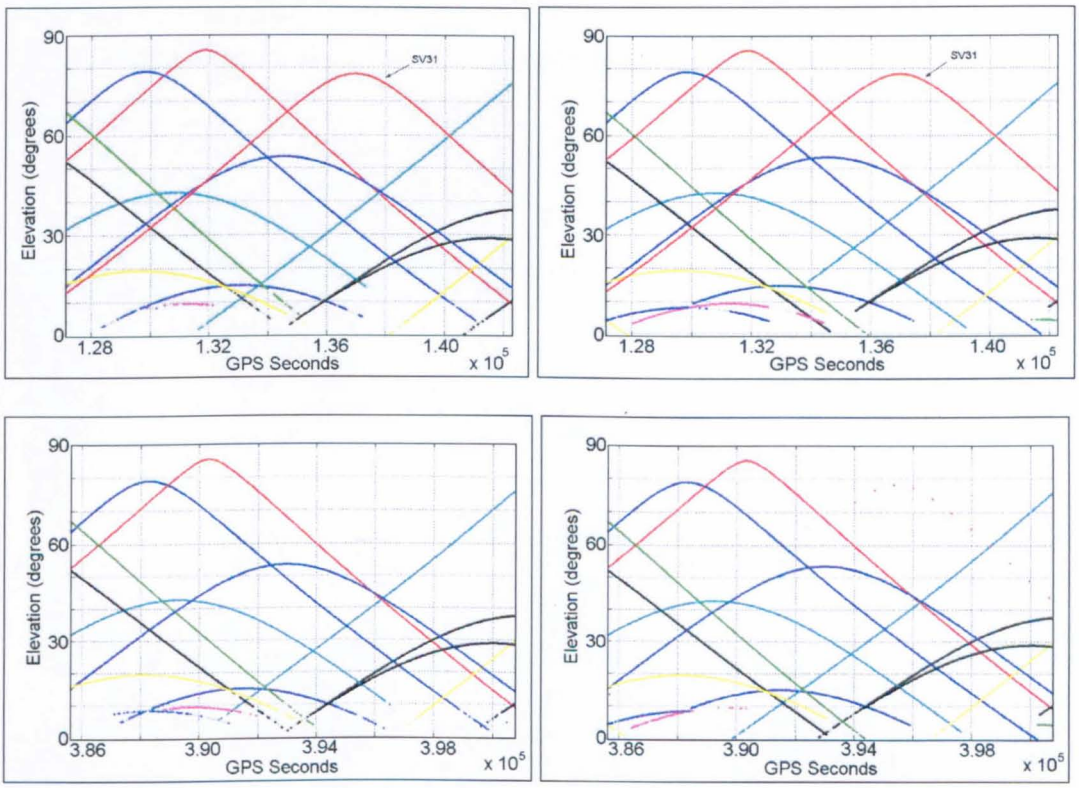

Figure 7.3 Satellite elevation against GPS seconds as seen from stations ref1 (left) and est (right) on 1st (top) and 4th (bottom) March 2004 during the Humber Bridge Trial.

With the absence of data from SV31, the effects were not obvious from the beginning of the observation period. This is due to a sufficient number of satellites being available for processing. The effects can be seen from the 132,500 GPS second mark onward where, at times, only a minimal number of 4 or 5 satellites were available, leading to a poor geometry, as can be seen from the GDOP values and the noisier position residuals on 4th March 2004.

From Figure 7.2, i.e baseline ref1 to twr1, the same situation was experienced with the satellite constellation on 4th March 2004. In this case, the position residuals were much noisier than for baseline ref1 to est, as station twr1 is located on the bridge tower, which is about 110 metres above ref1. Similar trends in the time series between days could mean multipath exists in the results, as mentioned earlier in Chapter 4, where the surroundings around twr1 could introduce both multipath and loss of sight to satellites. Comparing Figure 7.4 with 7.3, we can see that, there are instances where visibility to certain satellites from station twr1 was not possible.

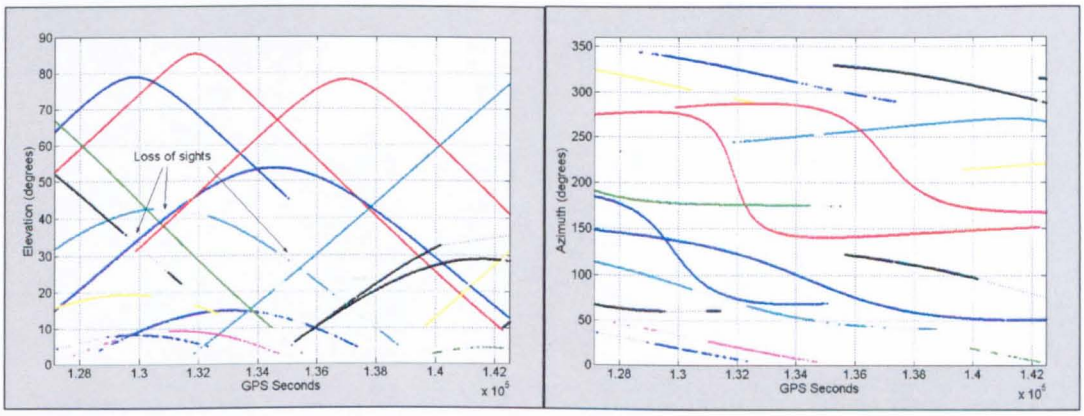

Figure 7.4 Satellites elevation (left) and azimuth (right) against GPS seconds as seen from station twr1 on 1st March 2004 during the Humber Bridge Trial.

Furthermore, the influence of multipath can be seen from the sky plots at station twr1 as shown in Figure 7.5, where much disturbed signals were obtained for satellites at the 60 degrees azimuth and 45 degrees elevation and on satellites at lower elevation i.e. below 30 degrees. The MP1 and MP2 are multipath values from equations relating a pseudorange and carrier phase of both frequencies as described in *Leick* [2004].

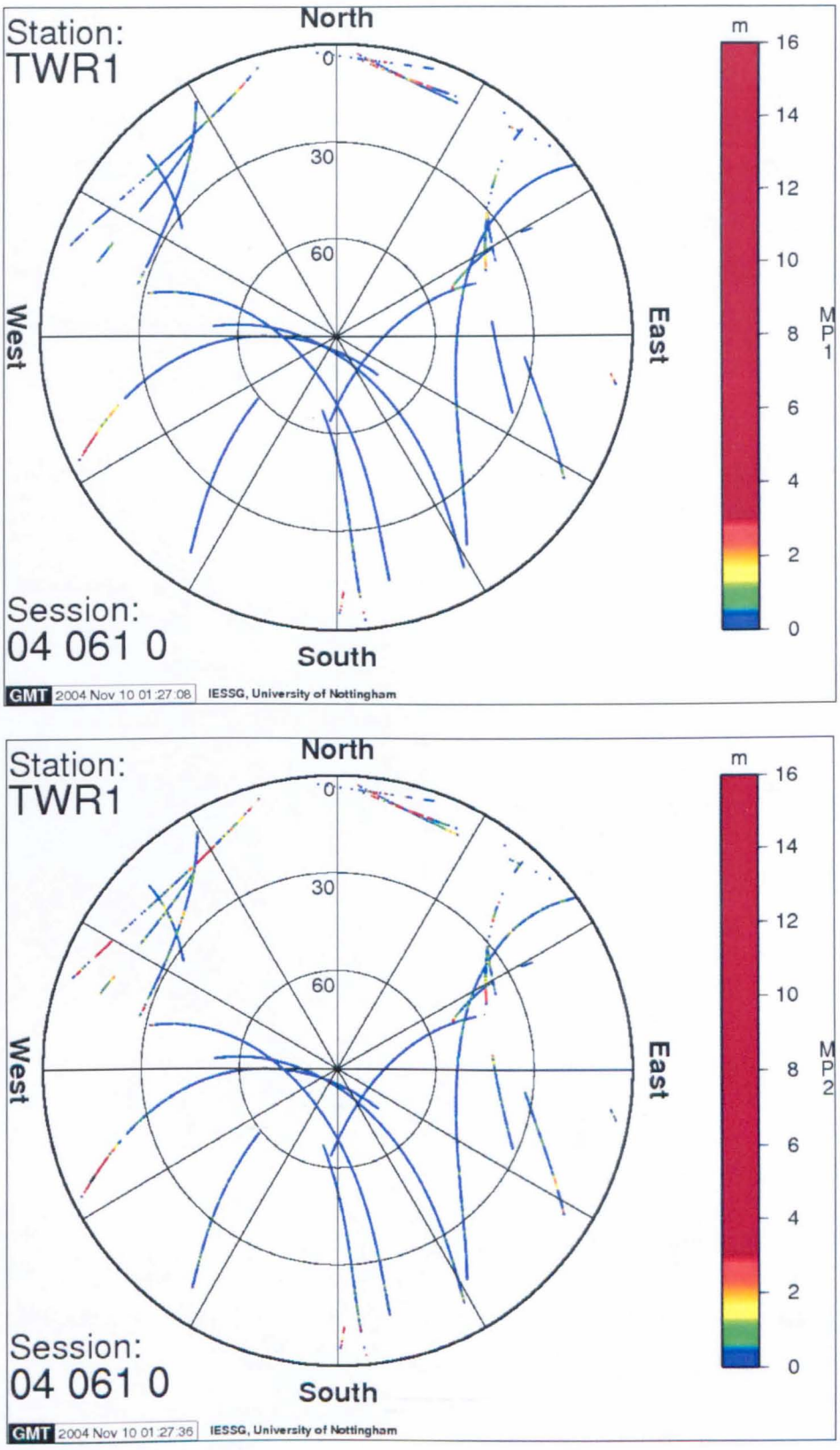

Figure 7.5 Sky plots of MP1 (top) and MP2 (bottom) from the RINEX file at station twr1 on DOY 61 (1st March 2004) during the Humber Bridge Trial.

Only a short period of common data were available for the three days, with a total of 2,864 seconds available for use with AF, for the detection of multipath, un-mitigated troposphere and movements. The period is for epochs from 127,137 GPS seconds up to 130,000 GPS seconds for day 1st March 2004, with its equivalent for day 2nd and 4th March 2004 taking into consideration the four minute advance of the constellation between consecutive days. For these selected epochs, the mean and standard deviation of the position residuals for each respective baseline can be seen in Table 7.1.

Baseline	dN (mm)		dE (mm)		dU (mm)	
01 March 04	Mean	Std. Dev	Mean	Std. Dev	Mean	Std. Dev
refl–est	-1.0	3.6	-2.1	3.7	-2.2	8.0
refl–twrl	7.5	9.4	-0.2	9.7	7.8	11.0
est–twrl	8.3	10.7	2.7	9.1	9.2	14.7
02 March 04						
refl–est	-3.0	3.8	-1.1	3.4	-9.6	8.8
refl–twrl	7.8	10.3	2.4	10.4	2.3	11.4
est–twrl	11.0	12.4	4.0	10.6	10.9	15.5
04 March 04						
refl–est	-1.4	3.7	0.5	3.2	1.1	7.8
refl–twrl	1.0	10.2	-0.3	10.9	8.5	11.0
est–twrl	2.7	11.8	-0.1	10.1	6.9	13.6

Table 7.1 Mean and Standard Deviation of the position residuals from selected epochs over the three days of the Humber Bridge Trial on 1st, 2nd and 4th March 2004.

Looking at the mean in the dN component, a possible bias (about 6mm) can be seen for baseline refl – twrl on the 4th when compared to 1st and 2nd March 2004. A similar bias can be seen for baseline est – twrl. However, considering the standard deviations these biases are not statistically significant.

Further investigations on the selected epochs for this trial were conducted as follows; a baseline formed by stations refl and est was investigated for multipath, and secondly, using both these stations as a reference and twrl as a rover, same day AF were performed followed by consecutive days AF using the COM part as described in the following sections.

7.1.1 Results for baseline refl to est

Station est is located about 600 metres south-east of refl with a difference in altitude of about -40 metres. AF was performed on consecutive days in two combinations for this baseline to test whether multipath exists. The first combination is between 1st and 2nd March 2004 position residuals time series and the second, with 2nd and 4th March 2004. Forward and Backward AF runs were carried out by interchanging the reference and desired time series between the two days for each combination. The results are shown in Figure 7.6. In the dN component, the effect of multipath (COM part) can be seen at about the 500 and 2,500 seconds mark (pink). Whereas in the dE component, it is only clear for the first 500 seconds (pink). In both components, the magnitude is quite small, i.e. less than ±10 mm. In the dU component, it is quite significant at the beginning and towards the end of the period concerned with a magnitude of about ±20 mm. The noise component (OUT part) is about the same magnitude as multipath for each component. The values for the minimum and maximum ranges in all three directions are shown in Table 7.2 and their RMS in Table 7.3. It is clear that the RMS in the dU component is much higher than the dN and dE components.

refl–est	dN (mm)		dE (mm)		dU (mm)	
OUT part	Min	Max	Min	Max	Min	Max
01–02 March	-10.2	8.2	-9.7	9.8	-20.7	22.6
02–04 March	-9.9	10.4	-11.2	10.9	-32.8	21.1
COM part						
01–02 March	-9.0	7.9	-5.5	7.3	-23.2	17.1
02–04 March	-7.9	8.5	-6.4	7.2	-14.1	17.7

Table 7.2 Minimum and Maximum values for the OUT and COM part from the AF between consecutive days for baseline refl – est in the Humber Bridge Trial on 1st, 2nd and 4th March 2004.

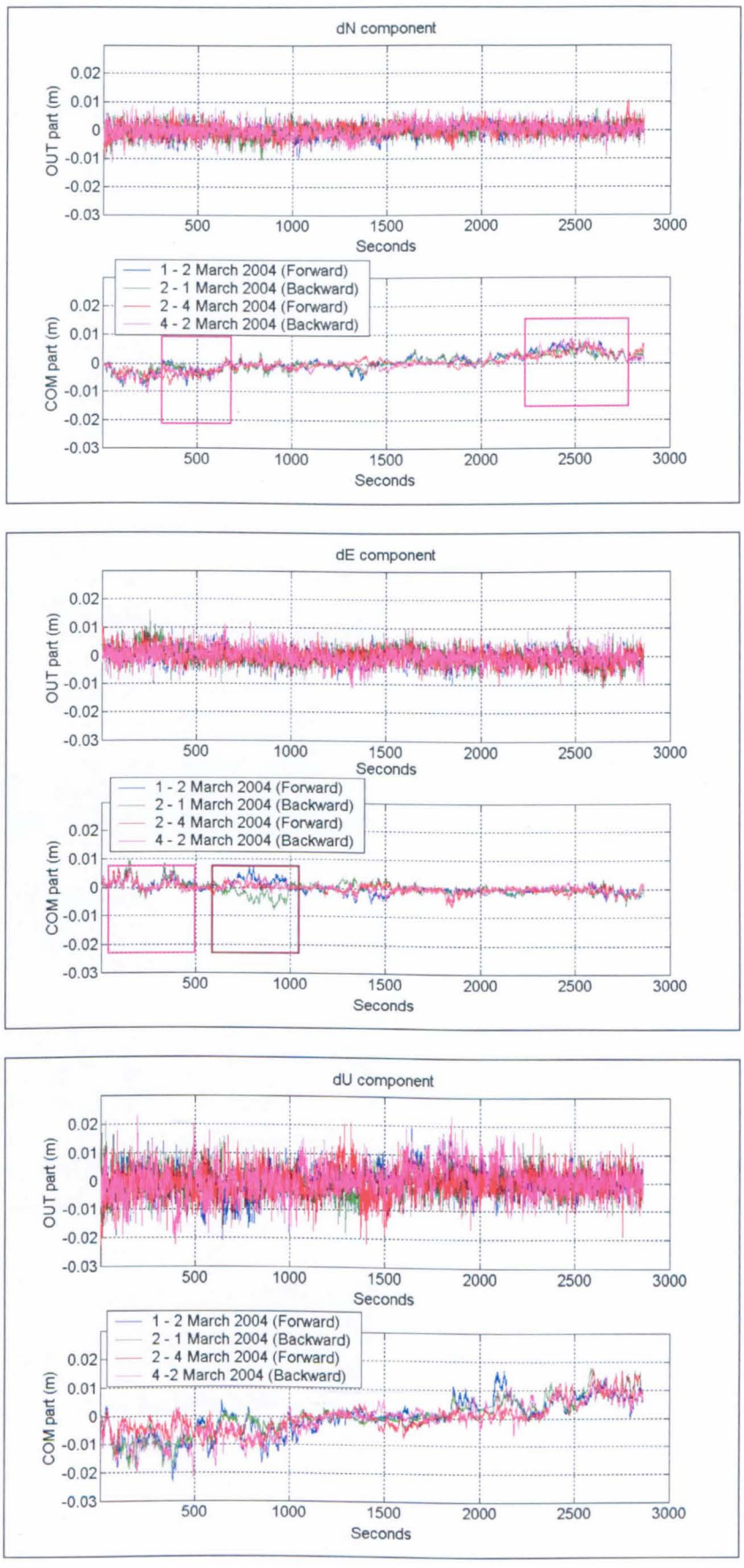

Figure 7.6 OUT and COM parts from the AF on consecutive days for baseline ref1 to est in the Humber Bridge Trial on 1st, 2nd and 4th March 2004.

refl–est	RMS (mm)		
OUT part	dN	dE	dU
01–02 March 2004	2.5	3.0	5.4
02–04 March 2004	2.5	3.0	5.6
COM part			
01–02 March 2004	3.0	1.8	7.1
02–04 March 2004	2.8	1.5	5.6

Table 7.3 RMS values for the OUT and COM parts from the AF between consecutive days for baseline refl – est in the Humber Bridge Trial on 1st, 2nd and 4th March 2004.

Two days	01–02 March 2004			02–04 March 2004		
Baselines	dN	dE	dU	dN	dE	dU
refl–est	0.5730	0.0398	0.6307	0.5121	0.1221	0.4588
refl/est–twrl	0.9099	0.8831	0.8489	0.9106	0.9322	0.8332

Table 7.4 Correlations from AF runs between consecutive days in the Humber Bridge Trial on 1st, 2nd and 4th March 2004.

The high values of correlation from AF (Table 7.4) suggest that multipath is the dominant factor for this baseline, especially when twrl is involved. The poor correlation recorded in the dE component for baseline refl – est show that only minimal multipath were present but looking at their plots in Figure 7.6, the magnitude of the variations are quite small, which is why poor correlation values were computed. The trends of epochs from 700 to 1,000 seconds (brown) were not multipath. This is shown by the differences in the results from AF in the forward (blue) and backward (green) directions. These differences are quite small, with a magnitude of only 10 mm, but could be caused by un-mitigated troposphere as both stations differ by about 40 metres in height.

7.1.2 Results for baselines refl and est to twrl

Same day AF was then performed using baseline refl to twrl and est to twrl on each of the three days (1st, 2nd and 4th March 2004). Forward run with baseline refl–twrl as reference and est–twrl as desired, and backward run vice-versa. Since it has been shown that between refl and est, there is some multipath (section 7.1.1), so, from AF, some differences in the trends were to be expected if baselines from both stations were used. The correlations for the same day AF above can be seen in Table 7.5. Their values show that good correlation can be seen in the dN and dE components but slightly lower for the dU component.

Baselines refl/est–twrl			
Same day	dN	dE	dU
01 March 2004	0.9522	0.9026	0.8233
02 March 2004	0.9635	0.9440	0.7979
04 March 2004	0.9622	0.9417	0.8100

Table 7.5 Correlations for AF runs on same day for the Humber Bridge Trial on 1st, 2nd and 4th March 2004.

The plots of the time series were as shown in Figures 7.7 (OUT part) and 7.8 (COM part). The OUT part is the noise while the COM part could contain the multipath, un-mitigated troposphere and movements of station twrl. We can see that there are variations between the results from forward and backward AF runs in both the OUT and COM parts, especially in the dU component for each day. This could be due to multipath, that exists at stations refl and est, as the differences mainly occur in the first 1,000 seconds and towards the end of the time series (pink) as found in section 7.11. The RMS for the OUT and COM part are as shown in Table 7.6, with the COM part having higher values than the OUT part.

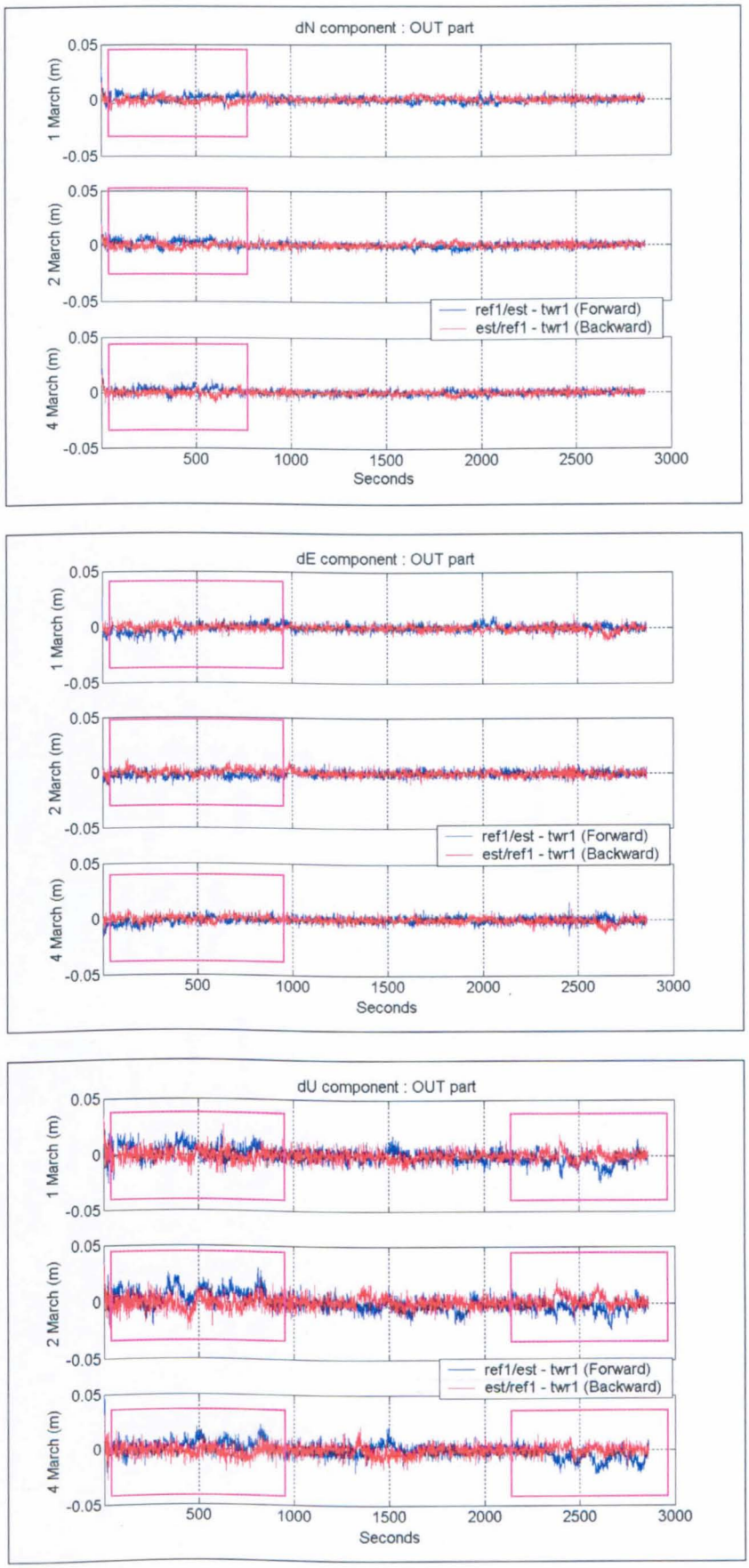

Figure 7.7 OUT part from the AF on same day for baseline ref1/est to twr1 in the Humber Bridge Trial on 1st, 2nd and 4th March 2004.

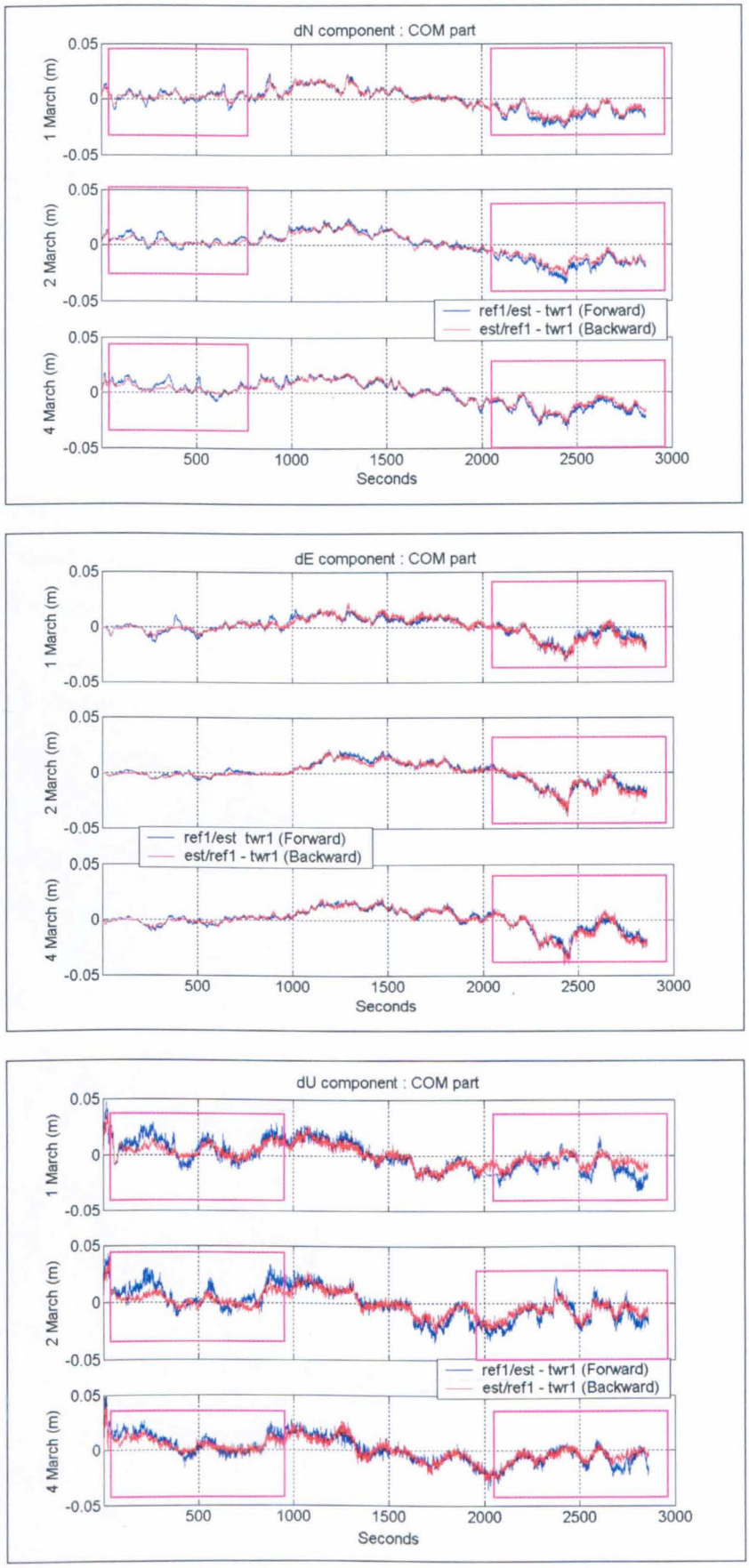

Figure 7.8 COM part from the AF on same day for baseline ref1/est to twr1 in the Humber Bridge Trial on 1st, 2nd and 4th March 2004.

RMS	OUT part (mm)			COM part (mm)		
refl/est–twrl	dN	dE	dU	dN	dE	dU
01 March 2004	3.1	3.5	6.6	10.2	8.3	13.1
02 March 2004	2.9	3.1	7.2	12.0	10.0	13.7
04 March 2004	2.8	3.2	6.7	11.4	9.5	11.7

Table 7.6 RMS values for the OUT and COM part from the AF on the same day for baselines refl – twrl and est – twrl in the Humber Bridge Trial on 1st, 2nd and 4th March 2004.

Further runs of AF using the COM part from Figure 7.6 between consecutive days were performed in two combinations (1st and 2nd, and 2nd and 4th March 2004 in forward and backward runs). The plots of the result are as in Figure 7.9.

Figure 7.9 shows that multipath is the dominant factor, as can be seen from the similarity in the patterns of the time series of the COM part. This is supported by the strong correlations as given in Table 7.4 for baseline refl/est to twrl. The multipath varies from –30 mm to 50 mm while the OUT part, which is the un-mitigated troposphere and movement, varies by about ±20 mm at most. In this case, it is not possible to identify and separate un-mitigated troposphere and movement from the OUT part.

RMS	OUT Part (mm)			COM Part (mm)		
refl/est–twrl	dN	dE	dU	dN	dE	dU
01–02 March 2004	3.3	2.3	5.2	11.5	9.8	12.7
02–04 March 2004	3.5	2.5	4.8	10.8	9.2	10.7

Table 7.7 RMS values for the OUT and COM part from the AF on consecutive days for baselines refl/est – twrl, using the COM part from same day AF, for the Humber Bridge Trial on 1st, 2nd and 4th March 2004.

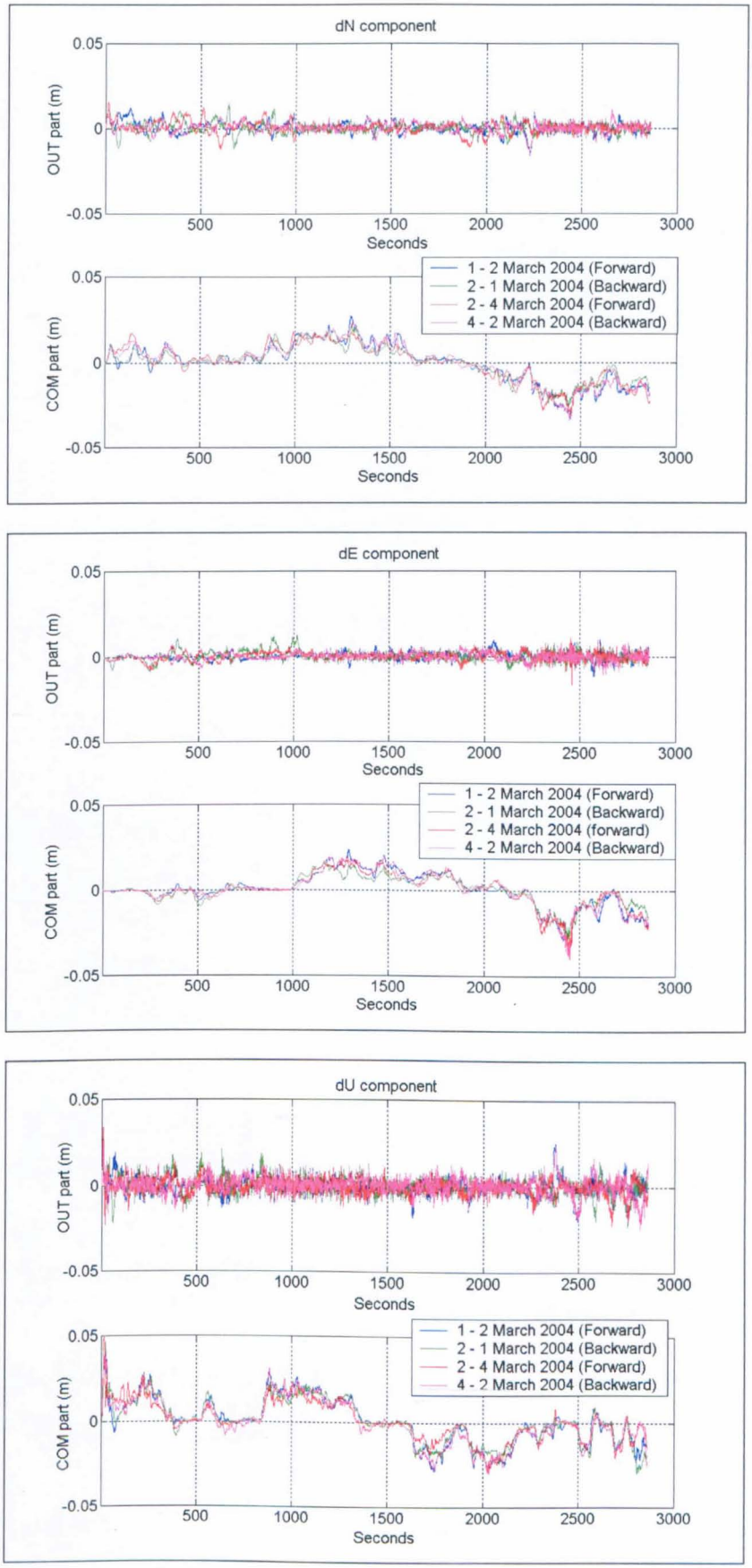

Figure 7.9 OUT and COM parts from the AF on consecutive days for baselines ref1/est to twr1, using the COM part from AF on the same day for the Humber Bridge Trial on 1st, 2nd and 4th March 2004.

What can be concluded from this trial is that, for the period in study, variations in the kinematic results were caused by multipath and not from the effects of un-mitigated troposphere or movement of the twr1 station. This is shown by the RMS values in Table 7.7, where the highest is in the dU component for the COM part and the effects of multipath were almost the same in all components. The multipath is mainly from structures around the station such as the walls of the tower and the cables supporting the bridge deck, which could greatly influence the signals from the satellites before they reach the receiver. This trial demonstrates that multipath is the major cause of the variations in the kinematic solution, where if it were not identified, it could be interpreted as movements by the engineers. With a difference in height of about 110 metres, assuming no movement at twr1, the RMS of the un-mitigated troposphere (the OUT part of Table 7.7) is at most $\pm$5.2 mm in the dU component and lesser in the dN and dE components.

7.2 Analysis of the Forth Road Bridge Trial, 8th to 10th February 2005

Station ref1 was computed with respect to OS active station EDIN (Edinburgh) and the coordinates were then used as control to compute the "true" positions of other Forth Road Bridge Trial stations. The coordinates and standard deviations of the respective Forth Road Bridge Trial stations can be seen in Appendix B (Table B4). It is evident that the computed geodetic positions have been achieved with a high precision, as shown by their respective standard deviations with the maximum being $\pm$3.4 mm. Plots of the position residuals on each of the three days from ref1 and ref2 to twre can be seen in Appendix F.

Full length plots for the whole duration of the three days (8th to 10th February 2005), of the position residuals for baseline ref1 – twre and ref2 – twre, together with their GDOPs were as shown in Figure 7.10 and 7.11. For baseline ref1 – twre, both stations were using dual frequency receivers of the same type (SR530 DF). It can be seen that period around the 300,000 and 340,000 GPS seconds on day 9th February 2005 (gaps in green) have unresolved ambiguities. Apart from that, there are also intermittent epochs where the ambiguities were not resolved.

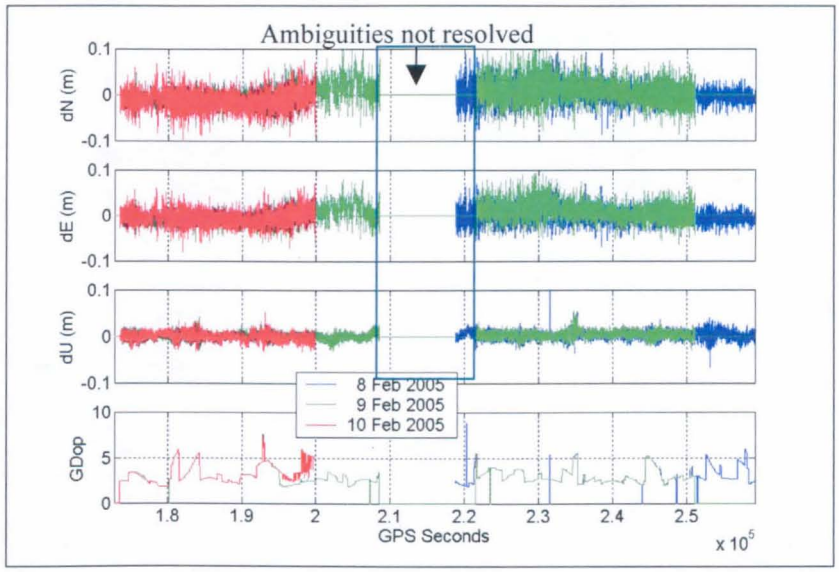

Figure 7.10 Position residuals and GDOPs for baseline ref1 to twre from three days of the Forth Road Bridge Trial on 8th (blue), 9th (green) and 10th (red) February 2005.

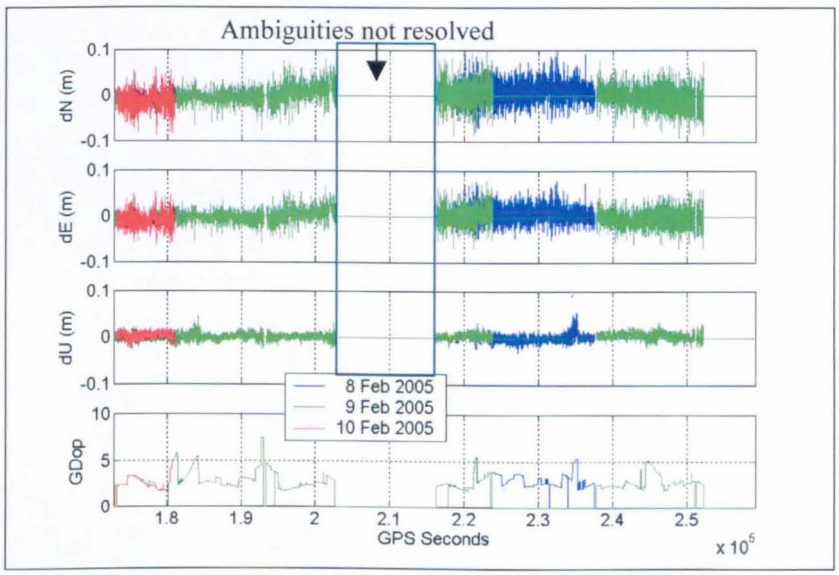

Figure 7.11 Position residuals and GDOPs for baseline ref2 to twre from three days of the Forth Road Bridge Trial on 8th (blue), 9th (green) and 10th (red) February 2005.

For baseline ref2 – twre, as can be seen in Figure 7.11, there are greater periods where ambiguities were not resolved. Due to results with unresolved ambiguities and CODE only solution, OTF kinematic processing had to be made in six sessions. The 6th session ambiguities were mostly not resolved and the 5th session also has periods with unresolved ambiguities towards the end of day 9th February. The receiver used at ref2 is the new Leica GRX1200. It has been noted that during

the period of observation, the receiver was having problems with the number of satellites in sight and at times, did not receive any signal. A check on the RINEX files showed that although the same satellite constellation was observed with dual frequency data recorded, lesser epochs were obtained at the ref2 station.

7.2.1 Common data sets

Although generally, the data were observed almost continously from noon on 8th February to 10 a.m. on 10th February 2005, there is very little common data between days. The major cause for this situation is that the data processed from ref2 came up with large gaps as can be seen in Figure 7.11 in the previous section. The only common data suitable for running AF was for the period between 00:08:26 to 02:13:09 hours on 9th February 2005 and advanced by 4 minutes for 10th February 2005. In seconds, they are equivalent to 259,706 to 267,189 and 345,866 to 353,349 GPS seconds on 9th and 10th February respectively, with a total of 7,484 seconds. Their GDOPs are almost the same which means that for the period concerned, the same constellation of satellites were used. The mean and standard deviation for each baseline for the selected epochs are given in Table 7.8.

Baseline	dN (mm)		dE (mm)		dU (mm)	
09 Feb 05	Mean	Std. Dev	Mean	Std. Dev	Mean	Std. Dev
refl–ref2	-3.2	2.8	-5.4	3.0	1.3	4.9
refl–twre	-7.1	9.1	-8.2	7.7	-0.2	6.0
ref2–twre	-3.9	9.0	-2.6	7.5	-1.7	5.4
10 Feb 05						
refl–ref2	3.6	2.8	6.1	2.9	-1.6	4.7
refl–twre	-9.1	16.8	-2.4	13.6	0.8	7.1
ref2–twre	-12.7	16.7	-8.5	13.4	2.6	5.9

Table 7.8 Mean and Standard Deviation of position residuals from selected epochs over two days of the Forth Road Bridge Trial, i.e. 9th and 10th February 2005.

Here, more consistent values can be seen for baseline refl – ref2 as they are both assumed to be static stations. Consistent values can also be seen in the dU component for baselines involving twre, but they vary in the dN and dE components, due to the variations of the position residuals in the time series which might be multipath, un-mitigated troposphere or movements.

7.2.2 Results for baseline refl – ref2

AF on two days was performed for baseline refl – ref2 [Forward (9^{th} as reference and 10^{th} as desired) and Backward (10^{th} as reference and 9^{th} as desired)] and the results showed that no significant multipath was present. From Figure 7.12, the highest value of multipath (COM part) is in the dU component with magnitude of up to $\pm$15 mm. Most of the time series have values of less than $\pm$10 mm, which were as expected as the distance between refl and ref2 is only 2.4 metres apart. The correlation of the time series between the two days AF were recorded as 0.3648 in dN, 0.2511 in dE and 0.3221 in dU. Although these values look small, as shown in Figure 7.12, the plots strongly suggest that some multipath is present because the plots from forward and backward runs of AF coincides, which means that the same trend exists on the two days. With these results, we can expect some variations from AF involving these two stations to twre. The RMS and the Minimum and Maximum values of each component are as shown in Table 7.9 and 7.10 respectively.

RMS Baseline refl–ref2	dN (mm)	dE (mm)	dU (mm)
OUT part	2.4	2.7	4.1
COM part	1.7	1.4	2.6

Table 7.9 RMS values for the OUT and COM parts from the AF on consecutive days (9^{th} and 10^{th} February) for baseline refl – ref2 in the Forth Road Bridge Trial.

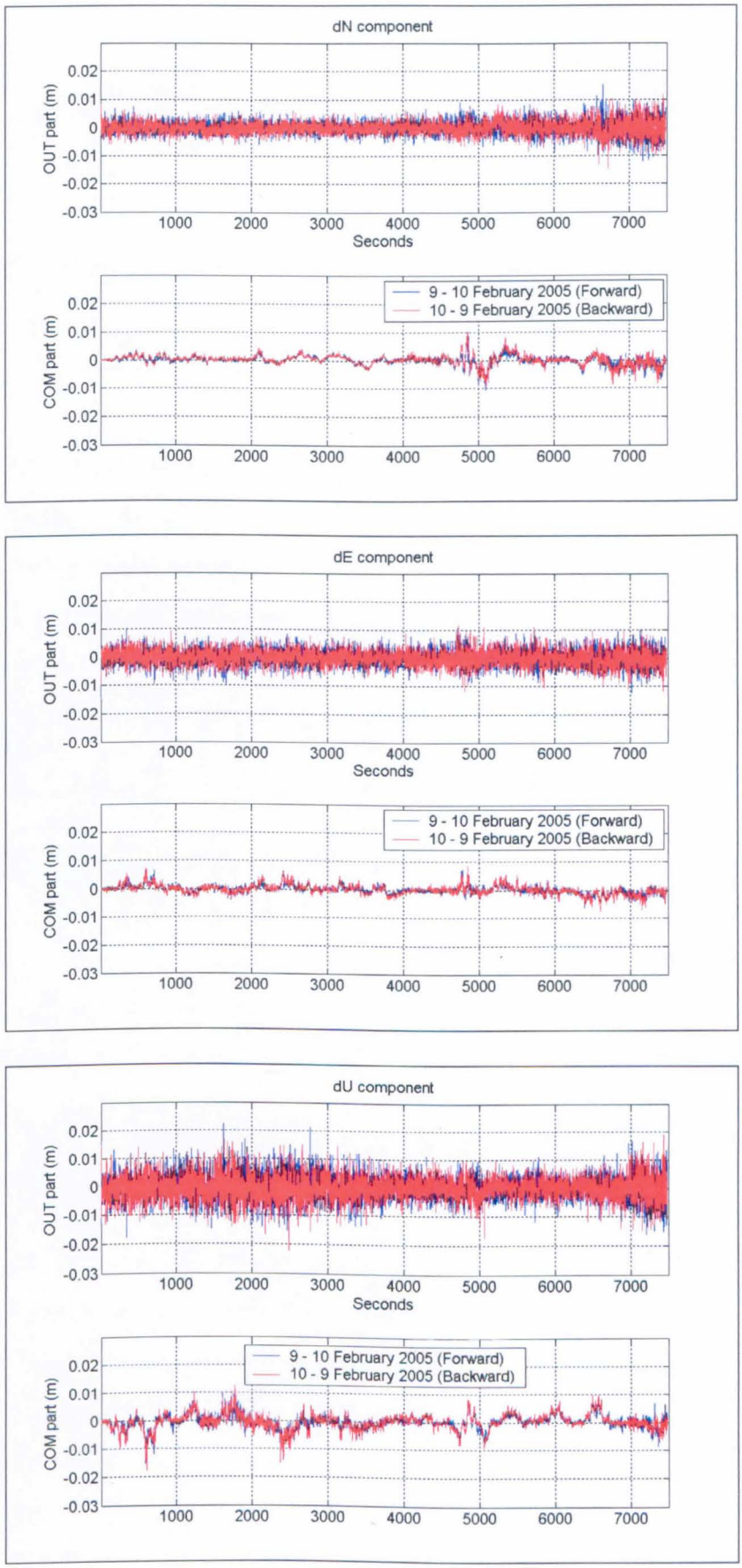

Figure 7.12 AF on two days for baseline ref1 – ref2 in the Forth Road Bridge Trial, i.e. 9th and 10th February 2005.

Baseline ref1–ref2	dN (mm)		dE (mm)		dU (mm)	
	Min	Max	Min	Max	Min	Max
OUT part	-13.0	14.3	-14.5	10.7	-17.7	22.2
COM part	-10.5	10.4	-6.2	7.2	-15.2	10.0

Table 7.10 Minimum and Maximum values for the OUT and COM parts from the AF on consecutive days (9th and 10th February) for baseline ref1 – ref2 in the Forth Road Bridge Trial.

The lower values of the RMS were expected for a very short baseline (2.4 m). As in the previous trials, the RMS for the OUT part exceed the COM part for this kind of baseline which means the noise dominates the position residuals. This can also be seen from the Max and Min values in Table 7.10. Although there are instances where the values reach as high as 22 mm, most of the epochs are below $\pm$10 mm for the dU component and lower for the dE and dN respectively.

7.2.3 Results for baselines ref1 and ref2 to twre

For these baselines, AF was performed firstly on the same day with ref1 – twre as reference and ref2 – twre as desired (Forward) and vice-versa (Backward) for 9th and 10th February 2005. Secondly, using the COM part from above, on consecutive days with 9th as reference and 10th February 2005 as desired (Forward), and vice-versa (Backward). The result from the same day AF is shown in Figures 7.13 (OUT part) and 7.14 (COM part) for all three components. It can be seen that the noise (OUT part) was successfully separated except for the slight spikes in the dN and dE components. The sharp spike in the dN plot for day 9th February, was from the forward run of AF with baseline ref1 – twre as reference and ref2 – twre as desired and does not appear in the backward run. The scenario is the reverse in the dE component. This is mainly due to the filter length that is being used in the Adaptive Filter script. When it is changed from the current value of 15 to 50 or higher, the sharp spike does not appear in the OUT part time series. However, the reason for retaining the filter length at 15 is, to ensure that sharp movements or vibrations can be extracted successfully by AF.

Looking at the COM part of Figure 7.14, which could consist of a combination of un-mitigated troposphere, multipath and movements, a different trend can be seen between the two days. Previously, for static stations, we have seen that the position residuals were highest in the dU component, but for this trial, it looks like it has the smallest variations as compared to the dN and dE components. This is shown by their RMS values in Table 7.11 and is an indication that movements could be the dominant factor here. The correlations for the results from same day AF can be seen in Table 7.12.

RMS	OUT part (mm)			COM part (mm)		
ref1/ref2–twre	dN	dE	dU	dN	dE	dU
09 Feb 05	2.7	2.8	3.9	8.6	7.0	3.9
10 Feb 05	3.0	2.9	3.7	16.3	13.0	4.8

Table 7.11 RMS values of OUT and COM part from AF on the same day (9th and 10th February 2005) for baselines ref1 and ref2 to twre in the Forth Road Bridge Trial.

ref1/ref2–twre	Day	dN	dE	dU
Same day AF	09 Feb 05	0.9511	0.9196	0.6287
	10 Feb 05	0.9863	0.9768	0.7502

Table 7.12 Correlations from AF on the same day (9th and 10th February 2005) for baselines ref1 and ref2 to twre in the Forth Road Bridge Trial.

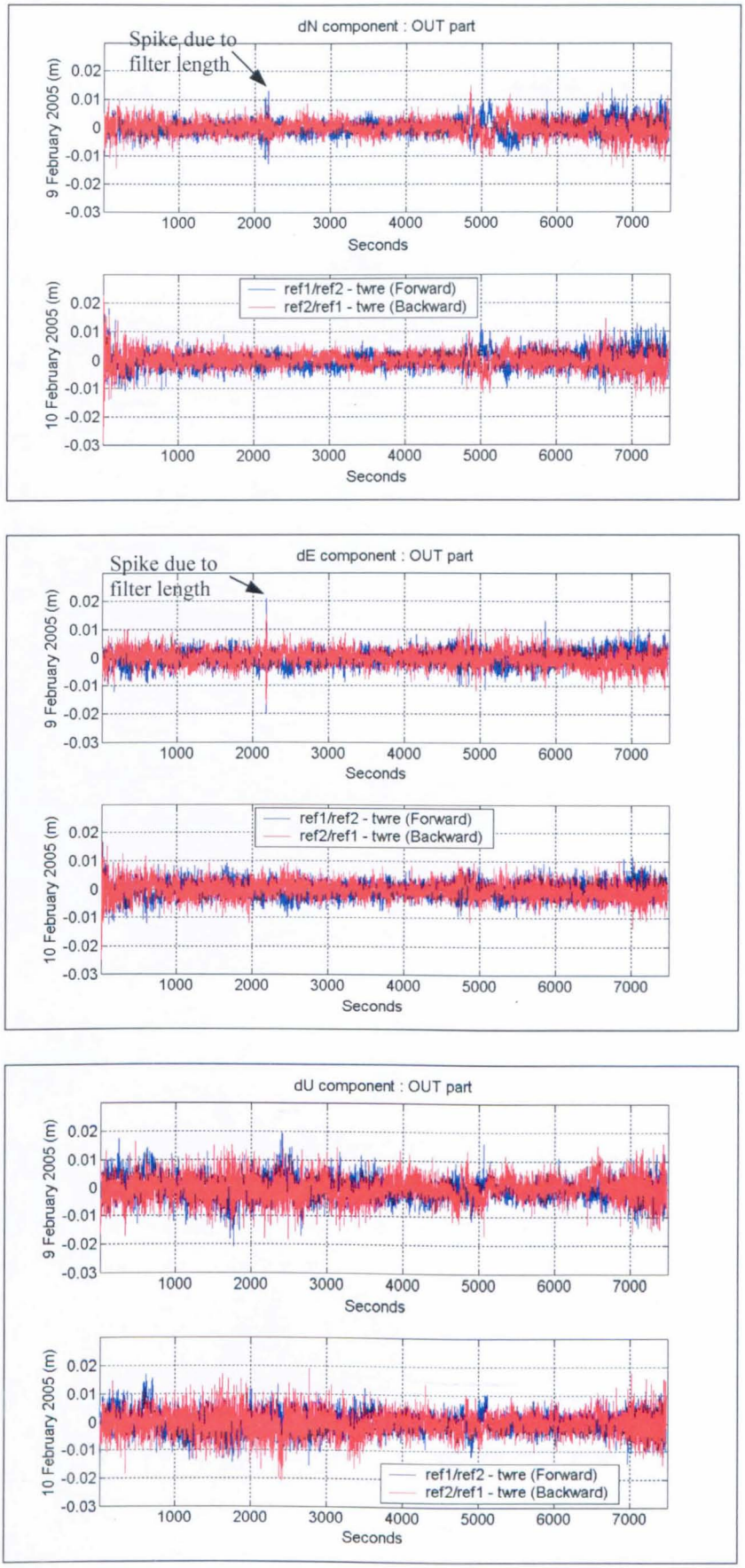

Figure 7.13 OUT part from AF on the same day (9th and 10th February 2005) for baselines ref1 – twre and ref2 – twre in the Forth Road Bridge Trial.

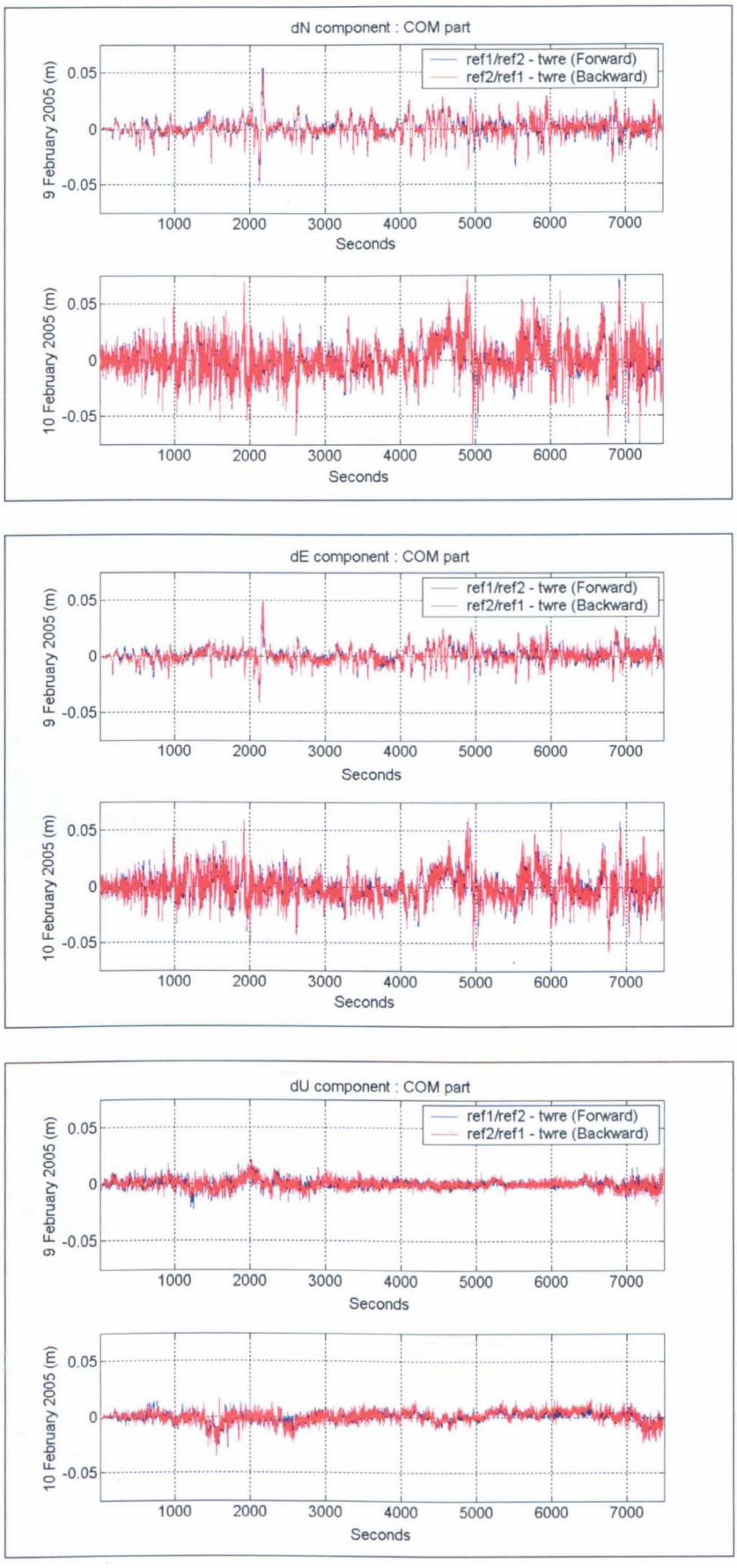

Figure 7.14 COM part from AF on the same day (9th and 10th February 2005) for baselines ref1 – twre and ref2 – twre in the Forth Road Bridge Trial.

Using the COM parts from Figure 7.14 above, AF was performed between the two consecutive days [Forward (9^{th} as reference and 10^{th} as desired) and Backward (10^{th} as reference and 9^{th} February 2005 as desired)]. The results are plotted in blue (forward) and red (backward) in Figure 7.15; their correlations were 0.0198 in dN, 0.0613 in dE and 0.1383 in dU.

These results are quite interesting, and very different from the results obtained for static stations. They are discussed in detail below.

7.2.3.1 Multipath

Looking at the COM part in Figure 7.15, in all three components there is no clear indication of the existence of multipath between the reference stations and the twre station. For example, in the dN component plot, there are significant differences between the forward and backward AF, which means that no exact match of the multipath pattern can be seen. There could be multipath at the 4,500 and 5,500 seconds mark, but it could also be similar patterns of movement on the two days. A more consistent pattern can only be seen in the dU component, at around the 1,500 seconds mark. The location of station twre is on top of the bridge tower, which was not heavily obstructed as experienced at twr1 in the Humber Bridge Trial. Whence, we can say that for this trial, no significant multipath is present. With this in mind, the COM part from Figure 7.14 represents a combination of the un-mitigated troposphere and movements. These are shown in Figure 7.16 using results from forward runs of AF only, as the backward runs produced similar results.

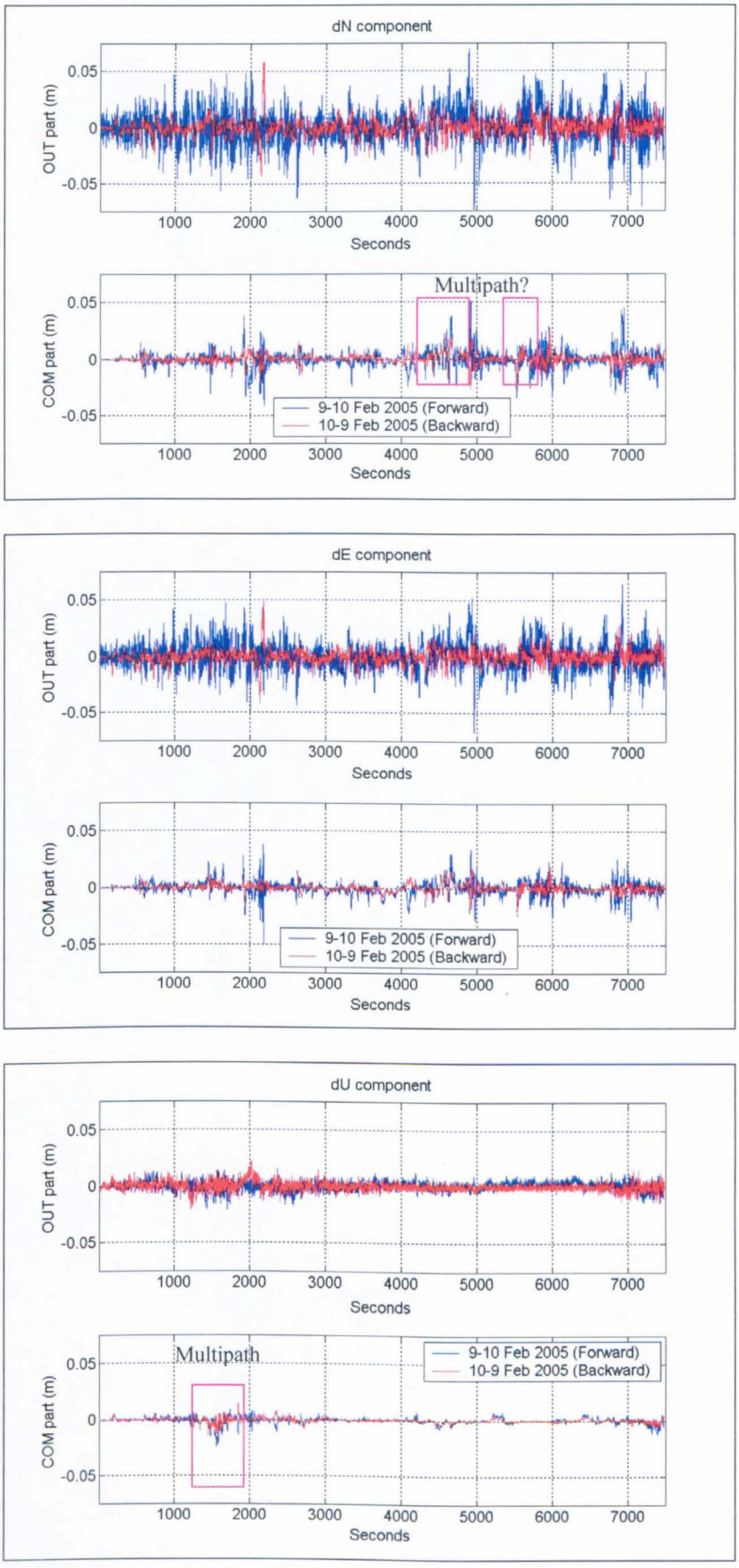

Figure 7.15 OUT and COM parts from AF on two days (9th and 10th February 2005) for baselines ref1/ref2 to twre in the Forth Road Bridge Trial.

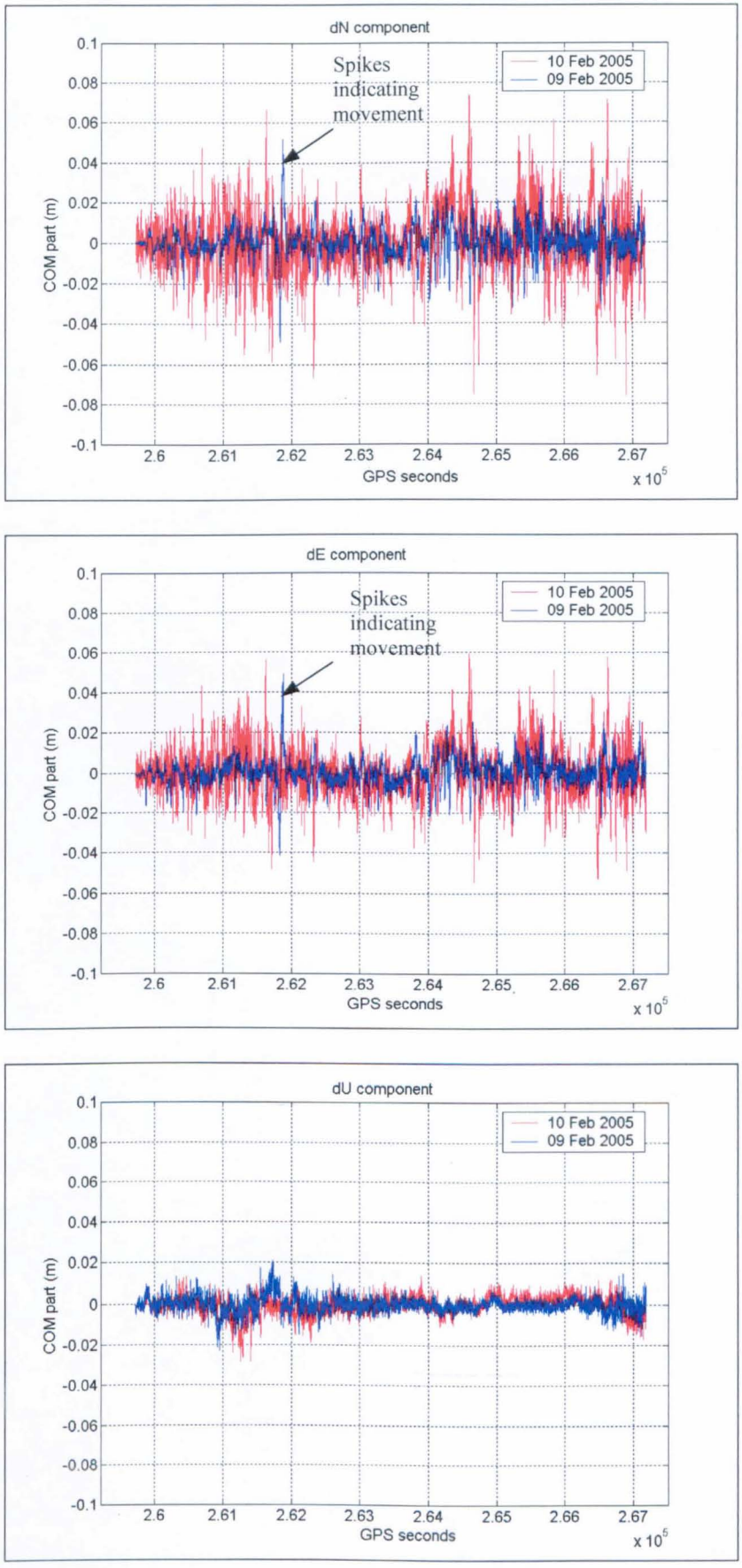

Figure 7.16 Plots of Un-mitigated Troposphere and Movements (COM part) between ref1/ref2 and twre on two days (9th and 10th February 2005) of the Forth Road Bridge Trial.

7.2.3.2 Un-Mitigated Troposphere

Based on the results from Chapter 6, using static stations, the variations of un-mitigated troposphere were maximal in the dU component. It is difficult to establish a threshold for the amount of un-mitigated troposphere to be expected as it varies between days, location and length of the baselines. If we are to consider the trends in the dU component, we can expect the effects of un-mitigated troposphere to be on average, about ± 10 mm. Of course, the variations in the dU component could also be related to movements in the dN and dE components, but considering movements in dN and dE of 4 cm for a 150 m high tower, this would account for less than 0.1 mm in dU.

Furthermore, the lengths of the baselines involved are about 750 metres, although the difference in altitude is higher than that of the University Trial i.e. 150 m, the location of the two ends of the baselines were in the same environment which differs from the University Trial and the Snowdon Trial. Whence, lesser effects from the un-mitigated troposphere should be expected as proven for the Humber Bridge Trial.

Figure 7.17, shows the Temperature in Celcius, Humidity in percentage, Wind speed in kilometres per hour and Wind Direction in degrees. From Figure 7.17, using the meteorological data, no unusual differences can be seen on the same day except for gradual changes in temperature and humidity, and variations in the wind speed. However, there are differences between days as shown by the four components of the meteorological data and this is reflected by the slight differences in the position residual plots as in Figure 7.16 (dU component). Since the meteorological data were obtained from one location, it is not possible to derive any relative differences between stations. These data were gathered at 30 seconds interval with the weather station placed at the centre of the middle span of the bridge deck. Comparing between Figure 7.16 with Figure 7.17, there is no indication of a significant relationship between the trends in the position residuals and the meteorological data.

Whence, for this trial, even though we know that difference in altitude does have some influence on the position residuals due to the un-mitigated troposphere, the impact of this might have been superceded by real movements.

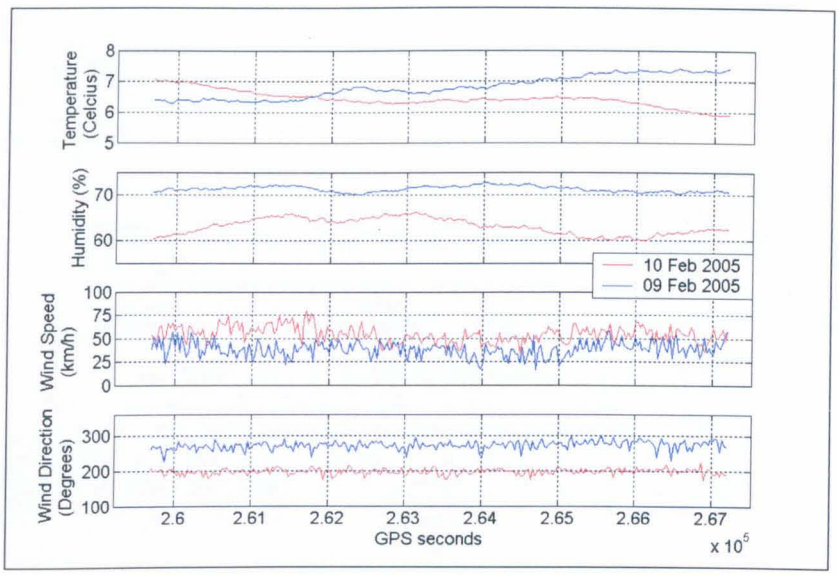

Figure 7.17 Plots of Meteorological Data on 9th and 10th February 2005, Forth Road Bridge Trial.

7.2.3.3 Tower Movements

Having identified the effects of multipath and un-mitigated troposphere in the time series, what is left to look at are movements. Looking again at the time series given in Figure 7.16 in the dN and dE components, there are some signs of movement on 9th February 2005, with larger deflections on 10th February 2005. The sharp spikes on 9th February 2005 (blue plot) just before the 262,000 GPS seconds mark are a clear sign of real movement.

A blow up plot for the period concerned (261,750 to 262,000 GPS seconds) can be seen in Figure 7.18. Such real movements of the tower could be caused by large and heavy vehicle(s) entering the bridge at the 261,800 and leaving at the 261,920 GPS second marks. Waves of deflection slowing down can be seen as the vehicle(s) near the exit. Whenever there is a movement in the positions (dN and dE component), the effect is the reverse for the dU component. Apart from the above, a lower band of movements can also be seen throughout the period of observation, which could be due to the effects of wind and light vehicles crossing the bridge.

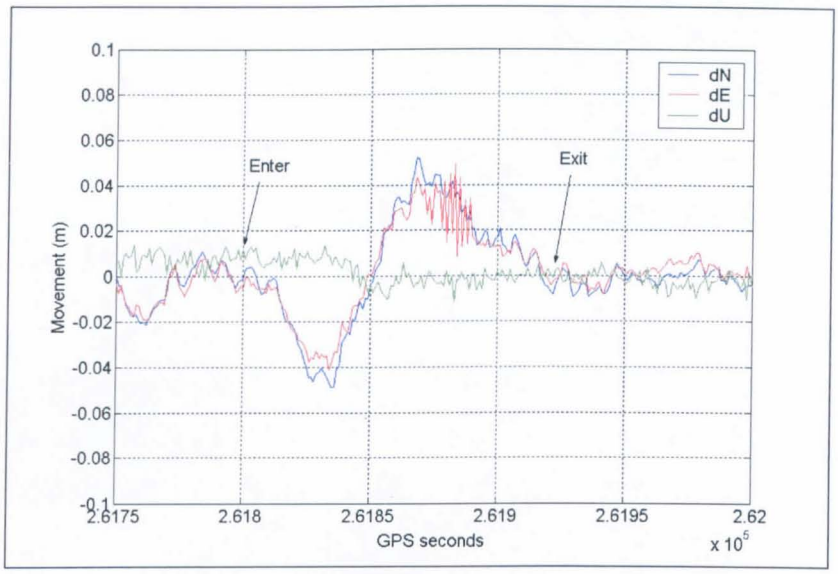

Figure 7.18 Movement of station twre for the period 261,750 to 262,000 GPS seconds on 9th February 2005 in the Forth Road Bridge Trial.

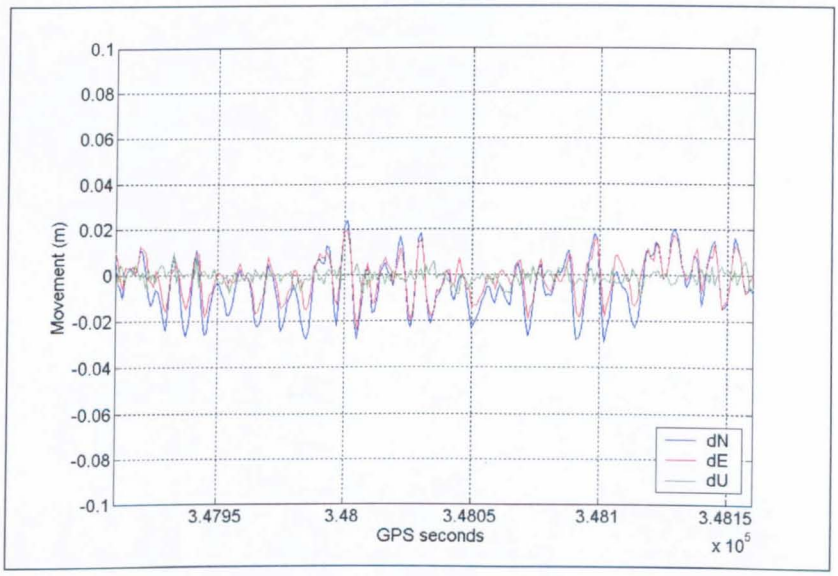

Figure 7.19 Movement of station twre for the period 347,910 to 348,160 GPS seconds (equivalent to period on 9th February as in Figure 7.18) on 10th February 2005 in the Forth Road Bridge Trial.

On 10th February 2005, much higher deflections can be seen in the time series. The wind was much stronger on this day as shown in Figure 7.17. The effects can be seen between epochs 260,800 to 262,500 GPS seconds in Figures 7.14 and 7.15. Higher variations can also be seen from the 263,391 to 266,713 GPS seconds period. This is actually the equivalent of 349,511 to 352,883 GPS

seconds for 10th February (01:05:51 to 02:01:23 hours UT) where, during this period the bridge was closed to all vehicles except for two 50 tonnes lorries. Figure 7.19 show the movements in all three components equivalent to period as of Figure 7.18 on 10th February. Only slight movements can be seen with a magnitude of around ±20 mm in the position components (dN and dE) and smaller in the dU component.

To further investigate whether the position residuals were dominated by real movement of the bridge tower, plots of the horizontal positions were produced as shown in Figure 7.20.

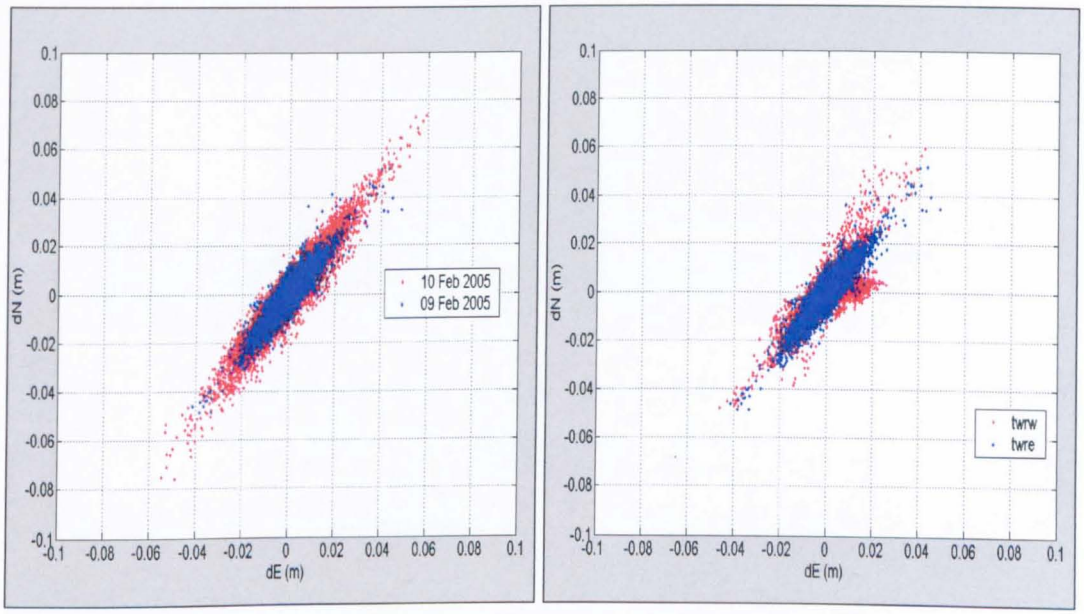

Figure 7.20 Horizontal positions of twre on 9th and 10th February 2005 (left) and twre and twrw on 9th February 2005 (right) for the Forth Road Bridge Trial.

The orientation of the bridge is about –3 degrees. The plots show that the position residuals have a direction of about 35 degrees, which suggests that the movements of the bridge tower are not in the bridge deck direction, but offset from this by 38 degrees clockwise, which could be due to the contribution of the wind coming from the North-North-West on 9th February and South-South-West on 10th February 2005. In terms of magnitude, a histogram plot of movements is given in Figure 7.21, where, it shows that for 09th February 2005, 98.4% of the position

residuals were 30 mm and below, with the highest of 66 mm at 261,868 GPS seconds (00:44:28 hours U.T.). For 10th February 2005, 86.2% of the position residuals were below 30 mm, 94.1% below 40 mm and 97.6% below 50 mm with the highest of 95 mm which occurs at 350,579 GPS seconds (01:22:59 hours UT).

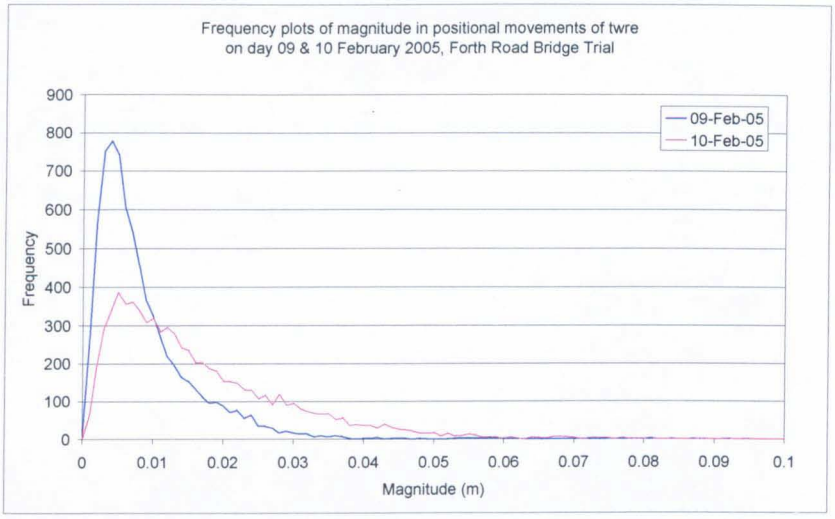

Figure 7.21 Frequency plots of magnitude in positional movements of twre ($\sqrt{dN^2 + dE^2}$) on 9th and 10th February 2005 for the Forth Road Bridge Trial.

Comparisons were also made using results from station twrw, which was located on the other side of the bridge deck but on the same tower as twre. Since the data was collected using a single frequency receiver (SR510), only common data on 9th February were available while common data for 10th February 2005 not available due to unresolved ambiguities. The positional plots together with results for twre on 9th February can be seen in Figure 7.20 (right). Poorer results were obtained for the twrw station but they still point to the same direction as twre, which suggests that real movement of the tower was dominant. The results which deviate from the common group were suspected to be multipath as twrw is using an AT502 antenna, which is not shielded from multipath like the choke-ring antenna used at twre.

To look at the effect of baseline length, the baseline from EDIN to twre was also processed. EDIN is nine kilometres away from ref1 and about twenty metres higher in altitude. The available data was from 262,800 to 288,879 GPS seconds. Only data on 9th February 2005 were available, hence, without common data, AF on same day and consecutive days cannot be performed. The position residuals are shown in Figure 7.22. Assuming no multipath present, we can see that with the longer baseline, higher variations in the positions were produced. If no data from ref1 were available, using only baseline EDIN – twre, the variations might be wrongly interpreted as movements. With only twre expected to move, it is highly likely that the points in the plots which depart from the red dots are not movements, but effects of un-mitigated troposphere due to the distance. Whence, the length of the baseline plays an important role for monitoring purposes.

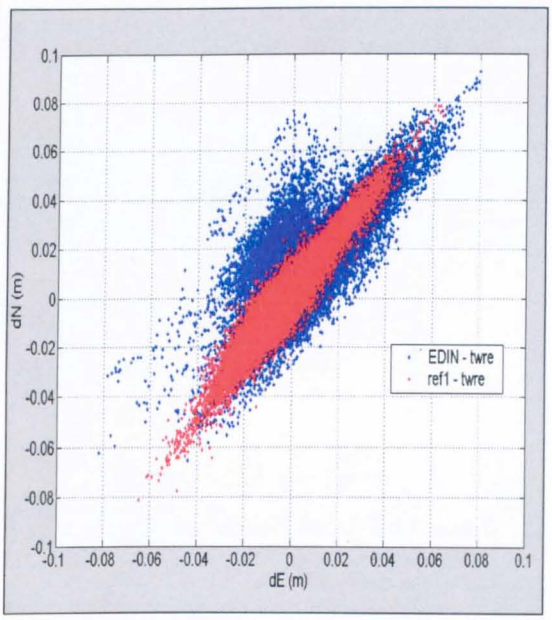

Figure 7.22 Horizontal positions of twre on 09th February 2005 computed from ref1 and EDIN for the Forth Road Bridge Trial.

7.3 Summary

It has been shown that multipath dominates the results from the Humber Bridge Trial and movements dominate the results from the Forth Road Bridge Trial. For the Humber Bridge Trial, the effects of un-mitigated troposphere are relatively small and difficult to be separated from movements. For the Forth Road Bridge Trial, the variations in the time series were considered to be real movements of the tower, contributed by the traffic loading on the bridge and wind. Based on results from Chapter 6, where the stations are static and un-mitigated troposphere dominates, the dU component recorded the highest variations in the position residuals time series. In this case for the Forth Road Bridge Trial, the dU component recorded the least variations. Hence, it is unclear if there were effects of un-mitigated troposphere, but even if it exists, the magnitude would be very small and would have been over shadowed by the real movements.

The conclusions of these tests are relevant to engineers as they show that real movements should only be considered once the effects of multipath and un-mitigated troposphere have been quantified, at least in terms of their magnitude if not in terms of their appearance as apparent movements.

Chapter 8

Comparing Virtual Reference Station Data with Actual Data

The concept of the VRS has been described in chapter 3. It is understood that the created virtual data would include the "correct" troposphere value for the particular station as it has been interpolated/extrapolated based from observations and computations made at existing known GPS stations [*Landau et al.*, 2003].

The VRS Network RTK system, as adopted by the Ordnance Survey of Great Britain is called OSNet [*Fane,* 2004], consists of the main HUB or Control Centre in Southampton, and the ground segment or physical network of reference stations on the ground spread throughout the United Kingdom, 27 to 98 km apart. Using data gathered from all reference stations, the HUB can compute models of ionosphere and troposphere from which VRS data can be created. For GPS mapping surveys, relative positions of a rover can then be computed with respect to a VRS. This brings the VRS nearer to the rover, which subsequently allows the mobility of the roving receiver to a greater distance from the actual reference stations. The Ordnance Survey are using Trimble software for this but Leica Geosystems AG are also using the same active station data for SmartNet, which is based around their SpiderNet software [*http://www.leica-geosystems.com*]

Using data for baselines lengths of 19 to 31 km, *Vollath et al.* [2002], made comparisons between actual and VRS data and found that for the ionosphere, with the VRS technique, an improvement factor of between 2 and 10 can be achieved, while the tropospheric residuals reduced by up to 40%, leading to improved positioning.

Restcher [2002] investigated the performance of a VRS network located in Southern Germany. For VRS baselines with a length of up to 35 km, the achievable precision for the horizontal component are always within ± 5 cm while for the height, larger standard deviations were obtained by a factor of 1.5 to 2 compared to the horizontal component.

Using an active GPS network with a distance of about 8 km from the nearest control station, *Lienhart* [2002] found that the precision of the plan positions and heights of single stations is better than 3 cm. The local positioning accuracy for shorter baselines (< 2 km) is about 1 to 2 cm if the two sites are occupied within one hour and about 3 cm otherwise. Although this result is better than that found by *Restcher* [2002], we have to bear in mind that the distance for the stations are much lower.

Landau et al. [2003] describes in detail how the corrections are computed for the VRS Network RTK system but still, it is not clear how the "actual" atmospheric and observation conditions are taken into account while generating the VRS data. For example, since the corrections are established relatively with respect to the nearest reference station, any un-mitigated atmospheric conditions at that reference station are suspected to be carried forward into the generated VRS data. This argument can then be extended to any multipath that is present at the reference station. This raises questions on the use of VRS data for monitoring purposes, as we have to be clear that apparent movements as shown by the position residuals are not treated solely as structural movements.

To investigate this, a second University trial as described in chapter 4 was conducted. The purpose was to see if VRS RINEX data can be an alternative if actual data were not available as a reference station in monitoring purposes. For this matter, virtual RINEX data were generated by the Ordnance Survey from their OSNet for each station where actual GPS observations were observed. Investigations were made, by comparing results from actual and virtual RINEX data in post processing.

The chapter starts with the details of the data processing and followed with the analyses of the results.

8.1 Preliminary Processing

Upon receiving the station coordinates, Colin Fane at the Ordnance Survey created virtual RINEX data for all stations, including NOTT. Here it should be noted that for the purpose of this thesis, whenever virtual data are referred to the 4 character ID will be preceded by a 'V', e.g. virtual data for twrl is vtwrl, for NOTT is VNOTT, etc.

To convert both actual and virtual data to kinematic mode, a "2" was inserted on a new line after the End Of Header in the RINEX file.

8.2 Static Processing

For the static processing, all of the actual data were processed with respect to station NOTT, using broadcast ephemeris and a 15 seconds epoch interval. The other parameters used were 15 degrees cut-off elevation angle and the *Saastamoinen* [1973] troposphere model with standard atmospheric parameters. The coordinates and standard deviations of the respective stations are given in Appendix B, Table B5.

All of the station coordinates were determined to a high precision, as shown by their standard deviations where the maximum value is 2.5 mm for station trel.

When the virtual data were available, static processing was also carried out by combining the data as

- From NOTT, i.e. with actual data to all stations with virtual data.
- From VNOTT, i.e. with virtual data to all stations with virtual data.

The results showed no significant differences in the station coordinates from these two mixed data combinations. However, when comparing the results based on purely actual data with the results based on purely virtual data, the station coordinates did have some differences. These are shown in Table 8.1. The highest differences of about 6 mm were recorded in the dU component for the stations

with difference in altitude of about 40 m. For stations at the same altitude, the differences in the dU component are minimal (less than 1 mm). This is also the case for all stations in the dN and dE components.

Station	dN (mm)	dE (mm)	dU (mm)
sf01	-0.5	0.0	0.3
sf02	-0.6	0.0	0.4
tre1	-0.7	0.0	0.2
tre2	-0.7	0.0	-0.1
twr1	-0.5	0.0	6.4
twr2	-0.6	0.0	6.1

Table 8.1 Differences in station coordinates when using purely actual and purely virtual data. The differences are results using virtual data minus results from actual data for the University Trial #2, 25th to 27th April 2005.

8.3 Kinematic Processing

Processing was carried out using the 1 second data for all three days. All possible baseline combinations were processed as follows,

a. Using actual data, i.e. from a station with actual data to a station with actual data,
b. Using virtual data, i.e. from a station with virtual data to a station with virtual data, and
c. Using mixed data, i.e. from a station with virtual data to a station with actual data.

8.3.1 Results

All baselines were computed successfully with the majority of the epochs having good GDOP of around 5 or lower, except for a short period of 2 minutes which happened around noon (130,000 GPS seconds) due to the number of satellites

available reducing as the geometry changed, as shown in Figure 8.1. At this time, the ambiguities were not resolved by Ski-Pro on DOY 115 (25th April 2005). There were also intermittent unresolved integer ambiguity epochs on DOY 116 and 117 (26th and 27th April 2005).

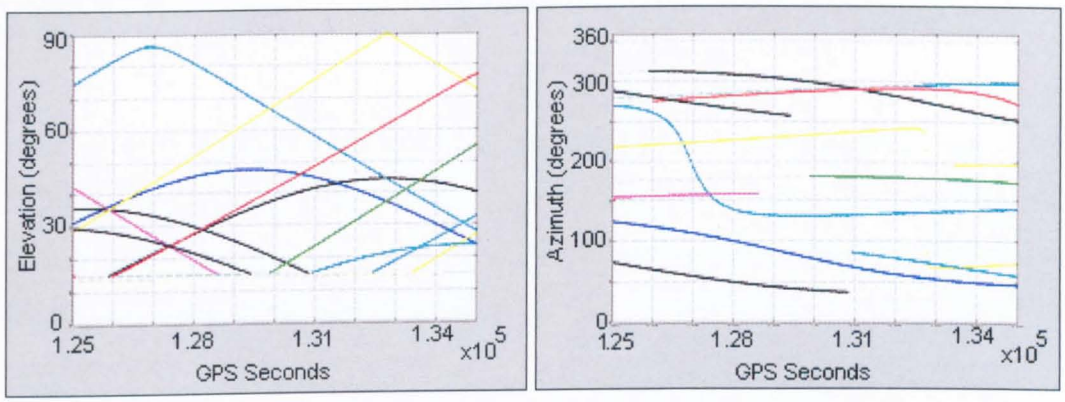

Figure 8.1 Plots of satellites elevation (left) and azimuth (right) as seen from NOTT on DOY 115 (25th April 2005) for the University Trial #2.

RMS	25 April 2005			26 April 2005			27 April 2005		
Actual data	Units in millimetres (mm)								
Baseline	dN	dE	dU	dN	dE	dU	dN	dE	dU
NOTT-sf01	4.4	5.7	5.9	4.7	5.8	7.6	6.9	8.3	11.4
NOTT-sf02	3.8	5.4	6.9	4.1	4.6	7.4	5.4	8.3	14.0
NOTT-tre1	3.4	5.3	6.3	4.0	5.3	8.3	5.6	9.0	12.8
NOTT-tre2	3.9	4.6	6.6	4.8	5.3	8.8	5.8	8.0	13.2
NOTT-twr1	3.3	4.3	5.5	3.6	4.9	8.0	5.8	8.1	13.7
NOTT-twr2	3.3	4.4	5.7	3.9	5.2	7.5	5.6	8.0	13.4
tre1-twr1	3.2	4.4	7.0	3.5	4.0	5.8	4.9	6.2	9.5
tre1-twr2	3.1	4.9	7.1	3.6	4.0	6.2	4.6	6.2	9.4
tre1-sf01	4.4	7.3	5.8	4.2	6.1	6.7	5.5	7.6	7.2
tre1-sf02	3.2	7.2	6.1	4.1	4.4	5.8	4.6	9.8	8.0
tre1-tre2	2.9	4.0	5.2	3.4	3.8	5.5	4.2	4.5	5.2
sf01-sf02	3.8	5.1	4.4	3.7	4.6	3.8	3.3	7.2	6.1
twr1-twr2	2.4	3.0	4.4	2.4	2.8	4.5	2.4	2.9	4.4

Table 8.2 RMS values for position residuals of baselines processed using actual data with Ski-Pro in kinematic mode for the University Trial #2 on 25th to 27th April 2005.

The RMS of the position residuals were computed from a total of 6,001 seconds i.e. from 10:04:00 to 11:44:00 hours for DOY 115, with a shift of 4 minutes for each consecutive day. Table 8.2 and 8.3 show the RMS values of the position residuals for the baselines processed using actual and virtual data respectively. Figure 8.2 presents the results for the baseline from NOTT and VNOTT in graphical form.

For the virtual data, the RMS values range from 0.1 to 4.1mm. This suggests that the interpolated corrections between the stations are quite small. Baselines of length a few metres show almost no differences at all whilst baseline lengths of up to two kilometres have slight differences in the troposphere resulting in slightly higher RMS values. Between days, DOY 117 (27th April 2005) have the highest variations which suggests the effects of troposphere were higher on that day.

RMS	25th April 2005			26th April 2005			27th April 2005		
Virtual data	Units in millimetres (mm)								
Baselines	dN	dE	dU	dN	dE	dU	dN	dE	dU
NOTT-sf01	0.7	1.0	2.5	1.0	0.5	2.1	0.7	0.9	2.9
NOTT-sf02	0.7	0.8	2.5	1.0	0.5	2.1	0.7	0.9	2.9
NOTT-tre1	0.9	0.9	2.7	1.2	0.6	2.5	1.1	1.0	4.0
NOTT-tre2	0.8	0.9	2.6	1.2	0.6	2.5	1.1	1.0	4.1
NOTT-twr1	0.7	0.4	1.9	0.7	0.7	1.3	0.9	0.9	3.0
NOTT-twr2	0.7	0.3	1.8	0.7	0.7	1.3	1.0	0.9	3.1
tre1-twr1	0.5	0.7	1.2	0.8	0.5	1.6	0.6	0.6	1.3
tre1-twr2	0.5	0.8	1.2	0.7	0.5	1.6	0.6	0.6	1.2
tre1-sf01	0.2	0.2	0.3	0.3	0.2	0.6	0.5	0.3	1.2
tre1-sf02	0.2	0.2	0.3	0.3	0.2	0.6	0.4	0.3	1.2
tre1-tre2	0.1	0.1	0.1	0.1	0.1	0.1	0.1	0.1	0.1
sf01-sf02	0.1	0.1	0.1	0.1	0.1	0.1	0.1	0.2	0.1
twr1-twr2	0.1	0.2	0.1	0.1	0.1	0.1	0.1	0.1	0.1

Table 8.3 RMS values for position residuals of baselines processed using virtual data with Ski-Pro in kinematic mode for the University Trial #2, 25th to 27th April 2005.

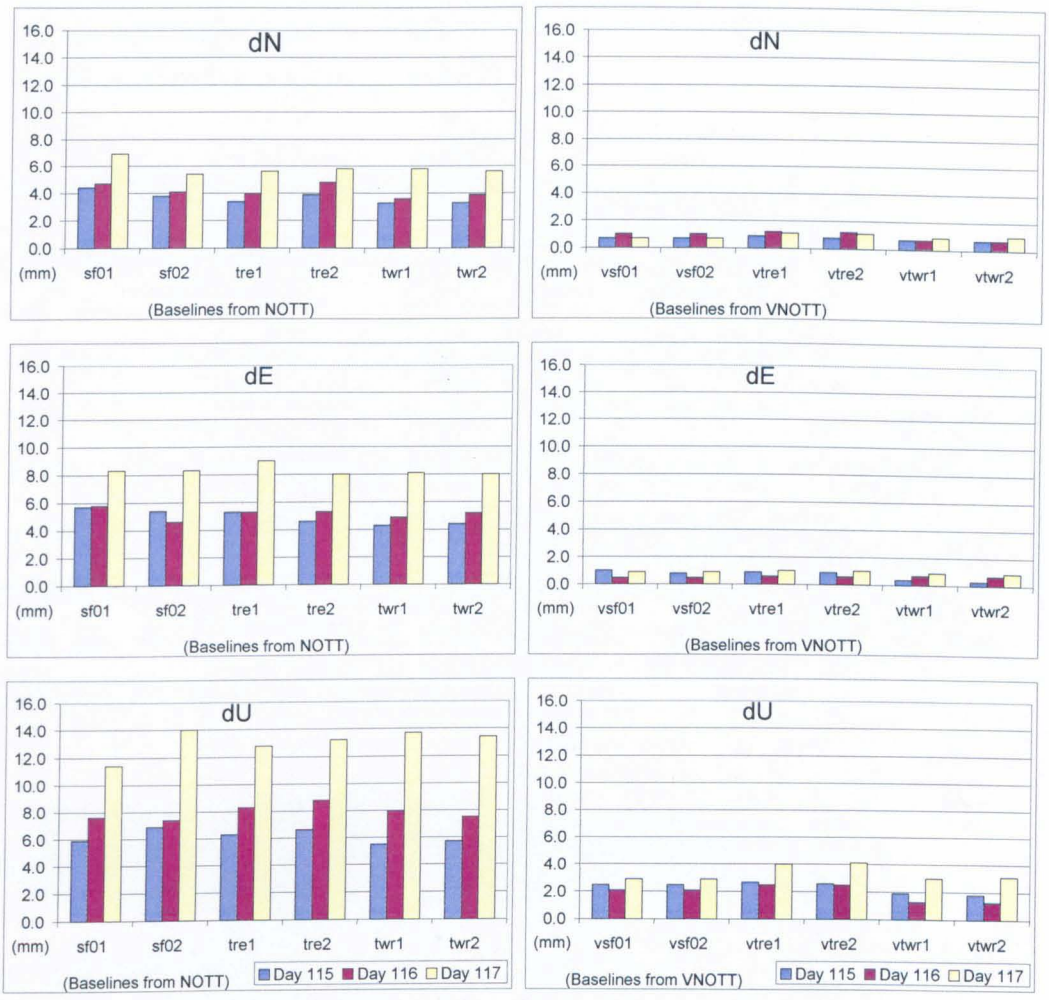

Figure 8.2 Plots of RMS values of position residuals for baselines from NOTT, processed actual and virtual data with Ski-Pro in kinematic mode for the University Trial #2 on 25th to 27th April 2005.

Considering the RMS values for the actual data, they vary from 2.4 to 14.0 mm. As compared to the RMS values for virtual data, the high values in the actual data could be due to real effects from un-mitigated troposphere, multipath and receiver noise. Even at a very small distance of a few metres, the RMS for the actual data reached as high as 6.1 mm. For these baselines, they should be experiencing the same troposphere, whence leaving multipath and receiver noise as the cause for the variations as shown by the RMS values. Station sf02 is located near a bus stop, which could contain multipath disturbance, as shown by its high RMS values. There are two kinds of multipath here, one is permanent multipath, where it repeats daily while the other is the temporary multipath created by passing large vehicles and buses stopping. Station twr1 and twr2 were on top of the tower

building and at 15 degrees elevation angle, so there should be no effects from multipath and, their RMS values should be purely an indication of the receiver noise and un-mitigated troposphere.

From Figure 8.2, it can be seen that the virtual data do take into account the real effects experienced by stations on a particular day. For example, on DOY 117 (27th April 2005), where the actual data RMS values were higher than the previous two days, the RMS values for the virtual data also rise. Considering results from virtual data alone, the RMS represents the relative troposphere as the rover virtual RINEX data were created based on the reference data where multipath and receiver noise will be mitigated. It can also be seen that, if VRS data are used as reference to compute the rover positions with actual data, it is expected that there will still be errors in the position residuals which, consist of multipath, un-mitigated troposphere and noise.

8.3.2 Does Multipath exist at OS active station NOTT?

As any virtual data is based on the actual data for the nearest reference station, i.e. NOTT in this case, it is important to ask if multipath exists at this active station. To investigate this, multipath (MP1 and MP2) plots from TEQC runs on NOTT RINEX data were produced as shown in Figure 8.3 for DOY 115 (25th April 2005). From the plots, there are signs of multipath at NOTT but the magnitude is less than 2 m, which occurs for satellites at lower altitude.

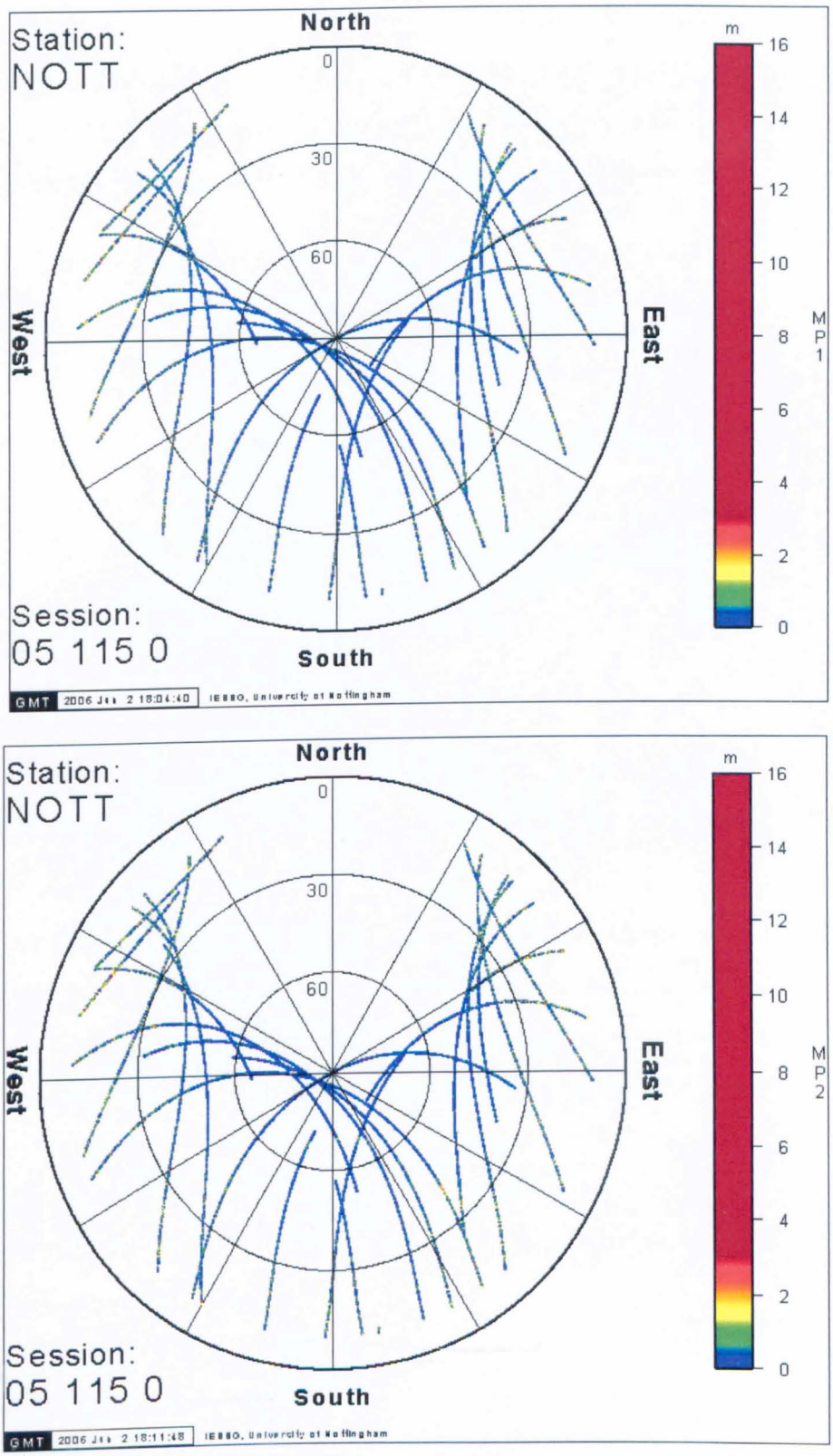

Figure 8.3 Sky plots of MP1 (top) and MP2 (bottom) from the RINEX file at station NOTT on DOY 115 (25th April 2005) during the University Trial #2.

8.3.3 Tests on baselines to station twr1

Using actual data, the plots of baselines from NOTT to twr1 can be seen for DOY 115 (25th April 2005) in Figure 8.4. The distance from NOTT to twr1 is less than two kilometres and the difference in height is about 40 metres.

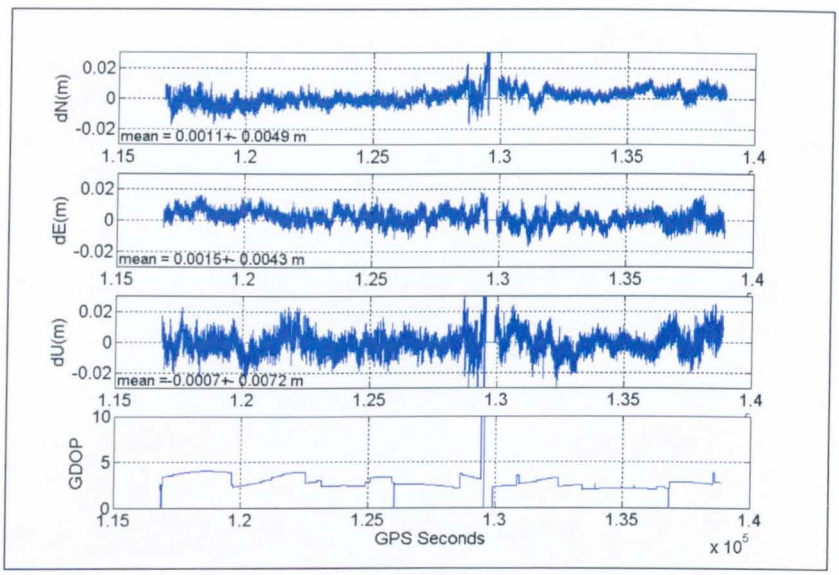

Figure 8.4 Plots of the baselines results for NOTT to twr1 using actual data on DOY 115 (25th April 2005) for the University Trial #2.

Plots of the same baseline using virtual data gave an almost straight line in all three components with very slight variations. This as expected as the virtual data "should be relatively free of all errors" such as troposphere and multipath. Hence, what we should get by using virtual data with actual data at an individual station is the absolute position residuals from the "true" coordinates of the respective station. Whereas, the result produced for baselines using virtual data is just representative of the modelled troposphere corrections that have been applied when creating the VRS data.

Computed baselines between NOTT and VNOTT produce "zero" differences in all components, the results for VNOTT to twr1 are the same as NOTT to twr1. This means that the virtual data for VNOTT is equivalent to the actual data for NOTT, which is perhaps not surprising if this OS active station was used as the nearest reference station in the creation of the virtual data. An inspection of the RINEX files for NOTT and VNOTT confirm this, as the pseudo-ranges are identical in both cases.

Figures 8.5 and 8.6 present the results for the mixed data cases at twr1 and twr2. On visual inspection it would appear that these are very similar to each other and to Figure 8.4, suggesting that the apparent movements are more likely to be "noise" in the actual data for stations twr1 and twr2 and that any differences in tropospheric delay between NOTT and twr1/2 have been modelled in the virtual data.

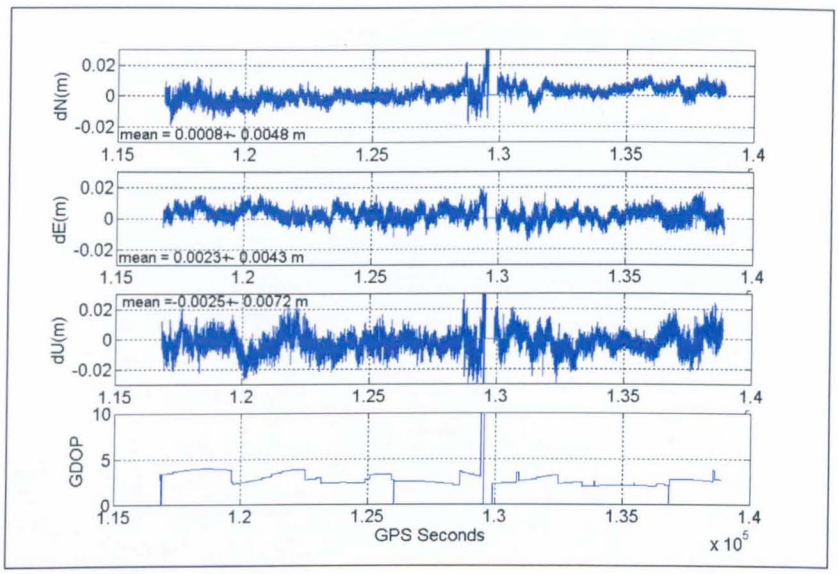

Figure 8.5 Plots of baseline vtwr1 to twr1, i.e. with virtual data (base) and actual data (rover) on DOY 115 (25th April 2005) for the University Trial #2.

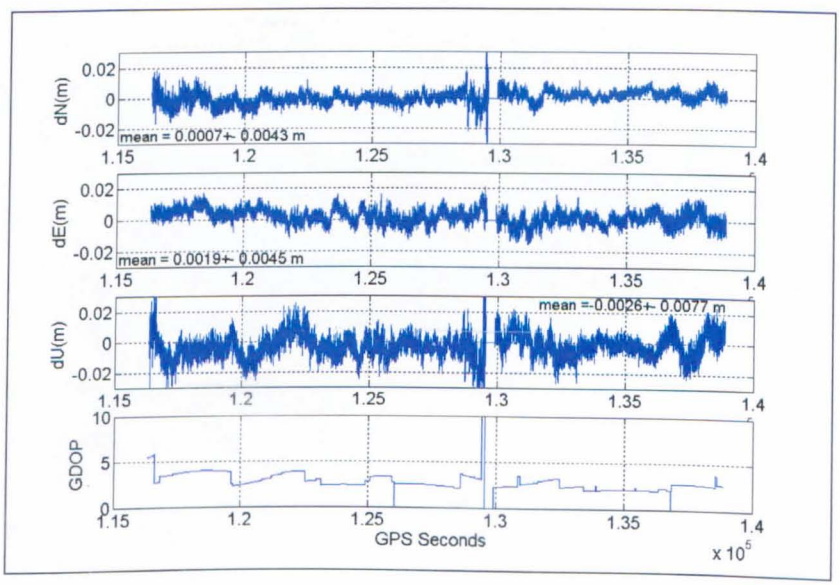

Figure 8.6 Plots of baseline vtwr2 to twr2, i.e. with virtual data (base) and actual data (rover) on DOY 115 (25th April 2005) for the University Trial #2.

Considering Figure 8.7, this argument is strengthened as even when using the virtual data, vtre1 with actual data twr1, effectively the same result is obtained as that shown in Figures 8.4, 8.5 and 8.6.

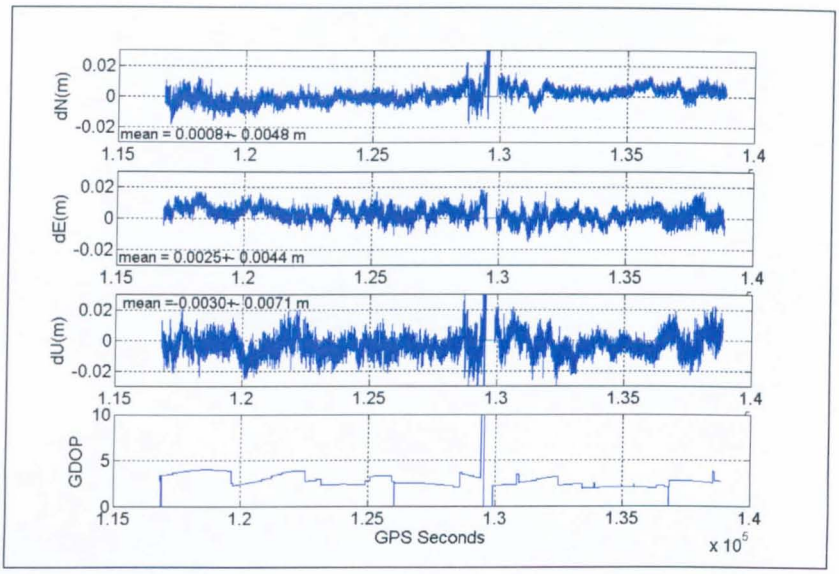

Figure 8.7 Plots of baseline vtre1 to twr1, using virtual and actual data on DOY 115 (25th April 2005) for the University Trial #2.

Considering a different combination of actual data, as in Figure 8.8, it is clear that the apparent movements here are a combination of the "noise" in the actual data for both stations, i.e. more likely to be multipath related than "un-mitigated tropospheric delay".

When the data for DOY 116 (26th) and 117 (27th April 2005) were processed, the same results as above were found. However, the trends were different between days and, as with their position residuals RMS plots in Figure 8.2, DOY 117 (27th April 2005) had the highest values, which could mean that observations for the day experiencing more un-mitigated troposphere and multipath.

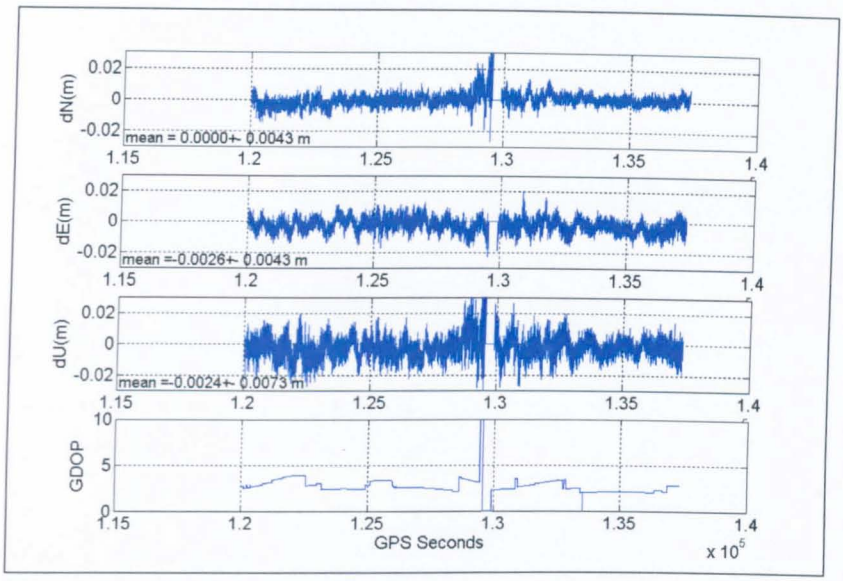

Figure 8.8 Plots of baseline tre1 to twr1, using actual data on DOY 115 (25th April 2005) for the University Trial #2.

8.3.4 Tests on baselines to sf01

Using actual data, the plots of baselines from NOTT to sf01 can be seen for DOY 115 (25th April 2005) in Figure 8.9. The distance from NOTT to sf01 is slightly above two kilometres and the difference in height is about -6 metres. Plots from NOTT to sf02 gave almost the same trend with slight differences.

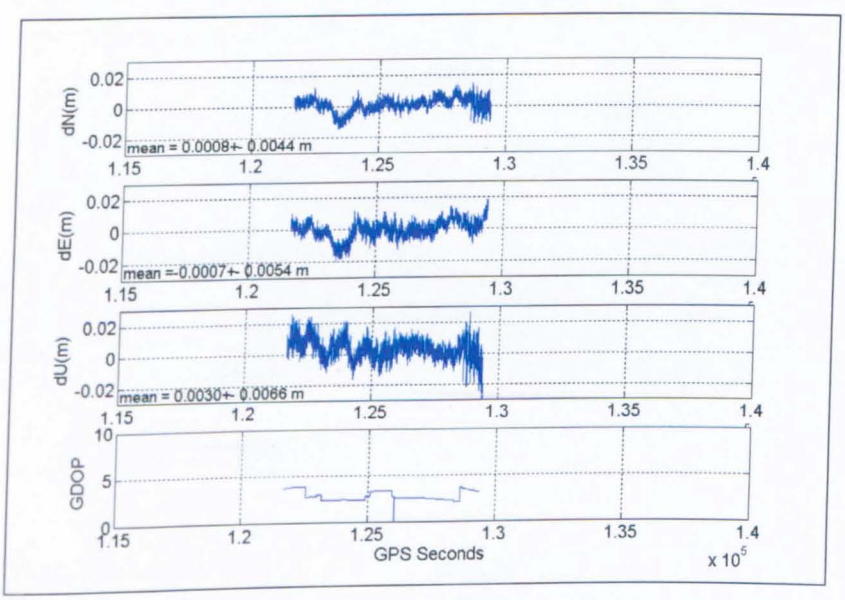

Figure 8.9 Plots of the baseline results for NOTT to sf01 using actual data on DOY 115 (25th April 2005) for the University Trial #2.

The results for VNOTT to sf01 are the same as NOTT to sf01. Further processing on sf01 between actual and virtual data (Figure 8.10), and vtre1 to sf01 (Figure 8.11) shows an almost identical result as in Figure 8.9. But using actual data for tre1 to sf01 shows a different trend (Figure 8.12). These show that the findings for sf01 concur with the findings for twr1.

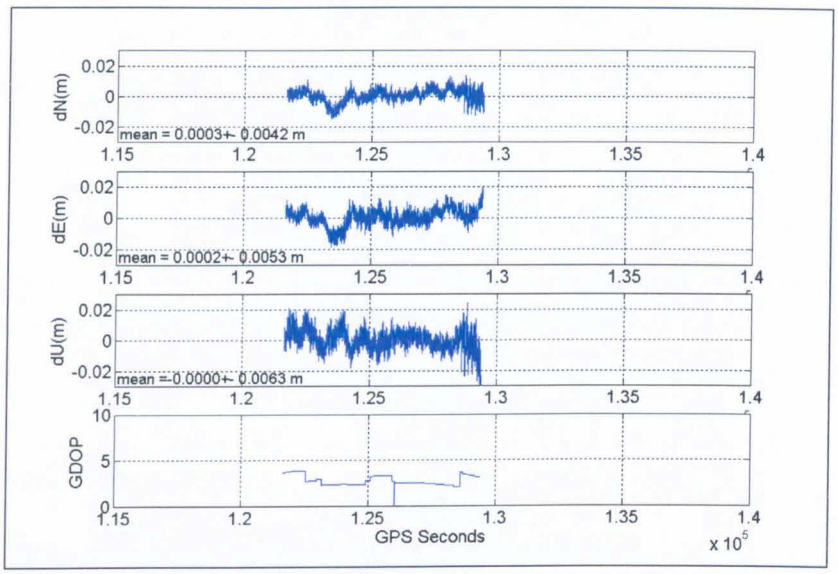

Figure 8.10 Plots of baseline vsf01 to sf01, i.e. with virtual data (base) and actual (rover) on DOY 115 (25th April 2005) for the University Trial #2.

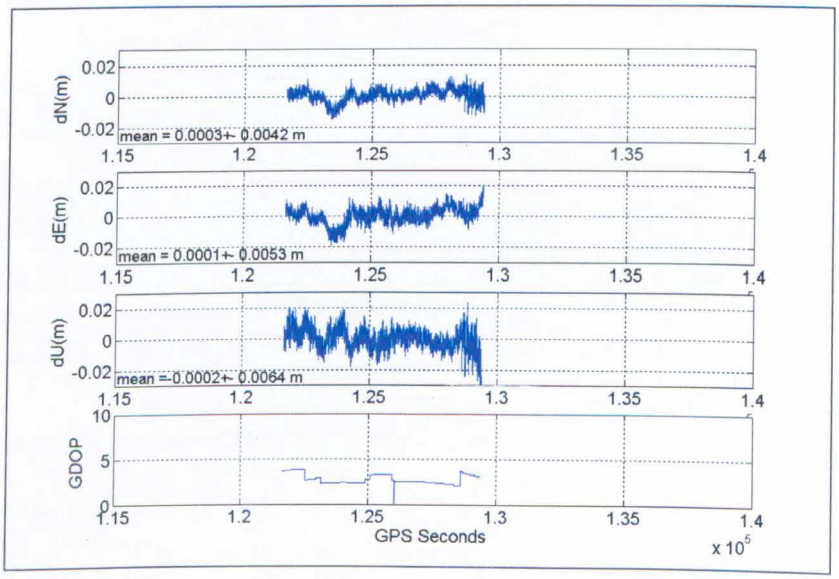

Figure 8.11 Plots of baseline vtre1 to sf01, using virtual and actual data on DOY 115 (25th April 2005) for the University Trial #2.

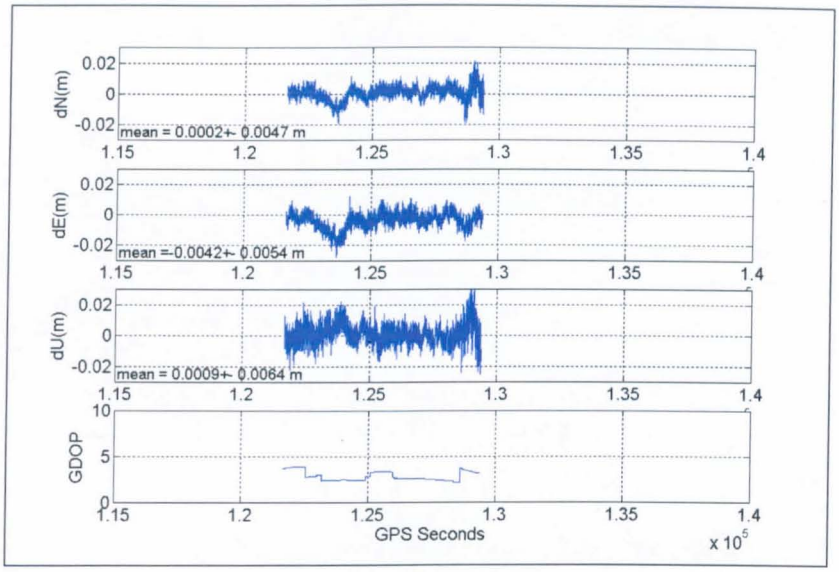

Figure 8.12 Plots of baseline tre1 to sf01, using actual data on DOY 115 (25th April 2005) for the University Trial #2.

8.4 Results Discussion

From the above findings, we can derive the following.

In general, for actual data, kinematic processing will compute a baseline with respect to a base station. The position residuals (δ) at a rover station for every epoch are then given by

$$\delta = \textit{Computed Position} - \textit{"True" position} \qquad [8.1]$$

Relatively, Δ will contain the following

$$\delta = (UT_r - UT_b) + (M_r - M_b) + (N_r - N_b) + (S_r - S_b) \qquad [8.2]$$

Where, UT – unmitigated troposphere, M – multipath, N – receiver noise, S – movement, and subscripts b and r are for base and rover respectively.

If $(S_r - S_b)$ equals zero (as the stations are assumed not to have moved)

$$\delta = (UT_r - UT_b) + (M_r - M_b) + (N_r - N_b) \qquad [8.3]$$

For virtual data, the position residuals (δv) at a rover station for every epoch are given by

$$\delta v = \textit{Computed virtual Position} - \textit{"True" position} \quad [8.4]$$

In this case δv will contain the following

$$\delta v = (UTv_r - UTv_b) + (Mv_r - Mv_b) + (Nv_r - Nv_b) \quad [8.5]$$

When using virtual data for the base and actual data for the rover, the position residuals (δmix) contain the following

$$\delta mix = (UT_r - UTv_b) + (M_r - Mv_b) + (N_r - Nv_b) \quad [8.6]$$

It is well known, that when using actual data from two receivers in a conventional zero baseline test

$\delta \neq 0$ as $\delta = N_{rec2} - N_{rec1}$

but $UT_{rec2} - UT_{rec1} = 0;$
$M_{rec2} - M_{rec1} = 0;$
$S_{rec2} - S_{rec1} = 0$

Considering a zero baseline test in which actual data from one receiver were used twice.

$$\delta = (UT_b - UT_b) + (M_b - M_b) + (N_b - N_b) + (S_b - S_b) = 0 \quad \text{or} \quad [8.7]$$

$$\delta = (UT_r - UT_r) + (M_r - M_r) + (N_r - N_r) + (S_r - S_r) = 0 \quad [8.8]$$

Similarly, for a zero baseline in which virtual data from one receiver were used twice.

$$\delta v = (UTv_b - UTv_b) + (Mv_b - Mv_b) + (Nv_b - Nv_b) = 0 \quad \text{or} \quad [8.9]$$

$$\delta v = (UTv_r - UTv_r) + (Mv_r - Mv_r) + (Nv_r - Nv_r) = 0 \qquad [8.10]$$

Now consider the case of mixed data at b, where b is actually the nearest reference station that is used to create VRS data. In this case

$$\delta mix = (UT_b - UTv_b) + (M_b - Mv_b) + (N_b - Nv_b) = 0 \qquad [8.11]$$

as $UT_b = UTv_b$; $M_b = Mv_b$; $N_b = Nv_b$

$= UT_{refl}$ $= M_{refl}$ $= N_{refl}$

However, this is not the case, eg. for baseline vtwrl to twrl as shown in Figure 8.5 when using mixed data at r where

$$\delta mix = (UT_r - UTv_r) + (M_r - Mv_r) + (N_r - Nv_r) \neq 0 \qquad [8.12]$$

as $UT_r \neq UTv_r$; $M_r \neq Mv_r$; $N_r \neq Nv_r$

because $UTv_r = fn\,(UT_{refl}, UT_{ref2}, \ldots\ldots, UT_{refn})$

$Mv_r = fn\,(M_{refl})$

$Nv_r = fn\,(N_{refl})$

In other words, the un-mitigated troposphere from the VRS data creation and the multipath and receiver noise at the reference station (refl) propagate into the virtual data and/or corrections used at the rover.

8.5 Summary

These tests show that by having an active station close to the area of interest, it is possible to create virtual data for stations which could be useful in helping to understand whether any apparent movements in the position residual time series emerging from the processing of actual data are due to troposphere or multipath (or in other cases real movements).

The created VRS data for a particular station will have the same characteristic as of the nearest reference station, in terms of multipath and receiver noise, but includes the expected tropospheric delay for the station. However, investigations on the VRS data when compared with actual data reveals that the tropospheric modelling used to account for the troposphere does not totally mitigate this effect.

Chapter 9

Conclusions, Recommendations and Suggestions For Further Work

9.1 Conclusions

The main research objectives as stated in chapter 1 were to

- Post-process GPS data in kinematic mode using Leica Ski-Pro Version 3.0 and compare the results with KINPOS.
- Identify the impact of un-mitigated troposphere for baselines with high differences in altitude.
- Identify the presence of multipath with the AF approach.
- Assess the quality of 3D position time series that could be provided to engineers for studies on the movement of structures.
- Investigate the use of VRS data for improved mitigation of tropospheric delay.

The findings for the above can be summarized as follows:

- Leica Ski-Pro Version 3.0 is a commercial software. Initially, it was thought that it only corrects for the hydrostatic delay since the actual algorithms used in it were unknown. Using KINPOS, comparisons were made on the position residuals and it was found that Leica Ski-Pro Version 3.0 attempts to correct for the total tropospheric delay, with the model given as equation [2.9b] in chapter two, and this was later confirmed by Leica Geosystems AG.

- It has been shown that as the baseline length increase, the effects of un-mitigated troposphere become greater. But it is not possible to quantify the exact amount or patterns of the effect as it depends on the location of the stations that form the baseline and varies from day to day. In terms of monitoring tall structures, it has been shown that difference in altitude, does not seem to have a systematic impact on the un-mitigated troposphere, based on the Snowdon Trial results in chapter six, where the magnitude of un-mitigated troposphere was almost the same for baselines with a fifty metres and one thousand metres difference in altitude. It was evident that if baseline lengths are kept to a minimum, as in the University Trial #1, smaller effects of the un-mitigated troposphere can be seen. However, it was demonstrated that the effects of the un-mitigated troposphere can be seen in all three components in the position residuals, not just in the dU component.

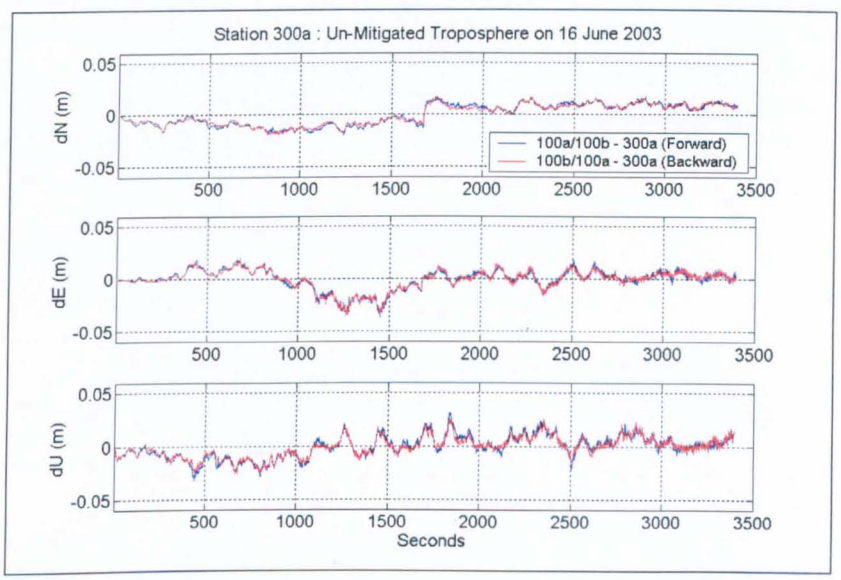

Figure 9.1 Un-Mitigated Troposphere in all three components from forward and backward AF runs from stations 100a and 100b to 300a on 16th June 2003 for the Snowdon Trial.

- Multipath can be identified with the AF approach for results on consecutive days, and further confirmed with results from a third day. Forward and backward runs of AF strengthen the identification of any existence of multipath. However, multipath could not be separated from un-mitigated troposphere, as found in chapter six, and from movements, as for the Forth Road Bridge Trial in chapter seven. It was concluded, therefore, that unless multipath dominates the position residuals time series, as can be seen from the

Humber Bridge Trial results, it will simply contribute to the magnitude of any apparent movements, as in the Forth Road Bridge Trial results.

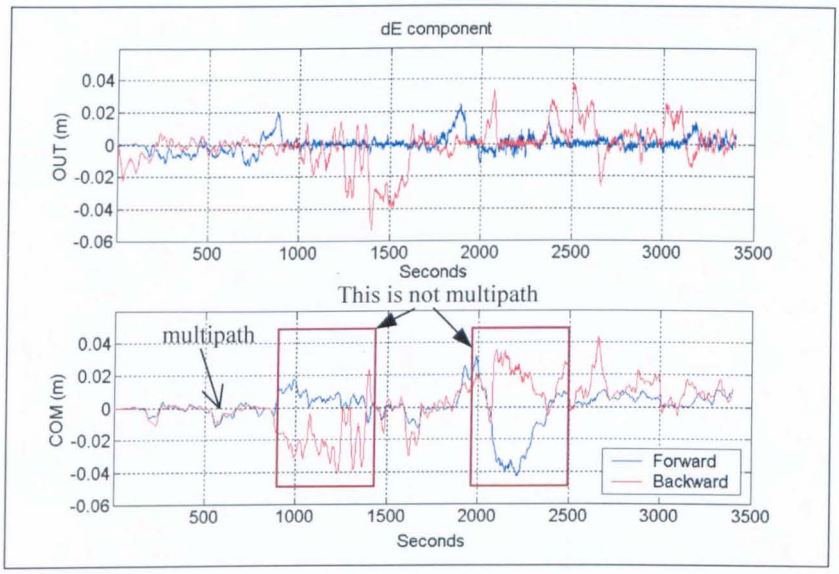

Figure 9.2 OUT (Un-Mitigated Troposphere) and COM (Multipath) parts of dE component from AF on two days (16th and 17th June 2003) for baselines 100a/100b to 400a in the Snowdon Trial. The COM part which should represent multipath could not be separated easily from un-mitigated troposphere.

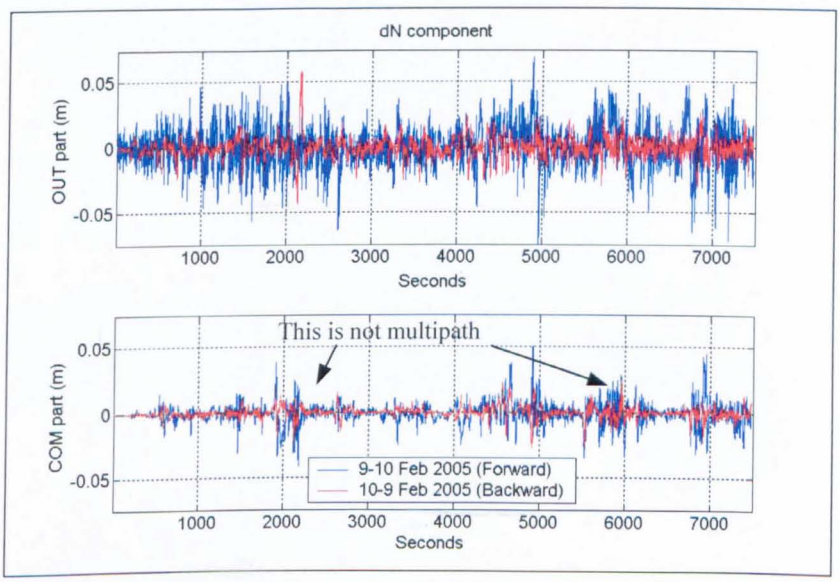

Figure 9.3 OUT (Movements) and COM (Multipath) parts of dN component from AF on two days (9th and 10th February 2005) for baselines ref1/ref2 to twre in the Forth Road Bridge Trial. The COM part which should represent multipath could not be separated easily from movements.

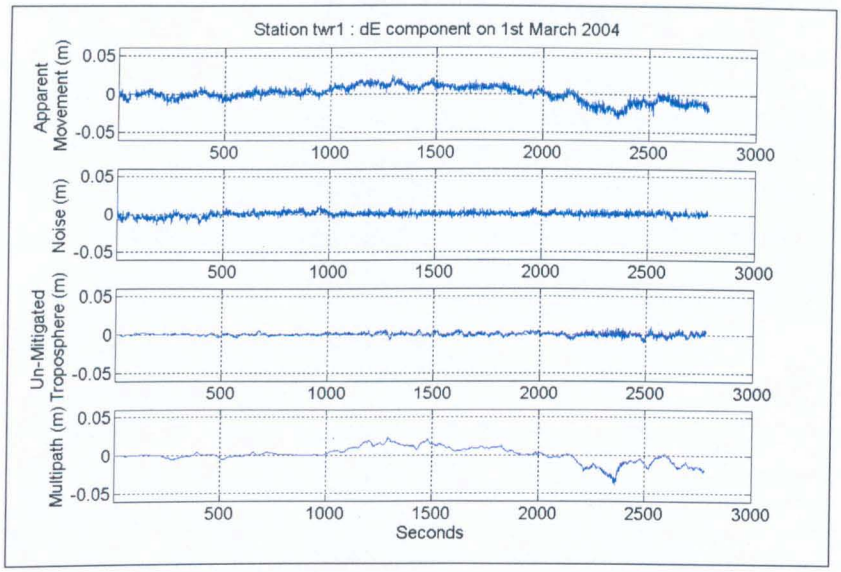

Figure 9.4 Apparent Movement at twr1 dominated by multipath in dE component on 1st March 2004 for the Humber Bridge Trial.

- Without a knowledge of the existence of un-mitigated troposphere and multipath, an engineer could easily mis-interpret apparent movements as real movements of a structure. The conclusions of these tests are relevant to engineers as they show that real movements should only be considered once the effects of multipath and un-mitigated troposphere have been quantified, at least in terms of their magnitude if not in terms of their appearance as apparent movements. These effects can result with apparent movements of magnitude up to ±40mm, however, these were dependent on the weather conditions and the location of the antennas.

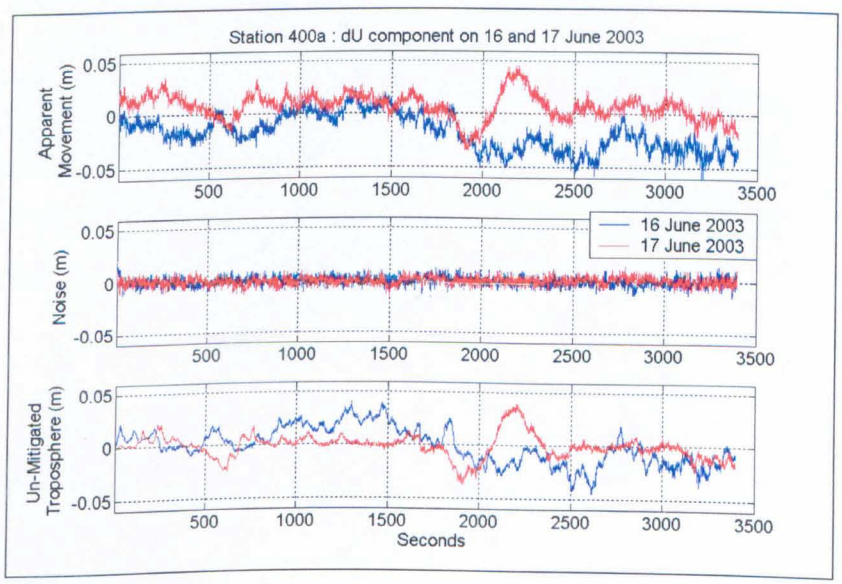

Figure 9.5 Apparent movement in dU component at station 400a dominated by un-mitigated troposphere on 16th and 17th June 2003 for the Snowdon Trial.

- Investigations on the VRS data as in chapter eight reveal that the tropospheric modelling used to account for the relative troposphere does not totally mitigate this effect. When compared to actual data for the same station, un-mitigated troposphere and multipath (from the reference station used to create the VRS data) still exists in VRS data.

9.2 Recommendations

For monitoring purposes, based on the conclusions of this research, engineers should consider the following recommendations:

- The baselines length from the reference to the monitored station should be as short as possible, to reduce the impact of un-mitigated troposphere aliasing as apparent movements, when using current commercial software or software with limited troposphere modelling capabilities.

- Analysis of time series of position residuals should include attempts to quantify the contributions of un-mitigated troposphere and multipath before any interpretation of real movements is carried out.

- The Adaptive Filter (AF) technique can be used to quantify the noise, un-mitigated troposphere, multipath and real movements. For best results, common data for at least three days should be used. By performing AF in Forward and Backward settings (interchanging the reference and desired time series), the trends of the output from AF can be validated.

9.3 Suggestions for further work

Based on the results of this research, the following further research could be carried out:

- Other methods should be studied to separate un-mitigated troposphere and real movements if it is not possible to use a short baseline length, e.g. further research using accelerometers [*Meng*, 2002] as an integrated unit should be investigated.

- To provide continuous data throughout the monitoring process, it is suggested to use additional peripherals such as pseudolites. Data gaps caused by un-resolved ambiguities due to corrupted signals or insufficient number of satellites available could then be filled.

- Further analysis of the movements of the towers in the Forth Road Bridge trial to investigate the influence of the bridge deck direction and wind direction on the observed movements.

References

Apostolidis, P. (2003). **Assessment of Multipath At North Shields Tide Gauge Continous GPS Station.** MSc Thesis, The University of Nottingham, UK.

Baueršíma, I. (1983). **NAVSTAR/Global Positioning System (GPS).** II., Mitteilungen der Satelliten-Beobachtungsstation Zimmerwald, No. 10, Astronomical Institute, University of Berne.

Behr, J. A., Hudnut, K. and King, N. (1998). **Monitoring structural deformation at Pacoima Dam, California, using continuous GPS.** Proceedings of the 11th International Technical Meeting of the Satellite Division of the Institute of Navigation, ION GPS-98, Nashville, TN, 15th–18th September.

Berg H. (1948). **Allgemeine Meteorologie.** Dümmler's Verlag, Bonn.

Bisnath, S.B., Mendes, V.B. and Langley, R.B. (1997). **Effects of Tropospheric Mapping Functions on Space Geodetic Data.** Proceedings of the IGS Analysis Center Workshop, Jet Propulsion Laboratory, Pasadena, Calif., U.S.A., 12th–14th March.

Boehm, J., Schuh, H. and Weber, R. (2001). **Influence of tropospheric zenith delays obtained by GPS and VLBI on station heights.** Proceedings of the IAG Symposium on Vertical Reference Systems, Cartagena, Colombia. 20th–23rd February.

Castleden, N, Hu, G.R., Abbey, D.A., Weihing, D., Øvstedal, O., Earls, C.J. and Featherstone, W.E. (2004). **First results from Virtual Reference Station (VRS) and Precise Point Positioning (PPP) GPS research at the Western Australian Centre for Geodesy.** Journal of Global Positioning Systems, Vol 3, No 1-2, 79-84.

Centipedia (2005). Internet site. (Last accessed 20th December 2005) http://www.centipedia.com/articles/troposphere/

Chadwell, C.D. and Bock, Y. (2001). **Direct estimation of absolute precipitable water in oceanic regions by GPS tracking of a coastal buoy.** Geophysical Research Letters, Vol. 28, No. 19, Pages 3701-3703, 1st October.

Chang, C.C. and Tseng, C.L. (1999). **Testing on Tropospheric Modelling for GPS Tracking Stations in Taiwan.** Geomatics Research Australisas. No. 70, pp 77-94.

Cheng, P., SHI, W.J. and Zheng, W. (2002). **Large Structure Health Dynamic Monitoring Using GPS Technology.** FIG XXII International Congress, Washington DC, USA, 19th–26th April.

Collins, J.P. and Langley, R.B. (1997). **Estimating the Residual Tropospheric Delay for Airborne Differential GPS Positioning.** ION GPS '97, 10th International Technical Meeting of the Satellite Division of the Institute of Navigation, Kansas City, Mo.,16th-19th September.

Collins, J.P. and Langley, R.B. (1998). **The Residual Tropospheric Propagation Delay: How Bad Can It Get?** Proceedings of the 11th International Technical Meeting of the Satellite Division of The Institute of Navigation, ION GPS-98, Nashville, TN, 15th–18th September.

De Jonge, P.J. and Tiberius, C.C.J.M. (1996). **The LAMBDA method for integer ambiguity estimation: implementation aspects.** Delft Geodetic Computing Centre, LGR series, No. 12.

Dodson, A.H., Shardlow, P.J., Hubbard, L.C.M., Elgered, G. and Jarlemark, P.O.J. (1996). **Wet tropospheric effects on precise relative GPS height determination.** Journal of Geodesy, 70, pp 188-202.

Dodson, A.H., Meng, X. and Roberts, G. (2001a). **Adaptive Method for Multipath Mitigation and Its Applications for Structural Deflection Monitoring.** International Symposium on Kinematic Systems in Geodesy, Geomatics and Navigation, Banff, Alberta, Canada, 5th – 8th June.

Dodson, A.H., Chen, W., Penna, N.T. and Baker, H.C. (2001b). **GPS Estimation of Atmospheric Water Vapour from a Moving Platform.** Journal of Atmospheric and Solar Terrestrial Physics, Vol. 63, pp1331-1341.

Duff, K. and Hyzak, M. (1997). **Structural Monitoring with GPS.** Public Roads, Spring 1997, Vol. 60, No. 4. Downloaded from the internet site. (Last accessed 24th January 2006).
http://www.tfhrc.gov/pubrds/spring97/gps.htm

Emporis (2005). Internet site. (Last accessed 20th December 2005).
http://www.emporis.info/en/bu/sk/st/tp/al/

Erener, A. and GÖKALP, E. (2004). **Mapping the Sea Bottom Using RTK GPS and Lead-Line in Trabzon Harbor.** FIG Working Week 2004. Athens, Greece, 22nd–27th May.

ESA (2006). **European Space Agency (GALILEO)** Internet site. (last accessed 12th February 2006).
http://www.esa.int/SPECIALS/Galileo_Launch/SEM4OD8A9HE_0.html

Euler, H.-J. and Ziegler, C. (2000). **Advances in Ambiguity Resolution for Surveying Type Applications.** ION GPS 2000, Salt Lake City, Utah, 19th–22nd September.

Fane, C.S. (2004). **An Empirical Analysis of The Performance of a Network RTK Solution.** MSc Thesis, The University of Nottingham, UK

Feta (2005). **Forth Road Bridge** Internet site. (Last accessed 23rd August 2005)
http://www.feta.gov.uk/

Ge, L.L, Chen, H.Y., Han, H. and Rizos, C. (2000). **Adaptive filtering of continuous GPS results.** Journal of Geodesy, 4 (7/8), 572-580.

Ge, L.L., Li, X., Peng, G.D., Rizos, C. and Ishikawa, Y. (2002a). **Intelligent Skyscrapper Monitoring System Based on GPS and Optical Fibre Sensors.** ION GPS 2002, Portland, Oregon, USA. 24th–27th September.

Ge, L.L., Janssen, V., Wang, Y.F. and Rizos, C. (2002b). **A Double Differencing Algorithm for GPS Derived Tropospheric Delay Corrections to Differential Radar Interferometry**. Downloaded from the internet site. (Last accessed 24th January 2006) http://www.gmat.unsw.edu.au/snap/publications/ge_etal2002c.pdf

Glenridge (2005). Internet site. (Last accessed 20th December 2005) http://www.glenridge.on.ca/megadoor/cbd028e.pdf

Gustafsson, F. (2001). **Adaptive Filtering and Change Detection.** John Wiley & Sons Ltd.

Häkli, P. (2004). **Practical Test on Accuracy and Usability of Virtual Reference Station Method in Finland.** FIG Working Week 2004, Athens, Greece, 22nd – 27th May.

Hansen, P. (1996). **On-The-Fly Ambiguity Resolution for GPS.** PhD Thesis, The University of Nottingham, UK.

Hatch, R. and Larsen, K. (1985). **Magnet – TI4100 GPS Survey Program, Processing Techniques and Test Results.** Proc. 1st Int. Symposium on Precise Positioning with the Global Positioning System, Washington DC, USA.

Haykin, S. (2001). **Adaptive Filter Theory.** Fourth Edition, Prentice Hall, Upper saddle River, New Jersey 07458.

HighTower (2006). Internet site (Last accessed 12 February 2006). http://mavrkyprojectphoto.blogspot.com/2006/02/highland-tower-collapse.html

Hofmann-Wellenhof, B., Lichtenegger, H. and Collins, J. (2001). **GPS: Theory and Practice.** Springer-Verlag/Wien 1997 (Fifth Revised Ed.), Austria.

Hopfield, H. S. (1969). **Two-quartic tropospheric refractivity profile for correcting satellite data.** Journal of Geophysical Research, Vol. 74, No. 18, pp. 4487-4499.

Hugentobler, U., Schaer, S. and Fridez, P. (2001). **Astronomical Institute of Berne, Troposphere Modeling and Estimation, Bernese GPS Software Version 4.2 manual.**

Humberbridge (2005). **Humber Bridge** Internet site. (Last accessed 23rd August 2005). http://www.humberbridge.co.uk/

IGS (2006). **International GNSS Service** Internet site. (Last accessed 12th February 2006). http://igscb.jpl.nasa.gov/components/prods_cb.html

Jensen, A.B.O. (2002a). **Investigations on the Use of Numerical Weather Predictions, Ray Tracing, and Tropospheric Mapping Functions for Network RTK.** Proceedings of ION-GPS/GNSS, 9th–12th September, Portland, Oregon, 2324.

Jensen, A.B.O., Tscherning, C.C. and Madsen, F. (2002b). **Intergrating Numerical Weather Predictions in GPS Positioning.** ENC GNSS-2002, Copenhagen, May.

Kaplan, E.D. (1996). **Understanding GPS Principles and Applications.** Artech House Inc.

Kashani, I., Wielgosz, P. and Grejner-Brzezinska, D. (2004). **The Double Difference Effect of Ionospheric Correction Latency on Instantaneous Ambiguity Resolution in Long-Range RTK.** ION GNSS, 17th International Technical Meeting of the Satellite Division, Long Beach, CA, 21st–24th September.

Kennie, T.J.M. and Petrie, G. (1990). **Engineering Surveying Technology.** Blackie, John Wiley & Sons, Inc.

Kijewski-Correa, T. and Kareem, A. (2003). **The Height of Precision.** University Of Notre Dame, Chicago, GPS World, September.

Kim, D., Jang, J and Kee, C. (2004). **Integer Ambiguity Search Technique Using Separated Gaussian Variables.** GNSS 2004. Sydney, Australia. 6th–8th December.

Kotthoff, H., Hilker, C. and Ziegler, C. (2005). **Strategy of Reliable Ambiguity Resolution for Static and Kinematic Applications.** Leica Geosystems AG, Switzerland. Downloaded from the internet site. (Last accessed 7th June 2005). http://www.leicaatl.com/support/gps/Technical_papers/AmbiguityStrategy.pdf

Landau, H., Vollath, U. and Chen, X. (2003). **Virtual Reference Stations versus Broadcast Solutions in Network RTK - Advantages and Limitations.** GNSS 2003, Graz, Austria, 22nd–25th April.

Landau, H., Vollath, U. and Chen, X. (2004). **Benefits of Modernized GPS/GALILEO to RTK Positioning.** GNSS 2004, Sydney, Australia, 6th–8th December.

Lau, L. (2004). **Investigations into Multipath Effects on GNSS Multiple-Frequency Single Epoch High Precision Positioning.** ION GNSS 17th International Technical Meeting of the Satellite Division, Long Beach, CA, 21st–24th September.

Leick, A. (2004). **GPS Satellite Surveying.** 3rd Ed., Dept of Surveying Engineering, University Of Maine, A Wiley-Interscience Publication.

Li, X., Rizos, C., Ge, L., Ambikairajah, E., Tamura, Y. and Yoshida, A. (2006). **Building Monitors: The Complementary Characteristics of GPS and Accelerometers in Monitoring Structural Deformation.** Inside GNSS, March.

Lienhart, W., Wieser, A. and Brunner, F.K. (2002). **Positioning by an Active GPS System: Experimental Investigation on the Attainable Accuracy.** FIG XXII Congress, Washington D.C., April.

Lovse, J.W., Teskey, W.F., Lachapelle, G. and Cannon, M.E. (1995). **Dynamic Deformation Monitoring of Tall Structure Using GPS Technology,** ASCE Journal of Surveying Engineering, 121, No. 1, pp 35-40.

Mader, G. L. (2006). **National Geodetic Survey (NGS)** Internet site. (Last accessed 20th January 2006). http://www.ngs.noaa.gov/ANTCAL/

Meng, X. (2002). **Real Time Deformation Monitoring of Bridges Using GPS/Accelerometers.** PhD Thesis, The University of Nottingham, UK.

Metoff (2005). **Met Office UK** Internet site. (Last accessed 20th December 2005) http://www.metoffice.com/education/secondary/teachers/

Misra, P. (2001). **Global Positioning System, Signals, Measurements, and Performance.** Ganga-Jamuna Press.

Niell. A. E. (1996). **Global mapping functions for the atmospheric delay at radio wavelengths.** Journal of Geophysical Research, 101, B3, pp 3227-3246.

Ogaja, C., Rizos, C., Wang, J. and Brownjohn, J. (2001). **High precision dynamic GPS system for on-line structural monitoring.** 5th International Symposium on Satellite Navigation Technology & Applications, Canberra, Australia, 24th–27th July, CD-ROM proc.

Parkinson, B.W. and Spilker, J.J. (1996). **Global Positioning System: Theory and Applications.** Volume I, American Institute of Aeronautics and Astronautics, Inc.

Pattinson, M. J. (2002). **Estimation of Tropospheric Delay from a Moving GPS Receiver.** PhD Thesis, The University of Nottingham, UK.

Restcher, G. (2002). **Accuracy Performance of Virtual Reference Station (VRS) Networks.** Journal of Global Positioning Systems, Vol. 1, No. 1: 40-47.

Rizos, C., Satirapod, C., Chen, H.Y. and Han, S. (1999). **GPS With Multiple Reference Stations: Surveying Scenarios In Metropolitan Areas.** 6th South East Asean Surveyors Congress, Fremantle, 1st–6th November.

Rizos, C. and Han, S. (2002). **Reference Station Network Based RTK Systems - Concepts and Progress.** International Symposium on GPS/GNSS, Wuhan, China, 6th–8th November.

Roberts, G.W., Dodson, A.H., Brown, C.J., Karuna, R. and Evans, R.A. (2000). **Monitoring the Height Deflections of the Humber Bridge by GPS, GLONASS and Finite Element Modelling.** IAG Symposia, Springer-Verlag, Vol 121, ISBN 3-540-67002-5, pp355-360, Berlin.

Roberts, G.W., Meng, X. and Dodson, A.H. (2001). **The Use of Kinematic GPS and Triaxial Accelerometers to Monitor the deflections of Large Bridges, Proc – Deformation Measurements and Analysis.** 10th International Symposium On Deformation Measurements, International Federation of Surveyors (FIG), Orange California, USA 19th–22nd March.

Roberts, G.W., Ogundipe, O. and Dodson, A.H. (2002). **Construction Plant Control Using RTK GPS.** FIG XXII International Congress, Washington, D.C. 19th–26th April.

Rutledge, D., Gnipp, J. and Kramer, J. (2001). **Advances in Real-Time GPS Deformation Monitoring for Landslides, Volcanoes, and Structures.** 10th International Symposium On Deformation Measurements, International Federation of Surveyors (FIG), Orange California, USA 19th–22nd March.

Saastamoinen, J. (1973). **Contribution to the theory of atmospheric refraction.** Bulletin Géodésique, 107, pp. 13-34.

Schueller, W. (1977). **High-Rise Building Structures.** John Wiley & Sons.

Staton, G. (2003). **Dodging The Invisible, The Recognition and Mitigation of RFI in GPS Data : A Receiver Comparison.** MSc. Thesis, The University of Nottingham, UK.

Tokay (2005). **Department of Geography and Environmental Sciences, UNIVERSITY OF MARYLAND BALTIMORE COUNTY (UMBC)** Internet site. (Last accessed 20th December 2005) http://www.research.umbc.edu/~tokay/index.html

Tor, Y.K. (2002). **L1, L2, Kalman Filter and Time Series Analysis in Deformation Analysis.** FIG XXII International Congress, Washington D.C., USA, 19th–26th April.

Tregoning, P., Boers, R., O'Brien, D. and Hendy, M. (1998). **Accuracy of absolute precipitable water vapour estimates from GPS observations.** *Journal of Geophysical Research,* 103, 28,701-28,7109, 1998

Treichler, J.R., Johnson, C.R. Jr. and Larimore, M.G. (2001). **Theory and Design of Adaptive Filters.** Prentice Hall, Inc. Upper Saddle River, New Jersey 07458. ISBN 0-13-040265-6.

USNO (2006). **Time Service Department, U.S. Navy** Internet site. (Last accessed 10th February 2006). http://tycho.usno.navy.mil/gps.html

Vollath, U., Landau, H. and Chen, X. (2002). **Network RTK Concept and Performance.** Proceedings of the GPS/GNSS Symposium, Wuhan, China, 6th–8th November.

Vollath, U., Brockmann, E. and Chen, X. (2003). **Troposphere: Signal or Noise?** Proceedings of ION-GPS/GNSS, Portland, Oregon, 9th–12th September.

Walsh, D.M.A. (1994). **Kinematic GPS Ambiguity Resolution.** PhD Thesis, The University of Nottingham, UK.

Wanninger, L. (2002). **Virtual Reference Stations for Centimeter-Level Kinematic Positioning.** Proceedings of ION-GPS/GNSS, Portland, Oregon, 9th–12th September.

Wanninger, L. (2004). **Introduction to Network RTK.** Downloaded from the internet site. (Last accessed 6th July 2005). http://www.network-rtk.info/intro/introduction.html

Wylde, G.P. and Featherstone, W.E. (1995). **An evaluation of some Stop-and-Go Kinematic GPS survey options.** Australian Surveyor, No. 3, Vol. 40, pp 205-212.

Yang, Y., Sharpe, R.T. and Hatch, R.R. (2002). **A Fast Ambiguity Resolution Technique for RTK Embedded Within a GPS Receiver.** Proceedings of ION GPS 2002, Portland, Oregon, 24th–27th September.

Zheng, Y., Feng, Y. and Bai, Z. (2004). **Grid Residual Tropospheric Corrections for Improved Differential GPS Positioning Over The Victoria GPS Network (GPSNet).** GNSS 2004, Sydney, Australia, 6th–8th December.

Appendix A

Guideline for the KINPOS Control File

These guideline were prepared based on the Outline of Kinpos written by Pattinson for his thesis [*Pattinson,* 2002]. Slight changes have been made to the original copy and only the description related to the settings in the control file will be mentioned here.

The control file [kinpos.ctl] is split into 3 different blocks, a Files block, an Options block and an Atmosphere block.

Below is an example of the control file used for Kinpos.

[Note : The lines in italic are the additional controls included for this project].

```
FILES
   INPUT
!REFREC RINEX base R:\Snowdon\RawData\static\100a1670.03O LEI503 XYZ
!      3826433.9838  -275635.2231  5078514.6210   1.5200
!KINREC RINEX b001 R:\Snowdon\RawData\static\100b1670.03O LEI503 XYZ
!      3826432.4000  -275619.6000  5078516.3000   1.6060

      EPH SP3 R:\Snowdon\RawData\Precise\igs12231.sp3
      AMBIGUITY NO  boatcp0h5.rep
      FIXREFSVN  NO 20
  END
  OUTPUT
     AZI  R:\Snowdon\results\kin\2run\1a3a16.azi
     ELE  R:\Snowdon\results\kin\2run\1a3a16.ele
     POS  R:\Snowdon\results\kin\2run\1a3a16.pos
     RES  R:\Snowdon\results\kin\2run\1a3a16.res
     TRO  R:\Snowdon\results\kin\2run\1a3a16.tro
     REP  R:\Snowdon\results\kin\2run\1a3a16.rep
END
END
```

```
 OPTIONS
   MODE 4  (1:standalone,2:diff_pse,3:diff_car, 4 diff_car&pse, 5:WL)
    DOPPLER  NO
    WL       NO
    SMOOTHPSE  yes  2
    FREQUENCY  0
    PSEUDERR 30.0d0
    DPSEUDERR 0.50d0
    CARRERR  0.010d0
    SDOPERR  0.1d0
    DDOPERR  0.002d0
    PROCNOISE     0.001d0
    INTERVAL      1.0d0  !epoch separation
    CONSTRAINT    NO   5.0
    START     YMDHMS 2003  6  16  09 04 03.00 !From 100a to all
    STOP      YMDHMS 2003  6  16  15 05 06.00 !From 100a to all
    TROP      1
    ELEVMIN  15.0
    NOACC     1
    POSITIONMODEL   CONSTACC
    TILT      NO  c:\GSTB\cycleslip\bu109458.02t
    PHASECENTRES YES
 END
 ATMOSPHERE
   BASE
     DRYMD  magnet     NEILL (KINPOS identify as NE not NI)
     WETMD  none       NEILL (KINPOS identify as NE not NI)
     SOLVE  none       DIRECT
     METDAT STD
     DELAY  NO
   END

   ROVER
     DRYMD  MAGNET     NEILL (KINPOS identify as NE not NI)
     WETMD  none       NEILL (KINPOS identify as NE not NI)
     SOLVE  NONE       DIRECT    0.00
     METDAT STD
   END
 END
```

Files Block

The files block specifies both the input and the output files for the program.

The input files may include multiple base station observation files, a roving receiver observation file, ephemeris files, an initial ambiguity file, and a slip file. The ephemeris file to be included can be in SP3 format or RINEX format. If in RINEX format, KINPOS uses the subroutines from CON2SP3 to convert to SP3 format. The observation files for the receivers can be in NOTT2 format, RINEX format, or MBN format, if logged directly to a laptop from a Z-Surveyor. The file type must be specified in the receiver identification lines. The fixed position of any base stations and the initial guess at the position of the rover are also included, along with the antenna heights. The positions can be in XYZ or GEO, whichever is specified, and the antenna heights are in meters. The antenna type should also be included here. Care should be taken that the correct coordinates are put in for the reference station. It is possible to use an input file containing the correct ambiguities for a session if these happen to be known. This may be useful for example if several processing runs of a data set are to be carried out to see what effect changing the random walk process noise has on the tropospheric delay estimates. Once the ambiguities have been resolved in the first run, the same ones can be used for all subsequent runs to make processing quicker. The FIXREFSVN option was added by the author to offer the option to have a defined reference satellite or not. A 'NO' option allows KINPOS to find it's own reference satellite while a 'YES' associated with the satellite number forces KINPOS to use that particular satellite as the reference satellite.

The output files specified here are the azimuth (AZI) file, elevation (ELE) file, position (POS) file, residuals (RES) file, troposphere (TRO) file and the report (REP) file. Here it should be noted that originally, only the position and report file were available, the others were added by the author. The position file shows the time tag, the position in geodetic and cartesian coordinates, and the standard deviation of the height estimates from the variance covariance matrix in the Kalman filter. The report file contains the time tag, the positioning accuracy of the solution, the number of satellites used, and the ambiguities for each satellite at each epoch in the correct form

to be read in if the option to do so is required. The AZI and ELE file shows the time tag with azimuth or elevation for each satellite used by KINPOS at each epoch. The residual file shows the time tag, total number of satellite, reference satellite and the residuals for each satellite available. The TRO file shows the time tag, ZTD at rover and base station and total number of satellite.

Options Block

The options block specifies the processing options for KINPOS.

- MODE – 1 is standalone, 2 is differential pseudo-range, 3 is differential carrier phase, 4 uses both differential pseudo-range and carrier phase, and 5 uses differential pseudo-range and wide lane carrier phase. The difference between mode 3 and mode 4 is that if at any point during processing the ambiguities cannot be resolved, the predicted position cannot be updated in the Kalman filter and so this is the one that is output and used to form the prediction for the next epoch. If the ambiguities are not resolved for any length of time, the position from mode 3 will therefore become inaccurate by meters and tens of meters very quickly. Mode 4 forms an estimated position based on pseudo-ranges every epoch and uses this as the predicted position in the Kalman filter for carrier phase observations. This ensures the estimated position does not degrade significantly over time, which ensures output positions are better when ambiguities are not fixed, and may also help regaining lock on the ambiguity values because the calculated ranges from the rover to the satellites will stay close to what they should be.

- DOPPLER – this option is set to 'YES' or 'NO' depending on whether Doppler measurements are to be used or not. The author has not had any Doppler data to use though, so it is not known what the program does with the Doppler data.

- SMOOTHPSE – this option is set to 'YES' or 'NO' depending on whether you want to smooth the pseudo-range observations or not. If this option is set to 'YES' then the pseudo-range observations will also try to detect and correct cycle slips to ensure that these do not contaminate the phase smoothed pseudo-range. It

is important to set this option to 'YES' if carrier phase is to be used, even if it is mode 3 and the pseudo-range is not wanted, otherwise no cycle slip detection routines will be used. If cycle slips were present then this could lead to incorrect ambiguities being resolved, or even make ambiguity resolution impossible. The value associated with this option is the data interval used in processing. The value input here is used to check for gaps in the data, and also governs what threshold value is used for cycle slip detection using the ionospheric residual. As the interval increases, cycle slips may be introduced that do not really exist. When the data interval is 15 seconds the threshold value is raised to try to decrease the number of false slips that are flagged, whilst still finding true slips. There is no theoretical basis for this increase though. The value that was chosen was the one that seemed to work the best for a particular data set that was being processed. It is important that the data intervals of the base receiver observation files are the same as or less than the data interval of the kinematic receiver observation file otherwise the program will not run.

- FREQUENCY – the options available are 1 (L1), 2 (L2), 0 (ionospherically free with float ambiguities), and 6 (ionospherically free with fixed ambiguities). Regardless of which frequency is specified here, both L1 and L2 observations will be used for ambiguity resolution. If the ambiguities are subsequently resolved, then the double difference observations in the frequency specified here will be corrected by the appropriate ambiguity. For L0 this will involve combining the L1 and L2 double difference integer ambiguities into non-integer values of L0 double difference ambiguities. For L6, the L1 and L2 ambiguities are not resolved. Instead the L1 and L2 float values are used and combined to form the ionospherically free float ambiguities.

- WL – This option specifies whether or not a separate search for the wide lane ambiguities is performed before the combined L1/Lw ambiguity search. This could be useful for longer baselines where it may be easier to resolve the wide lane ambiguity because of it's longer wavelength, and so fixing the wide lane ambiguities separately may then make it easier to resolve the L1 ambiguities in the combined L1/Lw search.

- PSEUDERR – the pseudo range measurement noise in meters.

- DPSEUDERR – the measurement noise for differential pseudo range measurements, in meters.

- CARERR – the measurement noise of the carrier phase observations, in meters.

- SDOPERR – the Doppler meadurement noise.

- DDOPERR – the differential Doppler measurement noise.

The measurement noise values specified here were left unchanged from those recommended by the original author of KINPOS Dr. Wu Chen.

- PROCNOISE – this is the random walk process noise in $cm/\sqrt{hr}$ for the tropospheric delay estimations. This value is redundant if tropospheric delay is not being estimated, i.e. the atmospheric option 'SOLVE' is set to NONE.

- INTERVAL – this is the tropospheric delay estimation interval in seconds. Position, velocity, and acceleration are always estimated every epoch. This option allows the tropospheric delay to be estimated at intervals greater than every epoch, although the value specified here must be divisible by the epoch interval. A value of 0.0 simply means that the delay will be estimated every epoch. This option is redundant if tropospheric delay is not being estimated, i.e. the atmospheric option 'SOLVE' is set to NONE.

- CONSTRAINT – this option allows the horizontal constraint method to be used for tropospheric delay estimation, rather than the standard kalman filter. If this option is specified then the horizontal position of the rover will be estimated first and then used to constrain the height and tropospheric delay estimates. If the option is set to yes then a value for the cut off angle in degrees should also be specified. This cut off angle is the one to be used for the height and delay estimation part of the program and may be the same or lower than the cut off angle for position specified in elevmin.

- START – this is the start time for processing and may be either in GPS week no. and seconds of week, or in year, month, day, hours, minutes and seconds. The marker GPS or YMDHMS before the time specifies which it is. It is important that the specified time is after the actual start of the base receiver observation files or the program will not run.

- STOP – this is the stop time for processing and may again be in GPS or YMDHMS.

- TROP – this option specifies the met data to use for providing tropospheric corrections. The options are 1 for no met data, 2 for Bomford standard data, and 3 for Bernese standard data. If a value of 1 is entered and there is no data so the MAGNET model is applied. If 2 or 3 are entered, then the standard meteorological data produced is then used in the Saastamoinen model to calculate tropospheric delays. A value of 0 means that no tropospheric correction will be applied. The standard data is used to calculate the tropospheric delay at the base and the rover, which is then used to correct the calculated ranges in the ambiguity resolution part of the software, unless the delay is being solved for in which case the estimated values are used.

- ELEVMIN – this is the cut off angle to be used, in degrees. Unless the horizontal constraint method is being used for delay estimation (signalled by putting yes for the constraint option), all observations to satellites below this angle will be ignored. If the horizontal constraint method is being used then the angle specified for constraint will either be the same as or lower than the angle specified here. If it is the same then no satellites below that angle will be used in any part of the program. If however the angle in constraint is lower, then only satellites below that angle will be ignored for the ambiguity resolution part. The angle specified here in elevmin will then be used as the cut off for estimating the horizontal position. All satellites used for ambiguity resolution will then come back in for the height and delay estimation.

- NOACC – this sets the number of epochs of data that will be accumulated before it is attempted to resolve the ambiguities in carrier phase mode. The minimum number that should be used here is 1. If when a processing run is started the

incorrect ambiguities are resolved, it may help to increase the number of accumulations.

- POSITIONMODEL – this defines which model is to be used for predicting the position of the rover in the Kalman filter. The two options are CONSTACC (constant acceleration) and RW (random walk). The Constant Acceleration model is the one that was put in by Dr. Wu Chen and the Random Walk model was introduced at a later date. It was thought that the Constant Acceleration model would give better position estimates in a marine environment where the motion is govern by tides and waves. In other applications it may be better to use the Random Walk model, although testing indicates that position estimates from processing runs using the different models give virtually identical results, probably due to the iterative nature of the estimation update process in KINPOS.

- TILT – for the RIGHt project it was essential to retrieve the height of the water level rather than the height of the antenna on the buoy. If set to yes, this option tries to account for the tilt of the buoy by using tilt and pressure data to correct the difference in height between the antenna and the water level. The tilt data may be included in an MBN file along with the raw data, or it may be in a separate file. If so then the file name and path should be specified here. If the tilt option is set to no then the vertical antenna height for the roving receiver specified in the files block will be used to correct the height estimates from processing.

- PHASECENTRES – for long baselines, or for baselines where mixed antenna types are used, the different phase centre offsets and variations may cause large errors, especially in height. If this option is set to yes then corrections for these effects will be applied during processing. The antenna types must be specified in the files block with the observation file identifiers, and at the present time may be one of three types, These are Leica or Ashtech choke ring (CHOKE), Ashtech marine (MARINE), and Ashtech ground plane (ASHGP). Additional antennas were added by the author to the getpcmod.for routine for different types of Leica antennas.

Atmosphere Block

The atmosphere block defines the atmospheric models and mapping functions to be used, and whether the delay is to be solved for. In the above example, the delay was modelled at the base station and the total tropospheric delay was estimated at the rover. This was because the distance between the base station and the rover was very short so the delay at both stations was highly correlated and could not be solved absolutely at both points.

All the following options apply to the base receiver. Several base receivers can be specified in the files block, but only one set of base atmospheric options can be applied.

- DRYMD – this specifies the model that will be used for the dry delay. The possible options are NONE, Saastamoinen, Hopfield, Black, EGNOS, and MAGNET, although in code only no model or the MAGNET model can be applied. If any of the others are chosen a warning message will appear. The dry mapping function must also be specified here. The possible options are Saastamoinen, Hopfield, Black, Marini, Chao, MAGNET, EGNOS, and Niell, but again not all are available in the code. Only the MAGNET, EGNOS, and Niell mapping functions can actually be applied. From this it can be seen that the only models and mapping functions that can be applied are the ones that do not require any meteorological data.

- WETMD – this specifies the model and mapping function to be used for the wet delay and has the same options as for the dry delay.

- SOLVE – this tells the software what delay if any is to be solved for. The options are NONE, ALL, and WET. If 'NONE' is entered then the delay will simply be modelled using the models specified in DRYMD and WETMD. If 'ALL' is specified then the total tropospheric delay will be estimated. If 'WET' is selected then the dry part of the delay (hydrostatic) will be modelled and the wet part will be estimated. If delay is to be estimated then it is recommended that the total delay is estimated rather than just the wet portion. If the delay is being solved for

then the software needs to know if it is solving for the delay directly (direct) or if it should find a scale factor (scale).

- METDAT – this simply tells the program whether there is meteorological data available or not. If 'STD' is specified then there is no measured met data and standard data has to be used. If met data is available then enter the file name along with the location of the file which contains the data. At the moment there is no routine to read and apply met data from a file though, so this option should be left on 'STD'.

- DELAY – this option says if the delay is known or not. The tropospheric delay may be known from a static GPS processing run or may have been measured using a WVR. If so then the value for the delay at certain epochs may be contained in a file and can be utilised by changing this flag from 'NO'. The possible options are that the same delay file is to be used for all base receivers (ALL), or different files are to be used at each base receiver. If this is the case then the 4 letters station ID is entered. The location of the file must then also be declared. If there is no delay file then the option is simply set to 'NO'.

All the atmospheric options for the rover are the same as the ones at the base receiver, except that you cannot choose to read the delays from a file. If the tropospheric delay is being estimated then because KINPOS is only used for short baselines at the moment, the delay cannot be estimated at both the base and the rover. The options should therefore be set to model the delay at the base, or to read in known values from a file, and then to estimate the total delay at the rover. If delay estimates are not needed then it is recommended that the delay is modelled at both the base and the rover.

Appendix B

Coordinates from Static GPS Processing Using Ski-Pro Version 3.0 for the

B1. Snowdon Trial

B2. Humber Bridge Trial

B3. University Trial #1

B4. Forth Road Bridge Trial

B5. University Trial #2

	Cartesian Coordinates (meters)			Geodetic Coordinates			Standard Deviations (m)			Relative Distance (km)
Station	**X**	**Y**	**Z**	**Latitude ϕ (N)**	**Longitude λ (W)**	**Ellipsoidal Height (m)**	**σX**	**σY**	**σZ**	
100a	3826433.9838	-275635.2231	5078514.6210	53° 07' 02."06927	4° 07' 12."56044	162.0349	-	-	-	0
100b	3826432.4166	-275619.6502	5078516.3120	53° 07' 02."17149	4° 07' 11."73137	161.7778	0.0013	0.0023	0.0014	0.015
200a	3828713.8498	-274148.6854	5077396.0600	53° 05' 44."27622	4° 05' 44."08482	568.6925	0.0001	0.0000	0.0001	2.721
300a	3831568.7475	-273060.9388	5076023.3325	53° 04' 05."97334	4° 04' 34."87678	1135.1451	0.0089	0.0006	0.0115	5.743
300b	3830923.0144	-272931.5596	5076494.8569	53° 04' 32."02670	4° 04' 30."41116	1119.5695	0.0000	0.0000	0.0001	5.240
400a	3833974.8335	-271317.6707	5073033.4131	53° 02' 08."99284	4° 02' 52."38218	114.0647	0.0035	0.0016	0.0046	8.689
400b	3833966.7890	-271309.0352	5073039.7908	53° 02' 09."34005	4° 02' 51."95039	113.9687	0.0082	0.0079	0.0104	8.687

Table B1. Cartesian and Geodetic Coordinates for stations in the Snowdon Trial processed in Static Mode with Ski-Pro Version 3.0.

	Cartesian Coordinates (meters)			Geodetic Coordinates			Standard Deviations (m)			Relative Distance (km)
Station	**X**	**Y**	**Z**	**Latitude ϕ (N)**	**Longitude λ (W)**	**Ellipsoidal Height (m)**	**σX**	**σY**	**σZ**	
LEED	3773717.8017	-109614.4560	5123816.0852	53° 48' 0."77451	1° 39' 49."65006	215.6051	-	-	-	80.315
ref1	3782349.2326	-29764.3994	5118416.8292	53° 43' 10."83387	0° 27' 03."12388	91.7934	-	-	-	0
est	3782787.5103	-29291.6990	5118047.8992	53° 42' 52."44152	0° 26' 37."16237	51.5661	0.0020	0.0017	0.0026	0.645
twr1	3782898.2979	-29751.0440	5118148.4386	53° 42' 51."38418	0° 27' 02."16013	200.2933	0.0019	0.0016	0.0023	0.549
ref2	3782346.9848	-29764.3890	5118418.4467	53° 43' 10."92343	0° 27' 03."12427	91.7672	0.0015	0.0019	0.0019	0.002
twr2	3782898.3004	-29751.0453	5118148.4382	53° 42' 51."38411	0° 27' 02."16020	200.2945	0.0019	0.0017	0.0023	0.549

Table B2. Cartesian and Geodetic Coordinates for stations in the Humber Bridge Trial processed in Static Mode with Ski-Pro Version 3.0.

	Cartesian Coordinates (meters)			Geodetic Coordinates			Standard Errors (m)			Relative Distance (km)
Station	**X**	**Y**	**Z**	**Latitude ϕ (N)**	**Longitude λ (W)**	**Ellipsoidal Height (m)**	**σX**	**σY**	**σZ**	
NOTT	3849254.9063	-80460.7907	5068085.0900	52° 57' 43."88780	1° 11' 50."91556	93.8240	-	-	-	2.376
sc01	3851191.4098	-81057.7227	5066606.2407	52° 56' 24."75556	1° 12' 20."70538	87.5400	0.0005	0.0020	0.0005	0.561
sc02	3851189.3963	-81059.2322	5066607.7996	52° 56' 24."83710	1° 12' 20."78846	87.5900	0.0019	0.0019	0.0021	0.563
tre1	3851619.6559	-80696.0360	5066281.9476	52° 56' 07."57689	1° 12' 00."86212	82.2225	0.0015	0.0019	0.0016	0.000
tre2	3851619.2571	-80698.4717	5066282.2682	52° 56' 07."59212	1° 12' 00."99294	82.2688	0.0010	0.0015	0.0010	0.002
twr1	3851064.6745	-79902.4341	5066778.0227	52° 56' 31."99842	1° 11' 18."9974	133.7205	0.0012	0.0008	0.0014	0.968
twr2	3851063.5923	-79900.8740	5066778.5118	52° 56' 32."03672	1° 11' 18."91508	133.4393	0.0010	0.0004	0.0012	0.970

Table B3. Cartesian and Geodetic Coordinates for stations in the University Trial #1 processed in Static Mode with Ski-Pro Version 3.0.

	Cartesian Coordinates (meters)			Geodetic Coordinates			Standard Errors (m)			Relative Distance (km)
Station	**X**	**Y**	**Z**	**Latitude ϕ (N)**	**Longitude λ (W)**	**Ellipsoidal Height (m)**	**σX**	**σY**	**σZ**	
EDIN	3575928.4704	-205860.6295	5259853.1434	55° 55' 29."21733	3° 17' 41."2518	119.0237	-	-	-	8.956
ref1	3569683.7305	-212280.8208	5263784.6461	55° 59' 17."34943	3° 24' 11."66144	96.7024	-	-	-	0
ref2	3569682.0687	-212282.5418	5263785.7339	55° 59' 17."41082	3° 24' 11."76623	96.7334	0.0015	0.0012	0.0011	0.002
twre	3568934.0712	-212291.2921	5264426.9639	55° 59' 49."00511	3° 24' 14."83192	210.9636	0.0029	0.0018	0.002	0.750
twrw	3568930.7335	-212312.8827	5264428.3556	55° 59' 49."08521	3° 24' 16."08678	210.971	0.0024	0.0023	0.0017	0.754

Table B4. Cartesian and Geodetic Coordinates for stations in the Forth Road Bridge Trial processed in Static Mode with Ski-Pro Version 3.0.

	Cartesian Coordinates (meters)			Geodetic Coordinates			Standard Errors (m)			Relative Distance (km)
Station	**X**	**Y**	**Z**	**Latitude ϕ (N)**	**Longitude λ (W)**	**Ellipsoidal Height (m)**	**σX**	**σY**	**σZ**	
NOTT	3849254.9063	-80460.7907	5068085.0900	52° 57' 43."88780	1° 11' 50."91556	93.8240	-	-	-	0.000
sf01	3851181.6512	-81062.7852	5066613.7841	52° 56' 25."15173	1° 12' 20."98739	87.7442	0.0012	0.0006	0.0014	2.019
sf02	3851180.4503	-81063.7143	5066614.7097	52° 56' 25."20027	1° 12' 21."03849	87.7711	0.0014	0.0013	0.0017	2.018
tre1	3851612.4357	-80674.9089	5066288.8537	52° 56' 7."90930	1° 12' 59."73929	83.1158	0.0012	0.0025	0.0013	2.367
tre2	3851611.2959	-80676.4023	5066289.7226	52° 56' 7."95485	1° 12' 59."82051	83.1413	0.0016	0.0016	0.0017	2.366
twr1	3851064.6625	-79902.4359	5066778.0167	52° 56' 31."99861	1° 11' 18."99751	133.7085	0.0009	0.0006	0.0009	1.894
twr2	3851063.5781	-79900.8498	5066778.5010	52° 56' 32."03689	1° 11' 18."91380	133.4218	0.0010	0.0005	0.0010	1.893

Table B5. Cartesian and Geodetic Coordinates for stations in the University Trial #2 processed in Static Mode with Ski-Pro Version 3.0.

Appendix C

Position residuals (and GDOPs) from Kinematic GPS Processing Using Leica Ski-Pro Version 3.0 for baselines from station 100a for the Snowdon Trial on 16th and 17th June 2003.

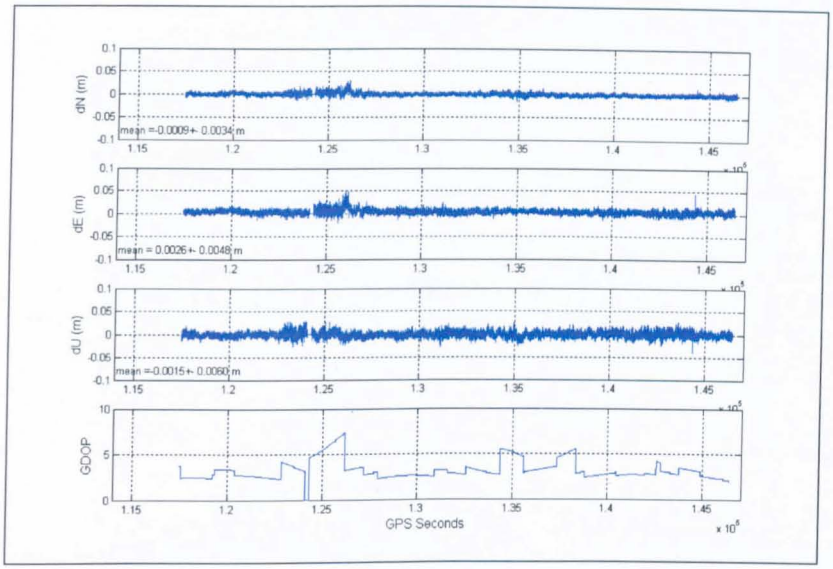

Figure C1. All position residuals and GDOPs for baseline 100a–100b from day 167 (16th June 2003) of the Snowdon Trial.

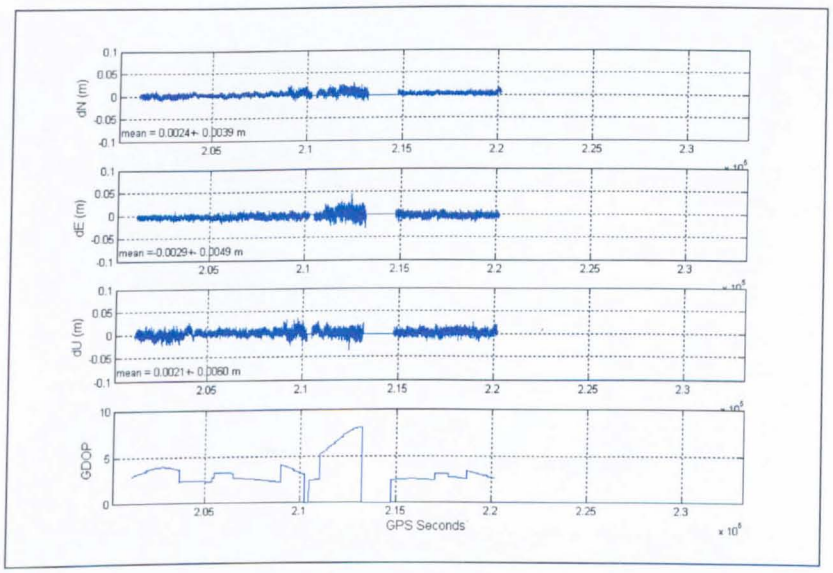

Figure C2. All position residuals and GDOPs for baseline 100a–100b from day 168 (17th June 2003) of the Snowdon Trial.

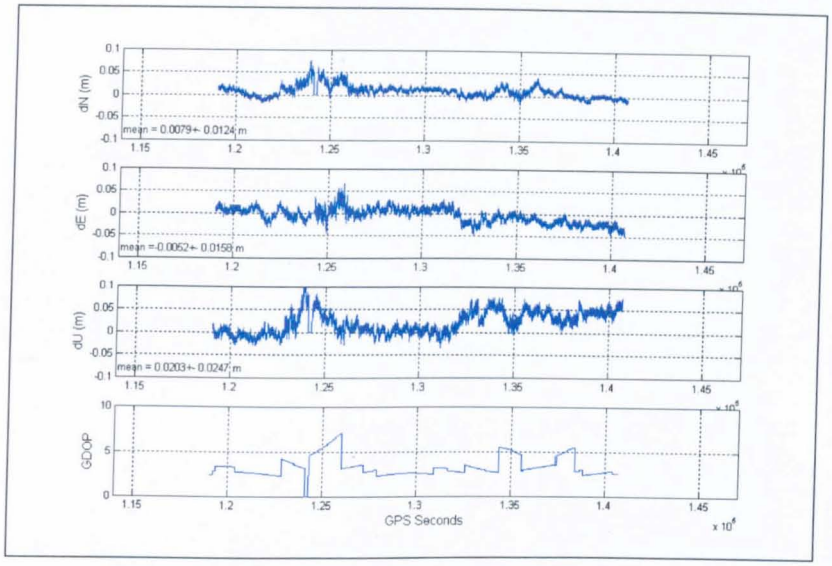

Figure C3. All position residuals and GDOPs for baseline 100a–300a from day 167 (16th June 2003) of the Snowdon Trial.

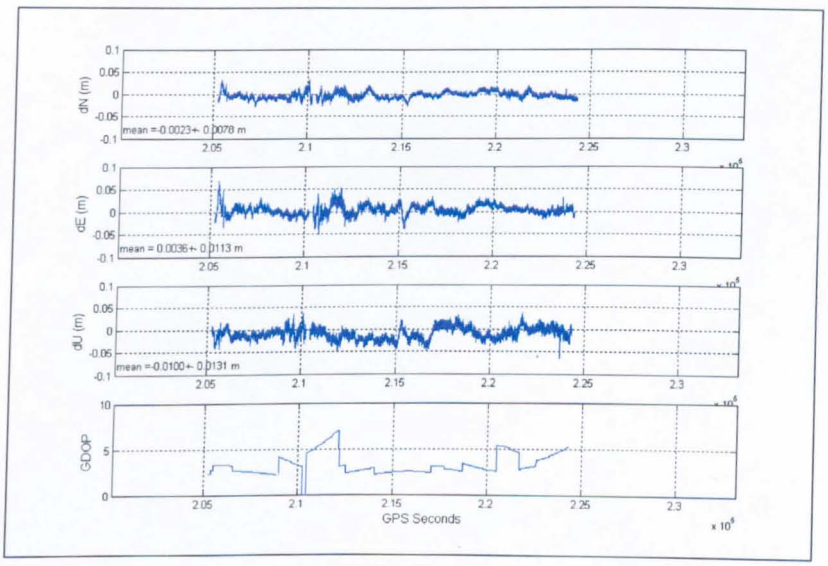

Figure C4. All position residuals and GDOPs for baseline 100a–300a from day 168 (17th June 2003) of the Snowdon Trial.

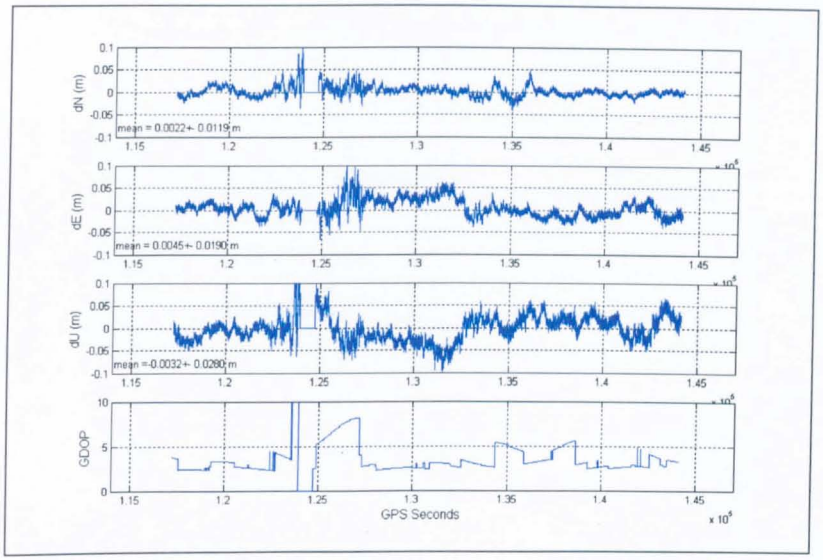

Figure C5. All position residuals and GDOPs for baseline 100a–400a from day 167 (16th June 2003) of the Snowdon Trial.

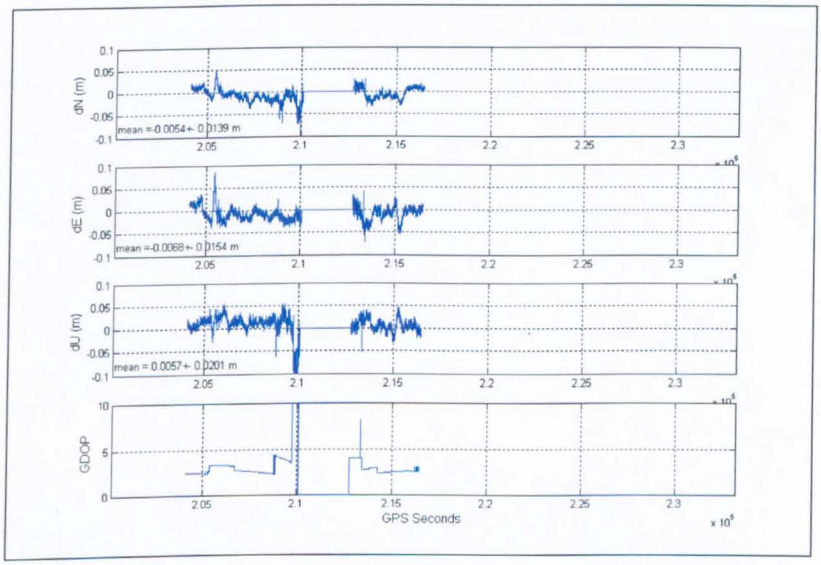

Figure C6. All position residuals and GDOPs for baseline 100a–400a from day 168 (17th June 2003) of the Snowdon Trial.

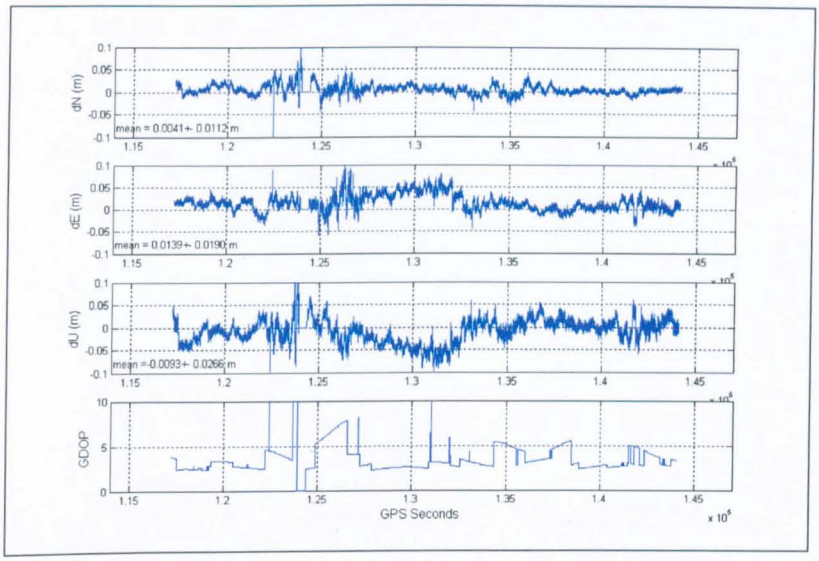

Figure C7. All position residuals and GDOPs for baseline 100a–400b from day 167 (16th June 2003) of the Snowdon Trial.

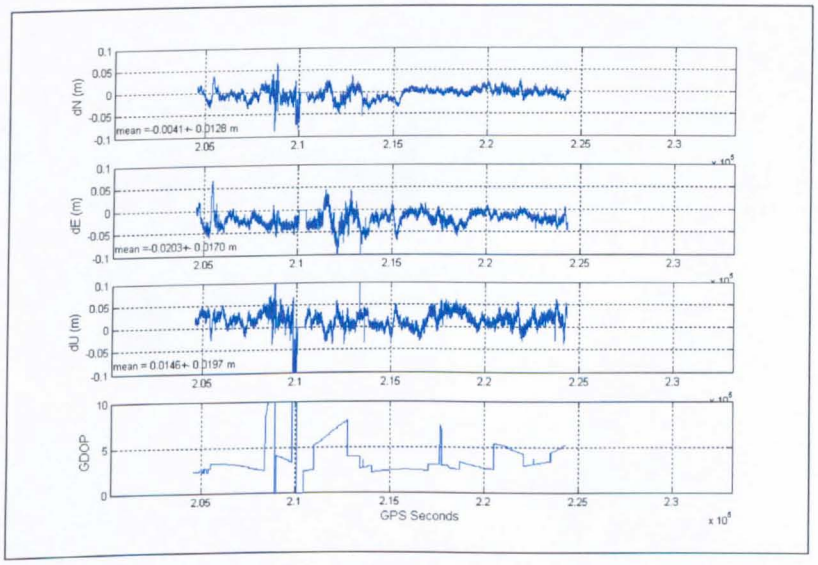

Figure C8. All position residuals and GDOPs for baseline 100a–400b from day 168 (17th June 2003) of the Snowdon Trial.

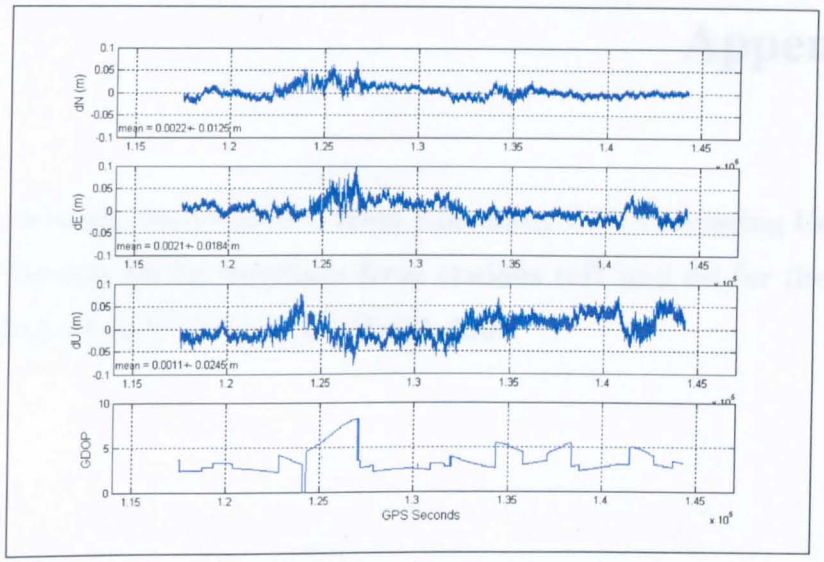

Figure C9. All position residuals and GDOPs for baseline 100a–200a from day 167 (16th June 2003) of the Snowdon Trial.

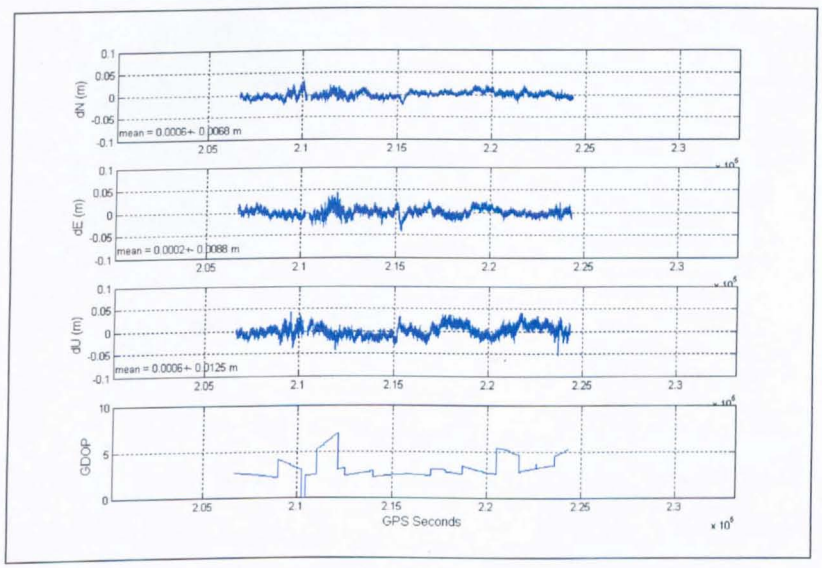

Figure C10. All position residuals and GDOPs for baseline 100a–300b from day 168 (17th June 2003) of the Snowdon Trial.

Appendix D

Position residuals (and GDOPs) from Kinematic GPS Processing Using Leica Ski-Pro Version 3.0 for baselines from stations ref1 and est for the Humber Bridge Trial #1 on 1st, 2nd and 4th March 2004.

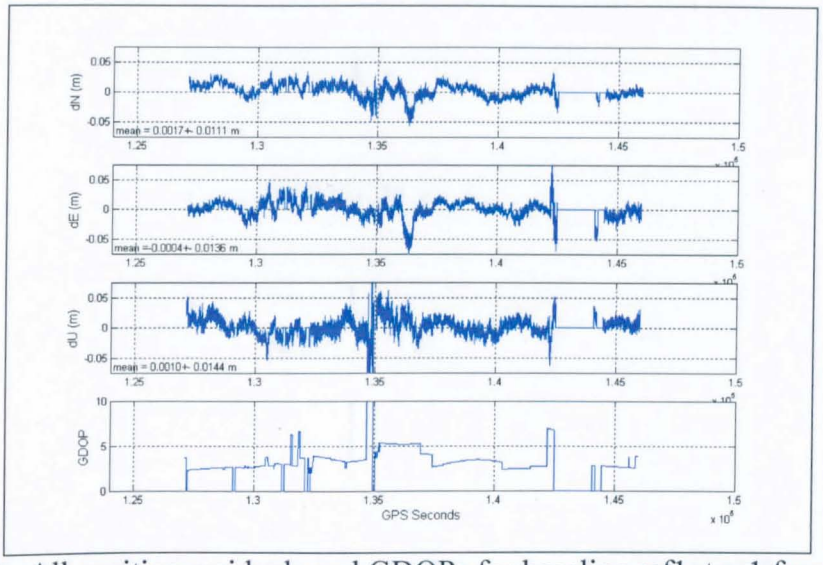

Figure D1. All position residuals and GDOPs for baseline ref1–twr1 from DOY 61 (1st March 2004) of the Humber Bridge Trial.

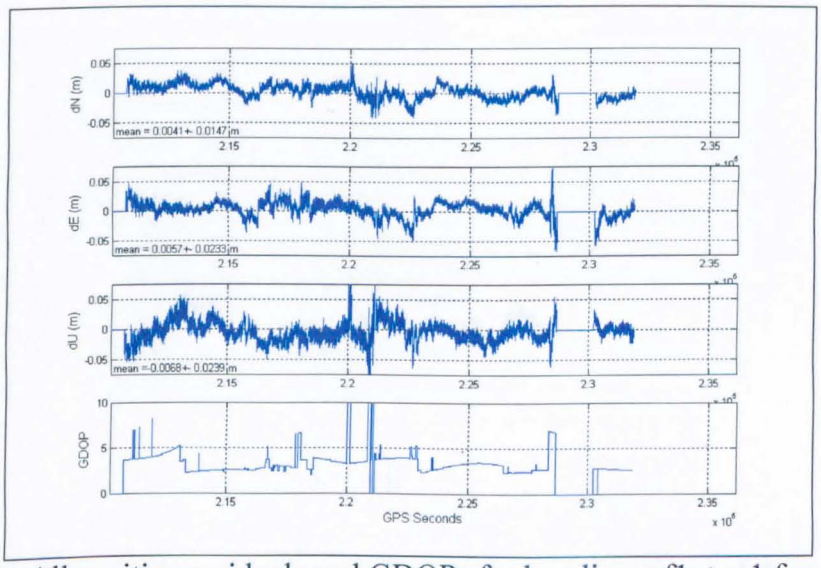

Figure D2. All position residuals and GDOPs for baseline ref1–twr1 from DOY 62 (2nd March 2004) of the Humber Bridge Trial.

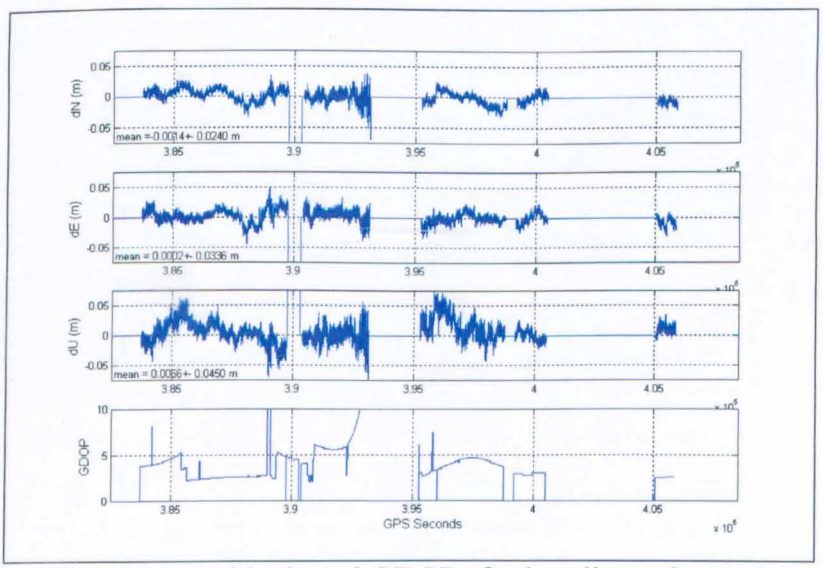

Figure D3. All position residuals and GDOPs for baseline ref1–twr1 from DOY 64 (4th March 2004) of the Humber Bridge Trial.

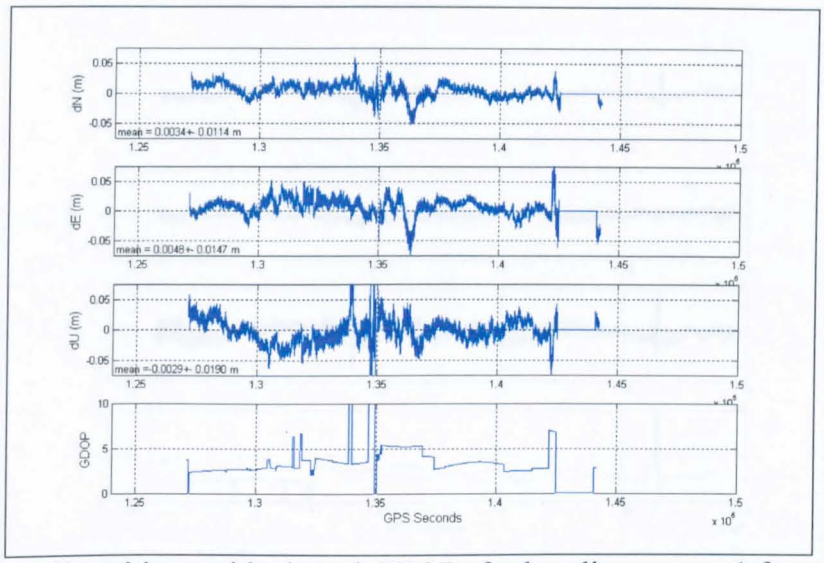

Figure D4. All position residuals and GDOPs for baseline est–twr1 from DOY 61 (1st March 2004) of the Humber Bridge Trial.

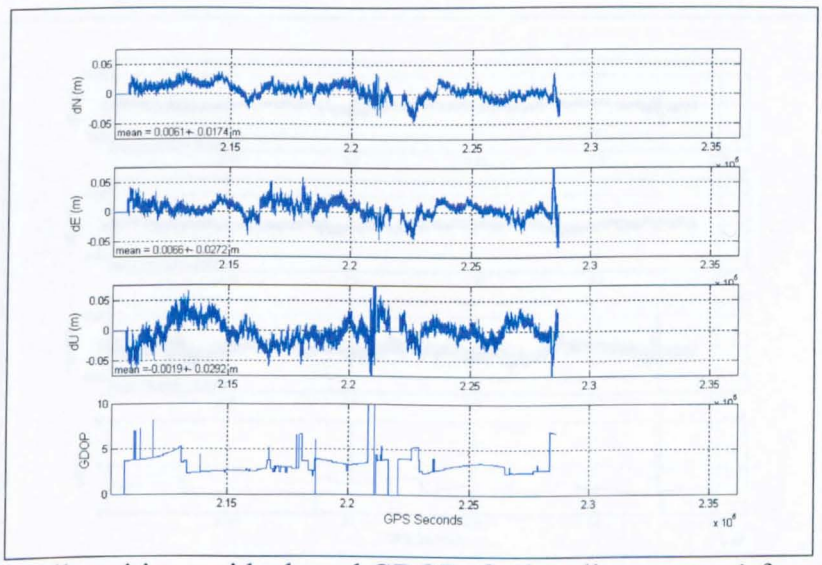

Figure D5. All position residuals and GDOPs for baseline est–twr1 from DOY 62 (2nd March 2004) of the Humber Bridge Trial.

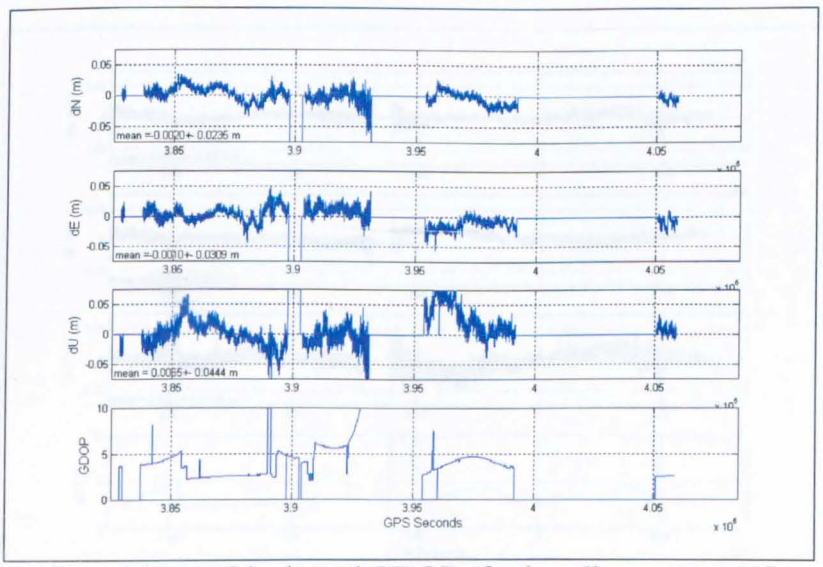

Figure D6. All position residuals and GDOPs for baseline est–twr1 from DOY 64 (4th March 2004) of the Humber Bridge Trial.

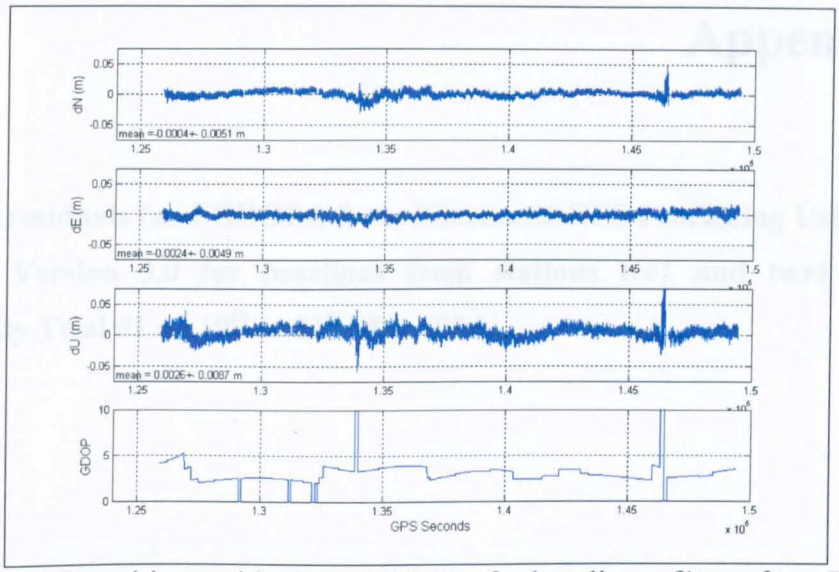

Figure D7. All position residuals and GDOPs for baseline ref1–est from DOY 61 (1st March 2004) of the Humber Bridge Trial.

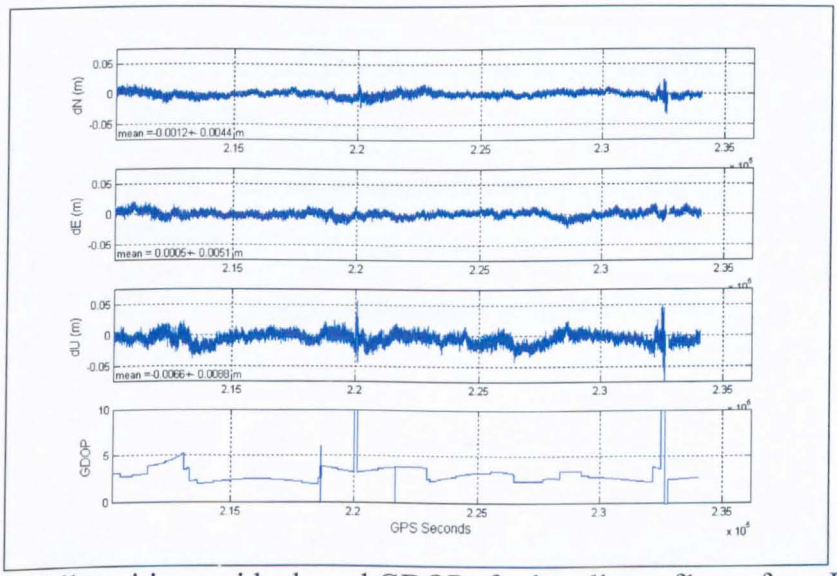

Figure D8. All position residuals and GDOPs for baseline ref1–est from DOY 62 (2nd March 2004) of the Humber Bridge Trial.

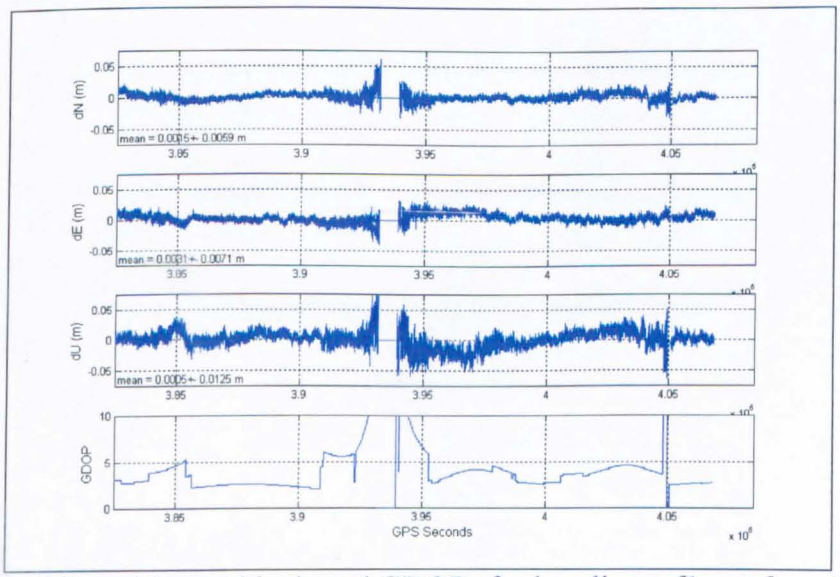

Figure D9. All position residuals and GDOPs for baseline ref1–est from DOY 64 (4th March 2004) of the Humber Bridge Trial.

Appendix E

Position residuals (and GDOPs) from Kinematic GPS Processing Using Leica Ski-Pro Version 3.0 for baselines from stations tre1 and twr1 for the University Trial #1 on 19th to 21st May 2004.

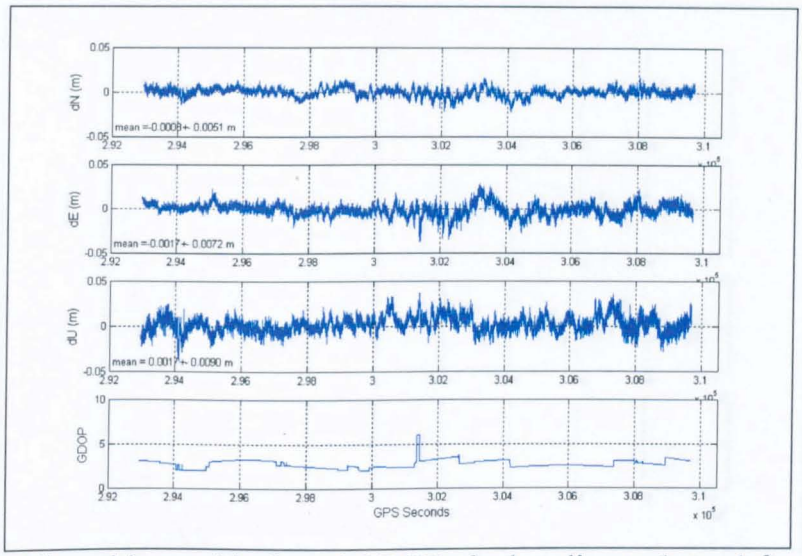

Figure E1. All position residuals and GDOPs for baseline tre1–twr1 from DOY 140 (19th May 2004) of the University Trial #1.

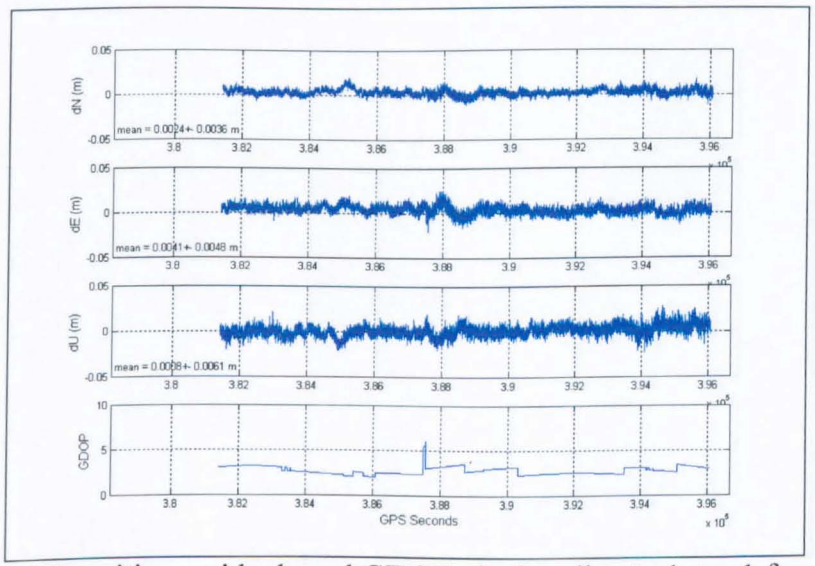

Figure E2. All position residuals and GDOPs for baseline tre1–twr1 from DOY 141 (20th May 2004) of the University Trial #1.

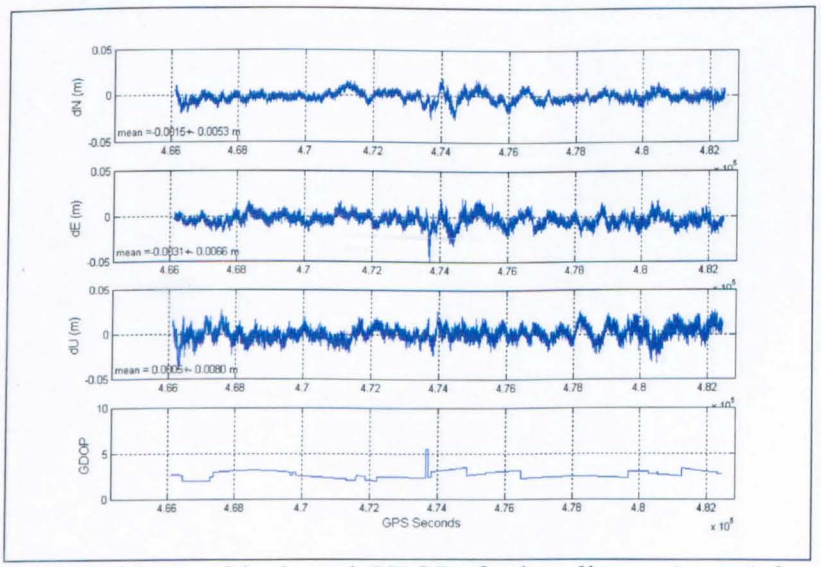

Figure E3. All position residuals and GDOPs for baseline tre1–twr1 from DOY 142 (21st May 2004) of the University Trial #1.

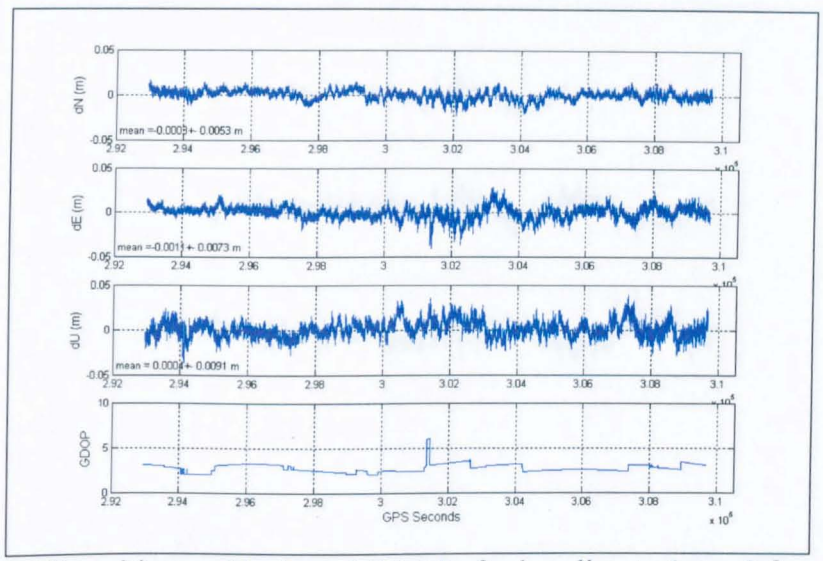

Figure E4. All position residuals and GDOPs for baseline tre1–twr2 from DOY 140 (19th May 2004) of the University Trial #1.

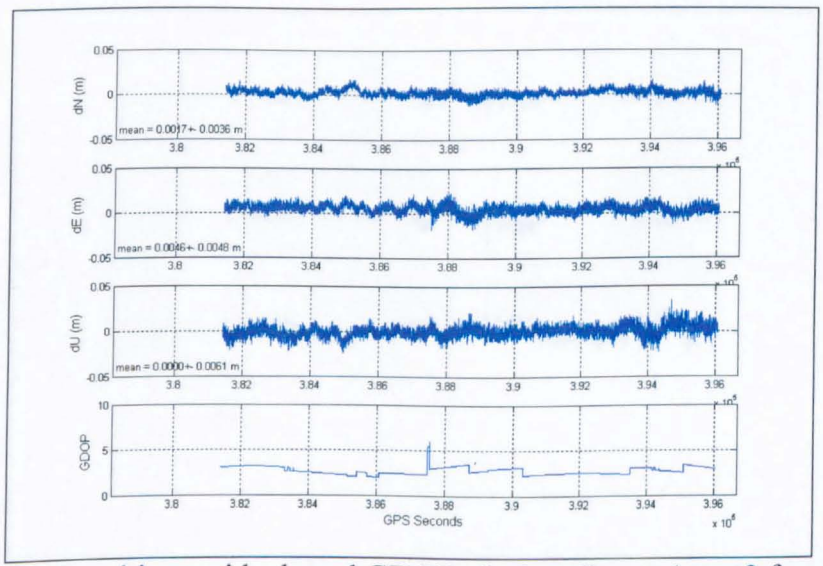

Figure E5. All position residuals and GDOPs for baseline tre1–twr2 from DOY 141 (20th May 2004) of the University Trial #1.

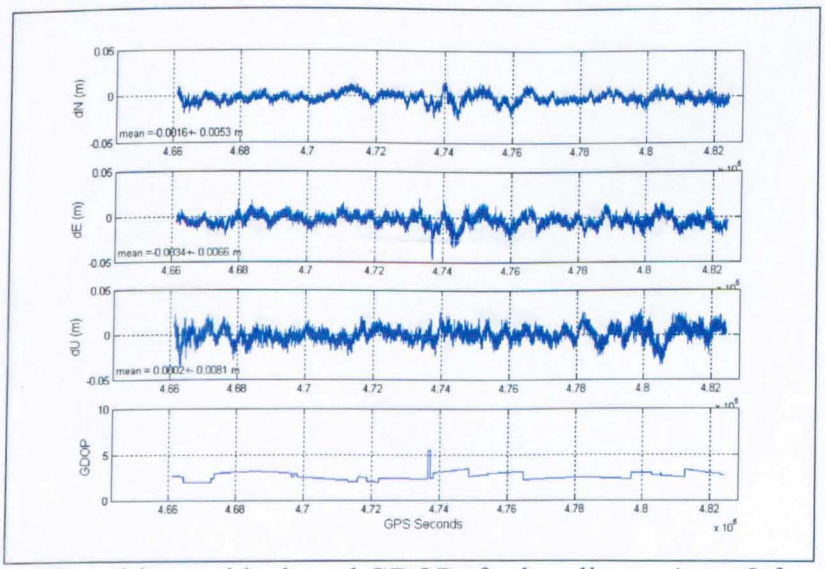

Figure E6. All position residuals and GDOPs for baseline tre1–twr2 from DOY 142 (21st May 2004) of the University Trial #1.

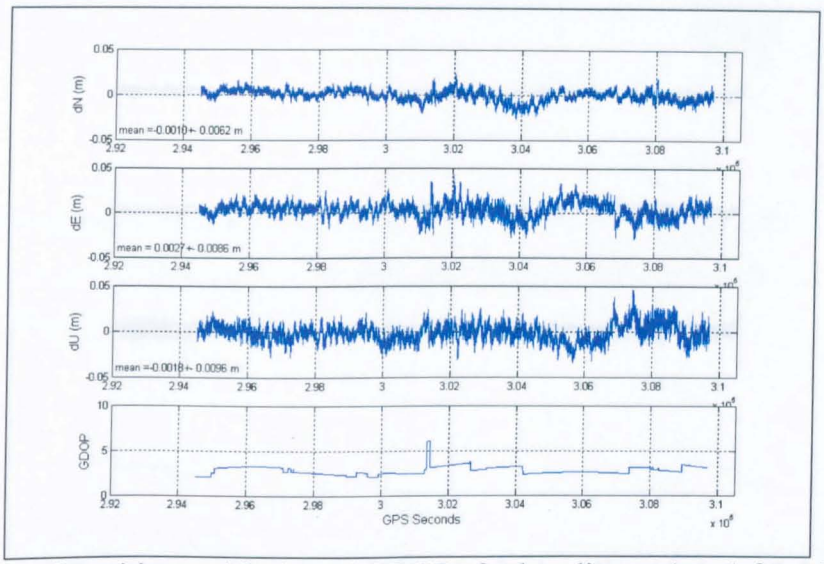

Figure E7. All position residuals and GDOPs for baseline tre1–sc1 from DOY 140 (19th May 2004) of the University Trial #1.

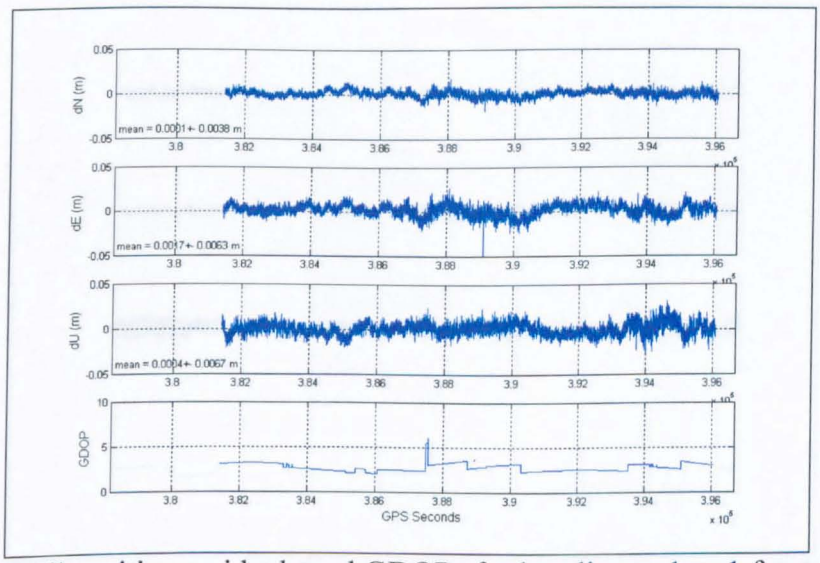

Figure E8. All position residuals and GDOPs for baseline tre1–sc1 from DOY 141 (20th May 2004) of the University Trial #1.

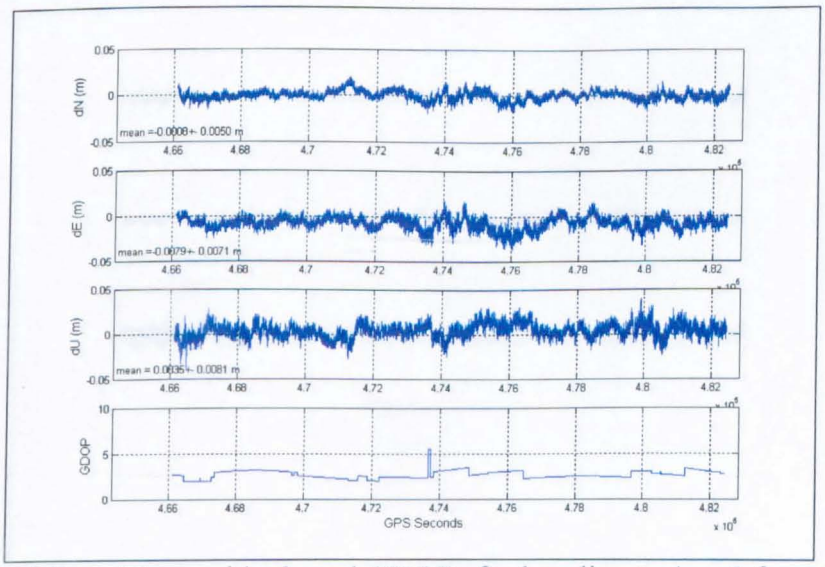

Figure E9. All position residuals and GDOPs for baseline tre1–sc1 from DOY 142 (21st May 2004) of the University Trial #1.

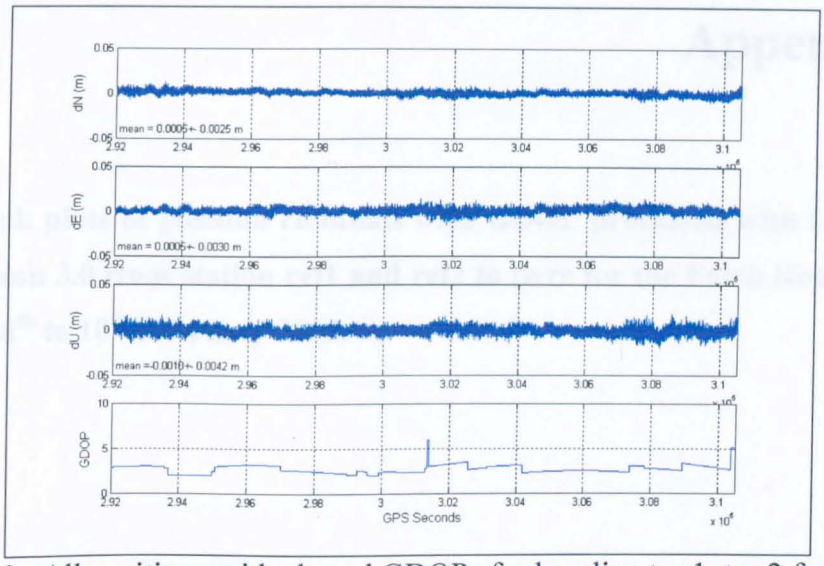

Figure E10. All position residuals and GDOPs for baseline twr1–twr2 from DOY 140 (19th May 2004) of the University Trial #1.

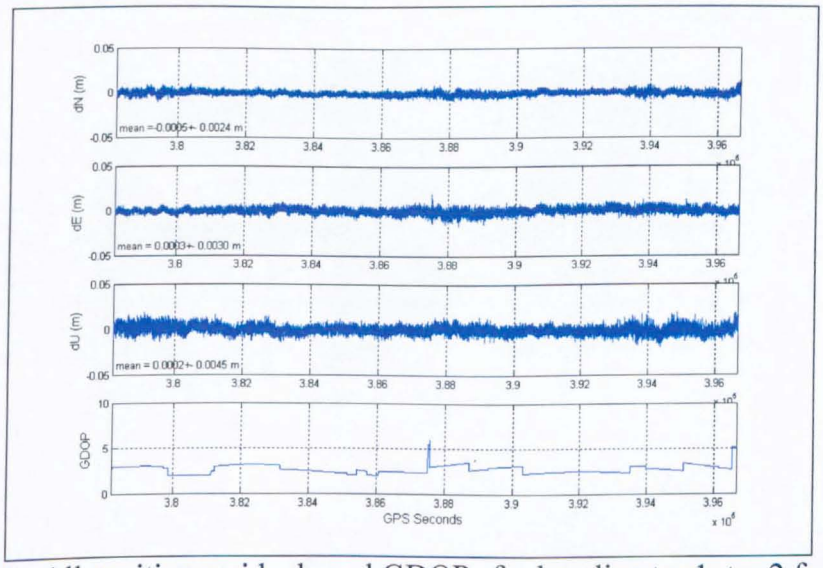

Figure E11. All position residuals and GDOPs for baseline twr1–twr2 from DOY 141 (20th May 2004) of the University Trial #1.

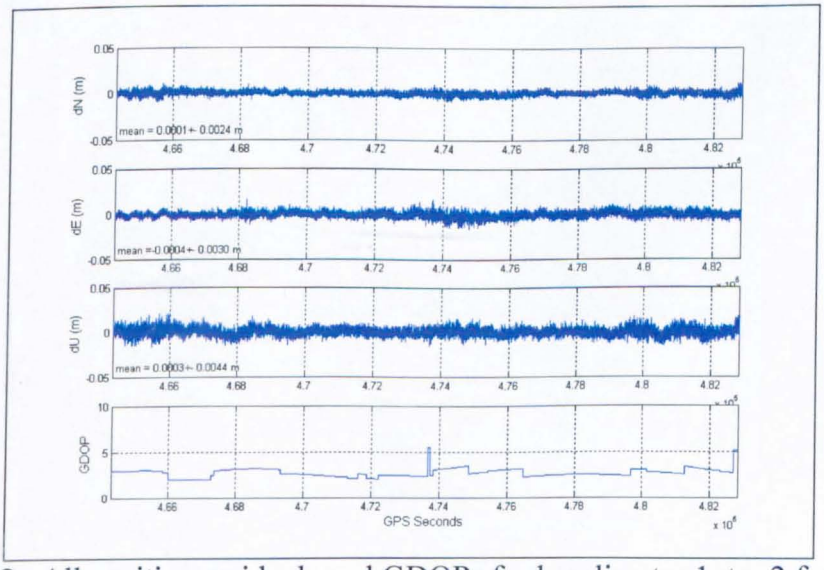

Figure E12. All position residuals and GDOPs for baseline twr1–twr2 from DOY 142 (21st May 2004) of the University Trial #1.

Appendix F

Full length plots of position residuals with GDOP processed with Leica Ski-Pro Version 3.0 from station ref1 and ref2 to twre for the Forth Road Bridge Trial on 8th to 10th February 2005.

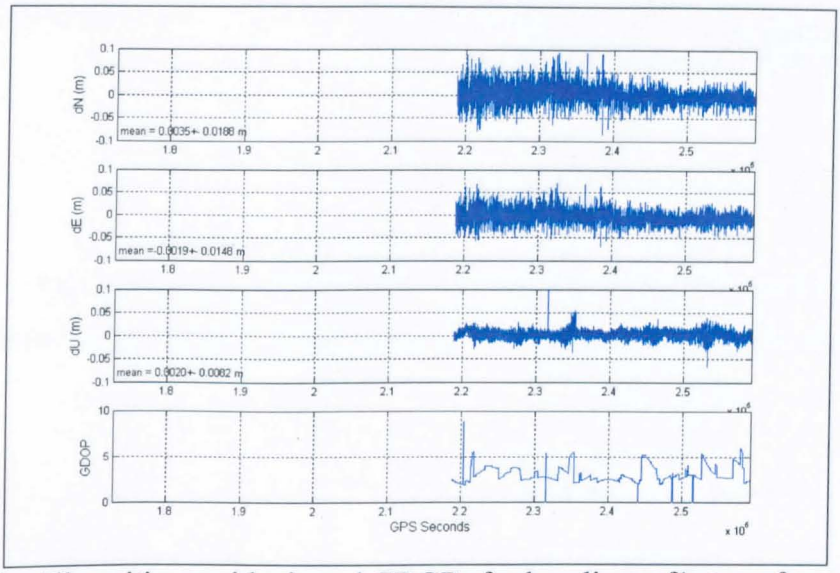

Figure F1. All position residuals and GDOPs for baseline ref1–twre from day 39 (8th February 2005) of the Forth Road Bridge Trial.

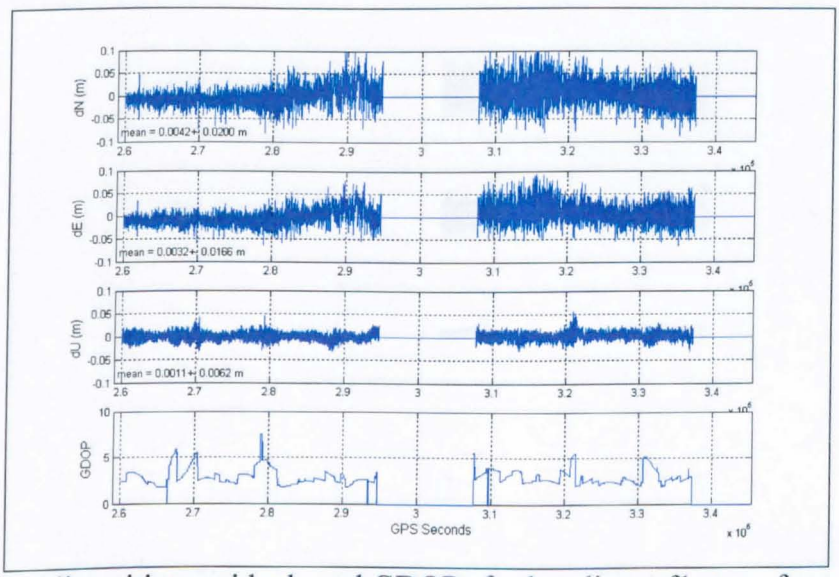

Figure F2. All position residuals and GDOPs for baseline ref1–twre from day 40 (9th February 2005) of the Forth Road Bridge Trial.

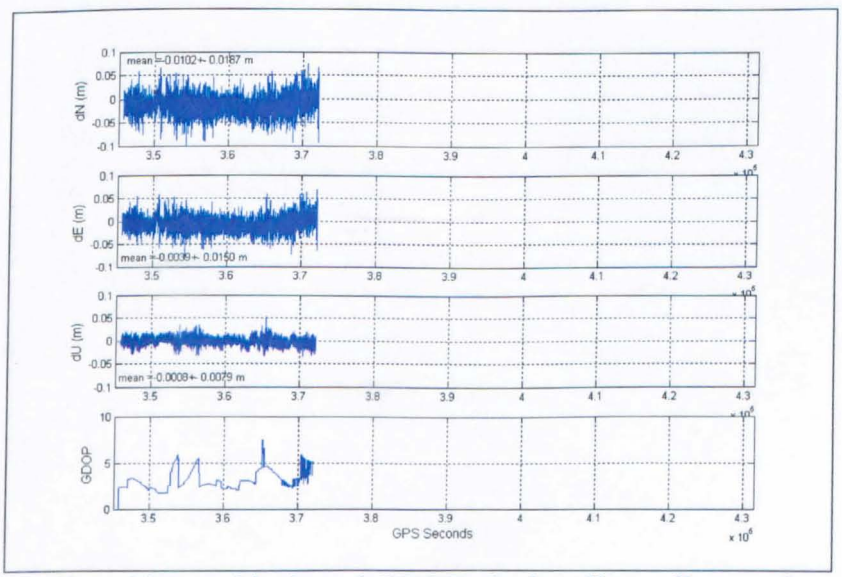

Figure F3. All position residuals and GDOPs for baseline ref1–twre from day 41 (10th February 2005) of the Forth Road Bridge Trial.

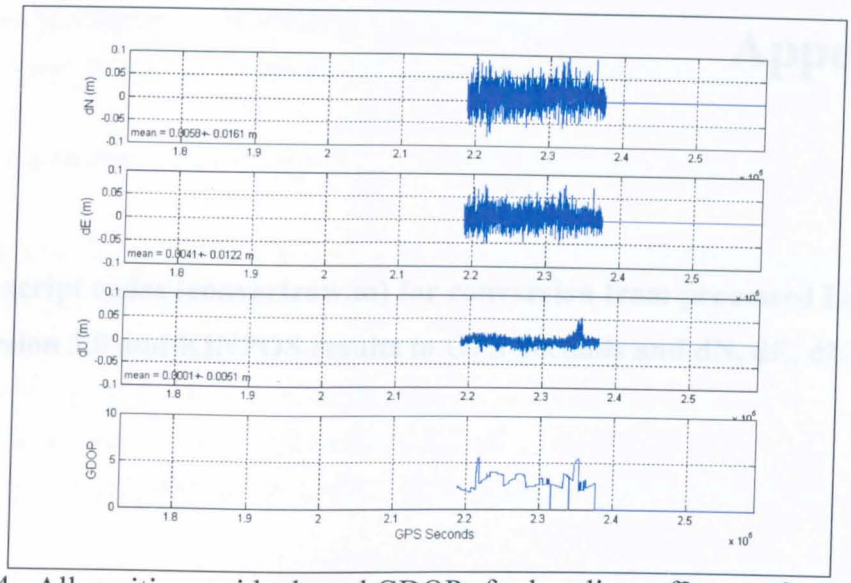

Figure F4. All position residuals and GDOPs for baseline ref2–twre from day 39 (8th February 2005) of the Forth Road Bridge Trial.

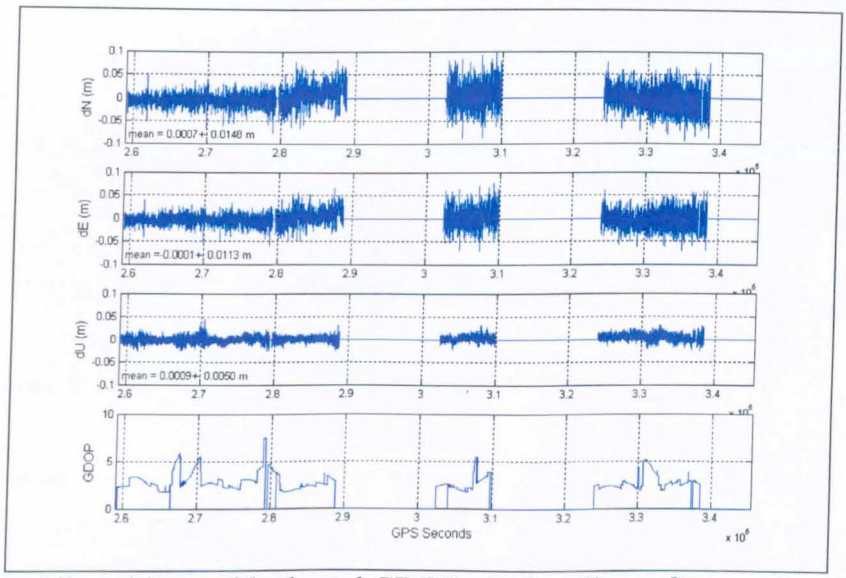

Figure F5. All position residuals and GDOPs for baseline ref1–twre from day 40 (9th February 2005) of the Forth Road Bridge Trial.

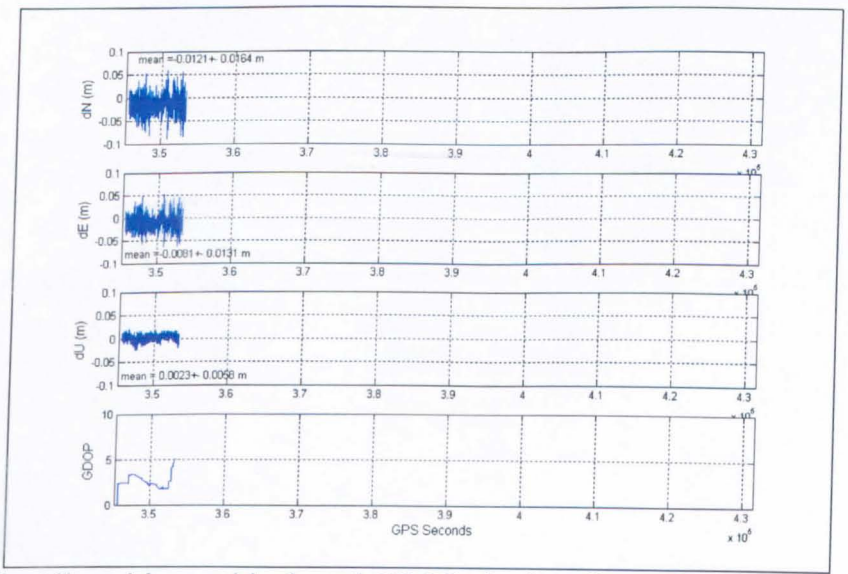

Figure F6. All position residuals and GDOPs for baseline ref1–twre from day 41 (10th February 2005) of the Forth Road Bridge Trial.

Appendix G

Matlab script codes (convertraw.m) for conversion from processed Leica Ski-Pro Version 3.0 and KINPOS results to GPS Seconds and dN, dE, dU.

```
% To read text files from SKI-PRO and KINPOS results
% And convert time to GPS seconds and coordinates from dX, dY, dZ to dN, dE, dU
%
%Sample from the Humber Bridge Trial
clear
% input the known latitude and longitude, X, Y, Z of points according to format
% can type in all known points.
longitud = 'W'   % 'E' for East or 'W' for West' no need to put the -ve sign
latitude = 'N'   % 'N' for North or 'S' for South
% Note : This is the correct format for DATA INPUT
%coord=' 53 42 51.38449   0 27  2.16063 3782898.2630 -  29751.0529 5118148.4080' %
example

%coord=' 53 43 10.83387          0 27  3.12388 3782349.2326 -  29764.3994
5118416.8292' %        ref1
%coord=' 53 42 52.44152   0 26 37.16237 3782787.5103 -  29291.6990 5118047.8992' %
        est
coord=' 53 42 51.38418   0 27  2.16013 3782898.2979 -  29751.0440 5118148.4386' %
        twr1

program = 1 ;  % 1 = SKI-PRO,  2 = KINPOS  input Software used

fail = 'e1w14'; % name of file excluding extension

%Day of week
day = 4 % day of the week
%   01 March 2004 (Mon) = 1
%   02 March 2004 (Tue) = 2
%   04 March 2004 (Thurs) = 4

if program==1
   extinp='.txt'
   initial = 'S'
else
   extinp='.pos'
   initial='K'
end;

extout = '.out';

basinp=strcat(fail,extinp);
basout=strcat(initial,fail,extout);
```

```
if program==1
[a1,a2,a3,a4,a5,a6,a7,a8,a9,a10,a11,a12,a13,a14,a15,a16,a17,a18,a19,a20,a21] =
textread(basinp,'%s%s%s%s%s%s%s%s%s%s%s%s%s%s%s%s%s%s%s%s%s%s%s');
a1=char(a1);
a22=a21;

else
[a1,a2,a3,a4,a5,a6,a7,a8,a9,a10] = textread(basinp,'%s%s%s%s%s%s%s%s%s%s');
a11=a5;
a12=a6;
a13=a7;
a21=a10;
a22=a9;
a1=char(a1);
a1=str2num(a1);
gsec=a1;

end;
%a1 is point number with time
%a11, a12, a13 is X, Y and Z
%a21 GDOP max
n=length(a1);

a21=char(a21);
a21=str2num(a21);

a22=char(a22);
a22=str2num(a22);

if program == 1
a1h=a1(:,(10:11)); %extracts hours in 2 digits string
a1m=a1(:,(12:13)); %extracts minutes in 2 digits string
a1s=a1(:,(14:15)); %extracts seconds in 2 digits string
a1sd=a1(:,(16)); %extracts the tenth of a second in 1 digits string
a1h=str2num(a1h); %convert hours from string to number
a1m=str2num(a1m); %convert minutes from string to number
a1s=str2num(a1s); %convert seconds from string to number
a1sd=str2num(a1sd);
a1s=a1s+a1sd/10

gsec=86400*day+(a1h*3600+a1m*60+a1s); %compute gps seconds
```

```
 if gsec>(86400*7)
    gsec=gsec-(86400*7)
 end;
 end;
 fid1=fopen('cek.txt','w')
 de=str2num(coord(1,1:3));
 mi=str2num(coord(1,5:6));
 se=str2num(coord(1,8:15));
 lat = (de+mi/60+se/3600)*pi/180; % latitude of rover in radians
 if latitude=='S' ;
    lat= -lat;
 end;
 fprintf(fid1,'lat = %d  %d   %8.5f  %13.8f  \n',de,mi,se,lat)

 de=str2num(coord(1,17:20));
 mi=str2num(coord(1,22:23));
 se=str2num(coord(1,25:32));
 lon= (de+mi/60+se/3600)*pi/180; % longitude of rover in radians
 if longitud=='W' ;
    lon= -lon;
 end;
 fprintf(fid1,'lon = %d  %d   %8.5f  %13.8f  \n',de,mi,se,lon)
 slat=sin(lat);
 clat=cos(lat);
 slon=sin(lon);
 clon=cos(lon);

 x=str2num(coord(1,34:45));
 y=str2num(coord(1,47:59));
 z=str2num(coord(1,61:72));

 fprintf(fid1,'lon = %12.4f  %12.4f   %12.4f  \n',x,y,z)
 fclose(fid1);

 a11=char(a11);
 a12=char(a12);
 a13=char(a13);

 a11=str2num(a11);
 a12=str2num(a12);
 a13=str2num(a13);
```

```
dn=((a11-x)*((-slat)*clon))+((a12-y)*((-slat)*slon))+((a13-z)*clat)
de=((a11-x)*(-slat))+((a12-y)*(clon))
du=((a11-x)*(clat*clon))+((a12-y)*(clat*slon))+((a13-z)*slat)

fid1=fopen(basout,'w'); % output baseline results in gpssecs, dN, dE, dU
for k=1:length(gsec)
if program == 1
   fprintf(fid1,'%d     %7.4f     %7.4f     %7.4f     %4.1f
%4.1f\n',gsec(k),dn(k),de(k),du(k),a21(k),a22(k));
else
   fprintf(fid1,'%d     %7.4f     %7.4f     %7.4f     %d     %d
\n',gsec(k),dn(k),de(k),du(k),a22(k),a21(k));
end;
end;
fclose(fid1);
```